LUMINESCENT PROPERTIES OF CdS(Te)

AND

THEIR APPLICATION TO NUCLEAR PARTICLE DETECTION

by

F. ESEN OZSAN, M.Sc.

A thesis submitted to the University of Durham

for the degree of

Doctor of Philosophy

July 1974

Department of Physics
Science Laboratories
Durham City

CONTENTS

ABSTRACT

Cadmium sulphide is a II-VI compound semiconductor with a wide band-gap of 2.53 eV at liquid nitrogen temperature, and is a good emitter of visible luminescence. Very efficient luminescent emission is observed at 600 nm when this material is doped with tellurium atoms at a concentration of 10^{18}-10^{19}/cc. The main purpose of the research reported in this thesis was to study the luminescent properties of CdS(Te) crystals and then to try to use them as scintillators in nuclear particle detection, particularly for γ-ray detection.

The use of different excitations, for example 5.5 MeV α- and 1 MeV β-particles, with CdS(Te) crystals containing different concentrations of tellurium and with varying stoichiometry produced some new results which led to further insight into the mechanism of luminescence in this material. Measurements made at temperatures between 80 and 300 K showed that the radiative recombination mechanism was dependent on the ionization density as well as the stoichiometry, and the tellurium concentration. At low temperatures, fast decay lifetimes of about 55 ns were observed with highly ionizing α-particles whereas the decay lifetimes were found to be about 220 ns with β-particle excitation. In general, the decay profiles were composed of two components, i.e. a fast, exponential part with a decay constant of about 25 ns, and a slow bimolecular part. The fast part was invariant with temperature, stoichiometry and tellurium concentration and was thought to be the intrinsic lifetime of the exciton trapped at the isoelectronic tellurium centre. Some of the radiative recombination was considered to come from the tunnelling of majority carriers from the conduction bands via electron trapping sites to the tellurium centres which had already trapped holes with a binding energy of

0.14 to 0.2 eV (as found from thermal quenching measurements). The 0.045 eV shift of the luminescence spectrum induced by α-particle and UV excitation, towards longer wavelengths relative to that excited by β-particles supported this idea.

CdS(Te) was found to be a very successful scintillator mainly because of its high luminescence efficiency (60-70%) and low band-gap. When a small thin platelike crystal was coupled to a silicon photodiode at low temperatures, a value of 24 eV per ion pair was obtained from the detection of 5.5 MeV α-particles. The successful growth of larger crystals with a volume of about 1 cc, which possessed similar properties to the original platelike crystals allowed the detection of various penetrating γ-rays with the same low values of energy for the creation of ion pairs.

ACKNOWLEDGEMENTS

I would like to express my gratitude to my supervisor, Dr. J.E. Bateman, for his kind guidance and assistance during the course of the research project. Many thanks are due to Professor G.D. Rochester and Professor A.W. Wolfendale for allowing me to use the facilities of the Department. I would also like to thank Dr. F. Ashton for encouraging me in this study. The help of the Physics Student Workshop staff headed by Mr. D. Jobling and Audio-Visual Section headed by Mr. M. Lee, are acknowledged.

I am grateful to Dr. J. Woods for allowing me to use the laboratory facilities of his group in the Department of Applied Physics and Electronics, and helping me with his interesting and useful discussions on the subject. A special acknowledgement must be reserved for Mr. J.R. Cutter, who has painstakingly grown all the CdS(Te) crystals used in this project.

I am indebted to M.E.T.U., Ankara, for financial support during the first year of this study, and U.N.E.S.C.O. for a grant covering the subsequent two years. The grant made by the Research Fund of Durham University towards the purchase of Si(Li) diode is also gratefully acknowledged.

Last, but by no means least, I would like to express my gratitude to my wife, Ayse, for her encouragement, support and practical help with the preparation of the thesis.

PREFACE

The work described in this thesis was carried out over the period 1970-1973 while the author was a research student under the supervision of Dr. J.E. Bateman in the Cosmic Ray Group of the Physics Department of the University of Durham.

The cryostats, their associated equipment and the electronics used in the radioluminescent measurements and in the detector works were designed by the author and some of the electronics were constructed by him. The cryostats were built in the Physics Department. All of the luminescent and optical measurements on tellurium-doped cadmium sulphide crystals and the detector measurements were carried out by the author except a few measurements which were recently made by Dr. J.E. Bateman in Rutherford High Energy Laboratories using the same experimental arrangements referenced in this thesis.

The growth of various CdS(Te) crystals used in this work were performed in the Applied Physics and Electronics Department of this University under the supervision of Dr. J. Woods. The author assisted with some of these growth runs and also controlled the growth parameters in the light of the luminescent and optical measurements made on them.

CHAPTER 1

INTRODUCTION

1.1 General

The radioluminescent properties of tellurium-doped cadmium sulphide, CdS(Te), have been studied with a view to developing an efficient scintillator for radiation detection (particularly of γ-rays). The radioluminescent decay, thermal quenching and quantum efficiency of a variety of crystals measured by means of single-photon counting techniques. Crystal boules of centimetric dimensions have been grown and have been shown to possess properties adequate for application to γ-ray scintillation counting.

Particularly encouraging properties of the material as studied recently (1-3) are its high luminescence efficiency (it appears that in most samples, 70% of the ion pairs produced by a charged particle produce photons of visible light on recombination) and rapid decay time (variable with doping and temperature from 5-500 ns). Taken with the high luminescence efficiency, the low band gap of CdS(Te) (2.5 eV as compared with 5.4 eV for NaI) can be expected to provide good overall scintillation counter statistics when a light detector of high quantum efficiency (such as a silicon photodiode) is used. A mean particle energy per ion pair of ∿25 eV is considered possible in such a device. This figure is singularly low for a scintillation detector and would appear to promise a γ-ray energy resolution intermediate between those of the solid state Ge(Li) detector and the NaI(Tl)-photomultiplier detector. Such a detector would be intermediate in all senses giving the stopping power of NaI(Tl) with a better energy resolution. The flexibility of the scintillation detection detector would be preserved while the

complexity and the cost would be less than that of a Ge(Li) device.

Much of the information obtained in the course of the present studies of CdS(Te) as a scintillator was expected to be of value in elucidating the luminescent properties of the material. Measurements of the luminescence efficiency, decay time, thermal quenching and spectral output are not only necessary for scintillation counter studies but also throw light on the mechanisms involved. The results available on CdS(Te) are rather restricted in scope and do not provide a serious test for the theory developed by Cuthbert (3) to explain the luminescent behaviour of the material. It is intended that the present work could contribute substantially in this respect by providing data on a wide range of sample grown under different conditions of doping level and stoichiometry.

Chapter 1 is devoted to a description of the general principles of radiation detection with particular stress on γ-ray detection. The optical and luminescent properties of CdS(Te) are reviewed in Chapter 2 with particular reference to their application to scintillation counting. Previous work on the material is also reviewed at that stage.

1.2 Nuclear Radiation Detection

1.2.1 Basic Principles

Fast moving particles such as α-particles, protons and β-particles in atomic radiation are detected by their effects on the matter through which they pass. They dissipate their energy in the ionization and/or excitation of the molecules of the material during the passage. It is this process (ionization, excitation) on which radiation detection systems are based. Uncharged particles, such as

γ-rays, are detected and measured in the same way because they produce secondary charged particles in their interaction with matter, as explained in detail in Section 1.3. For example, a γ-ray can transfer all or part of its energy to an electron in the absorbing material via the photoelectric and Compton process, and the ionization and excitation produced by this secondary electron may be used to detect the primary radiation. Neutrons following their interaction with matter, produce some charged secondary products, and they are detected in the same manner.

γ-ray detection is the most universally useful radioactive tracing and analytical tool known to science, medicine and industry. Therefore, much of the effort on nuclear radiation detection has gone into developing new forms of detector for γ-rays of MeV energies. On the other hand, the dependence of γ-ray detection on secondary quantum interactions in the detector material imposes special requirements on that material; namely, as large a mass/e as possible, and as high an atomic number as possible. The former increases the number of target atoms and the latter increases the photoelectric cross-section. Combining these factors with the other vital properties necessary to allow the ionization effect to be detected and amplified, seriously limits the choice of material and explains why only two types of γ-ray detector are commonly available (i.e. NaI(Tl) and Ge(Li) devices). In the present work on CdS(Te), the chief aim has been to produce a successful γ-detector. Since this imposes the most stringent requirements of any detection situation, the excellence of the device produced for any other radiation follows. Further, the (n,γ) reaction of thermal neutrons in cadmium offers the possibility of thermal neutron detection.

There are various types of radiation detector, e.g. gaseous proportional counters in which the free electrons produced by the incident particle are amplified in a Townsend avalanche; solid state junction detectors in which the electron-hole pairs are collected into an amplifier from the volume of the material by the high electric field in the junction region and scintillation counters in which the recombination of free carriers causes fluorescence which can be detected and amplified in a photomultiplier tube, (PMT). Further information about radiation detectors can be obtained from various books (4-6). In general, solid materials are preferred for γ-ray work because of the need for a high density target. As regards direct collection of ion pairs in the solid state, only silicon and germanium have been brought to the requisite degree of effective purity by means of lithium compensation to permit charge collection over the volumes necessary for γ-work (about 25 cc), and only germanium has an atomic number, Z = 32, high enough for reasonable detection efficiency in the 1 MeV region. The narrow band gap of germanium, while giving good ion pair statistics, also demands cryogenic operation.

Interest has focused therefore on the possibility of using binary semiconductors such as CdS, ZnTe and CdTe to give junction detectors capable of operation near room temperature. With band gaps near 2 eV, good ion pair statistics can be expected without excessive noise and leakage currents. However, the problem of achieving adequate purity and stoichiometric balance is severe and success is limited. Madden et al (7) have pointed out, however, a possible means of making use of these materials without making such severe demands on the crystal growth technology. By doping CdS with an isoelectronic impurity, tellurium, very efficient luminescent recombination centres can be

produced so that the material functions well as a scintillator of low band gap. Thus, one might expect good ion pair statistics and since light is relatively easy to collect from large volumes, the material with its γ-ray absorption coefficient comparable to that of NaI might be expected to make a good detector. In this work, therefore, we concentrate on the use of CdS(Te) as a scintillator.

1.2.2 The Scintillation Counter

The general arrangement of a scintillation counter is shown in Figure 1.1. The operation of this counter involves the following five stages:

(1) The absorption of the incident energy, E, by the scintillator

(2) The scintillation (luminescence) process in which a fraction of this incident energy dissipated is converted into emission of rE photons which are radiated in all directions.

(3) The transit of the emitted photons to the photocathode of the photomultiplier tube, PMT (N' = RrE photons arriving at the photocathode).

(4) Absorption of the photons and the production of N = arRe electrons at the photocathode where "a" is the photocathode quantum efficiency.

(5) The multiplication of the photo-electrons in the dynode structure of the PMT and the production of an electrical signal of amplitude N_A = GarRE at its output.

Each of the above stages is critical to the final performance of a scintillation detector and all must represent optimal conditions if the most desirable qualities of a radiation detector are to be realized, i.e. proportionally with particle energy and above all, good efficiency for detection.

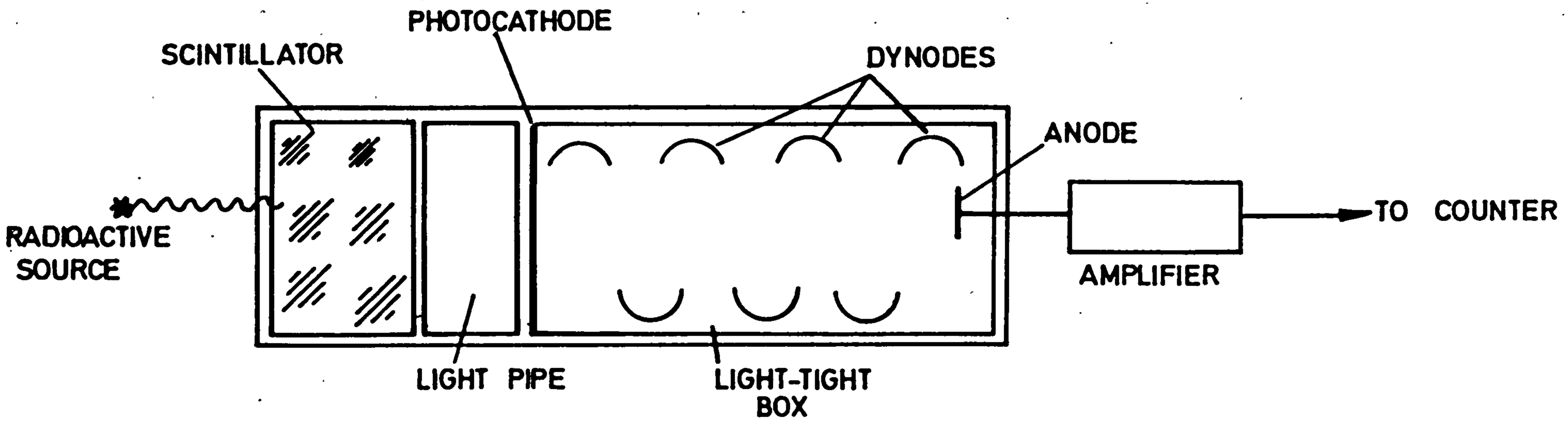

FIGURE 1·1 Scintillation counter with photomultiplier.

Stage (1) is particularly important in γ-detection in which case, unlike charged particle detection, the efficiency of detection is a strong function of the Z of the scintillator, its density and its volume.

Stage (2) often determines the linearity of response of the scintillator and the resolution obtainable. The luminescence efficiency of a material can be represented in various ways, e.g. the fraction of ion pairs which give rise to scintillation photons, or, more usefully the particle energy in eV required to produce a photon.

Stage (3) represents the problem of transferring the photons from the scintillator to the photon detector (here, the PMT). Losses of ∿50% regularly occur at this stage but, in general, the main problem is the dispersion introduced by the different optical paths the light rays take in reaching the photon detector. This dispersion is known as the transfer variance and is controlled principally by three factors: the optical transparency of the scintillator to its own light, the refractive index of the scintillator and the optical matching of the scintillator to the photon detector.

Stage (4) represents one of the most severe losses experienced in the whole process. The efficiency with which a photocathode can convert a photon into an electron is a rapidly decreasing function of the photon wavelength. This function is known as the quantum efficiency and its average value with a standard PMT rarely exceeds 15%.

Clearly, there are many factors to optimise in a scintillation counter if it is to function as a successful particle energy spectrometer. The difficulty is clearly demonstrated by the fact that, as far as γ-ray detection is concerned, only one system is generally in use, namely the NaI(Tl)-PMT. The other property of practical

interest is the response time of a detector. This is determined by the luminescent decay time of the scintillator and the band width of the photon detector. For general use, the response time should be sub-microsecond and if possible, a response of about 50 ns is highly desirable.

1.3 γ-Ray Detection and Spectrometry

1.3.1 Detection

Absorption of γ-rays on passing through a material is more complex than with charged particles. The latter dissipate their energy continuously in a sequence of numerous ionization and excitation events, and penetrate a certain distance, the range, into the absorber in doing so. Electromagnetic radiations on the other hand, are absorbed and scattered in single events. The three main processes involved in these electromagnetic interactions are the photoelectric effect, Compton scattering and pair production. The fraction f of the incident quanta (a beam of well-collimated γ-rays) which are absorbed, i.e. undergo one of these interactions, in their passage through a scintillator of thickness x, in cm, is

$$f = 1-\exp(-\mu x) \quad . \quad . \quad . \quad . \quad . \quad . \quad . \quad (1.1)$$

where

$$\mu = \sigma + \tau + \kappa \quad . \quad . \quad . \quad . \quad . \quad . \quad . \quad (1.2)$$

The constant μ is called the absorption coefficient, in cm^{-1}. The three terms, τ, σ and κ, characterize, respectively, absorption by the photoelectric effect, Compton scattering and pair production. Each of the absorption coefficients depends on the incident radiation energy, and on the nature of the absorber. Related detailed expressions can be found in various books (5,8-10).

The photoelectric effect (PE) occurs when a γ-photon penetrates matter, collides with an atom, loses all of its energy, and causes the ejection of an electron from one of the inner shells, usually the K shell. The ejected electron will have an energy, T_p, equivalent to the difference between the energy of the incident photon and the binding energy, B_e, of the electron, such that $T_p = E - B_e$. The electron vacancy is usually filled by an electron from an outer orbit. This electronic de-excitation is accompanied by the emission of a characteristic X-ray which can itself be absorbed in a similar fashion. In this way, the total energy of the original γ-photon is converted into the kinetic energy of one or more fast electrons. It will be noted that the secondary electron carries a unique energy. If the fluorescent X-rays do not escape the total energy deposited in the material equals the γ-energy. In scintillators, this energy is dissipated by the normal ionization processes which slow up a fast charged particle. In a γ-spectrum such as the one seen at channel number 750 in Figure 1.2, this energy corresponds to the photopeak. At low energies τ is the largest absorption component, but it decreases rapidly with increasing E, though with heavy elements it may still be appreciable up to a few MeV. This is clearly seen in Figure 1.3. The photoelectric absorption coefficient τ in a material with the atomic number Z and density ρ(g/cc) is given by

$$\tau = A \rho Z^4 E^{-7/2} \quad . \quad . \quad . \quad . \quad . \quad . \quad . \quad (1.3)$$

where A is constant. The photoelectric coefficient increases rapidly with atomic number and this explains the advantage of NaI as compared to germanium and silicon for γ-ray spectroscopy as seen in Figure 1.3.

Compton scattering (CS) is a process whereby the γ-photon, on collision with free or loosely bound electrons, imparts only a

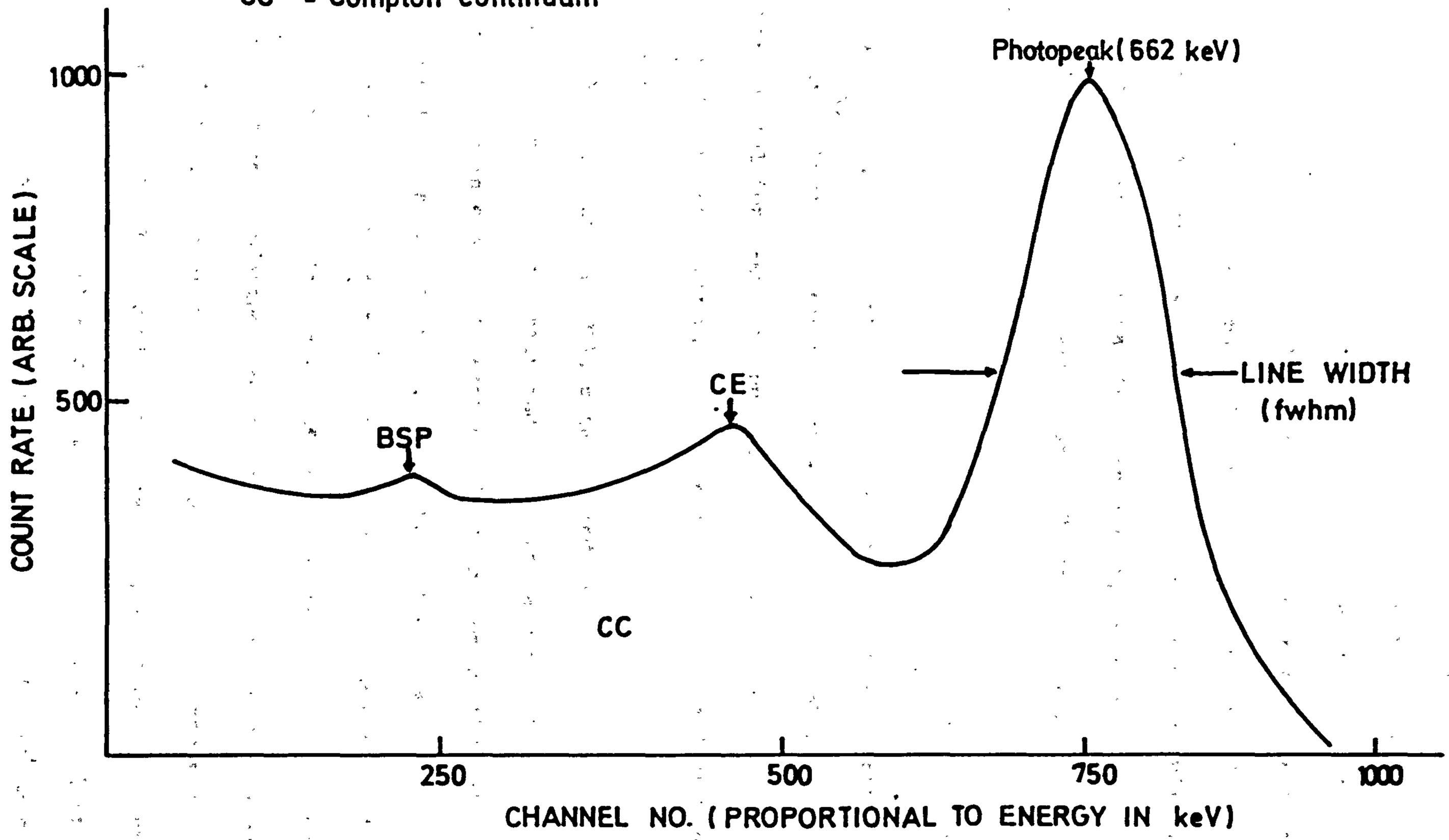

FIGURE 1·2 A gamma radiation spectrum (^{137}Cs).

fraction of its energy to the electron. The energy of the γ-photon must be high compared with the binding energy of the electron for this process to take place. As before, the energy of the scattered electron is absorbed by the scintillator and re-emitted in the form of light. Any fraction of the total incident energy can be transmitted in this way up to the kinematical limit. Thus unfortunately, depending on the angle of scatter a unique incident γ-ray energy results in a spectrum of pulse-heights varying from zero up to a value E' which is known as the Compton edge (see Figure 1.2) and is given by the relation:

$$E' = E/(1+\frac{1}{2\alpha}) \quad . \quad . \quad . \quad . \quad . \quad . \quad . \quad . \quad (1.4)$$

where $\alpha = \frac{E}{m_o c^2}$, $m_o c^2$ being the rest mass energy of an electron. The Compton distribution is rather flat at γ-energies of about 1 MeV and not very useful for γ-energy spectrometry. The Compton absorption coefficient does not vary much with the Z of the material and decreases steadily with E.

Pair production (PP), often called materialization, results in the creation of an electron and a positron and requires the incident photon to have an energy at least equal to the sum of the rest energies of the electron and positron, i.e. 1.02 MeV. The excess energy $T_{pp} = E-2m_o c^2$, is transformed into kinetic energy and shared by two members of the pair. At the end of its range the positron interacts with an electron, producing two annihilation radiation quanta each of energy 0.51 MeV. One or both of these annihilation photons may escape or they may be absorbed by the scintillator by the Compton or photo-electric process. The cross section κ for pair production increases with the energy and is roughly proportional to Z^2. As can be seen from Figure 1.3, the pair production process only contributes usefully

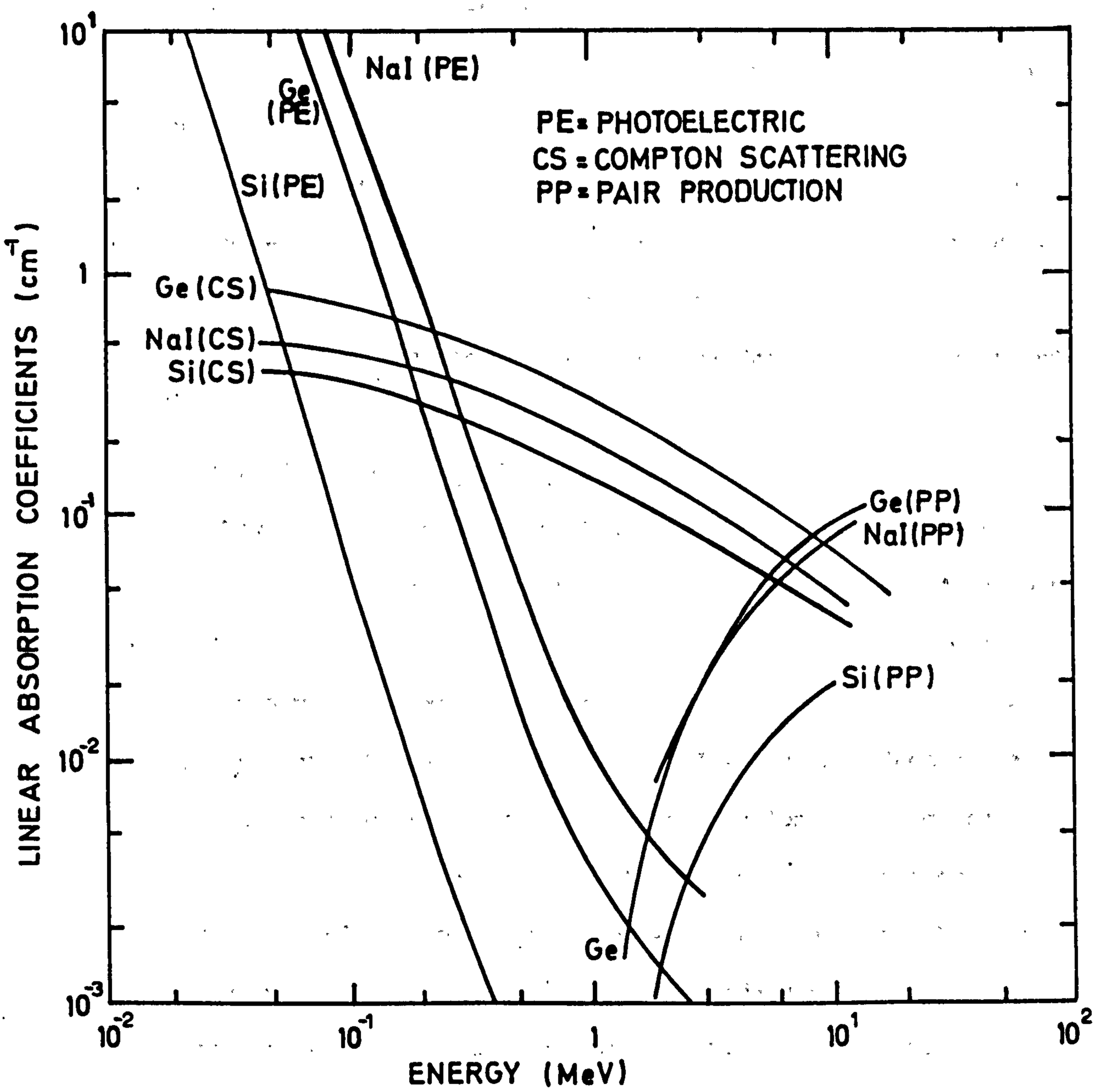

FIGURE: 1.3 Linear absorbtion coefficients versus γ-ray energy for sillicon, germanium and sodium iodide, from Bertolini and Coche (9).

at energies greater than 2-3 MeV which is not in general a region of great practical application.

In conclusion, we note that the absorption coefficient which is the sum of the partial coefficients τ, σ and κ goes through a minimum, since the cross section of the photoelectric effect and Compton effect decrease whereas that of pair production increases, with increasing photon energy. This minimum occurs at an energy which increases as the atomic number of the detector material rises.

1.3.2 Detection Efficiency

The interaction ratio f of a scintillator used for the detection of γ-rays or X-rays is defined as the fraction of photons incident on the front surface of the scintillator which undergo interactions with the scintillator leading to a dissipation of some of their energy. For a collimated beam of γ-rays incident normally on a scintillator of thickness x, the interaction ratio, given by the Equation 1.1, is identical with the detection efficiency. The complexity in γ-detection arises, however, from the fact that each of the three interaction processes yields secondary electrons whose energies are related in different ways to E. The relative numbers of each group of electrons depend on the relative magnitudes of the associated absorption coefficients τ, σ and κ for the scintillator and the energy E. At low E, where the photoelectric absorption is high, it is possible to obtain a value of f approaching unity, and by using large scintillators containing high Z materials (e.g. NaI, CsI) it is possible to obtain high detection efficiencies at higher values of E. The detection efficiency of an NaI(Tl) scintillator for 0.662 MeV γ-rays improves from 0.49 to 0.74 when a

1 in. x 1 in. crystal is replaced by a 2 in. x 2 in. one, as reported by Birks (5) (Table 1.1).

In Figure 1.4, we have represented schematically the various interactions which γ-rays of less than 1 MeV energy can have with a crystal. Choosing NaI(Tl) as our model material, we see from Figure 1.3 that at energies less than 100 keV the large τ ensures that most of the γ-rays are absorbed by the photoelectric (PE) process (II in Figure 1.4), and a Gaussian shaped peak is obtained in the pulse-height spectrum as seen in Figure 1.2. The Compton distribution is negligible. However, at energies near the Iodine K edge (33 keV) the fluorescent X-rays can escape from the surface of the crystal giving a double peaked spectrum with corresponding energies E and $E-B_e$ (see process I in Figure 1.4).

Above 100 keV, the main absorption process becomes the Compton effect and 50% or more of the interactions may be contained in the Compton distribution (III in Figure 1.4). However, if the volume of the crystal is large enough, reabsorption of the wavelength shifted photon is possible by the PE process and again the pulse-height reaches a value corresponding to the total energy of the incident gamma (IV in Figure 1.4). Thus even at energies approaching 1 MeV, a good full energy peak is observed with a reasonable efficiency. This is seen clearly in Table 1.1 where the calculated detection efficiencies (f) and the full energy peak (sometimes called photo-peak) efficiencies (f_p) are given for various dimensions of NaI(Tl) crystals and γ-ray energies. When the ratio of the number of counts in the photopeak to the total number of γ-photons detected is multiplied with f, f_p is obtained. It is clear that for a material such as NaI or CdS, minimum volumes are of the order of a few cc and good working values are around 100 cc.

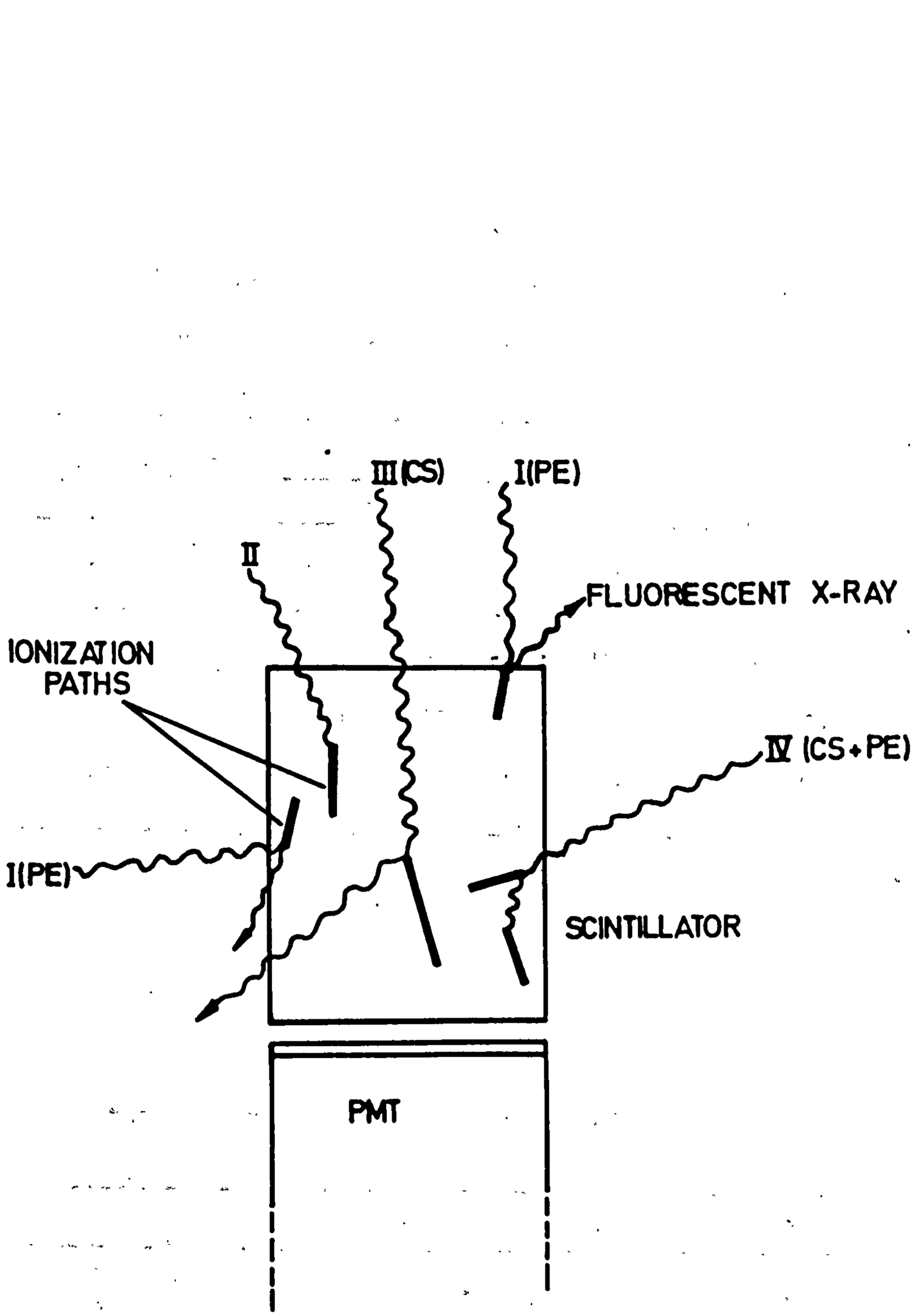

FIGURE 1.4 Various γ-ray interactions which could be involved in a scintillator.

TABLE 1.1

Calculated detection efficiencies and full energy peak efficiencies for NaI crystals for a broad parallel beam, Birks (5)

Crystal size	Radius	1 in.		1 in.		2 in.		2 in.	
	Height	1 in.		2 in.		1 in.		2 in.	
Energy, MeV		f	f_p	f	f_p	f	f_p	f	f_p
0.279		0.79	0.65	0.95	0.82	0.79	0.67	0.95	0.85
0.661		0.49	0.19	0.74	0.36	0.49	0.22	0.74	0.43
1.33		0.37	0.08	0.60	0.17	0.37	0.10	0.60	0.23

TABLE 1.2

Properties of some scintillators from Madden et al (7) and Birks (5)

	NaI(Tl)	CsI(Tl)	NE102	CdS(Te)
Absolute efficiency at room temperatures	13%	6%	3%	Variable 10-20%
Decay time constant of fast component	0.23 μs	1.0 μs	2.5 ns	Variable about 0.2 μs
Emission peak (room temperature)	410 nm	565 nm 595 nm	400 nm	630 nm
Z of highest component	53	55	6	48
Transparency	good	good	good	to be investigated
Stability in air	poor	good	good	good
Density, g/cc	3.7	4.5	1.2	4.8

Increasing the volume of a scintillator the efficiency figure improves but, unfortunately, the light collection and the pulse-height (energy) resolution suffers. Figure 1.2 shows a typical pulse-height spectrum obtained with a 1 in. diameter by 1 in. deep cylinder of NaI(Tl) which has a resolution figure of about 8% to 662 keV γ-rays. If a 3 in x 3 in crystal is used, this resolution becomes poorer (i.e. 12%).

1.3.3 Energy Resolution

For a constant value of incident radiation energy, E, successive events will give an average value of N photo-electrons in the PMT, but the statistical nature of the processes involved will cause individual deviations from the mean value, with a standard deviation of $N^{\frac{1}{2}}$. Because of this, the peaks in the energy spectrum have a finite width. The energy resolution of a detector, which represents the ability of the detector to separate lines with neighbouring energies, is measured in terms of the full line width at half maximum (fwhm) of a spectral peak, as seen in Figure 1.2. This quantity can be expressed as a percentage of the incident energy or in terms of energy measured in electron volts.

There are various factors affecting line broadening in an energy spectrum. Thus the finite energy resolution of a scintillation counter (11,12) originates from the fluctuations in the following processes:

(1) Light production in the scintillator itself,

(2) Light collection at the photocathode,

(3) Production of electrons at the photocathode,

(4) Collection of photoelectrons at the first dynode,

(5) Electron multiplication in the PMT.

The number of photons produced by each monoenergetic event may vary because of local variations in the luminescence efficiency and production statistics. Nothing can be done to decrease this effect except increasing the luminescence efficiency of the scintillator so that the variance in photon production will be less effective. Because of the variations in optical geometry, the efficiency of light collection varies considerably (13). So, a detection event near the phototube window will result in a greater pulse-height than a distant detection event of the same energy transfer. Self-absorption, reflection losses, light trapping and inefficient light piping may all contribute to this reduction in optical collection efficiency and therefore increase its fractional variance. Consequently, it is most important to choose a scintillator with good optical quality, with complete transparency to its own light. Reflective coverings of scintillators (14) can increase the photon collection efficiency. As for the production of electrons at the photocathode, this is controlled by the photoelectric quantum efficiency of the window-cathode system and the spectral matching between scintillator and photocathode. The uniformity of the photocathode response over its area must be well maintained for good resolution. Electron collection at the first dynode is determined by the cathode-first dynode structure and the potential between them. Recently developed photomultipliers (15) with a high gain first dynode of GaP have led to a big reduction in this variance. The variance in electron multiplication processes in the photomultiplier tube is controlled by the voltages applied to the first few dynode stages and by the structure of the tube.

The point in a scintillation system at which the resolution is most critically determined is that at which there is the smallest number of statistical entities. This is just after the photocathode

of the PMT and the mean particle energy required to produce one photoelectron (ω) is therefore a very important parameter, reflecting as it does the ultimate statistical usefulness of a given signal. Assuming Poisson statistics, we have (for numbers of photoelectrons greater than about 10) the fwhm of the peak given as:

$$\Delta E \text{ (fwhm)} = 2.35 (\omega E)^{\frac{1}{2}} \quad . \quad . \quad . \quad . \quad . \quad . \quad (1.5)$$

Calculating the resolution to be expected from a 662 keV γ-ray with a NaI(Tl) scintillator a figure of about 4% for $\Delta E/E$ is obtained (5). In practice, 8% is observed. Various experimenters (5,11,12) have shown that this extra variance arises from the differential light collection from the volume of the crystal, i.e., the transfer variance. As Figure 1.4 indicates, γ-rays can interact uniformly throughout the volume of the scintillator. The solid angle of the photon detector and the various reflection paths can change very substantially according to the locus of origin of the light. Reflective coatings again help to minimize this problem but no adequate solution has ever been found. Clearly, the optical quality and refractive index of the scintillator very much determine the transfer variance.

1.3.4 Performance of Various γ-Ray Detectors

The choice of a γ-detector is made according to the application required (9,16). The type and the size of the detector, and the radiation energy to be measured control the performance. Figures 1.5 and 1.6 show the energy resolution and efficiency of various γ-detectors with respect to incident energy.

There are several types of scintillators being used as γ-ray counters. The interesting properties of the three principal scintillators including CdS(Te) for comparison purposes are given in Table 1.2.

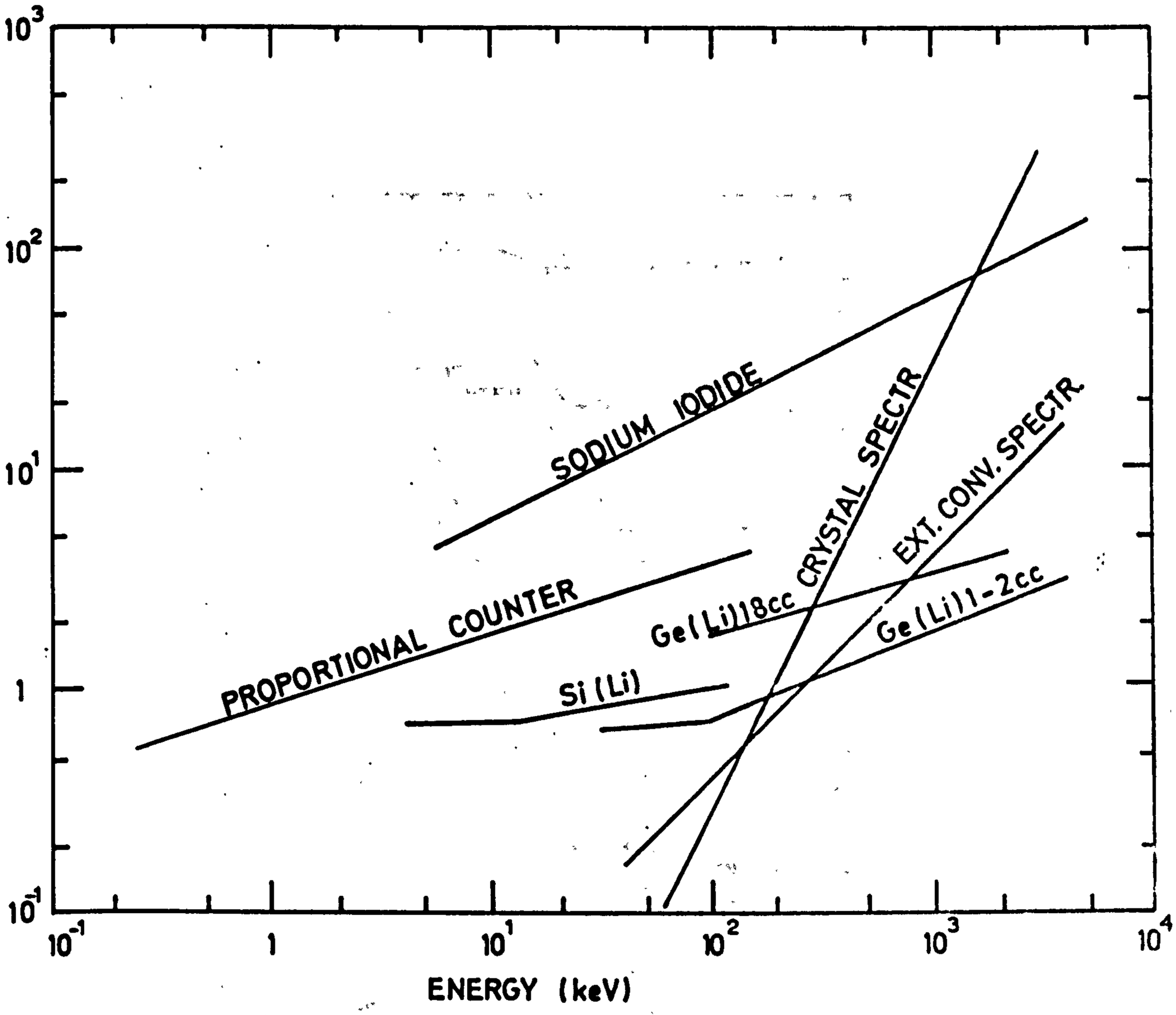

FIGURE 1.5. Resolution versus photon energy for different γ-ray spectrometers, from Bertolini and Coche (9).

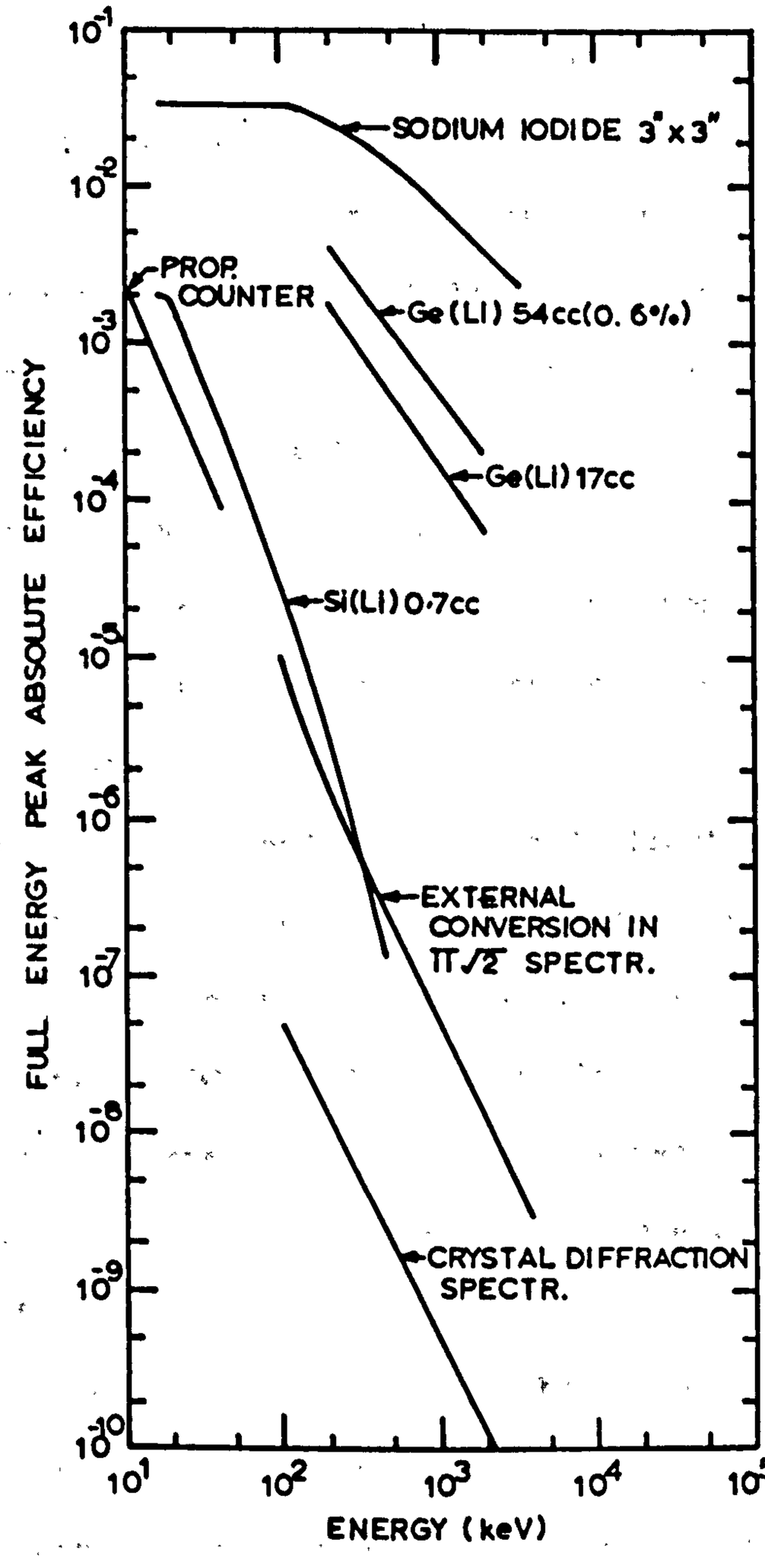

FIGURE 1.6 Absolute full energy efficiency versus photon energy for different γ-ray spectrometers, Bertolini and Coche (9).

The essential properties required for a good γ-scintillator as mentioned already are high Z, good luminescence efficiency (i.e. low ω), good optical quality and the ability to be grown to centimeter dimensions or larger. A final concern is for a short luminescent decay lifetime (less than 1 μs).

Sodium iodide doped with 0.1% mole fraction of thallium is to date the most common and important scintillator for γ-ray and X-ray spectrometry. It possesses all the essential properties, except that the lifetime is rather long (about 0.23 μs) with several very slow secondary components. It has a further disadvantage is being hygroscopic which limits its flexibility. But high detection and photopeak efficiencies are easily obtainable as shown in Table 1.1, because it has a high Z and because it is possible to grow very large size (up to 11 in. x 11 in.) single crystals, which are good for total absorption spectrometry (17,18).

Caesium iodide doped with 0.1% mole fraction of Tl has similar properties to NaI(Tl) as seen in Table 1.2. It is non-hygroscopic, but its scintillation efficiency is less than NaI(Tl); its emission spectrum lies between 500 and 600 nm, creating spectral matching problems when it is used with common PMT's. Since its γ-absorption coefficient is greater than that of NaI(Tl), a smaller volume of CsI(Tl) can be used for a given efficiency.

Because of their low density (about 1 g/cc) and the low Z of their constituent elements, organic scintillators, Birks (5), have much lower γ-ray absorption coefficients than inorganic scintillators. Consequently, the organic scintillators do not compare with these alkali halide scintillators for routine γ-ray spectrometry. However, they possess two advantages over inorganic scintillators, namely a fast decay time, and in the case of liquid or plastic solutions, practically no

limitation on size. The former property is important in the fast coincidence detection of γ-rays. Should the application call for fast timing or coincidence measurements, it should be noted that a figure of merit for such applications is provided by the ratio of light output to scintillation decay time (10); thus, NaI(Tl) and even CsI(Tl) become quite competitive with the organics, in the region of lower energies where the relative light output of the organics is low.

In recent years, semiconductor detectors have started to replace scintillation counters in many applications (19). The main advantage they offer is their good energy resolution which is due largely to their narrow band gaps and consequent low energy per ion pair. It turns out that a large number of measurements previously performed with traditional spectrometers (in particular, NaI scintillators), can be repeated using semiconductor detectors with better results. At low energies, as it can be seen from Figure 1.5 and 1.6, Si(Li) gives good results. Ge(Li), with its higher Z, behaves better at high energies. When excited with ^{60}Co γ-rays, a 20 cc Ge(Li) detector gives an energy resolution of 0.23%, but its photopeak efficiency compared with that of 3x3 NaI(Tl) is as low as 3% (20).

A very large number of studies and measurements are based on the analysis of a γ-ray spectrum. The results obtainable depend to a large degree on the amount of information that can be extracted from the γ-ray spectrum, and on the precision of this information. In these cases, a large total absorption peak uniquely related to the γ-ray energy is essential. Nuclear physics experiments, e.g. decay scheme studies, the production of γ-rays from nuclear reactions, short nuclear lifetime measurements, etc., provide a major field of application for γ-ray spectrometry (9,10,16). However, a growing and ultimately more important field of application is that of materials' analysis by means

of X-ray fluorescence and neutron activation. Here, the identification of particular γ- and X-rays from a given atom is the vital concern, and efficiency is not too much of a problem. Thus very good photopeak resolution is the prime requirement. On the other hand, in many other applications where the photon energies are known (tracer experiments, flow experiments, etc.) only the detection efficiencies are required. This is particularly true in autoradiography in medicine where the requirement that the patient lie motionless for a considerable time (about 30 minutes) severely limits the technique. In this case, counting efficiency is the vital parameter.

In a very few applications in particle physics, fast timing is a particular requirement as well as the ability to tolerate high instantaneous rates. In this case, neither alkali halides scintillators nor Ge(Li) detectors offer acceptable performance.

Thus Ge(Li) detectors are used in materials' analysis, NaI(Tl) detectors in medicine, and plastic scintillators in nuclear physics. The fact that performance is usually a compromise in some respect in most applications implies a continuing search for new γ-ray detecting materials.

1.4 Search for New γ-Ray Detectors

1.4.1 Main Requirements

The requirements made on any new γ-ray detecting material are stringent and may be summarised as follows:

(1) Low effective energy per ion pair (or photoelectron) in the final detection system. This leads to good ion pair statistics (and finally good γ-energy resolution as given in Equation 1.5), and is determined ultimately by the band gap of the material. Thus a Ge(Li) detector yields 2.6 eV/ip whereas a NaI(Tl) detector yields about 150 eV per photoelectron.

(2) High photopeak detection efficiency. This depends on the detector having both a high Z and a large volume, hence large crystals are necessary. CsI(Tl) is superior in this respect over all alternatives; the mean Z is 54 and very large crystals of many cubic inches can be grown.

(3) Fast response times. None of the high resolution, high efficiency materials yield this. Figures of around or less than 50 ns would be ideal.

Development of semiconductor detectors, e.g. Ge(Li), Si(Li), has fulfilled one of the above mentioned requirements for new γ-ray detectors, namely superior energy resolution due to their low band gaps. Germanium, Z=32, has a much larger photopeak efficiency than silicon, Z=14, and thus is a much more desirable material for γ-ray detectors. On the other hand, the relatively small band gap of germanium requires temperatures near -190°C for optimum operation as opposed to temperatures of +20°C to -75°C for silicon detectors. Another disadvantage of Ge(Li) detectors is the requirement of permanent cryogenic storage in vacuum due to their susceptibility to surface contamination and the high room temperature mobility of the compensating lithium.

The availability of large volume materials in γ-ray detectors is quite a critical matter. Large single crystal growth for the production of usable detectors must be achieved. Without this, the question of the use of any new γ-ray detector material remains purely academic. Optical quality is the main limiting factor in growing large scintillators. In semiconductor detectors, the main size-limiting factor is the obtainable trapping length (21). The maximum volume reported in Ge(Li) detector is about 100 cc (22).

1.4.2 New Materials Developed

Most of the work on new γ-ray detector development has concentrated on semiconductors (16,21,23,24). This is natural since in semiconductors one may hope to achieve direct collection of the ion pairs created by a charged particle. This leads directly to an extremely low energy per ion pair and therefore, potentially at least, to good energy resolution. However, the necessary combination of properties in a semiconductor is particularly stringent (see Gunnersen, 25). A list of the band gaps and atomic numbers of various materials is given in Table 1.3. There are two approaches which may offer improved performance characteristics in comparison with Ge(Li) detectors: A high Z, narrower band gap semiconductor such as InSb, when operated at liquid helium temperatures, could provide higher photopeak efficiencies and narrower line widths (fhwm), or, on the other extreme, wide band gap semiconductors such as CdTe can be used at room temperature and above. As a practical matter, a band gap of about 1.4 eV or greater gives rise to thermally generated currents sufficiently small to allow room temperature operation of high resolution detectors.

The critical comparison among these new detectors is made by looking at their respective electron and hole trapping lengths, $L_{e,h}$, which can be expressed as (22)

$$L_{e,h} = \mu_{e,h} \tau^{+}_{e,h} E \quad . \quad . \quad . \quad . \quad . \quad . \quad . \quad . \quad (1.6)$$

where $\tau^{+}_{e,h}$ is the mean carrier lifetime for which a carrier (electron or hole) remains free in the depleted region, $\mu_{e,h}$ is the drift mobility of the respective carrier, E is the electric field. Trapping lengths of microns can be quite acceptable for many semiconductor device applications, while for radiation detectors it is often desirable to collect charge over distances measured in centimeters.

TABLE 1.3

Atomic numbers and band gap energies of some materials from Muggleton (16) and Miller (21)

Material	Atomic number	Band gap (eV)
Ge, germanium	32	0.66
Si, silicon	14	1.1
CdTe, cadmium telluride	48 , 52	1.4
GaAs, gallium arsenide	31 , 33	1.4
HgI_2, mercuric iodide	80 , 53	2.1
SiC, silicon carbide	14 , 6	2.2 - 3.3
ZnS, zinc sulphide	30 , 16	3.65
CdS, cadmium sulphide	48 , 16	2.4
InSb, indium atimonide	49 , 51	0.17

The enormous advantage of silicon and germanium over other materials at the present time is due to their long trapping lengths in the range of meters. The current leading contenders such as CdTe, GaAs and HgI_2 have trapping lengths of millimeters. The others, such as GaP, InP, PbO, PbI_2 etc. are very poor, with short trapping lengths of microns or less.

Much work has been carried out on CdTe (26-30). A resolution of 16% has been obtained with 662 keV γ-rays, at room temperature, but when the crystal size is increased, the performance is limited by heavy trapping which causes incomplete charge collection; the consequent variability of pulse-height with position of the γ-ray interaction in CdTe reduces the full energy efficiency below that expected. But there is a steady improvement in spectral performance of CdTe (21). Even at the lowest level, however, CdTe devices have definitely entered an area in which they can be directly applied, as small medical probes for example.

Because of its numerous device applications, GaAs has received much attention. There has been a continuous effort to grow high purity samples of many III-V compounds and the increased understanding of GaAs from the theoretical point of view, has enabled the fabrication of useful nuclear radiation detectors (31).

Most recently HgI_2 has been introduced as a γ-ray detector (24,30). With its very high Z and wide band gap it offers and attractive detector potentiality. It also exhibits good carrier transport properties. A ^{60}Co γ-ray spectrum obtained with a small size crystal of HgI_2 has given a very well resolved peak with 10% energy resolution; this is attributable to the very high Z and high density (7.7 gm/cm^3) of the detector material, but difficulty is being experienced in reproducing the above results.

The low band gap of semiconductors and the consequent low values of energy per ion pair make them an attractive proposition as detector materials. However, the extreme difficulty of achieving the required degree of purity (less than 1 ppm) to permit the successful operation of large volume junction detectors has led to extremely slow development in the exploitation of materials such as GaAs and CdTe as detectors. Madden et al (7) have pointed out that the benefit of the good ion pair statistics of semiconductors may be realized by making use of the recombination radiation. In general, recombination luminescence is much less sensitive to impurities and stoichiometry than free carrier lifetime. Madden et al therefore studied the well known II-VI compounds, CdS and ZnTe, doped with isoelectronic impurities such as tellurium and oxygen. In both cases satisfactory luminescent efficiencies and decay lifetimes were recorded. The results on CdS(Te) were encouraging in view of the high luminescence efficiency and fast decay lifetimes which promise to make CdS(Te) a useful scintillator (Table 1.2).

The narrow band gap of CdS (2.5 eV) gives better ion pair statistics than the alkali halides (band gap of about 5 eV), but also results in the recombination luminescence being at appropriately longer wavelengths. Thus, the major emission band of CdS(Te) is centred on 600 nm at which wavelength no PMT photocathode has a reasonable quantum efficiency. Special tubes for laser applications are beginning to appear but, up until now, an S20 photocathode has been the best available with about 7% quantum efficiency at 600 nm. This poor efficiency largely negates any advantage which the use of the semiconductor scintillator may have gained. Fortunately, another type of light detector is now available in the form of the cryogenic silicon photodiode, application of which to scintillation counting has been developed by Bateman and Özsan(32).

With a high quantum efficiency (∿70%) at 600 nm, the silicon photodiode can fulfil the requirement posed by the semiconductor scintillator in order to make an efficient composite scintillation counter. The cryogenic operation of the photodiode maintains the photon detector noise at very low levels (32) and also allows direct optical coupling of CdS(Te) to the photodiode since the scintillator operates best at low temperatures, e.g. 100 K (7). A principal feature of the present work is the investigation of the properties of a radiation detector which consists of a crystal of CdS(Te) coupled to a cryogenic silicon photodiode.

1.5 Scintillation Detection with Silicon Photodiodes

It has been shown by Bateman (33-35) that the silicon photodiode is a good detector of scintillation light at longer wavelengths, e.g. from CsI(Tl) at 500-600 nm. However the performance of the composite scintillator-photodiode detector is seriously limited by the high room temperature noise of the photodiode. This problem has been solved (32) by adapting a cryogenic Si(Li) particle detector to be used as a photodiode. The success of this procedure was shown by the 0.85% fwhm energy resolution observed with 50 MeV protons when a CsI(Tl) photodiode detector was used (32). (A detector composed of a NaI(Tl)-PMT combination can yield only 2% fwhm for 50 MeV protons). The noise limitation is almost completely removed by cryogenic assembly which reduces the system noise width by more than a factor of ten from 25 keV(Si) to 1.9 keV(Si), i.e. to 530 ion pairs fwhm.

The fortunate fact that CdS(Te) has nearly maximal luminescence efficiency at 100 K, the operating temperature of the Si(Li) diode, removes the need for the thermally insulating light pipe which reduced the coupling efficiency in the case of the CsI(Tl) detector. The

spectral matching of the CdS(Te) light output to the plateau of 70% quantum efficiency in the silicon photodiode response (36) indicates that we have a fairly ideal combination of scintillator-photon detector.

1.6 The Previously Reported Performance of CdS(Te) as a Scintillator

Madden et al (7) have studied the scintillation properties of platelike CdS(Te) crystals of the order of 100 microns or less in thickness. The photoluminescence spectra of CdS(Te) crystals show two emission bands, at 600 nm and 730 nm. The temperature and Te concentration control the efficiency of these bands. For lightly doped samples (less than 10^{19} Te/cc), the 600 nm band is dominant both at low temperatures and at room temperature. At 100 K, the luminescence efficiency of this band was found to be as high as 70% (2), but the efficiency quenches considerably at higher temperatures.

The response of CdS(Te) platelets to 5 MeV α-particles was examined at temperatures between 100 K and 300 K. The scintillations were detected by a PMT and the corresponding pulses were compared in height, shape and spread (fwhm) with those from a plastic scintillator. In this way, the first evaluation of the performance of CdS(Te) as a scintillator was obtained. The results were encouraging in many senses. At room temperature, CdS(Te) produces pulse-heights which are 7 times greater than those of the plastic scintillator, but decay times are slower, about 300 ns at this temperature. At 100 K, the results were even better, i.e. 23 times greater pulse-heights and 100 ns decay time. A direct consequence of the improvement in pulse-height is the increase in the fwhm resolution. At low temperatures, the resolution obtained for CdS(Te) in these scintillation measurements was 15% whereas the

plastic scintillator gives only 24% α-energy resolution.

The properties of CdS(Te) are matched well to the silicon photodiode so that a composite scintillation detector, CdS(Te) - Si(Li), becomes an attractive proposition in the radiation detection field. However, the platelets are not adequate for γ-detection. A large volume of scintillator with good optical qualities has to be grown in order to absorb highly penetrating γ-photons.

Attempts made by Madden et al to grow the large single crystals suitable for a useful scintillator resulted in very poor luminescent and optical properties. The growth of this type of crystal presents serious problems. Fortunately, in our University we have a group with long experience of growing CdS crystals. Clark and Woods (37) have reported a technique capable of producing large single crystals of undoped CdS of good optical quality, and it was hoped that modification of their technique might lead to the successful growth of large crystals of CdS(Te) (i.e. 1 cm diameter by a few centimeters long). It was considered that successful growth of a useful (i.e. with good luminescent and optical properties) crystal of this size would indicate that the large crystals required for scintillation counting could be grown by scaling up the technique.

1.7 Conclusion

It now appears likely that it will be possible to develop a new scintillation detector, using a CdS(Te) scintillator coupled to a silicon photodiode.

This new detector should provide a useful variety of properties as a nuclear particle detector (particularly for γ-rays). We might expect a stopping power comparable to that of NaI(Tl) with a pulse-height resolution considerably better than that of NaI(Tl) but not as

good as that of Ge(Li). (See in Figure 1.7, the comparison of the 662 keV γ-ray energy spectra obtained by NaI(Tl)-PMT and Ge(Li) detectors with the expected spectrum obtainable by a CdS(Te)-Si(Li) detector). The response time would be as fast and (in some cases) much faster than that of NaI(Tl) and the format of a cryogenic scintillation counter still permits a degree of flexibility and robustness not found in Ge(Li) detectors. The principal problem initially was to succeed in growing large (several cc) crystals of CdS(Te) with properties typical of the platelets grown by Madden et al (7). This means high luminescence efficiency with good optical quality. It is fairly clear that if volumes of a few cc are realised, scaling up to hundreds of cc should be relatively straight forward. Beyond the initial stages, the problems of light collection from a material of high refractive index must be tackled in the context of coupling to a silicon surface.

The properties of the sample grown have been assessed by measurements of the decay lifetime, quenching curve and luminescence efficiency. The former have been done using a single-photon counting technique. It addition it was hoped that the data obtained from the programme which covered vapour grown platelets and boules with stoichiometry controlled towards excess cadmium and sulphur as desired, would contribute to the understanding of the luminescent processes in CdS(Te). In the technique described in Chapter 4 we have the ability to stimulate the crystal with α-particles and β-particles. The 250:1 difference in the ionisation density produced by these particles introduces a further diagnostic condition, not so far applied to this material.

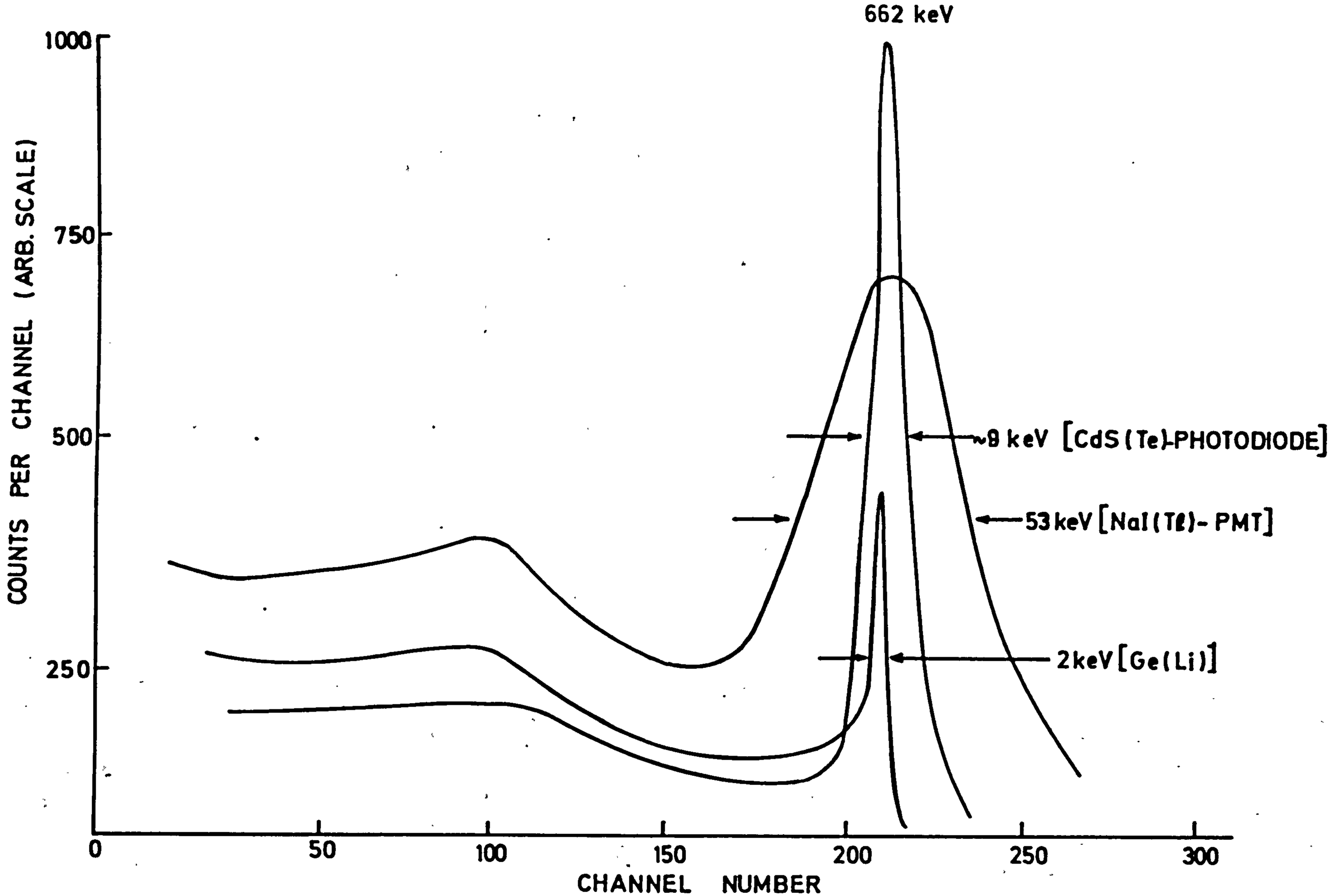

FIGURE 1.7. Comparison of ^{137}Cs γ-ray spectra measured by NaI(Tℓ)-PMT and Ge(Li) detectors with the expected spectrum obtainable by a CdS(Te)-Si(Li).

CHAPTER 2

OPTICAL AND LUMINESCENT PROPERTIES OF CdS(Te)

2.1 Introduction

The luminescence of II-VI compounds has been extensively studied with regard to the radiative recombination mechanism and the nature of the centres responsible for luminescence, and it has been shown that impurities and native defects are the centres responsible for luminescence. The quality of a crystal affects the results considerably. Due largely to the availability of good thin single crystal platelets of the wurtzite group II-VI semiconductors CdS, CdSe, and ZnS, rather more work has been done and more information has been obtained on these materials than on others. A detailed review of the physical and chemical properties of II-VI compounds has been given by Aven and Prener(38).

Much of the research work on these compounds, particularly on CdS, ZnS, and CdTe, has been stimulated by their many technological uses as phosphors and photoconductive devices. In this chapter, previously reported optical properties of CdS doped with tellurium will be reviewed. Most of the properties of CdS(Te) are determined by the host material, CdS, when the Te concentration is low, i.e. around 10^{18}-10^{19} atoms/cc. Therefore, we will begin with a short review of the related properties of CdS.

2.2 Luminescence in CdS

2.2.1 Some Parameters

When electromagnetic radiation propagates in a material, it is attenuated because of energy absorption, by a factor $e^{-\alpha x}$ where α is the absorption coefficient and x is the propagation distance.

Generally speaking, the absorption of those photons of energies lower than the smallest energy gap (the direct band gap in II-VI compounds) is relatively weak and arises from the interaction with the crystalline imperfections and the material appears to be transparent to its own radiation. It is a matter of long experience that in order to obtain values of α of 1 cm^{-1} or less in "pure" CdS, the purity of the crystal must also be high. Thomas and Hopfield (39) have reported a value of 0.8 cm^{-1} at 600 nm in CdS crystals at low temperatures. A detailed study of the optical absorption of group II-VI compounds have been made by Dimmock (40). All these studies have shown that more growth and experience is necessary to obtain better crystals with low absorption coefficient. Another interesting property referred to by Moss (41), is that the transmission of single crystals of CdS in the absorption edge region increases when the temperature is low. This property matches our requirement very well since we want to make use of this material at low temperatures.

A detailed survey of the refractive index of CdS crystals has been given by Moss (41), Gobrecht and Bartschat (42) who examined this property at 293 K and at 93 K. At 600 nm, the corresponding values were found to be 2.5 and 2.47 respectively.

Another important parameter is the magnitude of the band gap which is 2.58 eV as given by Hopfield and Thomas (43).

2.2.2 Radiative and Non-radiative Recombination

Ionizing radiation will, in one way or another, produce free holes and electrons in a semiconductor. This energy may be transferred deeper into the crystal by electron-hole pair diffusion, or by exciton diffusion. The diffusion of holes and electrons and particularly of excitons in CdS has been the subject of considerable controversy, claims

having been made of diffusion lengths of up to several millimeters, although such figures have been challenged(44).

If semiconductors are to be used as scintillators one had to consider how these holes and electrons recombine to produce light. Not all of the electrons and holes produced recombine radiatively. Usually most of the carriers recombine non-radiatively. In fact, in pure CdS non-radiative recombination is more probable. The precise mechanism of radiative and non-radiative recombination can be quite complicated and is by no means fully understood. However, by introducing some impurities such as donors, acceptors or isoelectronic substituents (see Section 2.3) into host material it is possible to increase the probability of radiative recombination with consequently higher luminescence efficiency. Te in CdS performs this job. Electrons and holes produced in the material may recombine radiatively at such centres more efficiently as indicated by Madden et al(7), and some 70% quantum efficiency (fraction of the electrons and holes which recombine radiatively) is obtainable at low temperatures in CdS(Te)(2). (There is not a great difference between the definitions of "quantum efficiency" and "luminescence efficiency" as will be explained in Chapter 3).

The photoluminescent spectrum of pure single-crystal CdS at low (liquid helium) temperature and under high excitation intensity exhibits many narrow lines in the region 486 - 510 nm, and broad emission bands between 510 and 560 nm. Narrow lines occur only at low temperatures at energies slightly less than the band gap energy(45). These transitions arise from states which are loosely bound and so radiate only weakly with phonon cooperation. These transitions correspond to the annihilation of an exciton which is bound to a neutral donor or acceptor. (They are named I_2 and I_1 respectively).

The broad band emission, known also as green edge emission, consists of bands with replicas of lower intensity at longer wavelengths through the simultaneous emission of one or more longitudinal optical phonons(46). They occur at comparatively high temperatures (78 K), and are associated with phonon effects. The origin of these broad bands has been the subject of a great deal of controversy. Colbow and Yuen(47) have recently shown that the green edge emission in CdS is associated with distant donor-acceptor pair recombination.

Free electrons and holes produced in CdS by ionizing radiation can decay non-radiatively in various ways, one of these involves Auger processes. In such a process, the electron and hole of the exciton recombine and the energy of the bound exciton is transferred to the second electron (on the donor) or hole (on acceptor) which is ejected from the impurity with a large kinetic energy which is rapidly lost as heat as the carrier cascades down by emitting phonons(7). The important point here is that if more than two mobile particles are able to come together, there is a good chance that non-radiative Auger recombination can occur. It seems likely that as electrically active impurities are added the chances of three body collisions occurring are increased, leading to non-radiative Auger transitions. In the light of these remarks, it would appear desirable to have a luminescent centre at which both hole and electron are captured so that recombination is rapid and that such a centre while electrically neutral should not provide extra holes and electrons making possible non-radiative Auger recombination. Isoelectronic traps provide solutions to these requirements.

2.3 Isoelectronic Traps

It sometimes happens that when a host atom in a semiconductor is replaced by an impurity atom from the same column of the periodic

table, i.e., an isoelectronic substitution, the impurity atom can trap a hole or an electron. When this happens, we talk about an isoelectronic trap. Since the substituents are isoelectronic, they do not possess a net charge nor do they provide extra holes or electrons, in this they are to be distinguished from donors and acceptors.

Although there have been various studies of isoelectronic traps, so far no satisfactory theoretical solution has been given of this phenomena. To form an isoelectronic trap, the electronic states of the impurity atom must differ significantly from those of the atom it replaces in order to produce a local potential capable of binding a hole or an electron (48). If such a condition is fulfilled, the substituting atom may provide a bound state within the forbidden gap for a hole-electron pair or exciton. Whenever the electron (hole) is tightly bound in the potential well of the isoelectronic substituent, it binds a hole (electron) via the normal long range Coulomb interaction. The second particle characterizes the centre as an isoelectronic acceptor (donor). Thus, ZnTe(O) and GaP(N) are isoelectronic acceptors, since the impurities (O and N respectively) have greater electron affinity than the host anions (Te and P respectively). Bi in GaP and Te in CdS, on the other hand are isoelectronic donors.

It is interesting to note that all presently known isoelectronic traps are substances of limited solubility in the host crystal. This is reasonable, since the condition of the isoelectronic substituent being sufficiently different from the atom is replaces, makes it substitution energetically unfavourable and so limits its solubility (48,49).

The properties of the materials containing isoelectronic traps have been subjected to various studies and experiments. Some examples

are ZnTe(O), GaP(N), GaP(Bi) (49-52), and CdS(Te) (2,3,53). At low temperatures, such traps can emit light with luminescent efficiencies approaching unity and rapid exponential decay times are observed. For example, the 600 nm emission band of CdS(Te) has a 70% efficiency at low temperatures and 300 ns decay time (2).

2.4 Experimental Results on CdS(Te)

2.4.1 Introduction

Various investigators have studied the luminescence of Te-doped CdS. An important point to note at this stage is that all the results obtained so far, and to be described in this chapter, were from thin platelike crystals. Aten and co-workers (53) have described some of the properties of such CdS(Te) crystals. They showed that tellurium substituting isoelectronically for sulphur at a concentration of $2x10^{18}$ atoms/cc could trap a hole and subsequently an electron, and luminescence occurred at 77 K in a broad band near 600 nm. At room temperature this luminescence was largely quenched. Photoconduction due to Te was also described. They concluded that Te gave rise to centres with an energy level of 0.2 eV above the top of the valence band.

Cuthbert and Thomas (2) have also examined the optical properties of CdS(Te) in detail. They discovered a second emission band at 730 nm, which was observed when the tellurium concentration exceeded 10^{19} atoms/sec, and which remained unquenched at room temperature. Both bands were rather broad and lacking in any fine structure even at 4 K. The temperature dependence of the luminescent decay time of both bands were examined. It was concluded that the two bands were associated with bound electron-hole recombination at (a) isolated,

and (b) nearest-neighbour pairs of tellurium atoms on sulphur sites.

Roessler (3) made a more detailed study of the luminescence in CdS(Te) by examining the variation of the luminescent emission with temperature and with excess donor and acceptor concentrations. He showed that a simple configurational coordinate model could be used to explain the shape of 600 nm band. He also suggested that the room temperature photoluminescent spectrum could be used to estimate the Te concentration in the sample.

Cuthbert (1) has examined the free carrier lifetimes in CdS(Te) over a wide temperature range, and showed that these data correlate very well with the previously reported luminescent decay time data. Differential equations, formulated to describe the temperature-dependent kinetics, were solved to obtain the transient luminescent and free carrier decay profiles.

In the next sub-sections, a detailed description of the above mentioned results on emission, absorption, lifetime and thermal quenching characteristics of CdS(Te) will be given.

2.4.2 Optical Emission and Absorption Spectra

In general at sufficiently low temperatures (4 K), an electronic transition will contribute both a broad multiphonon component and a sharp zero-phonon line to the optical spectrum, where the relative intensities are determined by the strength of the electron-lattice coupling (3). In the present system, CdS(Te), no sharp line structure is seen because of the strong phonon interaction with the lattice, and both the emission and the absorption spectra consist of broad bands. The absence of sharp lines in spectra has limited the

detailed knowledge which could otherwise be obtained. When sharp lines are not seen, several less direct techniques (54) are usually employed to identify band spectra such as time-resolved spectroscopy and the measurement of decay lifetimes of emission bands,etc.

The photoluminescent emission from CdS(Te) crystals with different tellurium concentrations, [Te], has been examined by Cuthbert and Thomas (2), and Roesler (3). Their results are consistent; two distinct broad bands were seen at low temperatures, as demonstrated in Figure 2.1(a). The relative intensities of these bands is controlled by the tellurium concentration and either one can be preserved alone with appropriate crystal composition as shown in Figure 2.1(b) and (c).

At 20 K, the peak of the high energy (orange) band is centred at 2.09 eV(593 nm), has a half-width of 0.2 eV and, for crystals containing less than 10^{18} atoms/cc of tellurium, is the only band present in the spectrum. This featureless band, peaked near 600 nm, is very similar to the emission at 77 K reported by Aten et al (53). At room temperature, this band is broadened (to 0.37 eV) and shifts slightly to 2.04 eV (607 nm). Additional structure between 2.2 eV (563 nm) and 2.4 eV (516 nm) is often observed, particularly at low temperatures and in lightly doped crystals (Figure 2.2). This structure is the familiar edge emission from CdS and is not connected with the presence of tellurium.

As the tellurium concentration increases, the low-energy band appears initially as a weak shoulder on the 2.09 eV band and eventually completely dominates the spectrum for (Te) above $3x10^{20}$ atoms/cc. The peak position of this band depends on [Te] as well as varying non-monotonically with temperature. For a sample containing $2x10^{20}$ atoms/cc of tellurium, the peak is centred at 1.72 eV (720 nm)

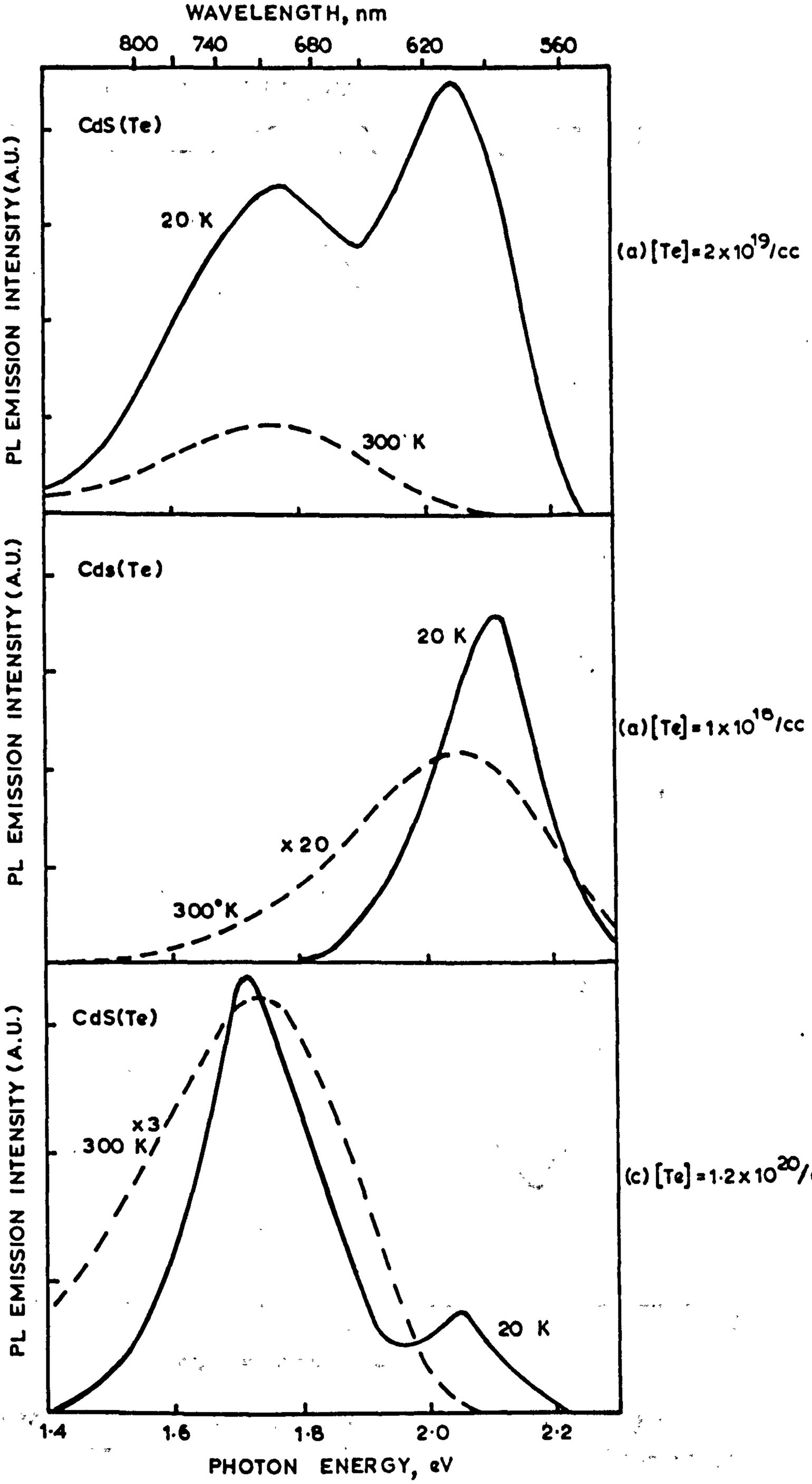

FIGURE 2.1 Photoluminescent (PL) emissions from CdS samples of different Te concentrations excited by 435 nm radiation, from Roessler (3).

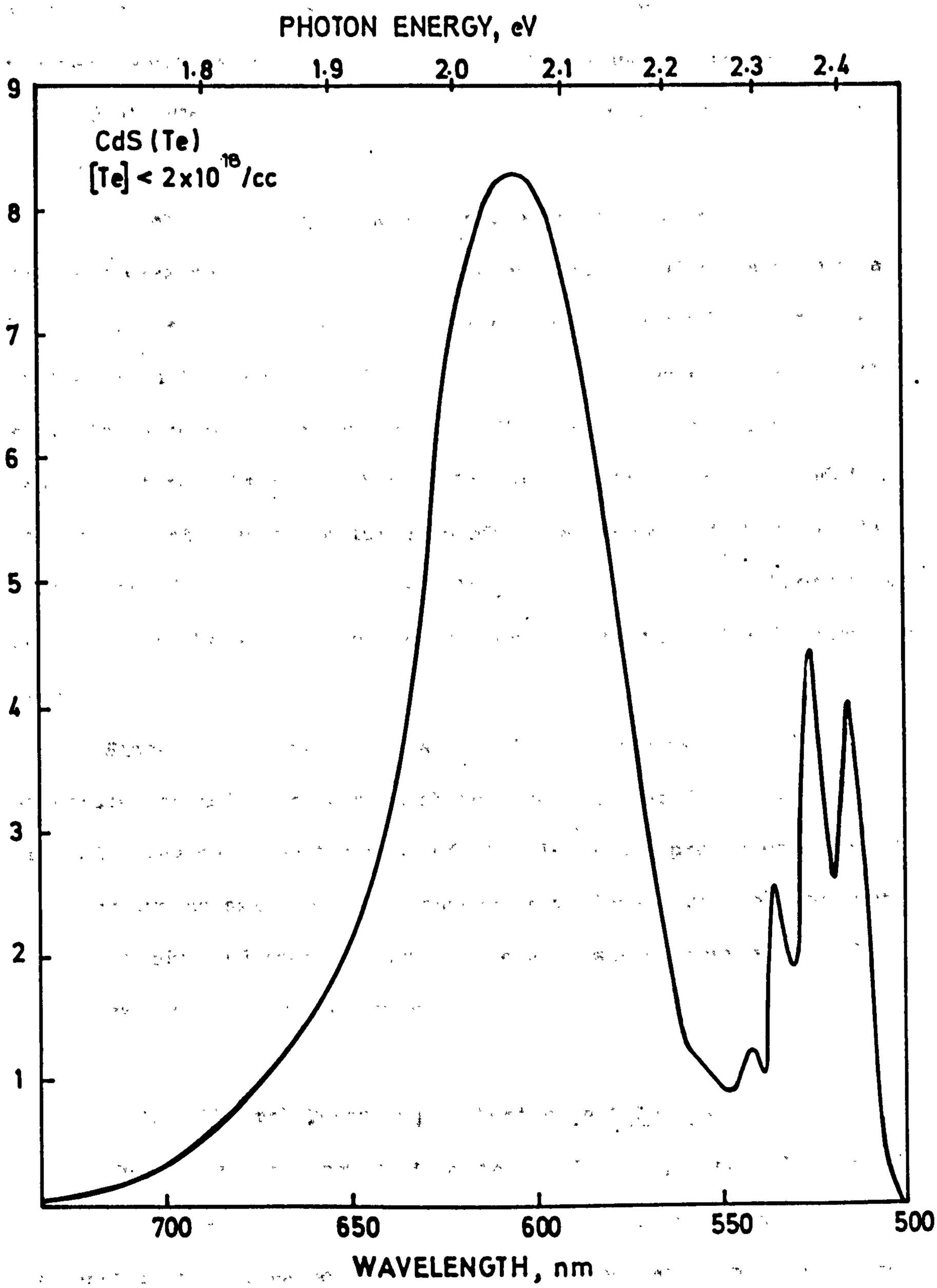

FIGURE 2·2 Luminescent emission of a CdS(Te) sample at 4·2K excited by an electron beam, from Cuthbert and Thomas (2).

at 20 K and has a half-width of 0.23 eV. Roessler has shown that the peak position and the half-width of the orange emission band at 300 K in CdS(Te) can be used to find the tellurium concentration in the sample.

The absorption spectra of a series of tellurium-doped crystals has been examined by Cuthbert and Thomas (2). Heavily doped crystals had a dark red colour due to absorption below the band-gap produced by the tellurium, whereas lightly doped crystals were organge to the eye. The absorption measurements at 25 K were structureless; there was no distinct absorption band. It was also found that the addition of small quantities of tellurium produced a pronounced shift of the absorption edge to low energies. They concluded that the broadening and shift in the absorption spectra were due to tellurium isoelectronic traps.

Since both emission and absorption spectra were found to be structureless and contained no sharp lines, it was difficult to determine any detailed features of the electronic processes associated with the two emission bands. Consequently, less direct methods were used to study band spectra such as the analysis of thermal quenching and decay times of luminescence.

2.4.3 Thermal Quenching of Luminescent Intensity

The radiative recombination in CdS(Te) was, generally, thought to be the decay of an exciton trapped at a tellurium atom. As the temperature is increased, however, thermal ionization of the exciton, first the electron and subsequently the hole, occurs. A released hole may be retrapped at a tellurium atom or alternatively it may be captured by some "killer" centre, for example, and lost to any

radiative decay process. The probability of non-radiative decay increases with temperature and depends on the factor exp(-U/kT), where U is the thermal activation energy associated with the liberation of the hole from the tellurium trap and k is the Boltzman constant (3). The net luminescence efficiency, R, is clearly

$$R = P_r/(P_r+P_n) = I(T)/I(0) \quad . \quad . \quad . \quad . \quad . \quad (2.1)$$

where P_r and P_n are the probabilities of radiative and non-radiative transitions, respectively, with associated decay times τ_r, τ_n. I(T) and I(O) are the luminescent intensities at temperatures T and O K respectively.

It is a common practice to determine the activation energy, U, by fitting the data on the thermal quenching of luminescence to and expression of the form

$$I(T) = I(0)/(1+A\exp\frac{-U}{kT}) \quad . \quad . \quad . \quad . \quad . \quad .(2.2)$$

where 'A' is a constant. The validity of equation 2.2 is clearly restricted to systems with a single excited state and associated single decay times τ_r and τ_n. Using the slope at the high temperature side of the quenching curve of the 600 nm band, different authors have estimated the activation energies as 0.167 eV (53), 0.19 eV (2) and 0.20 eV (3) for CdS(Te).

Cuthbert and Thomas (2) used electron beam excitation to obtain the thermal quenching data of luminescence, which is given in Figure 2.3. They examined the thermal quenching of both emission bands. It was observed that the low energy band was not quenching at low temperatures as was the higher energy 600 nm band, but was gradually quenching above room temperature.

Roessler on the other hand used photon excitation to examine the quenching of the 600 nm band of various CdS(Te) crystals.

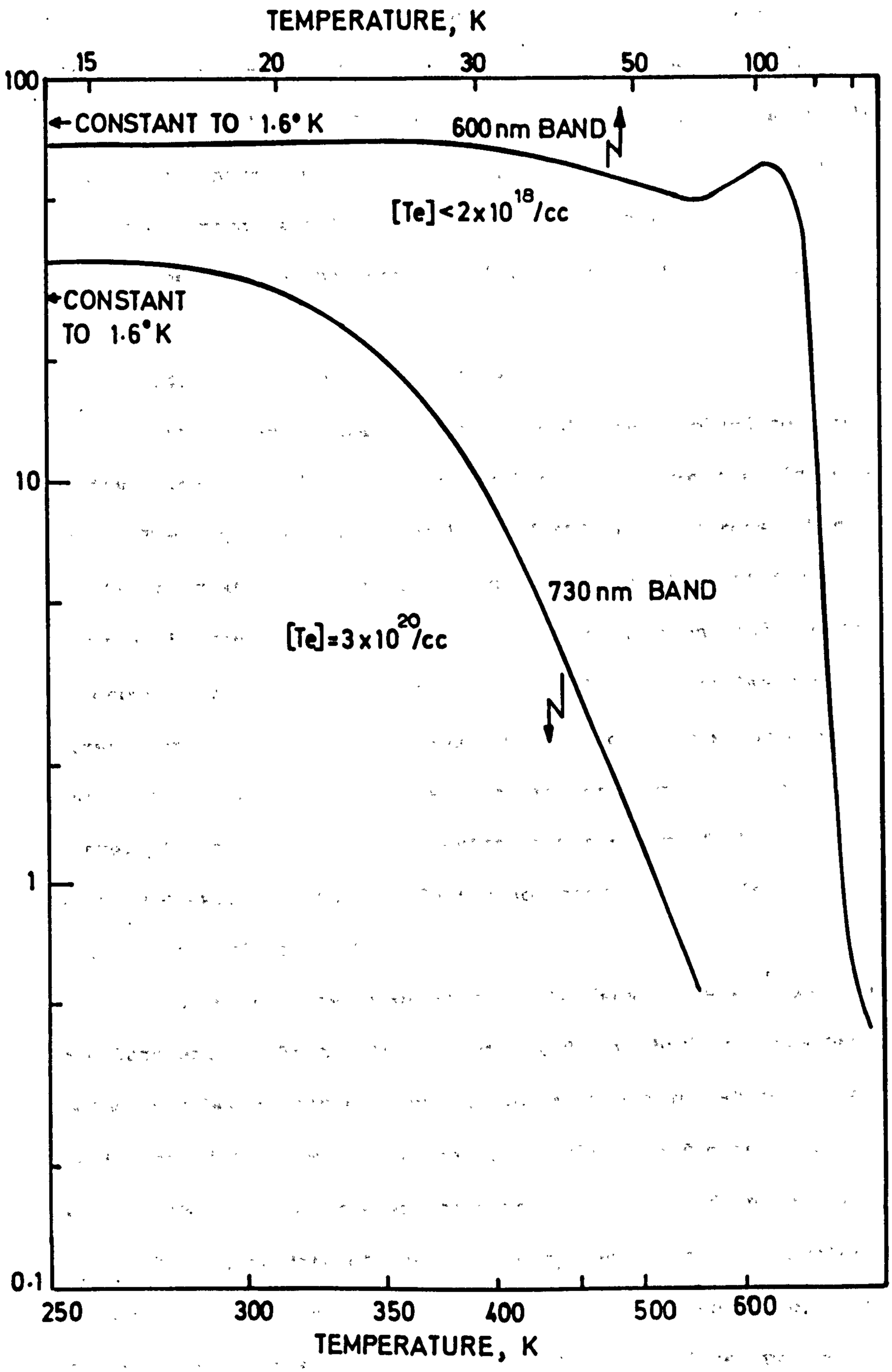

FIGURE 2.3 Luminescence efficiency variation with temperature of CdS (Te) crystals, from Cuthbert and Thomas (2).

Since UV excitation is absorbed close to the surface recombination effects become important and his results therefore were slightly different from those of Cuthbert and Thomas. Even for the samples of same concentrations of tellurium, there was a variation in the activation energies calculated, ranging from 0.175 to 0.225 eV. This can be seen in the quenching data given in Figure 2.4.

2.4.4 Luminescent Decay Times

Cuthbert and Thomas (2) have used time-resolved spectroscopy to investigate the decay of the total emission from the high energy band. They have used a pulsed beam of 400 keV electrons. The decay of the integrated light intensity of the 600 nm band at 4.2 K is given in Figure 2.5, which shows that this emission band decays exponentially with a decay time, τ, of 0.30 μsec, at least for the first microsecond. If there was any additional emission near to this band, it would be seen as an additional component in the decay curve. In fact only a small deviation was observed at longer times which was explained as an effect associated with shallow donor and acceptor impurities in CdS(Te).

The temperature dependence of the decay time was examined and Cuthbert and Thomas found that the decay which was exponential below 40 K became non-exponential above this temperature. The variation of $t_{1/e}$, with temperature is shown in Figure 2.6. $t_{1/e}$ is the time for the emission to fall to 1/e of intial value.

The decay data of the low energy band were more complex and consequently provided less information about the nature of this band. Cuthbert and Thomas (2) have shown that this band decayed non-expeonentially with time, the intial decay time of which was found to be about 0.65 μsec.

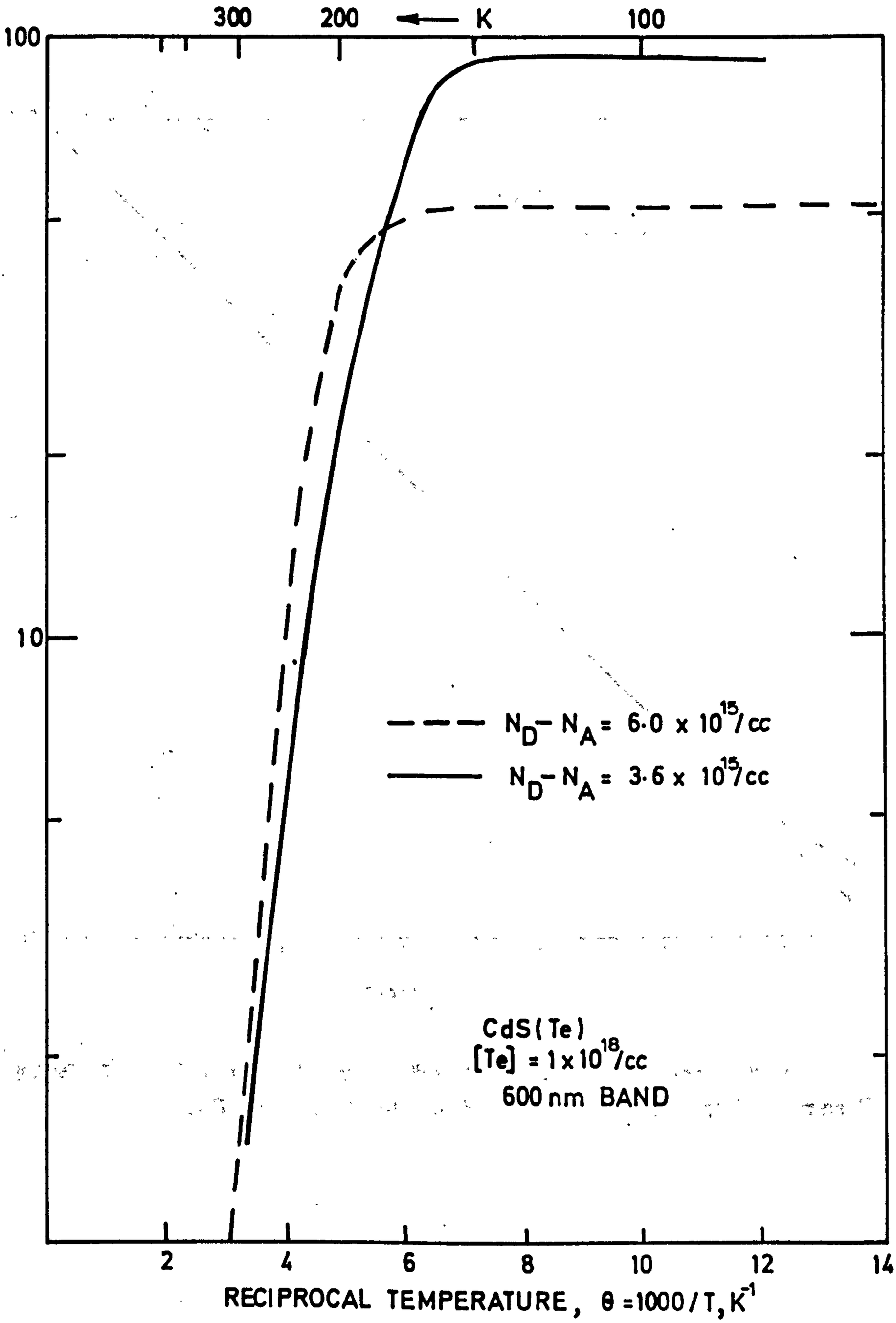

FIGURE 2·4 Temperature quenching of the luminescent emission from two CdS(Te) samples having different impurity concentrations, from Roessler (3)

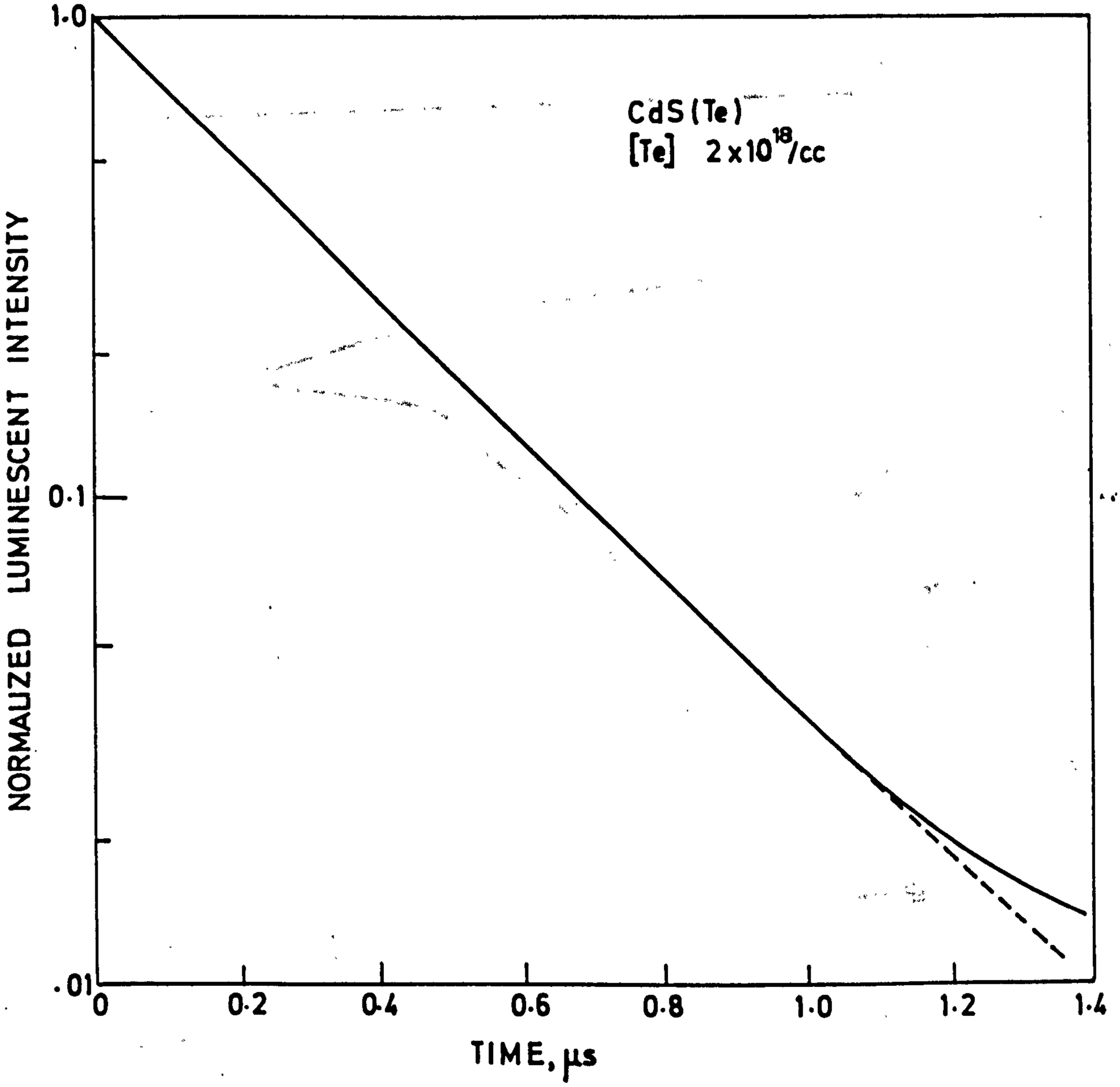

FIGURE 2.5 The time decay of the light sum from the 600nm CdS(Te) band at 4.2K, from Cuthbert and Thomas (2)

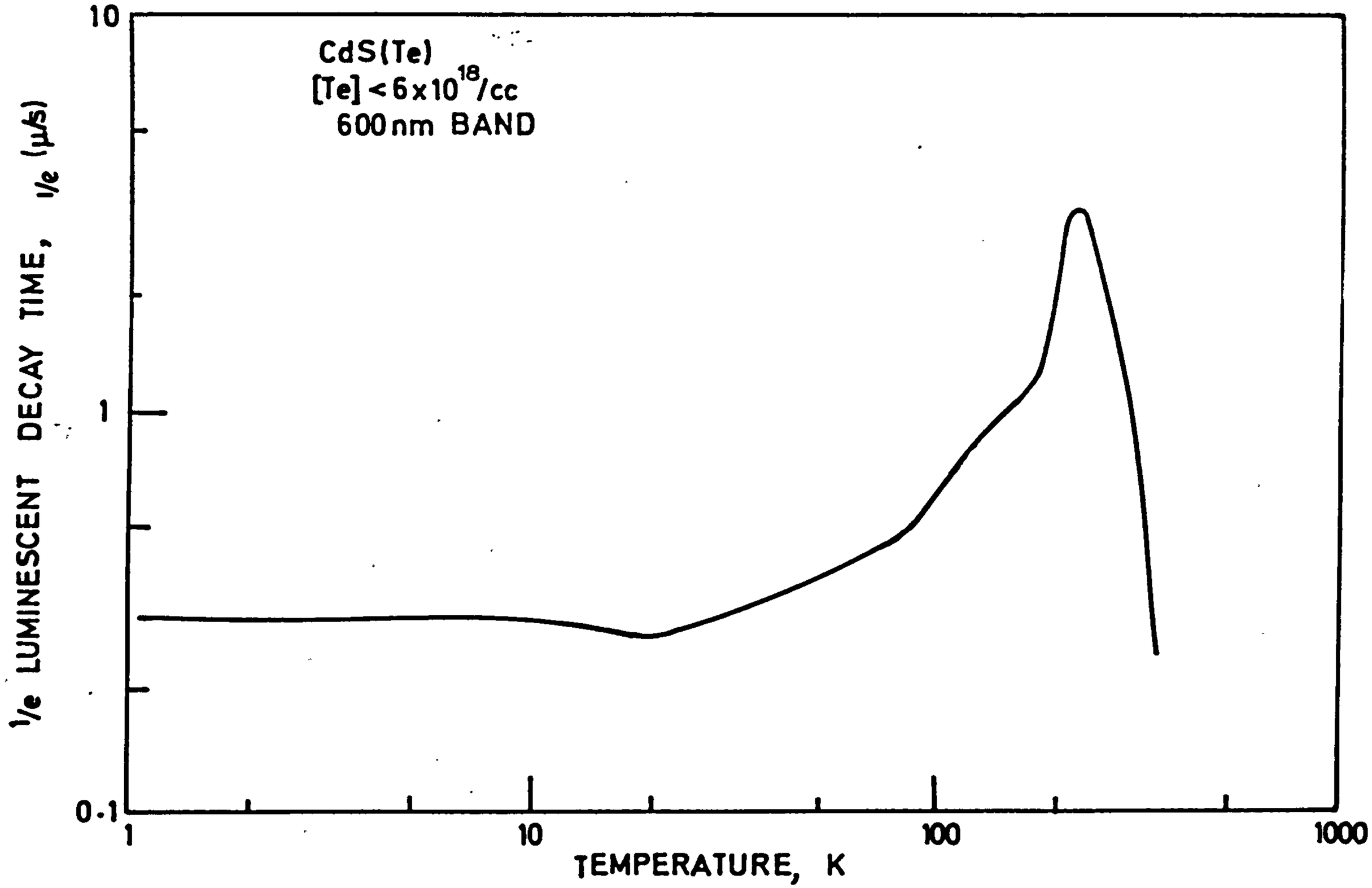

FIGURE 2.6 1/e Luminescent decay time variation of a CdS(Te) crystal with temperature, from Cuthbert and Thomas (2)

Roessler (3) studied the high energy band only and found a similar decay time, i.e. 200-300 ns at low temperatures.

2.4.5 Interpretation of Results

Since no zero-phonon line was observed in the luminescent emission spectrum of CdS(Te), it is not a simple matter to understand the luminescence in this material where all that is observed is two broad emission bands in the regions of 2.09 eV and 1.72 eV. However, measurements of the thermal quenching and decay curves of these luminescent emissions have provided some information about the optical transitions involved in CdS(Te).

The higher energy band has been attributed to the radiative annihilation of excitons bound to isolate Te atoms on S sites. Using a radioactive-tracer technique, Goede and Nebauer (55) have confirmed that this emission band is due to Te centres and not to intrinsic defects as might have been suspected from the appearance of a similar band in undoped CdS crystals. Further, from the proportionality between the intensity of the luminescent emission and the Te concentration they concluded that the Te centres were isolated Te atoms and Te-Te associates played no important role here. When Cuthbert and Thomas (2) applied the technique of time-resolved spectroscopy to this high energy emission band, they found no spectral changes in CdS(Te) emission with time. This evidence and the exponential decay were given as supporting reasons for supposing recombination to occur at a single centre rather than at distant donor-acceptor pairs.

The luminescent efficiency of the high energy band depends upon the stability of the trapped exciton. Because tellurium has a lower electron affinity than sulphur it is expected that the hole

will be trapped first, the electron subsequently being bound coulombically. The thermal quenching curve which gives roughly the variation in luminescence efficiency, was found to be almost constant up to 150-200 K; then the efficiency started to drop as seen in Figure 2.4. This was explained as follows (3): when the temperature is increased towards 200 K the electrons will largely have been ionized but the holes will remain bound. The probability of radiative electron-hole recombination near a tellurium atom is thus constant initially but begins to decrease as the temperature is increased beyond 200 K, when the holes become thermally ionized. The activation energy for hole ionization was determined from the slope of the thermal quenching curve and was found to vary between 0.175 eV and 0.225 eV for lightly doped samples (3). The variation in the Te concentration and the presence of uncontrolled impurity donors and acceptors from sample to sample were cited as the reasons for these variations in activation energy.

Roessler (3) has tried to explain the high energy emission using a simple configurational coordinate model. Theoretically he found the binding energy of the exciton to the tellurium atom to be 0.22 eV, making use of the estimated energy of 2.36 eV for the no-phonon line, which was not observed experimentally at all. Cuthbert (1) has tried to show the correlation between the free carrier decay time and luminescent decay time in CdS(Te) and set up some differential equations to describe these decays. He calculated the binding energy of an electron bound to Te atom to be 20 meV.

The low energy band in CdS(Te) was dominant at the higher Te concentrations. The luminescent decay was found to be non-exponential. No precise explanation has been offered for this decay so far. The possibility of this band being associated with donor-acceptor pair

recombination was checked by Cuthbert and Thomas (2) and was eliminated, since time resolved spectroscopy showed no shift of the emission band. Cuthbert and Thomas calculated an activation energy of 0.6 eV for this band from the thermal quenching data. They suggested that low energy emission was from excitons bound to deeper trapping levels. As Roessler (3) has also suggested, these centres might be pairs or larger groupings of Te atoms at nearest-neighbour sulphur sites, the binding energy increasing correspondingly.

2.5 Conclusions

The luminescent and optical properties of CdS(Te) have been outlined in this chapter. Studies made so far which have hitherto been confined to the platelike crystals of this material have shown that the isoelectronic traps in CdS introduced by Te atoms produce two distinct broad band emissions, in the region of 2.1 eV (600 nm) and 1.7 eV (730 nm) whose parameters are controlled by the temperature of the sample and the concentration of tellurium impurities.

When the Te concentration is greater than 10^{19}-10^{20} atoms/cc the low energy (red) band begins to dominate the emission. There is no precise explanation of this red emission in the literature. It has been suggested that pairs of larger grouping of Te atoms on nearest-neighbour sulphur sites may be the centres responsible. Measurements made on this band have shown a slow and non-exponential decay time ($\tau_{1/e}$ = 0.8 μs at 78 K) and a low luminescence efficiency (of about 35% and constant from 1.6 K up to room temperature) as given by Cuthbert and Thomas (2). Besides having low luminescence efficiency, the crystal becomes opaque because of the considerable shift of the absorption spectrum towards longer wavelengths at high Te concentrations. As a result of the poor luminescent and optical

properties no use of this red band has been suggested for device application, instead the orange band has attracted all the attention of the researchers. Its superior properties fit the requirements of scintillation counting as already mentioned by Madden et al (7). (See Table 1.2 in Chapter 1).

When the concentration of Te is reduced to between 10^{18}-10^{19} atoms/cc, we start to see the effect of another broad band but this time very efficient, emission band near 600 nm. The luminescence efficiency of this orange band at low temperatures is about twice that of the red band, i.e. 70%, but it is quenched rapidly at room temperature (2). Roessler (3) tried to increase the efficiency of this band at room temperature by introducing excess donors which, in turn, caused slow decay components to appear in the decay time data.

As Cuthbert and Thomas (2) have shown, the luminescent decay of the orange band is exponential and faster at low temperatures (300 ns at 10 K). Cuthbert (1) tried to explain the fast decay crystals in terms of free carrier effects. Henry and Nassau (45) have calculated a theoretical luminescent decay life-time of 27 ns which agrees poorly with the figure of 300 ns measured by Cuthbert and Thomas. Explanations given for the orange band are more consistent and precise. The band is considered to be due to excitons trapped on the isolated Te atoms.

Another important advantage when the Te concentration is low is the increased transparency of the crystal. When the Te concentration is $1x10^{19}$ atoms/cc, the absorption length at 600 nm is about 1 cm (not very difference from pure CdS), whereas this value becomes about 0.3 cm for a Te concentration of $1.7x10^{20}$ atoms/cc (2). Taking into consideration the high efficiency and fast decay of the

orange emission from CdS(Te), together with the increased transparency, this material is clearly more suitable for device application, especially as a scintillator in radiation detection. With its favourable optical and luminescent properties at low temperatures, CdS(Te) fits scintillation detector work very well in all respects. The luminescent emission from CdS(Te) at 600 nm matches the spectral response of a silicon photodiode. In addition, thermal matching is also good (both devices operate more efficiently at low, cryogenic temperatures).

If the scintillator is to be used as a gamma-detector the relevent properties of CdS(Te), i.e. high Z, high luminescence (scintillation) efficiency in the required spectral range, fast decay, transparency to its own radiation, and thermal matching are not in themselves sufficient. A larger volume crystal with at least the same properties as platelets has to be available in order to detect highly penetrating gamma-photons, as explained in detail in Chapter 1. So far, none of the investigators have been able to grow large boules of CdS(Te) with properties similar to those of platelets, nor has enough effort been devoted to the problem of obtaining an absorption length of more than one centimetre.

Clearly more experimental work is necessary on CdS(Te) to elucidate the physical phenomena involved and to grow large crystals with the required quality and impurities. This can only be achieved by growing more CdS(Te) crystals (both platelets and boules) and measuring their optical and luminescent properties using various techniques. The method developed by Clark and Woods (37) for the growth of large CdS boules has proved most useful for the realization of the first requirement, i.e. large crystals with the correct

emission properties. Then, using the powerful techniques, e.g. the measurement of the luminescent decay times by single photon counting, we have been able to learn more about the physical processes involved.

In what follows we describe the growth of platelike crystals of CdS(Te) with low Te concentration (since we were only interested in the 600 nm band) and our attempts to reproduce the results already obtained by others. Later we concentrate on the growth of CdS(Te) samples with large volumes with which it has been possible to develop a composite scintillation counter for γ-ray detection.

CHAPTER 3

GROWTH OF CdS(Te) CRYSTALS AND THE PRELIMINARY RESULTS

3.1 Introduction

The CdS(Te) scintillators studied in the present work were grown by the group in the Department of Applied Physics and Electronics of this University which specialises in the growth and study of II-VI compounds in general and CdS in particular. Dr. John Woods supervised the growing procedures which were carried out by Mr. John Cutter. The author assisted with some of the growth runs.

3.2 Growth of Platelike Crystals of CdS(Te)

Clearly, the first task was to grow the CdS(Te) platelets successfully used by Cuthbert and Thomas (2) and check that their results could be reproduced in respect of the parameters relevant to scintillator performance, i.e. luminescent efficiency and decay lifetime. The crystals were grown by a vapour-transport process (also referred to as the "flow method") using argon as a carrier gas. The method is basically similar to that employed by Cuthbert and Thomas (2).

The crystal growing apparatus is shown in Figure 3.1. To produce the platelets, a stream of purified argon gas at 100-200 cc/min was passed first over a silica boat containing (5N) semiconductor grade CdTe from Koch-Light Ltd., and then over a similar boat containing Optran grade CdS (BDH Ltd) which was maintained at a higher temperature. The boats were situated in a long silica tube with 40 mm bore, which itself was contained in a single-zone electric furnace. The two boats were separated from one another by a mechanical spacer so that their positions and therefore their temperatures could

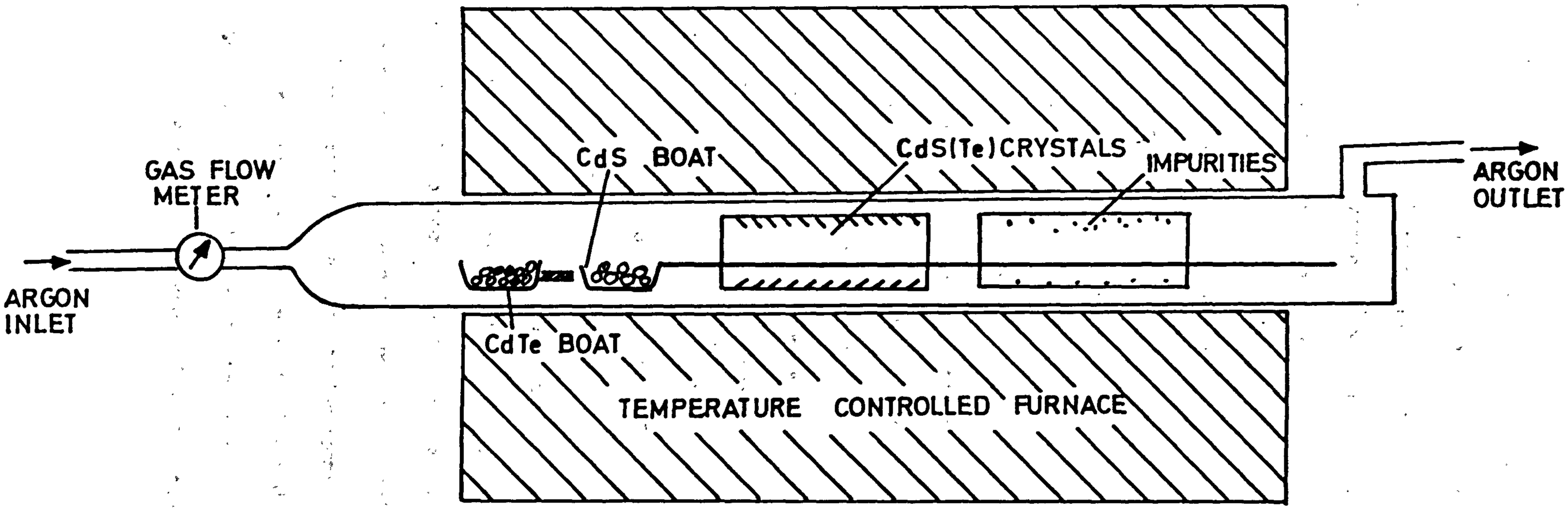

FIGURE 3.1 Schematic diagram of platelike CdS(Te) crystal growing apparatus.

be reproduced from run to run. This was necessary because, although the 50 gm charge of CdS was held at 1150°C, the charge of CdTe of about 1.8 gm was situated near the mouth of the furnace close to the argon inlet and consequently was held at a temperature which was difficult to measure. This temperature probably lay around 600-900°C.

The vapour condensed and the crystals grew on a silica liner, downstream from the charge end of the silica container, at a temperature ranging from 700 to 1000°C. Each run was terminated before either charge of sulphide or telluride had evaporated completely. This ensured that the vapour over the growing crystals was of roughly constant composition throughout the growth period. The second liner on the right hand side of the first one as seen in Figure 3.1, was used to collect any volatile impurities and any unreacted elements. The relative positions and temperatures of the boats containing the charges were determined by trial and error. Each run lasted about 24 hours. Only two trials were required before crystals containing concentrations of Te between 10^{18} and 10^{19}/cc were successfully produced.

The experimental growth conditions used in the three different runs which produced useful platelets are given in Table 3.1. Large numbers of small orange coloured crystals, which were either rod-like or platelets, were obtained in a single run. All of the samples examined had crystallised in the hexagonal modification with the c-axis either lying parallel to the axis of a rod or in the plane of a platelet. Platelets varied in thickness in the range of 100 microns or less and were in the range of millimetres in length and width.

TABLE 3.1

Main growth conditions of the three different platelike crystals of CdS(Te)

Run No.	Argon flow cc/min.	CdS Charge		CdTe Dopant	
		Amount (gm)	T(^{o}C)	Amount (gm)	T(^{o}C)
106	200	54.10	1150	0.65	900
108	100	50.41	1150	1.54	600
110	100	50.55	1150	1.83	600

TABLE 3.2

Tellurium concentrations of various CdS(Te) crystals

Run No.	Concentrations, Atoms/cc			
	A	B	C	Average
511	8.8×10^{19}	11.5×10^{19}	8.1×10^{19}	9.5×10^{19}
512		L.T. 1.1×10^{18}	L.T. 1.1×10^{18}	1.1×10^{18}
513	5.3×10^{18}	3.5×10^{18}	6.4×10^{18}	5.1×10^{18}
518	7.2×10^{18}	-	-	7.2×10^{18}
534	8.0×10^{18}	8.7×10^{18}	8.9×10^{18}	8.6×10^{18}
535	9.1×10^{18}	9.5×10^{18}	10.2×10^{18}	9.7×10^{18}
108	1.56×10^{19}	1.63×10^{19}	1.1×10^{19}	1.43×10^{19}

(L.T. = Less than)

3.3 Properties of the Grown CdS(Te) Platelets

3.3.1 Tellurium Concentration Measurements

The concentration of tellurium in CdS affects its optical properties, as already mentioned in Chapter 2. Consequently, the concentration measurements were carried out parallel with the crystal growth runs in an attempt to produce crystals with the required optical and scintillation properties. In addition, the knowledge of concentration is a vital factor if it is to be demonstrated that the luminescence bands under discussion are indeed associated with the tellurium rather than other chemical impurities or physical defects.

Two methods were used to measure the Te concentrations in CdS, namely X-ray, fluorescence and atomic absorption. Measurements by X-ray fluorescence were made in the Geology Department of this University. The atomic absorption measurements were carried out in the Department of Geology in the University of Aston and at A.E.R.E. Harwell. The X-ray fluorescence method proved quite inadequate at the concentrations of interest giving errors of a factor of 2. Much more accurate results to within approximately ±20 ppm (w/w) were obtained from the atomic absorption analysis.

The Te concentrations of crystals from the same growth run were found to vary by as much as a factor of 2 (see Table 3.2). This is a common problem in crystal growth from the vapour phase because it is rather difficult to maintain the physical conditions (e.g. temperature, vapour pressure) constant throughout. In practice, therefore, at least three groups of crystals were selected from each run for concentration measurements. Table 3.2 shows the Te concentration in atoms/cc, of various CdS(Te) samples, among which only the crystals from run No. 108 were platelets, while the others were boules.

The spread of values is evident and the concentration figures are considered to be within an error of approximately $\pm 0.42 \times 10^{18}$ as determined by the atomic absorption technique used.

3.3.2 Luminescent Properties of the Platelets

Three basic parameters of the platelike crystals were examined initially:-

(1) the photoluminescent emission spectrum,

(2) the decay lifetime of α-particle induced luminescence, and

(3) the luminescent efficiency.

Emission spectrum analysis of CdS(Te) crystals was necessary, especially for spectral matching, since CdS(Te) scintillators were required for use in conjunection with a photodiode to produce a composite radiation detector as explained in detail in Chapter 1. Besides, it was necessary to compare the luminescence of our crystals with that reported by the earlier workers on CdS(Te), and to check the existence of the emission band centred near 600 nm at low temperatures which was required for our cryogenic scintillation detector.

As-grown platelets were mounted on the copper block of a vacuum cryostat, and their emission spectra were determined by chopping the luminescence radiation before passing it through a Barr and Stroud double monochromator, type VL2. The emergent light was detected with an EMI 9558 photomultiplier which has an S20 type photocathode. The output from the photomultiplier was fed into a Brookdeal lock-in amplifier, type 401, and finally displayed on a chart recorder. Such a system provided very good signal-to-noise figures.

In these first emission studies, ultraviolet excitation was used. This was provided by a 250 W compact source, mercury lamp, suitably filtered by Chance Glass OX1 and a 10% solution of $CuSo_4$ to isolate the 365 nm line. The function of the $CuSO_4$ was to eliminate the mercury red line at 710-730 nm which would otherwise interfere with the low energy band emission from CdS(Te). A copper-constantant thermocouple was used to determine the temperature of the sample.

All of the photoluminescence curves shown in this chapter have been corrected for monochromator dispersion and photomultiplier response. The emission intensities are plotted as the relative emitted energy per unit wavelength interval. Figure 3.2 shows the spectral emission distributions of two different platelets, 108S3 and 110S2. The emission bands shown in this figure are very broad. In CdS(Te) 108S3, the high energy band centred at 600 nm was predominant at low temperatures, 81 K, and there was no red band at this temperature, instead there was a long tail to the 600 nm band on the longer wavelength side. At room temperature, the picture was different. The orange band seen at low temperature was quenched and the red band predominated. This had a broad distribution. These results are very similar to those discussed by Cuthbert and Thomas (2). The platelet 110S2 was tested in the same manner. The same structureless broad band around 600 nm was observed at 81 K. There was also a weak emission on the shorter wavelength side of this band. This unresolved contribution is attributed to edge emission, which is a property of the bulk, CdS, as explained in Chapter 2 (see Figure 2.2). At room temperature, sample 110S2 showed a rather different picture compared with 108S3. There was no red band but a very broad orange distribution centred at 630 nm. A comparable shift of the orange band with temperature has also been mentioned by Cuthbert and Thomas.

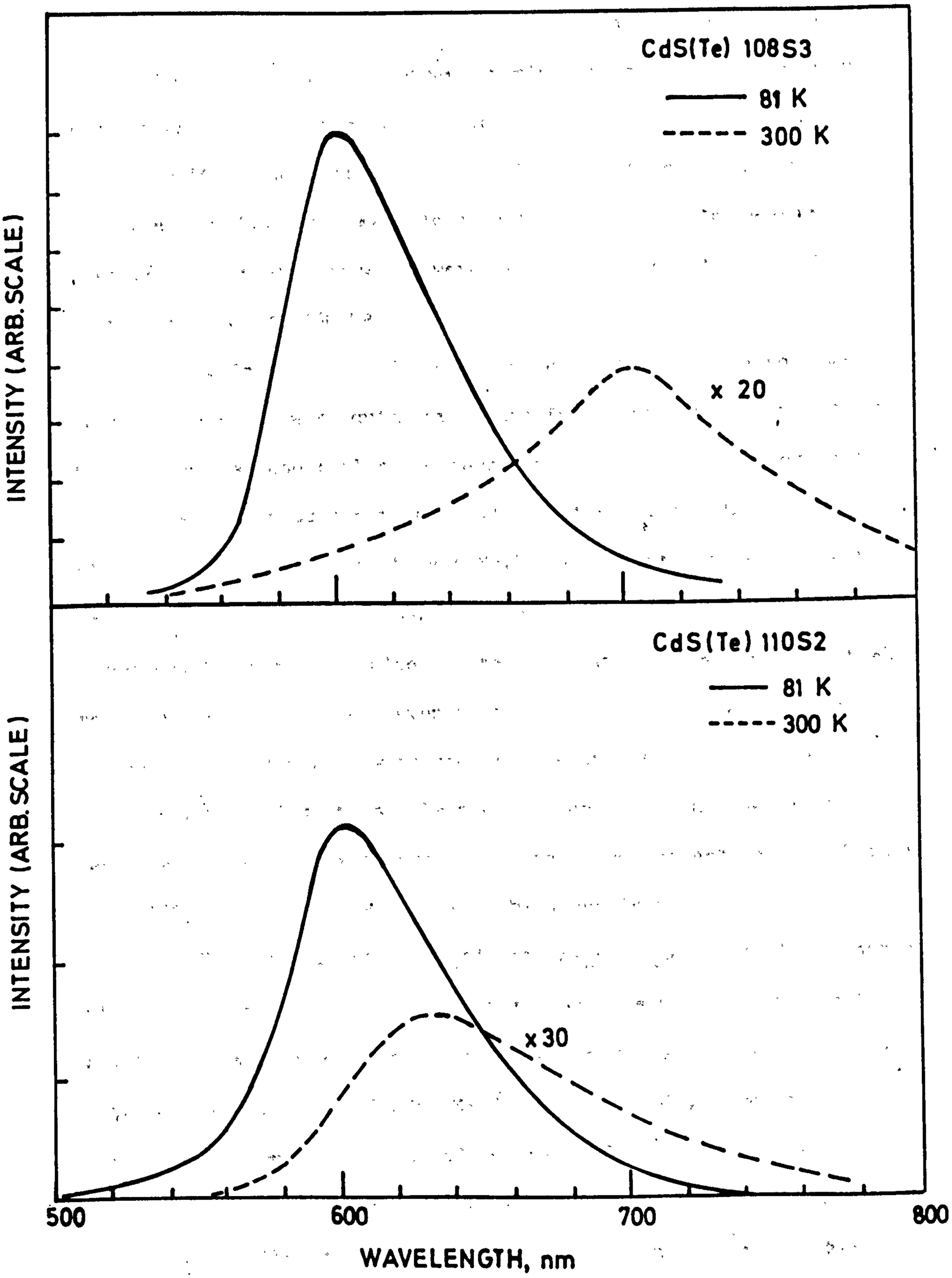

FIGURE 3.2 Luminescent emission spectra of two different CdS(Te) platelets excited by 365nm UV radiation.

Another important parameter, the decay lifetime of the scintillation light pulses originating from the orange emission of the excited CdS(Te) platelets was examined next. In these preliminary measurements, the current pulses at the output of a photomultiplier, Mullard / type 56AVP) were analysed with the help of an oscilloscope (Tektronix 543B). 5.5 MeV alpha-particles from ^{241}Am were used to irradiate the platelets which were kept in a cryostat optically coupled to the PMT (56AVP).

The decay times of the luminescence measured in this way on various platelets were quite promising for scintillation applications. Although non-exponential the decays, in general, were faster than those reported by Cuthbert and Thomas. At 80 K, the 1/e decay times of the pulses from the platelets No.108 were found to be in the range of 50-100 ns, whereas Cuthbert and Thomas (2) found values near 300 ns, using 400 KeV electron pulse excitation. At room temperature, the measured decay times were even shorter (about 15 ns) which again emphasises the contrast with the results of Cuthbert and Thomas (i.e. 1 μs). Using the single-photon counting technique, more precise measurements were carried out on the radioluminescent decay lifetimes of CdS(Te) crystals. Details will be given in Chapter 5.

The luminescence (scintillation) efficiency which is another vital parameter in scintillation work was measured by exciting the crystals by alpha-particles. These measurements were made using a cryogenic silicon photodiode, K-22 of Simtec Ltd., to which the crystals were optically coupled by means of a transparent silicon compound. The CdS(Te) scintillator and the photodiode were both kept at 80 K using the cryostat described by Bateman and Özsan (32); the technique described by them was used to determine the response of the scintillators to the exciting ionizing radiation. Calibration of the

system with monochromatic γ-rays permitted the number of ion pairs produced in the silicon detector by the light pulse to be accurately calculated.

The work of Cuthbert and Thomas has shown that the quantum efficiency of the 600 nm band is very high, i.e. 70% at 4.2 K and 40% at room temperature. In this context quantum efficiency means the fraction of electron-hole pairs which recombine radiatively, which is a measure of luminescence efficiency. The high refractive index of CdS and the coupling of a sample to a photon detector introduce uncertainties of the order of 50% into absolute measurements of the light output. Comparison of different samples is possible to better accuracy if the geometries are identical and the internal absorption is not significant. In general, however, it is only possible to set a lower limit to the efficiency.

A platelet of CdS(Te), 108S1, was chosen to obtain the pulse-height distribution of the scintillator-photodiode combination described above. Hence the luminescence efficiency for irradiation with 5.5 MeV ^{241}Am α-particles at 90 K could be calculated. The distribution is given in Figure 3.3. The peak corresponds to a signal of 2.2×10^5 ion pairs in the photodiode so that each ion pair requires 24 eV of particle energy for its creation. This low value indicates a high efficiency for scintillation detection which is attributed to the high radioluminescent efficiency of CdS(Te) at low temperature and its matching spectral response to the silicon photodiode.

In general, the number of electron-hole pairs, N, created in the silicon following the absorption of one α-particle with energy E in the CdS(Te) is

$$N = \frac{E}{\omega} CRT \quad . \quad . \quad . \quad . \quad . \quad . \quad . \quad . \quad . \quad (3.1)$$

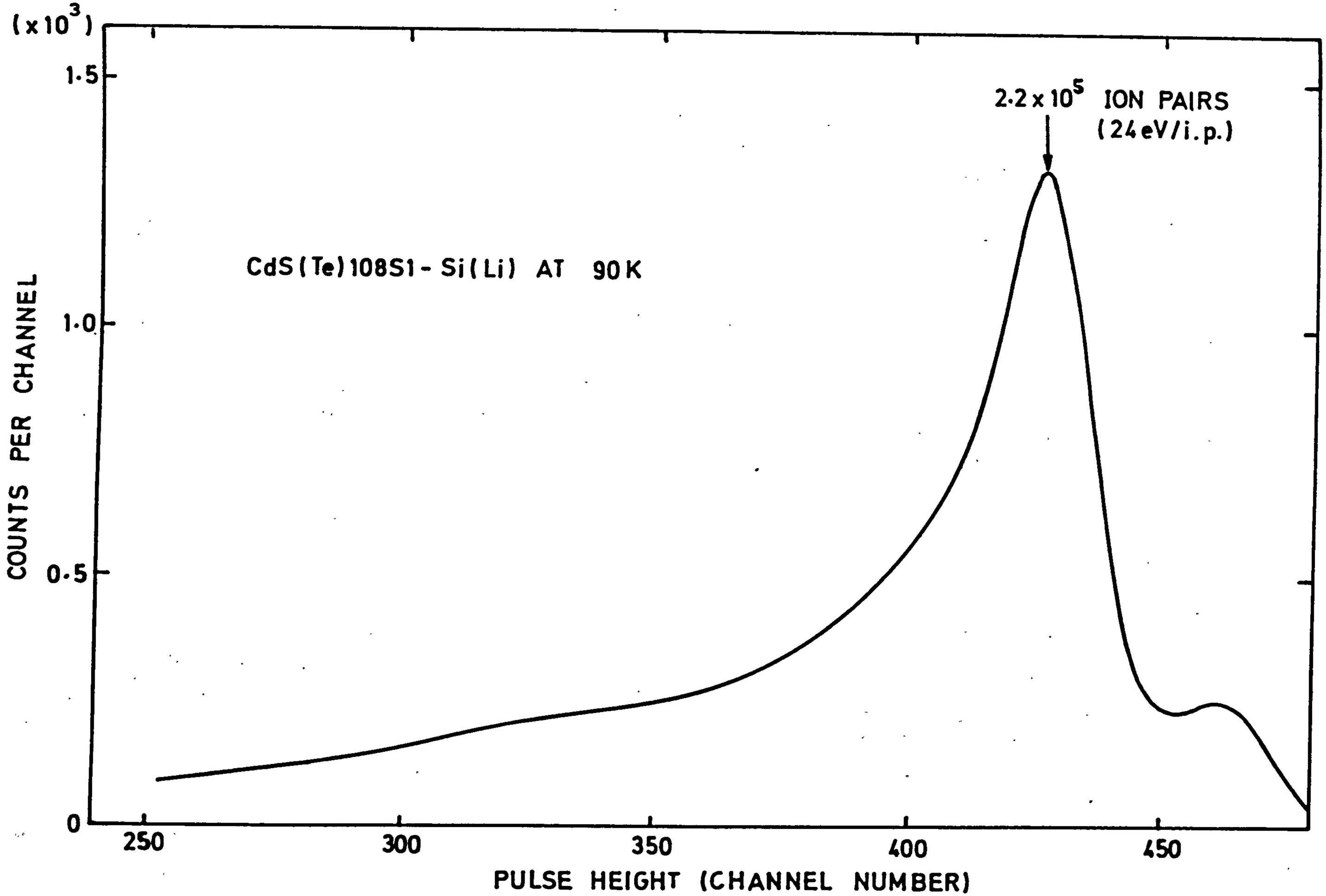

FIGURE 3.3 Pulse-height distribution of 5.5 MeV α-particles detected by the CdS(Te)-Si photodiode.

where ω = particle energy to create one electron-hole pair in the CdS(Te) ($\omega \sim 3\ E_G = 7.5$ eV), C = capture efficiency of the free carrier at the luminescence centres, R = radiative recombination (luminescence) efficiency and T = the transfer efficiency of photons from the scintillator into electron-hole pairs in the silicon.

If we write $N = E/W_{eff}$ where W_{eff} is the observed effective energy to produce one electron-hole pair in the silicon, then

$$W_{eff} = \frac{\omega}{CRT} \quad . \quad . \quad . \quad . \quad . \quad . \quad . \quad . \quad . \quad . \quad (3.2)$$

Now $W_{eff} = 24$ eV and $\omega = 7.5$ eV, so that if we assume a transfer efficiency T = 0.5, we get RC = 0.625. The produce RC is the quantum efficiency used by Cuthbert and Thomas and the value 62.5% is clearly in good agreement with their estimate.

These first results on the luminescent properties of platelets, i.e. fast decay times, high luminescence efficiency and matching spectral response are encouraging for scintillation detection work, and demonstrate that the production of large crystals with similar properties would be of great interest for γ-ray detection.

3.4 Growth of the Boules

Vapour-grown platelets are adequate for absorbing the shallowly penetrating alpha and beta radiation. However, crystals of greater volume are required for absorbing the more deeply penetrating gamma radiation as explained in Chapter 2.

Madden et al (7) who studied the application of CdS(Te) to scintillation counting used the same platelike crystals as Cuthbert and Thomas (2). Their attempts to prepare large crystals with properties similar to those of the platelets were not successful. The luminescent response of large crystals has always been found

weaker than that of the small vapour grown platelets. More recently Mikulyak (56), of the same laboratory, has described attempts to produce somewhat larger crystals of CdS(Te) by coalescence within a heated charge. Partial success only was achieved. In contrast with this experience, it was found that the modification of the vacuum sublimation technique described by Clark and Woods (37) to grown boules of CdS leads to large crystals with good isoelectronic luminescence properties.

With Clark and Woods technique, it is possible to grow crystals of CdS(Te) with centimetre dimensions. With this arrangement, the boules are grown by sublimation down a temperature gradient in a controlled pressure of cadmium or sulphur vapour. The controlled pressure is obtained by maintaining a reservoir containing excess cadmium or sulphur at a constant temperature during the growth sequence. Such an arrangement is shown in Figure 3.4. A charge of CdS is distilled from one end to the other of a vertical silica capsule. The capsule which is evacuated to 10^{-6} torr is connected via a narrow orifice to a reservoir which may contain either cadmium or sulphur. The reservoir is held at a constant temperature during the growth by means of the lower furnace so that a fixed vapour pressure throughout the system is established. During the growth which takes 7-14 days, the capsule is pulled through the furance at 0.1-0.2 mm per hour.

Using Clark and Woods method and a charge of 25 gm of undoped CdS flow crystals, two optimum conditions were established for the growth of undoped boules, some 4 cm long and 1 cm in diameter. These were, (a) charge at 1080 C with excess sulphur in the reservoir at 310^{o}C and, (b) charge at 1150^{o}C with cadmium in the reservoir at 550^{o}C. Experience showed that when crystals doped with 10^{18}-10^{19} cm^{-3} of tellurium were required, this could be achieved in two ways. In the

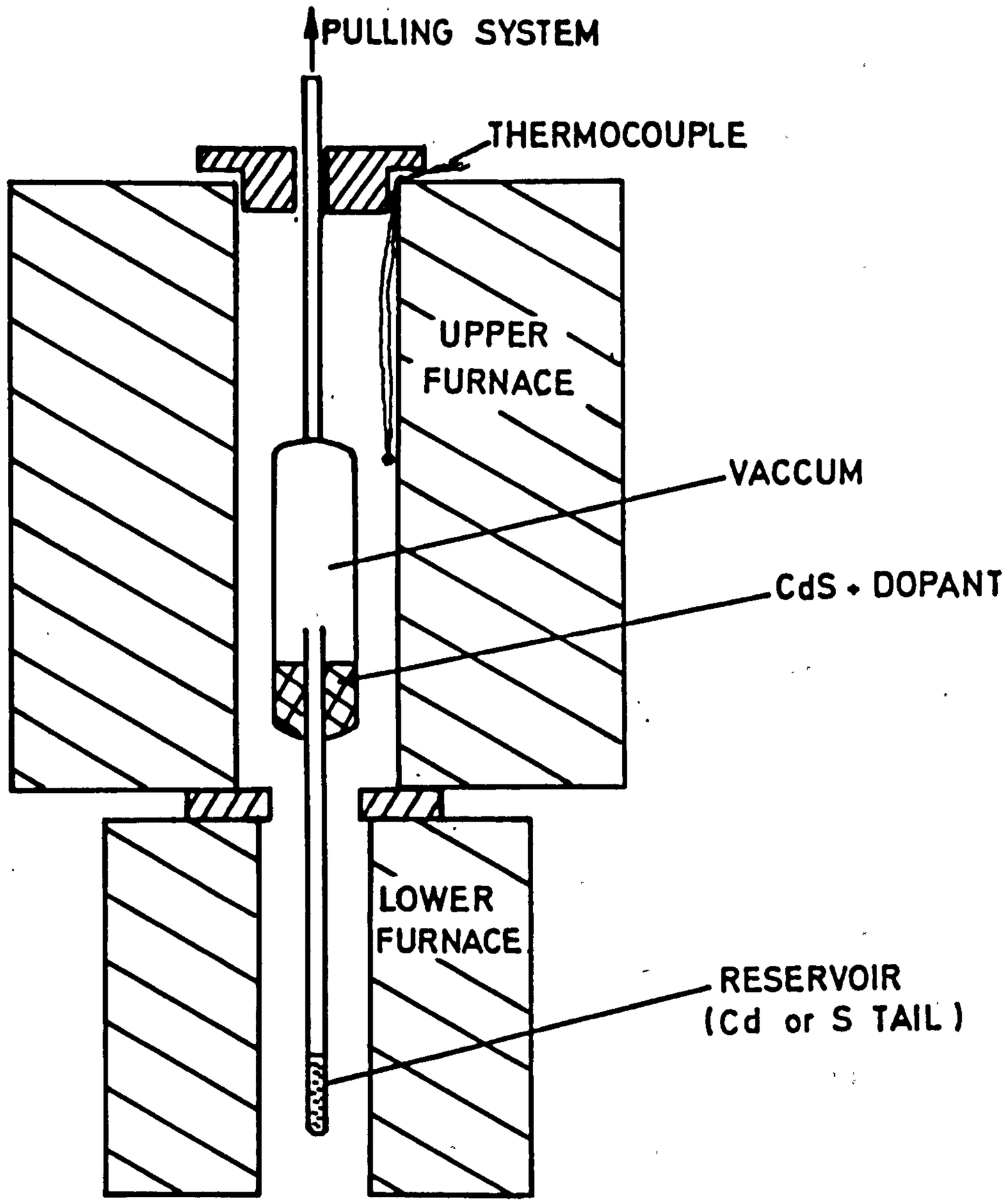

FIGURE 3.4 Furnace arrangement for growing large boules of CdS(Te).

first, 6.25 mgm of CdTe was added to the 25 gm charge of CdS. This was then loaded into a capsule connected to a reservoir containing elemental sulphur. The optimum conditions for growth of a boule of good crystalline perfection were then found to be obtained with a charge temperature of 1150°C and a reservoir temperature of 250°C. In the second arrangement, 12.5 mgm of elemental tellurium was added to the 25 gm charge of CdS and excess cadmium was used in the reservoir. With this combination optimum growth occurred with a charge temperature of 500°C. With both arrangements, slightly less transparency was obtained than when undoped crystals were grown, but boules of some 3 cm long and 1 cm in diameter with a mass of 16-20 gm were produced quite consistently. A photograph of a large CdS(Te) crystal grown in this manner is shown in Figure 3.5.

The growth conditions used in the various runs to produce large crystals are shown in Table 3.3. Some of the crystals grown with the arrangements outlined above exhibited a polycrystalline structure and contained cracks. But, there were very good large single CdS(Te) samples grown among them, e.g. CdS(Te) 512. Crystals grown using sulphur in the reservoir had a light orange body colour and were transparent. Their optical quality was superior to that of crystals grown with a cadmium reservoir at 550°C. These latter boules were rather dark. However, when the temperature of the cadmium reservoir was reduced to 500°C, good transparency was again obtained. The tellurium concentrations in the boules have already been given in Table 3.2.

3.5 Preliminary Survey of the Properties of the Boules

In this section, we will describe only briefly the preliminary results obtained on the as-grown boules of CdS(Te) since the detailed

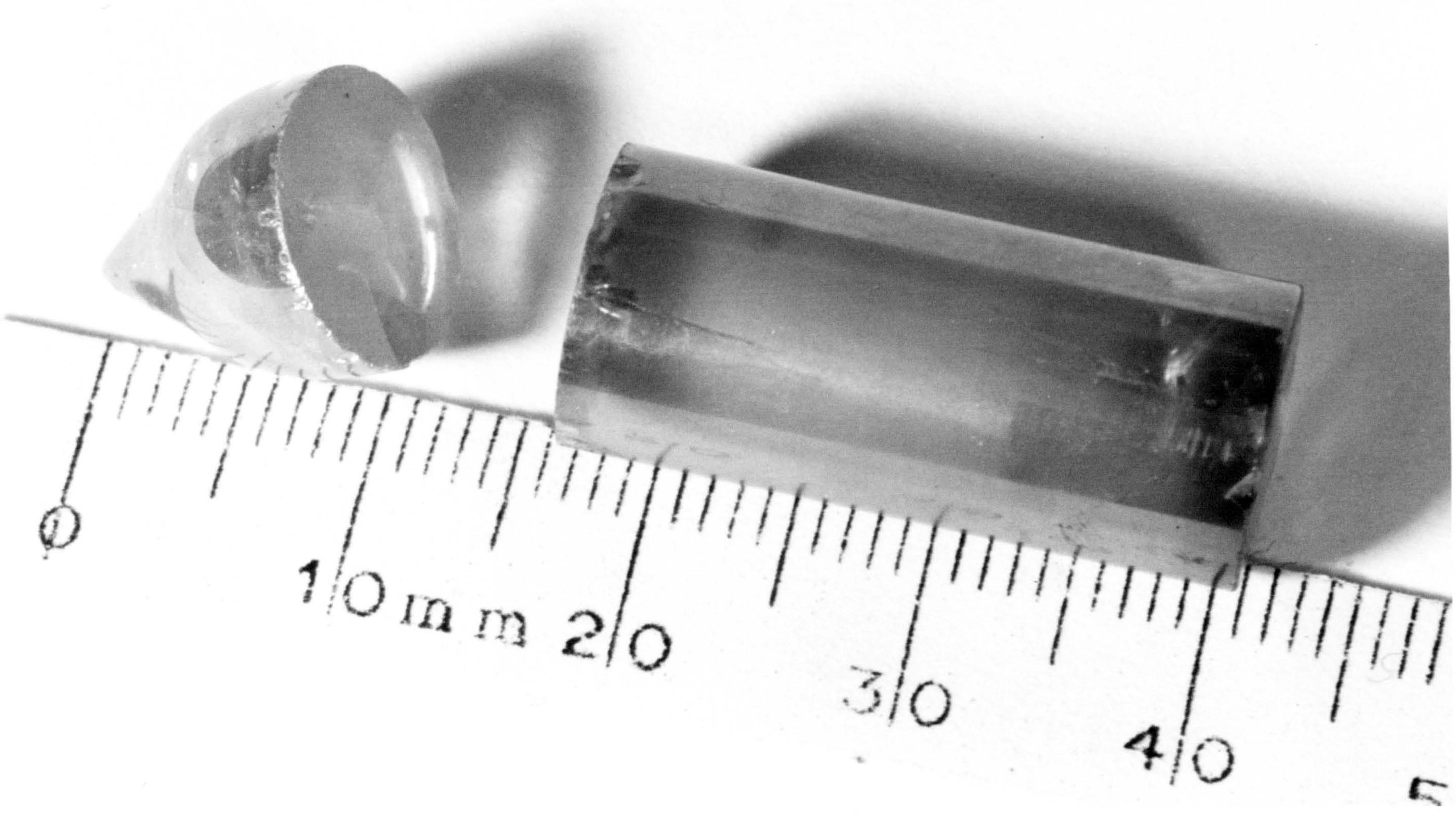

FIGURE 3.5 A CdS(Te) boule grown with Clark-Woods technique (37)

TABLE 3.3

Main growth conditions of the various boules of CdS(Te)

Run No.	Reservoir (Tail)		Dopant	Amount (mgm)	Temperature of upper furnace (^{o}C)
	Material (0.2 gm)	T(^{o}C)			
511	S	310	CdTe	250	1080
512	S	310	CdTe+(S)	6.25+(500)	1080
513	Cd	550	CdTe	6.25	1150
518	Cd	550	Te	12.5	1150
534	Cd	500	Te	12.5	1150
535	S	250	CdTe	6.25	1150

description of the various other investigations on these large crystals will be given later in Chapters 5 and 6.

The photoluminescence from the as-grown CdS(Te) boules was examined using the same system as described in Section 3. Since the transparency of these large crystals was not as good as the platelets, less efficient luminescent emission from them was unavoidable. But, the spectral distribution of the photoluminescence was found to be the same as that of the platelets. The heavily doped 511S2 crystal, containing 9.5×10^{19} atoms/cc of Te, (see Table 3.2) was reddish in colour in the daylight at room temperature. Figure 3.6 shows the photoluminescent emission from this sample at 81 K and 300 K. Even at low temperatures, the red band at 700 nm was apparent just beside the orange band at 600 nm. The other boule examined, 512S2 (containing 1.1×10^{18} atoms/cc of Te), had a better optical quality and provided more encouraging results. A more efficient 600 nm band was observed together with an unresolved edge emission band at 81 K, see Figure 3.6. The efficiency of this band began to drop and the peak position shifted towards longer wavelengths when the temperature was increased. At room temperature this sample was light orange in colour and was more transparent than the first sample, 511S2.

The decay times of the 600 nm emission from the boules when excited by the 5.5 MeV alpha-particles were examined in the same manner as for the platelets, i.e., the current waveforms from a fast photomultiplier were displayed on an oscilloscope. The sample 512, which had the best optical quality had a 1/e decay time of about 12 ns at 80 K, indicating that the luminescent decay times from the boules and platelets were of comparable magnitude although there were some slight variations in the shapes of the decay curves. With

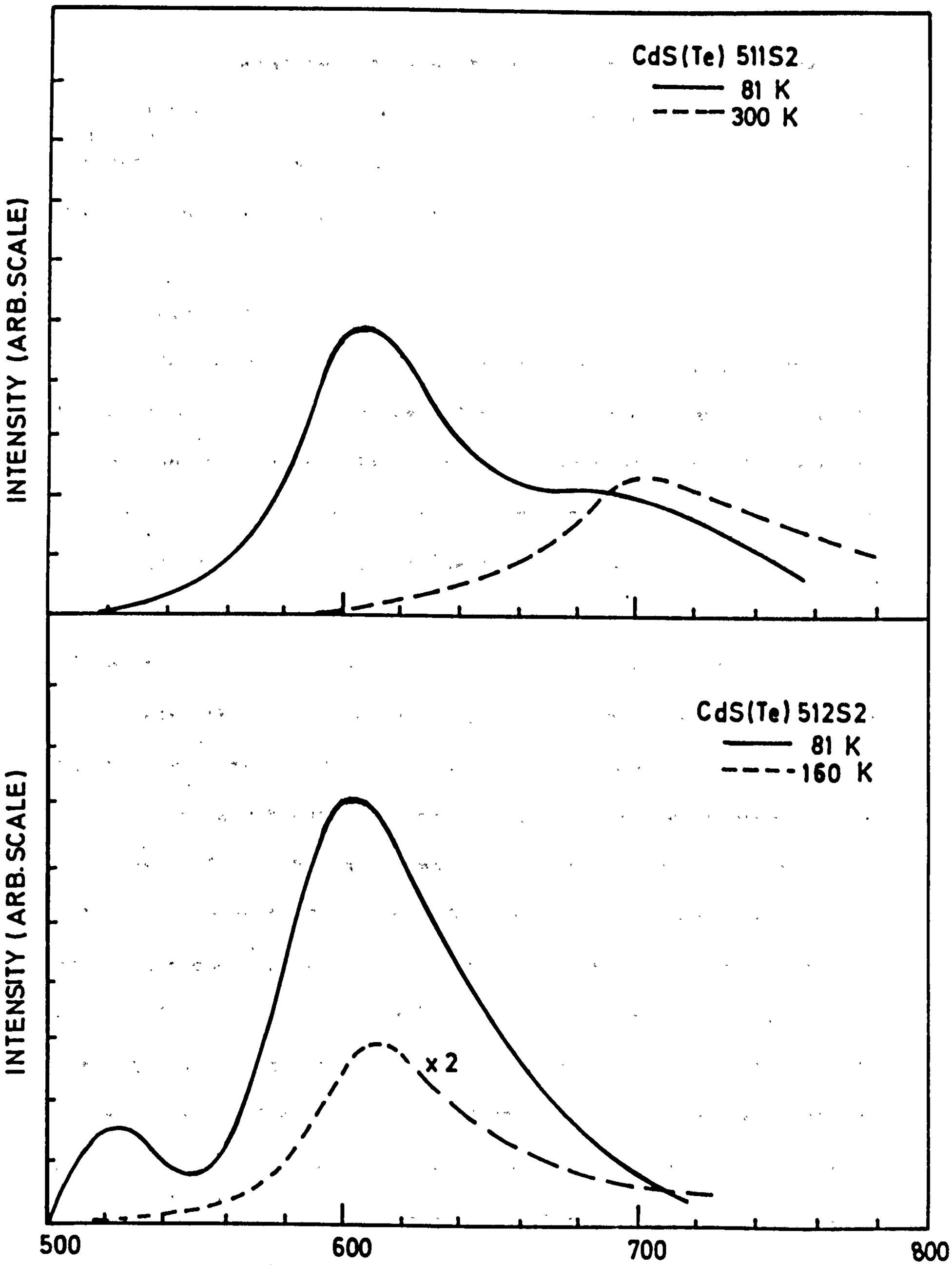

FIGURE 3.6 Luminescent emission spectra of two different CdS(Te) boules excited by 365 nm UV radiations.

increasing temperature the decay times from the boules became shorter as did those from the platelets. A detailed investigation of the various decay curves was made using single-photon counting techniques. The results will be given in Chapter 5.

3.6 Discussion

Te-doped CdS crystals in the form of small platelets and large boules have been grown successfully. An initial examination of their luminescent properties clearly showed that these crystals have considerable potential for use at low temperatures (80-100 K) as scintillators in conjunction with cryogenic photodiodes.

Our platelets were grown in essentially the same manner as those used by Cuthbert and Thomas (2). When excited by 5.5 MeV α-particles they exhibited very similar radioluminescent properties to those reported by Cuthbert and Thomas. Namely, at low temperatures, an efficient and broad emission band at 600 nm was observed. A quantum efficiency of 60-70% was estimated for this orange emission with the help of a cryogenic Si photodiode. On this occasion, the performance of the proposed radiation detector, i.e. CdS(Te) scintillator-Si(Li) photodiode was checked and a low eV/ip value was found from the detection of the α-particles. The low band gap and the high radiative recombination efficiency of the CdS(Te) platelet together with its good spectral matching and direct coupling facility to the Si photodiode resulted in this low value (24 eV) of energy loss per ion pair. Further study on this detector will be described in Chapter 6.

The high efficiency of the 600 nm band was thermally quenched at higher temperatures. On the other hand, the low energy (red) emission band at 700 nm which was observed in the crystals having

high Te concentrations was not as efficient as the 600 nm band, so it has not been studied in this work. In summary, the only difference between the present results and those of others on platelets was observed on the decay times of the luminescence. At low temperatures, the decays were found to be non-exponential with 1/e decay times of less than 100 ns whereas Cuthbert and Thomas found an exponential decay with a time constant of 300 ns. Our results are more encouraging for scintillation applications because faster radiation detectors are always preferable, especially in γ-ray detection as explained in Chapter 1.

Previous workers have only been able to grow the small platelets; their attempts to grow larger volumes of CdS(Te) crystals with the similar properties to those of the platelets were not successful. On the other hand, with the early investigations on the boules grown by us by means of the Clark-Woods technique similar radioluminescent properties of large crystals and small platelets were observed. The optical quality of these crystals varied from one growth run to another, depending upon the growth conditions. Often, crystals grown in excess sulphur and with low Te concentrations were found to have better optical quality and hence transparency. It is quite apparent that to grow large single crystals with a high purity and optical quality is not an easy matter. More work and long experience is necessary in order to understand the growth mechanism involved and to achieve consistent growth of large single CdS(Te) crystals with good transparency.

At this stage, it seems that the major obstacle to the use of CdS(Te) as a useful scintillator has been removed. Before the response of such a scintillator to various radiations, especially

to penetrating γ-rays were investigated, an extensive experimental work on the luminescent and optical properties of this material, with particular emphasis on the boules, is necessary so that the physical process involved in this crystal could be elucidated and any practical problem met in the device application with this material could be dealt with easily. For this purpose, one should carry out more radioluminescent measurements using different and more powerful techniques.

CHAPTER 4

EXPERIMENTAL TECHNIQUE

4.1 Introduction

In general, three measurements characterize the radioluminescent properties of a material - (1) the luminescent efficiency, (2) the thermal quenching of luminescence emission and (3) the luminescent decay characteristic. In the case of CdS(Te) the radioluminescent efficiency is best measured by means of a silicon photodiode and these measurements are described in Chapter 6. To measure the thermal quenching and the decay characteristics single photon counting techniques (SPCT) were used. A special cryostat was designed so that the investigations could be made at various temperatures, i.e. between 80 and 300 K. A second cryostat (see Chapter 6) was built for the studies of the new radiation detector, i.e. the CdS(Te) scintillator - Si(Li) photodiode combination and for the examination of radioluminescence efficiency.

4.2 Measurement of the Decay Profiles

4.2.1 General Remarks

The simplest and most common method employed in the measurements of decay profiles of luminescence is to couple the scintillator examined to a high speed PMT and to study the shape of the output pulse, using a fast oscilloscope. However, the poor photon statistics of any one light pulse preclude accurate measurement of the decay data from this observed profile.

After the development of SPCT by Bollinger and Thomas (57) it has become a relatively simple matter to investigate various luminescent decays and measure the decay time of radioluminescence. The main principle of the technique used in the present work is the measurements by means of a time-to-amplitude converter, (TAC), of the time between

the start of the light pulse, and the detection of the first photon by stop PMT in the shower of photons of which the luminescent decay is composed. The result is registered in the memory of a multichannel pulse-height analyzer (MCA). By repeating this procedure a large number of times, the time distribution of the first photons is obtained in the MCA and the curve corresponding to this distribution is the desired decay profile as will be proved in Section 4.2.5.

By counting the individual photoelectron produced in the PMT by the single photons, the yields of many pulses are added until the required statistical accuracy is achieved (see Section 4.2.4). Thus, profiles with about 10^7 photons can be derived.

4.2.2 Experimental Arrangement

The experimental arrangement developed for the measurements of luminescent decay from the CdS(Te) samples is illustrated schematically in Figure 4.1. Figure 4.2 shows a photograph of the whole arrangement.

In order to study the decay of the luminescence produced by the excitation of the scintillator we require a zero-time signal that has a known relation to the time of excitation. Since CdS(Te) exhibits a sub-nanosecond rise time in its radioluminescent output when stimulated by a fast charged particle, this time signal was simply obtained by collecting a large fraction of the light flash coming from the scintillator. The start-PMT (see Figure 4.1) was used for this purpose. By sensing the formation of the first few photoelectrons at the cathode of this fast PMT (56 AVP), a pulse was formed which characterized the starting time of the light flash, i.e. the zero-time pulse. This approach limits the application of the technique to the study of luminescent decays with sharp rise times (i.e. $\lesssim$ 10 ns). CdS(Te) has

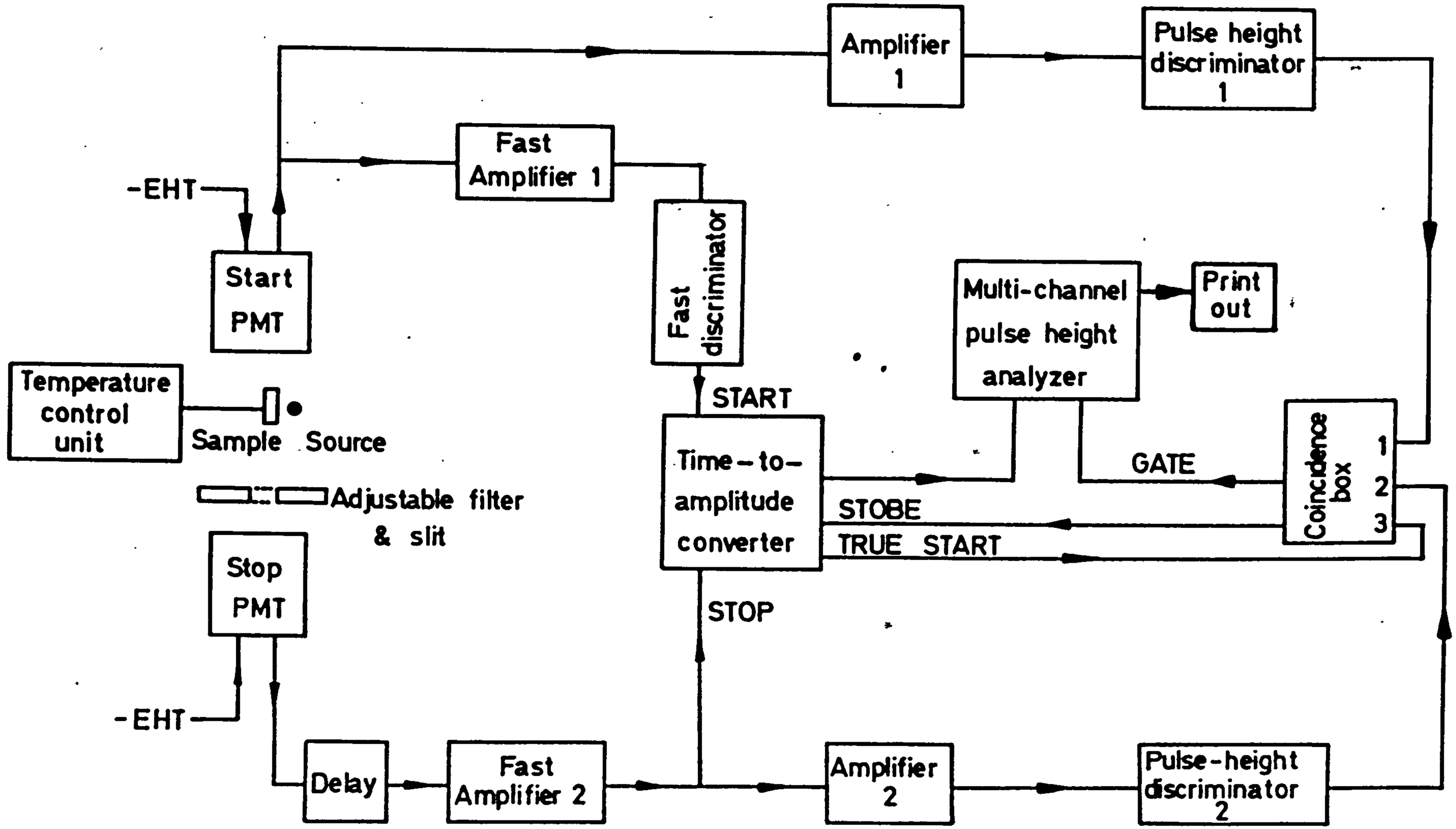

FIGURE 4.1 Schematic diagram of the experimental arrangement used for the measurement of scintillation decay time.

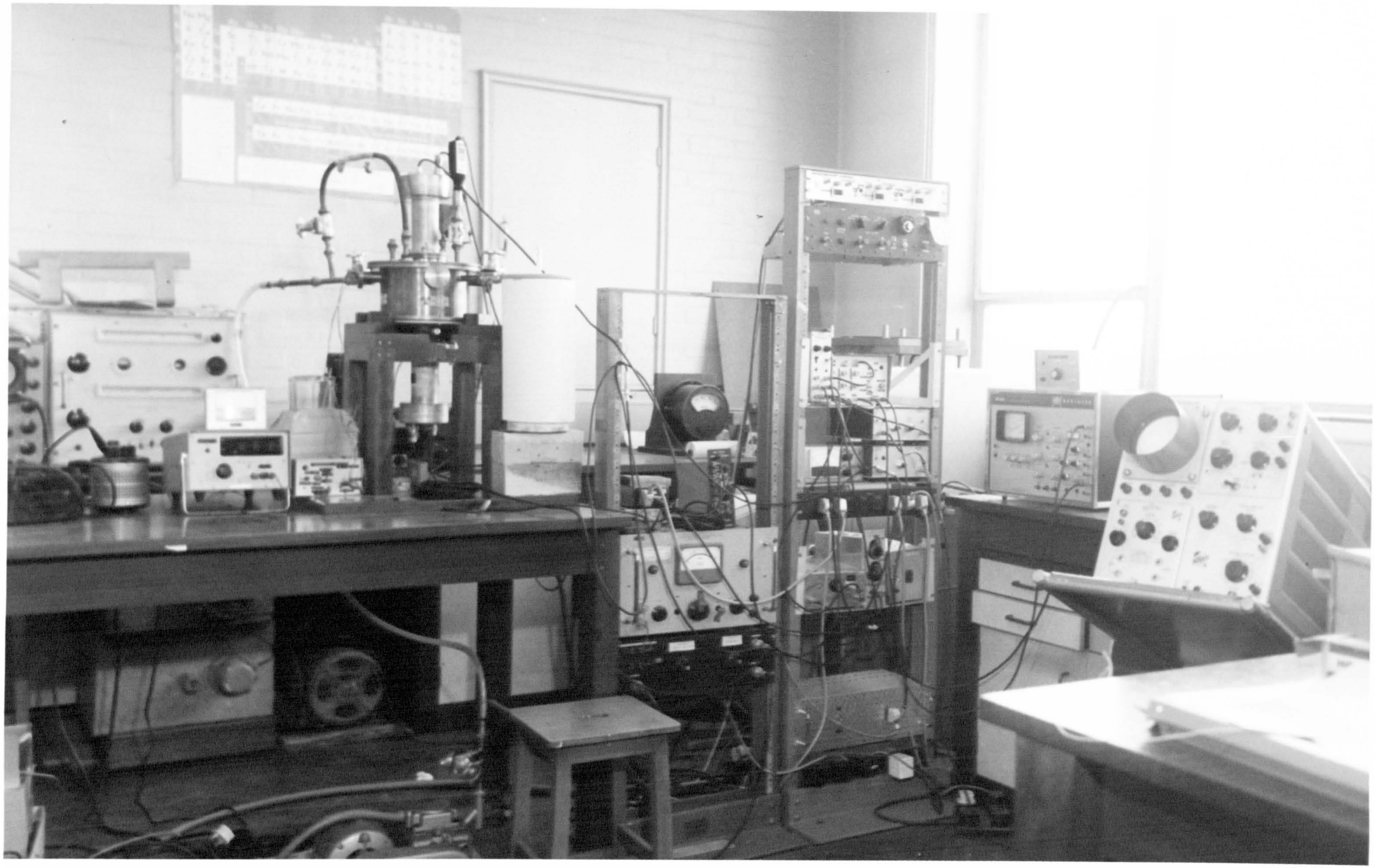

FIGURE 4.2 A view of the experimental arrangement used for the luminescent measurements of the CdS(Te) crystals

been shown to exhibit rise times of the order 1 ns. Use of radioactive sources removed one of the constraints associated with a pulse accelerator and permitted the use of the wide range ionization densities available between β-particles and α-particles.

A second PMT, i.e. the stop-PMT, scanned the same scintillator in the cryostat from a greater distance. An adjustable slit was used to control the intensity of light striking this PMT to ensure that the stop-PMT detects an average number of photons which is less than one per scintillation. This condition must be preserved if the resulting pulse-height distribution in the MCA is to be a faithful representation of the decay function. Since the single photons will be counted with this PMT, it must be a fast, high gain, but low noise device. The EMI 9597, was chosen for this purpose. It has an S-20 photocathode to suit the 600 nm output of CdS(Te) and the typical anode pulse rise time and fwhm are 2 ns and 3 ns respectively. The high noise rate of the 50 mm diameter S-20 photocathode was drastically reduced by means of a magnetic collimator (see later).

The difference in time between the zero-time pulse and the first single photon pulse to arrive from the sample was measured by converting the time difference into a pulse-height using the TAC. Then, the resulting time distribution of these single photons was accumulated in the MCA. To achieve this result electronically, the current pulse from the start-PMT was fed into the two amplifiers operated in parallel (see Figure 4.1). The output signal from the preamplifier (fast amplifier 1) was fed to the input of the fast discriminator. This unit produced a fast narrow pulse at the leading edge of the input start signal. This zero-time pulse was applied to the start input of the TAC (Ortec 437A), to initiate the cycle. The discrimination level of this fast branch of the system was so adjusted that a trigger

was obtained only for signals greater than that corresponding to 3-4 photons. This ensured that the time delay between the start of the scintillation and the zero-time pulse was as small as possible. It is worth mentioning at this stage that another important advantage of the SPCT is its linearity, which is mainly controlled by the linearity of the TAC, but is not particularly dependent on the linearity of the other units in the system, such as the PMT's and amplifiers.

The single-photon pulse from stop-PMT which carried the time information of the luminescent decay phenomena was first amplified by the fast amplifier 2. The delay introduced by the 50Ω coaxial cables in this series branch was used to control the starting time position of the decay displayed on the MCA. The output of this fast preamplifier was fed into two parallel branches. One went to the stop input of the TAC. If any cycle had already been started in this TAC by the zero-time pulse, this cycle was terminated by the arrival of the stop pulse. The output of the TAC is a pulse whose amplitude is proportional to the time difference between the start and stop input pulses. This information in amplitude was sent to the MCA (NS-605, an 512 channel PHA) and stored in its corresponding channel which was calibrated with respect to time as explained in Section 4.2.4. In this way the decay distribution was obtained in the MCA, and the data was displayed on the MCA oscilloscope or printed out on paper by the teletype.

The quality of the observed decay distribution was considerably improved by judicious selection of triggers in the discrimination system operated in parallel (Figure 4.1). With this arrangement, not every output from the TAC was stored in the MCA. The operation of this unit was gated by the coincidence system (the slow selection channels) in order to eliminate unwanted pulses triggering the system.

The principal functions of the slow selection channels are,

(i) to improve the time resolution by selecting in both channels only

those pulses which drive the fast discriminators hard and (ii) to ensure that only pulses with many photons (i.e. genuine particle induced events) are accepted by the start channel. These requirements thus were met by adding a slow coincidence circuit to the system. Start and stop pulses were fed to its respective inputs through the slow (1 μs time constant) amplifiers 1 and 2 and pulse-height discriminators 1 and 2 respectively. The signals that were selected in amplitude and shaped by these discriminators were applied to the respective inputs of the coincidence box, the output of which controlled the gating at the input of the MCA. With this arrangement, only the coincidences caused by sufficiently large anode pulses were registered in the memory of the MCA. Thus, noise triggers from the start-PMT were eliminated.

The thermal (dark) noise originating from the stop-PMT cannot be eliminated with the same ease, because both the electrons constituting the noise and the single photoelectrons are not distinguishable in shape. However, by decreasing the working area of the photocathode with the aid of the focusing electrode of the PMT and the magnetic collimator (EMI, type C121), the dynode system could be made blind to the electrons from the cathode with the exception of those emitted by this small area at the very centre of the cathode. Gradual cooling of the PMT through the cold cryostat also improved its performance and further decreased the dark current noise. With these precautions the noise of the stop-PMT was reduced considerably (1-2 counts/sec.).

In the coincidence box, adjustable delays and widths were introduced separately to the input start and stop pulses (1 and 2) so that the coincidence arrangement in time was made possible. The coincidence box also provided output terminals for inspection of the delayed and shaped start and stop pulses and for measurement of their rates. Because of the delays introduced in the coincidence processes,

the TAC output pulse passing to the MCA was strobed externally with an auxiliary pulse delay and width circuit 3.

4.2.3 The Cryostat

A vital part of the experimental arrangement used with the SPCT was the thermally controlled cryostat. While the results of Cuthbert and Thomas indicated that it is interesting to have data at liquid helium temperatures, our interest in a practical application and the fact that the luminescence efficiency remains practically unchanged between 4 K and 80 K justified our restricting the investigation to the temperature range from 80 - 300 K.

The general requirements of the cryostat can be summarized as follows:

(1) It should contain a liquid nitrogen reservoir, a sample holder with a heater assembly and temperature controller, facilities for exciting the scintillator, an adjustable slit in the light path to the stop-PMT, and the housings for the two PMT's.

(2) It should be light-tight.

(3) It should be vacuum-tight to maintain the liquid nitrogen inside the cryostat and the temperature stability of the sample throughout each decay run. This, in return, will help the heater to maintain the temperature of the sample constant at any value between 80 K and 300 K throughout a decay run.

(4) The start-PMT must be as near to the sample as possible in order to collect most of the scintillation light, whereas the stop-PMT may be some distance from the sample since it requires at most one photon from every scintillation.

The detailed drawings and a photograph of this cryostat are given in Figure 4.3 and Figure 4.4 respectively. The liquid nitrogen reservoir with its filling pipes, and the front section of the start-PMT

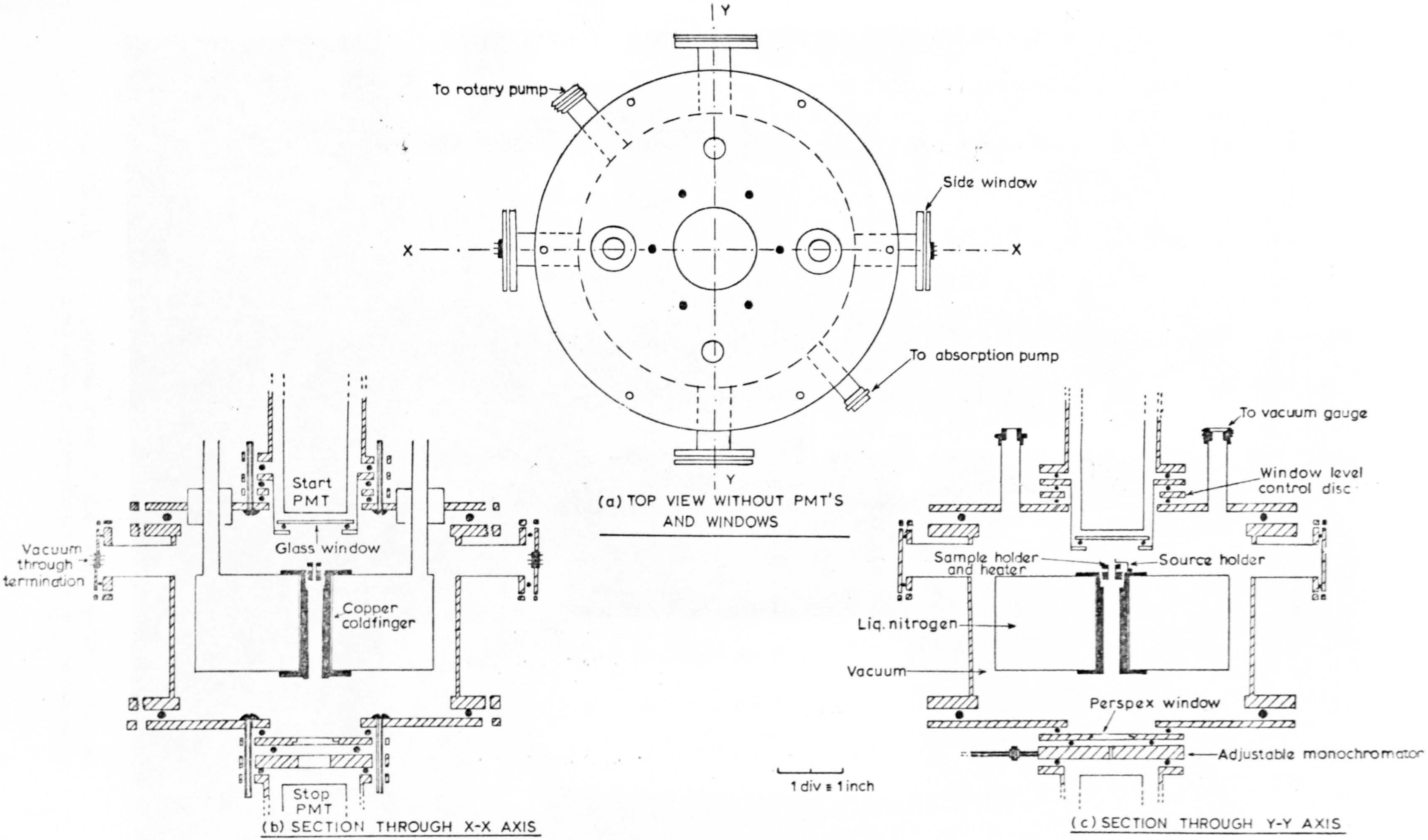

FIGURE 4·3 DETAILED DRAWINGS OF THE DECAY SYSTEM CRYOSTAT

FIGURE 4.4 A general view of the decay system cryostat used with single-photon counting technique

housing were made from stainless steel to ensure better insulation (see Figure 4.5), whereas brass was used for the other sections of the cryostat. The unit itself was made completely light- and vacuum-tight with the O-rings used. The volume of the reservoir was about 3 litres which was enough to keep the sample at liquid nitrogen temperature for some 15 hours without any refilling as long as the vacuum inside the cryostat was preserved at about 0.015 torr. A simple cryogenic adsorption pump made by us using aluminium calcium silicate (molecular sieve type 5A from BDH Chemicals Ltd.) was found to produce a satisfactory vacuum.

A tight copper pipe (cold finger) was inserted through the hole in the centre of the reservoir and held by copper flanges at each end to maintain the sample holder at low temperature as the nitrogen level inside the reservoir gradually dropped. The heater assembly was screwed to this copper cold finger at the top, and an adjustable and firm source holder was just located beside it as shown in Figures 4.3 and 4.5. The sample, properly fixed on a thin copper plate was put at the top of the heater unit in such a way that it could see both PMT's.

The design considerations for a satisfactory heater are:

(1) It should permit a stable temperature to be maintained in the sample throughout each decay run.

(2) By varying the voltage across the coil, it should be possible to obtain any temperature between 80 K and 300 K.

Using different materials, geometry, and heating elements, various heater assemblies were designed and tested. At the end, the heater unit illustrated in Figure 4.6 was found to be most successful.

The heater and sample holder assembly was made from three pieces soldered to each other. The top and bottom pieces were made from highly conductive copper whereas the connecting piece was a thin

FIGURE 4.5 An inner view of the decay cryostat

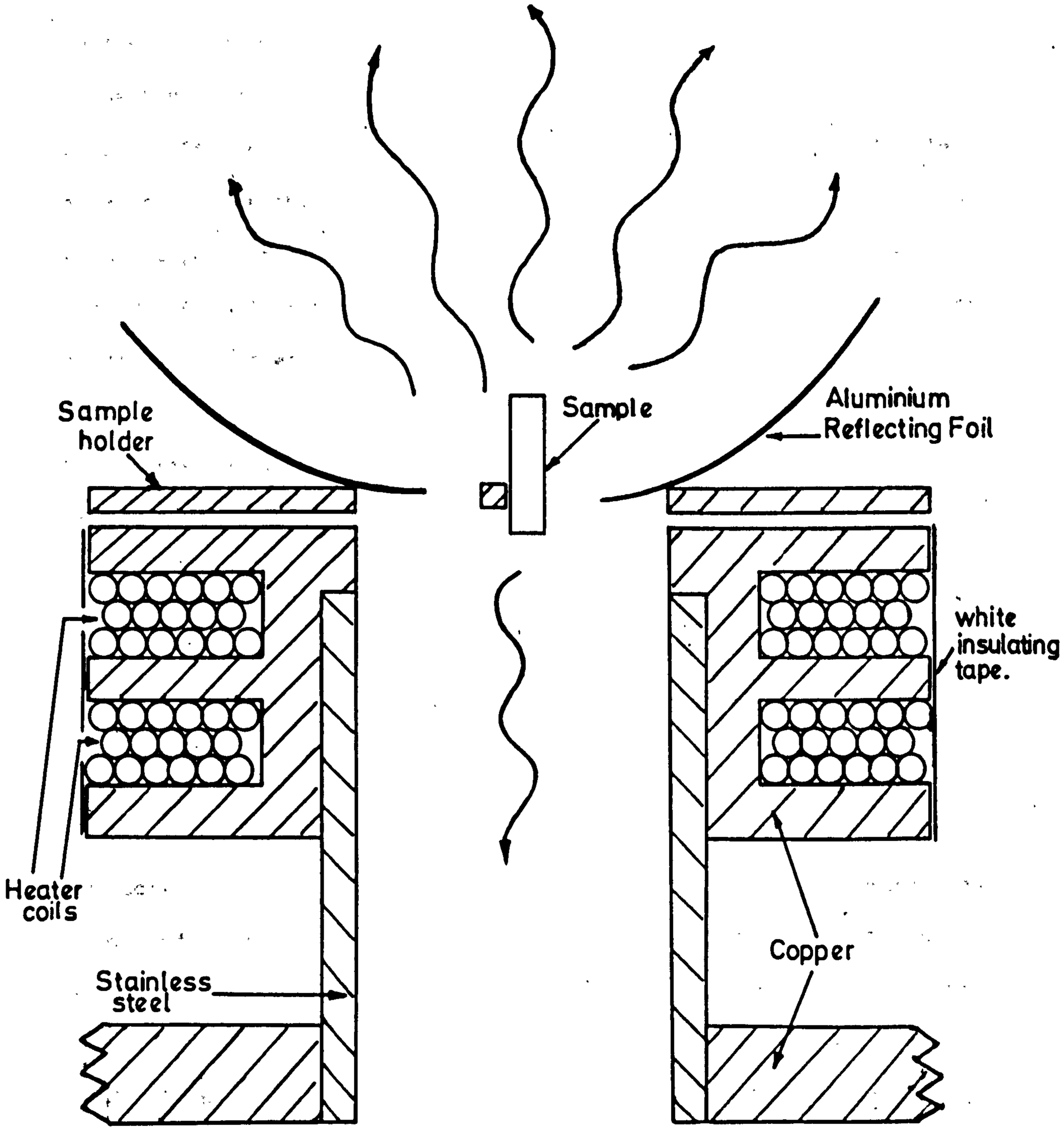

FIGURE 4.6 The cross-section of the sample holder and the heater assembly of the cryostat.

wall stainless steel pipe which is a poor conductor of heat. Consequently, any heat generated by the coils in the two grooves of the sample holder could easily balance the heat loss through the stainless steel pipe over the entire temperature range. The sample attached to a thin copper disc was situated at the top of the heater as shown in Figure 4.6. Silicone grease smeared between the sample disc and heater maximized the thermal coupling. A copper constantan thermocouple was located on the same disc near to the sample to measure the temperature. The reference junction of this thermocouple system was held at room temperature.

The start-PMT was located as near to the sample as possible in order to detect most of the scintillation. The aluminium reflecting foil around the sample improved the light collection. The stop-PMT was placed further away from the sample. The longer light-path and smaller solid angle caused fewer photons to be detected by the lower PMT. Furthermore, the rate of the single photons detected by this PMT could be controlled by the adjustable slit. The monochromator was also used to view the decay at a selected wavelength. The PMT's were at atmospheric pressure and were insulated from the vacuum inside the cryostat by the windows as shown in Figure 4.3. The window materials used (glass and perspex) were fully transparent in the spectral region studied.

4.2.4 Measurement of the Decay Profile

The photocathode of a PMT converts a photon into a low energy electron (with some finite probability $Q(\lambda)$ known as the quantum efficiency). This results in a gaussion current pulse at the anode of the device. In an ordinary scintillation counter, say NaI(Tl), the number of photoelectrons in a pulse is so great that they pile up on

each other to yield a current waveform resembling the decay curve but with characteristic statistical noise superimposed as illustrated in Figure 4.7(a). If, now, we attenuate severely the light between the scintillator and the PMT, and if the PMT has a very fast anode pulse response, the signal degenerates into a distribution of a single photon pulses (Figure 4.7(b)). Clearly, counting these in a narrow interval at a time t after t = 0 would result in a measurement of the decay curve as t was varied. This is the sampling approach of which Cuthbert and Thomas used a variant.

An alternative approach is to use a TAC and MCA. In this case, however, the recording system has the property that it records only the time interval between t = 0 and the <u>first</u> photon pulse and then goes dead for several microseconds. This is clearly useless for the case shown in Figure 4.7(b). However, the simple solution is to attenuate the light pulse still further until <u>at most one</u> of the photons produces a photoelectron pulse in the stop-PMT, as in Figure 4.7(c). Our knowledge of Poisson statistics, however, tells us that there will always remain a certain probability of finding two or more photons in a decay and that such events produce a deficit in the measured decay relative to the original light flash. As will be shown in the next section on dead time corrections, it is relatively easy to determine the maximum error introduced by this effect. Simple mathematics shows that the maximum fractional error (i.e. at long times in the decay) tends to the value of the ratio of the triggering rates in the stop and start channels (defined as stop-to-start ratio). Thus, a 0.02 ratio gives a maximum error of 2% at the times long compared with the characteristic time constant of the decay. The topic of the direct observation of a decay function by means of SPCT at low stop-to-start rates has recently been discussed in detail by Miehe et al (58).

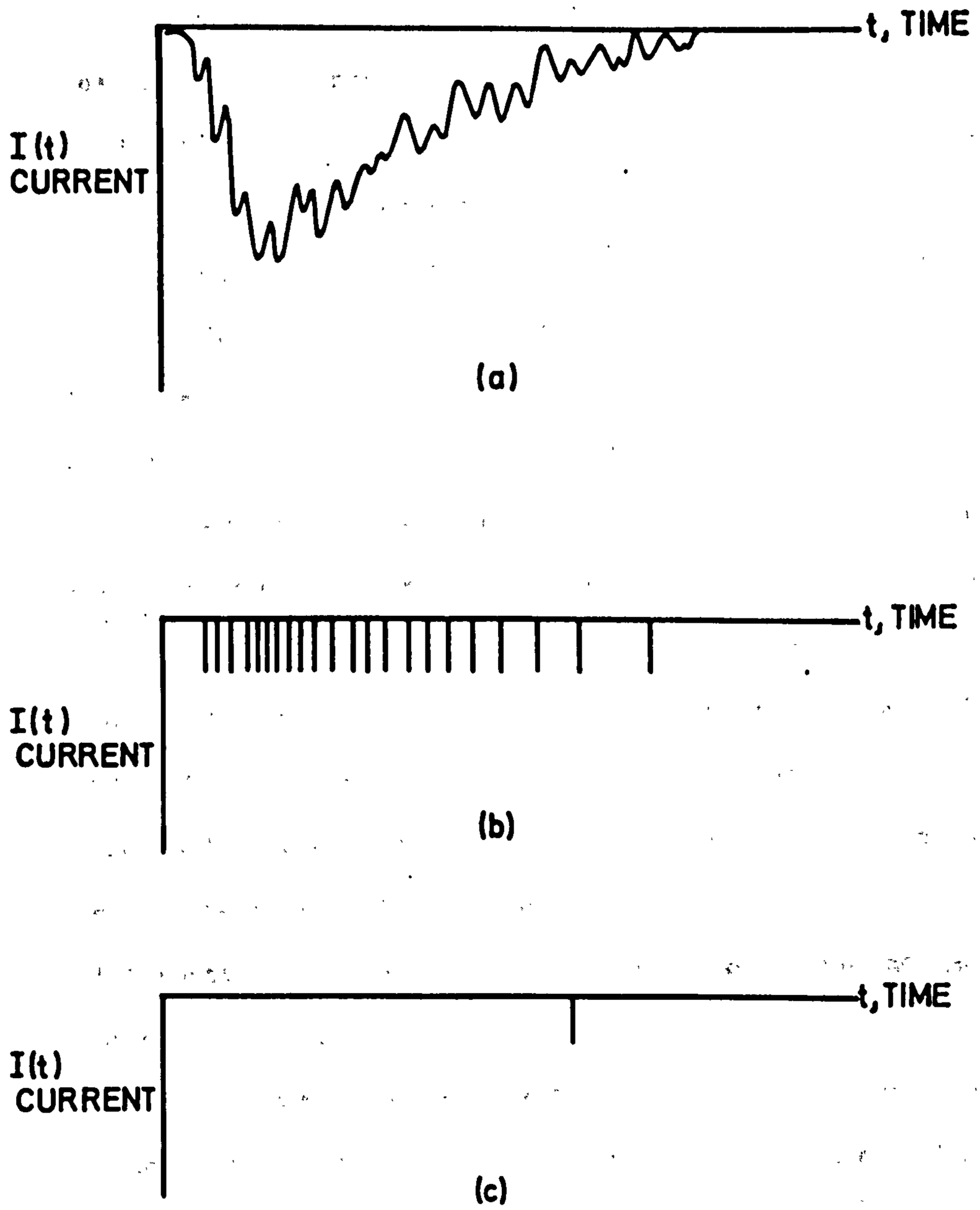

FIGURE 4.7 Current waveforms from a fast PMT scanning a scintillator. Light from the scintillator is not attenuated in (a), attenuated in (b) to see the photon distribution, heavily attenuated in (c) to detect only <u>one</u> single photon per scintillation.

4.2.5 Performance of the System and Correction Factors

Before starting the luminescent decay time measurements some test runs were carried out so that the performance of the electronics could be better understood. First, the linearity of the system was checked, then the time scale of the MCA was calibrated. Finally, the factors contributing error to the decay data were investigated.

The linearity of the system was checked in the following way: A sample scintillator used in the cryostat was excited by 5.5 MeV α-particles which produced successive random excitations. The resultant scintillations were detected by the start-PMT only, while a random photon source (a tungsten lamp) was used to excite the stop-PMT. The stop rate was kept very low, about 1/50 of the start rate. This test run was continued for some time to obtain better statistics. At the end of this run, a flat spectrum in the MCA was observed as expected (one would expect a constant number of counts in all channels when there is no time correlation between the TAC-start and stop pulses). The differential nonlinearity of 2% introduced by the TAC used was negligible for our purpose.

The time scale of the TAC-MCA combination was calibrated using pulses with constant and precise delays. To achieve this, the output pulses from a mercury pulser were fed directly into the start input of the TAC while the delayed output from the same pulser was applied to the stop input of the TAC. Calibrated 50 ohm coaxial cables were used as delay elements. In this way, the outputs from the TAC were collected in one channel of the MCA since there is a constant time difference between the TAC-start and -stop pulses. By varying the delay, the channel widths of the MCA were calibrated for the various ranges of the TAC, covering the range from 0.14 ns/channel to 2.24 ns/channel.

The over-all time resolution of the system should be examined since the observed decay curve is a convolution of the actual decay with the time resolution function (59). This time resolution function can be deduced from the measurements of decay curves for a fast scintillator. Here, ZnO(Ga) was chosen as the test scintillator. This has a decay time of about 0.45 ns (Nuclear Enterprise Data Sheet). The response of this sample to ^{241}Am α-particles was measured using this system. The result, shown in Figure 4.8, provided information about the time resolution function. A fwhm of about 2.3 ns was estimated from these distributions which implied a half-width $\Delta t_{1/e}$ of 1.5 ns at 1/e of the maximum. In the literature, the reported values of the half-width ($\Delta t_{1/e}$) lie between 1 ns and 6.8 ns (57,61). As the shortest decay time measured on our CdS(Te) samples was about 10 ns, it was possible to determine the decay times from the slope of the decay.

The shape and the fwhm of the observed time resolution function depends on various factors, e.g.

(1) The variations in the responses of both PMT's (noise, after-pulsing, transit time fluctuations, etc.),

(2) The type of the scintillator and its optical coupling to the start-PMT, since the time fluctuations of the start signal depend on the integrated scintillation intensity,

(3) The performance of the electronics (pulse-height triggering and selection).

In Section 4.4.2, it was shown that the noise and after-pulsing originating from the start-PMT can be eliminated electronically by setting limitations on the height of the selected start pulses and making use of a coincidence technique; but, the noise from the stop-PMT cannot be handled with the same ease since both the noise and single

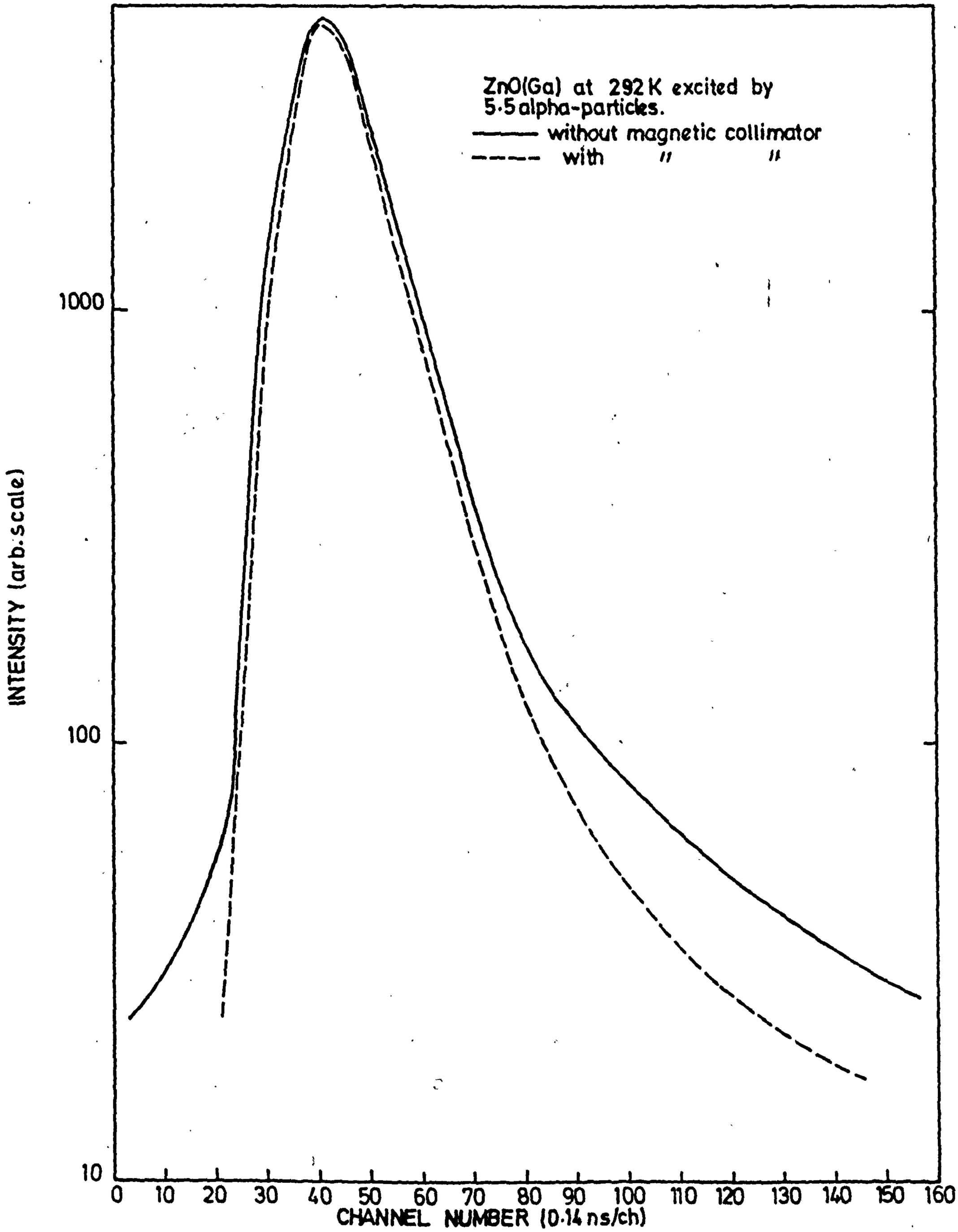

FIGURE 4.8 Decay profiles of ZnO(Ga) obtained with our system.

photons carrying the signal are identical in character. Here, however, the magnetic collimator located on the photocathode of the stop-PMT improved the all-round performance. The stop-PMT noise came down from 21370 counts/sec to 25 counts/sec, and the consequent improvement in the time resolution was seen as a sharper leading edge and a shorter tail on the right-hand side of the distribution (see Figure 4.8). In addition, the transit time fluctuations in the PMT were made less effective by maintaining the EHT of the PMT's constant throughout the measurements (59).

The start-PMT should be coupled to the scintillator as closely as possible, in order to give a large zero-time signal with minimum time jitter. This condition was difficult to achieve in the arrangement because it was necessary to maintain some separation between the photocathode and the sample for thermal insulation. This reduced the amplitude of the light pulses considerably which was not desirable, because the time resolution of the system was critically dependent on the shape (the amplitude and the rise time) of the start light pulses. The aluminium reflecting foil was introduced around the sample simply to improve this light collection (Figure 4.6).

On the other hand, the amplitudes of the light pulses from a CdS(Te) scintillator vary from sample to sample and from temperature to temperature, depending upon the optical quality of the crystal examined and its luminescence efficiency. At low temperatures, the time resolution observed from the decay profiles was very good, e.g. $\Delta t_{1/e} \simeq 2$ ns, because the luminescence efficiency from the crystals was high. In this case, the error on the decay times derived from the decay profiles was very low, e.g. $\sim$ 1%. At higher temperatures, the luminescence efficiency of the CdS(Te) crystals dopped considerably. This, in turn, caused poor time resolution, so that the value of $\Delta t_{1/e}$

increased (see Table 5.1 of Chapter 5). In this case, an error of $\sim$ 2-3% was anticipated. To determine the decay times more precisely, it is possible to unfold the decay curve (59,60) using various resolution functions, but the level of accuracy already achieved was adequate for our purpose. So, no extra effort was devoted to this problem. In general, the variations in the time resolution were kept as low as possible throughout by making careful adjustments to the start channel electronics, e.g. the EHT of the PMT and the threshold levels of the discriminator, for each data run.

The background emanating from the chance coincidence is another instrumental effect encountered in these decay time measurements. Fortunately, the chance coincidences of early and delayed pulses were almost negligible in our experiments because the peak intensity is much larger (about 10^3) than the background level in the decay curve. If the two values are comparable, it is always possible to subtract the background.

The raw data stored in the MCA at the end of each decay run is a direct analogue of the luminescent light decay as long as the count rate is very low. At high count rates, however, the probability of observing more than one photon in a cycle of the experiment becomes significant. If, in any cycle (particle excitation), the total probability of detecting a photon by the stop-PMT is high, then the measured photon detection probability will be distorted. The TAC will nearly always be started by the photons detected near the beginning of the time distribution, and it will then be unavailable later in time with the result that a shorter decay distribution will be observed. Consequently, the probability $P_1(t)$ of detecting the first photon at time t will not be equal to the illumination function i(t) which is also defined as the probability of detecting a single photon at time t.

This type of error in SPCT is called the pile-up (dead-time) error and various considerations and correction techniques are described in the literature (62-66).

Coates (62,65) has shown that, at low count rates, the error in the decay lifetime due to pile-up is constant at long times and equal to the ratio N of the stop to the start rates. N can be measured easily in our system by a scaler connected to the outputs 1 and 2 of the coincidence box (Figure 4.1). At higher stop rates, the pile-up correction becomes more difficult and complex as indicated by Davis and King (64). They suggested an experimental approach to find the pile-up correction. The technique requires the incorporation of an inhibit circuit. Detection of photons after the first one, produces an inhibit signal to the TAC so that the delayed first photon coming to the start of TAC to initiate the cycle is inhibited. In this case, only events that contain single photons are counted. On the other hand, the most recent development to avoid the dead-time correction in SPCT have come after the introduction of a new high-gain first-dynode PMT. If we use such a PMT together with an amplitude selector in the stop channel of the system, we can avoid photon pile-up since this sort of PMT can distinguish between one, two or three photoelectrons by amplitude measurement. With such a system, the stop rate can be even made higher (58).

In our measurements, we have always used low stop rates so that N was less than 0.02. In this case, the pile-up error is well defined and negligible. We can prove the validity of this assumption in the following way: Let us define $P_2(t)$ and $P_3(t)$ as the probability of obtaining a second photon or third photon at time t. We can write,

$$Ni(t) = P_1(t) + P_2(t) + P_3(t) + \ldots \quad (4.1)$$

where Ni is the number of photons detected by the stop-PMT per

... and $P_1(t)$ is the observed decay distribution. Consequently the higher the values of $P_2(t)$ and $P_3(t)$, the larger the error one expects in the decay data. $P_2(t)$ which is a measure of the loss due to one previous stop photon, can be written as

$$P_2(t) = P_1(t) \cdot P_1(o,t) \quad \ldots\ldots (4.2)$$

where

$$P_1(o,t) = \int_o^t P_1(t')\, dt' \quad \ldots\ldots (4.3)$$

is defined as the probability of one event having occurred any time up to time t. Similarly, we can write for $P_3(t)$, i.e.

$$P_3(t) = P_1(t) \cdot \int_o^t \int_o^{t'} P_1(t'')dt'' \cdot P_1(t')dt' \quad (4.4)$$

in our case, we have

$$\int_o^{t_{max}} P_1(t')dt' = N \quad \ldots\ldots (4.5)$$

The fractional importance of $P_2(t)$ can be written as

$$\frac{P_2(t)}{P_1(t)} = \int_o^t P_1(t')\, dt' \quad \ldots\ldots (4.6)$$

At long times, the right hand side of the above expression becomes equal to N. So, the worst error in the distribution becomes constant and equal to N. If the stop to start ratio is 1/50, then a 2% correction is required at long times with less at shorter times.

Similarly, the fractional importance of $P_3(t)$ is

$$\frac{P_3(t)}{P_1(t)} = \int_o^t \int_o^{t'} P_1(t'')\, dt'' P_1(t')\, dt' \quad .. (4.7)$$

This becomes equal to N^2 at long times. If N = 0.02, the fractional error coming from the loss due to two previous photons is as low as 0.04%.

Let us consider that the observed decay function is an exponential one and $t_{max} >> \frac{1}{k}$ for convenience of integration. Using Equation 4.12, we can write

$$N = \int_o^{t_{max}} P_1(t')\, dt'$$

$$= \int_o^{t_{max}} A\, e^{-kt'}\, dt' \quad \ldots\ldots\ldots \quad (4.8)$$

If $t_{max} \longrightarrow \infty$, the above expression becomes

$$N = -\frac{A}{k} \left[e^{-kt}\right]_o^{\infty} = \frac{A}{k} \quad \ldots\ldots\ldots \quad (4.9)$$

the fractional importance of $P_2(t)$ as derived from Equation 4.6 is

$$\frac{P_2(t)}{P_1(t)} = \int_o^t Ae^{-kt'}\, dt$$

$$= -\frac{A}{k} \left[e^{-kt}\right]_o^t$$

$$= \frac{A}{k} (1-e^{-kt}) \quad \ldots\ldots\ldots \quad (4.10)$$

$$= N(1-e^{-kt})$$

To the second order we can always approximate Equation 4.1 to

$$i(t) \simeq P_1(t) + P_2(t) \quad \ldots\ldots\ldots \quad (4.11)$$

Using the Equations 4.10 and 4.11 we see that the correction to be made to the decay data at $t \sim 2\tau$ has only risen to 0.9 N which equals 1.8% if N is 0.02 again.

For non-analytic decay functions, the integral $\int_o^t P_1(t')dt'$ can be evaluated numerically and the correction calculated exactly. However, keeping $N \ll 1$ is clearly a good way of making sure that the

error due to pile-up is small and well defined so that it can usually be neglected.

4.3 Measurement of Thermal Quenching of Luminescence Intensity

The luminescence efficiency of CdS(Te) crystals varies with temperature as described in Section 2.4.2. From measurements of the thermal quenching of the luminescence intensity, it is possible to derive useful physical information, e.g. the activation energies of the luminescent centres.

Fortunately, it is possible to use the same measuring technique, i.e. that described in the previous section, to obtain the quenching data for the CdS(Te) samples. The TAC and the MCA were not used for these measurements. Instead the variation in the stop-rate with respect to the sample temperature was recorded. The stop-rate was again kept very low as for the decay time measurements in order to avoid the pile-up problem. The adjustable slit was very helpful in controlling the intensity of the photons detected.

The mechanical stability of the CdS(Te) crystal and the source of excitation are very critical factors. Any movement of these components during a measurement creates large errors in the stop-rate due to changes in the optical acceptance of the stop-PMT. Proper arrangements were made inside the cryostat to maintain the mechanical stability of the crystal and the source.

During each measurement, the temperature of the sample was varied step-wise from the lowest obtainable temperature to room temperature using the heater shown in Figure 4.6. At the same time, the stop rate and temperature were recorded. Each individual measurement was repeared several times in order to check the possibility of error originating from mechanical movement.

The noise from the stop-PMT plays an important role in the quenching measurements. Near room temperature, the noise figure became comparable with that of signal. Thus, the noise was always subtracted from the recorded signal value. Better results were obtained when the noise of the stop-PMT had been reduced to a minimum with the help of the magnetic collimator used and the gradual cooling through the cold cryostat.

4.4 Conclusion

The experimental techniques and the electronic arrangement used in the work described in this thesis have been described. SPCT which is the main technique used in decay time and thermal quenching measurements of luminescence has been discussed in detail. It has been shown that the instrumental error introduced into the observed decay curves is well defined and can be estimated when it is not negligible. For present purposes, the accuracy of $\sim$ 1% in decay time measurements at temperatures near 100 K and 2-3% near 300 K was quite adequate. The pile-up error is constant and equal to the ratio N of stop to start rates at long times. This error becomes even smaller for shorter intervals of time. As long as N is kept low, e.g. $\sim$ 1/50, this technique can provide a measure of reasonably precise decay time, and thermal quenching data for the CdS(Te) crystals without any necessity for a pile-up correction.

The thermal quenching measurements were found to be very straightforward, accurate and repeatable with within $\sim$2% provided care was taken that the sample and source did not move during thermal cycling.

PAGE
NUMBERS
CUT OFF
IN
ORIGINAL

CHAPTER 5

MEASURED RADIOLUMINESCENT PROPERTIES OF CdS(Te) CRYSTALS

5.1 Introduction

Some preliminary results of the measurements of the luminescent properties of our CdS(Te) crystals have been described in Chapter 3. Here, a wider range of measurements on the various CdS(Te) crystals using the techniques described in Chapter 4 are discussed.

The main aim of these measurements is to contribute further to the understanding of the luminescent emission process in this material. Our samples were doped with low Te concentrations (10^{18} - 10^{19} atoms/cc) so that good optical quality was preserved. The 600 nm band was therefore dominant in the emission spectrum and the contribution from 700 nm emission band was negligibly small as shown in Chapter 3. For this reason, in most of the measurements made here on the orange emission band no optical filter was used to isolate this band from the total emission, instead the total light coming directly from the sample was examined. On the other hand, some measurements were made to determine whether the luminescent decay profiles varied with the wavelength of emission and whether the emission band shifted with decay time.

Since we did not have a helium cryostat almost all the data (decay profiles and thermal quenching of the radioluminescent emission, radioluminescent emission spectra) were obtained at temperatures between 70 K and 300 K. The highly ionizing α- and less densely ionizing β-particles were used to induce luminescence in this material. Sometimes γ-rays were used as well (in the scintillation efficiency measurements).

From the many small platelets grown in each crystal growth run the best looking crystal was selected for these measurements. With the boules, a small and a clean piece cut from the boule was used. The same sample

from any growth run was used throughout a series of measurements and the variations in the observed results among different samples from the same growth run were not significant. Thus, instead of naming the sample by the numbers such as 108S8, 512S1, only the crystal growth number is given, viz. 108, 512.

5.2 Further Emission Spectra Data

5.2.1 Radioluminescent Emission Spectra

Using UV excitations, the luminescent emission spectra of various CdS(Te) samples were measured at various temperatures and the corresponding results have been shown in Chapter 3. These results confirmed the existence of a very wide (fwhm of about 45 nm), structureless emission band, located around 600 nm, which quenches rapidly at room temperature. Since radioactive sources were used to study the decay profiles and the thermal quenching of the luminescent emission, it was interesting to check whether there was any change in the emission spectra when the samples were excited by different radioactive sources.

Initially 5.5 MeV α-particles from an ^{241}Am source were used to stimulate the radioluminescence in thin platelet crystals. The sample and the source were located inside the photodiode cryostat (a detailed description of this cryostat can be found in the next chapter). An adjustable monochromator based on the MS-1 graded interference filter (400-700 nm) of Barr and Stroud Co. was located between the sample and the PMT (D224B with S-20 photocathode). The amplified and discriminated single-photon pulses from this PMT were counted by a scaler.

With this arrangement, the radioluminescent emission spectra from various CdS(Te) samples were obtained basically at two temperatures, i.e. at 80 K and 300 K. Since the monochromator used had a wide band-pass (30 nm), one could not expect to observe the detailed spectral

distributions. Even so, these distributions provided useful information for comparison purposes. The necessary corrections to the recorded emission intensities due to the spectral responses of the photocathode and graded filter were made. The resultant luminescent intensities were plotted as the relative energy emitted per unit wavelength interval.

The α-induced radioluminescent emission spectra from the platelet 108, and boules 511 and 512 are shown in Figure 5.1 (a), (b) and (c) respectively. The same broad emission band centred around 590-600 nm was observed at low temperatures. This band showed the expected shift towards longer wavelength as the temperature was increased. At room temperature, the measurements were less accurate because of the low signal levels from the sample.

If the radioluminescent emission spectra shown here are compared with the photoluminescent emission spectra given in Chapter 3, one finds almost the same distributions at low temperature; but, some differences are apparent at room temperature. This is clearly seen if the room temperature photoluminescent emission spectrum of sample 108S3 (Figure 3.2) is compared with its radioluminescent emission spectrum (Figure 5.1(a)). The latter has more light in the shorter wavelength region of the emission spectrum.

5.2.2 The Photoluminescent Emission Spectra at Very Low Temperatures

The lack of structure in the luminescent spectra of CdS(Te) crystals presents something of a puzzle for the understanding of the mechanism involved. In particular, the absence of a zero-phonon line is unfortunate and it was felt desirable to confirm the results of previous workers (2,3) by investigating the photoluminescent spectra

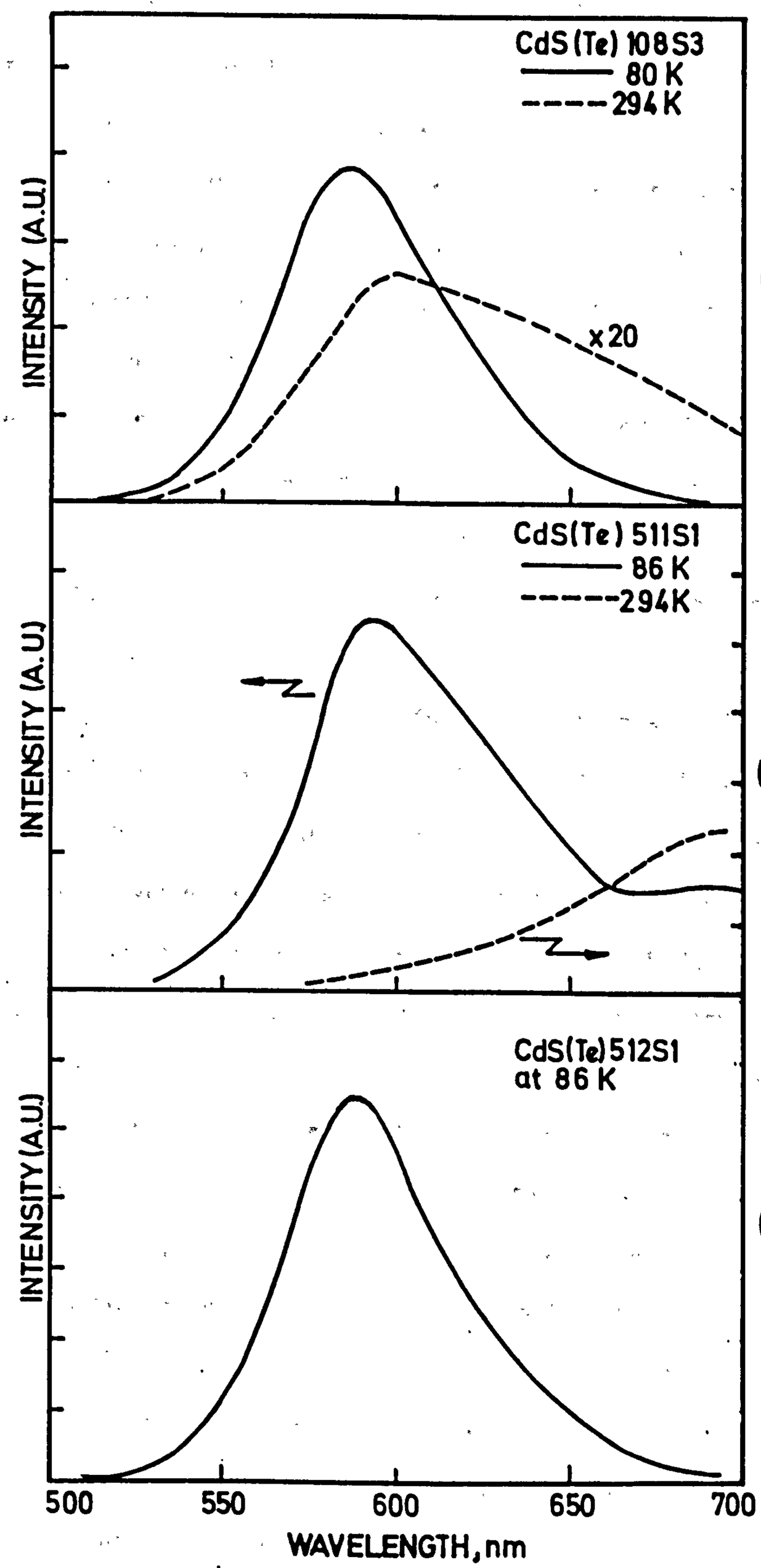

FIGURE 5.1 Radioluminescent emissions from various CdS(Te) samples excited by the 5.5 MeV alpha-particles from a ^{241}Am source.

at the very low temperatures permitted by the helium cryostat of the Department of Applied Physics and Electronics. Mercury and Tungsten lamps were used for excitation (with suitable filters) and an Optica spectrometer (CF 4NL) measured the output distribution.

In this way, using different wavelengths of excitation, the photoluminescent emission from various CdS(Te) samples, both platelets and boules, were scanned at temperatures starting from 10 K up to 80 K. There was no sign of a sharp zero-phonon line or of much weaker phonon sidebands in the blue region of the spectrum as observed by Henry and Nassau (45) in pure CdS; only green edge emission peaks were found. On the other hand, the broad orange emission band centred at 590 nm was always present. The peak position of this orange band did not change with temperature but the fwhm of this peak narrowed a little bit towards low temperature, i.e. 42 nm at 80 K and 40 nm at 10 K when excited by the UV light at 365 nm. It is certain that some part of the broadening observed was instrumental in origin. Figure 5.2 shows the photoluminescent emission spectrum of the boule 512 at temperature 10 K when excited by the same UV light. The intensity of the luminescent emission is plotted in terms of relative emitted energy per unit wavelength interval. This spectrum is very similar to the one given by Cuthbert and Thomas (Figure 2.2). The green edge emission peaks of CdS at 515, 522, 530 and 540 nm can easily be seen in this picture. The same edge emission peaks were observed in the platelets 108 and boule 513, but not in the boule 518 (the concentration of Te atoms in various CdS(Te) samples examined here are tabulated in Table 5.1).

In the temperature range 10 K to 80 K there was no visible change in the efficiency of the orange emission band. On the other hand, a considerable decrease in the efficiency of edge emission bands was observed when the temperature was raised from 55 K to 70 K. In general,

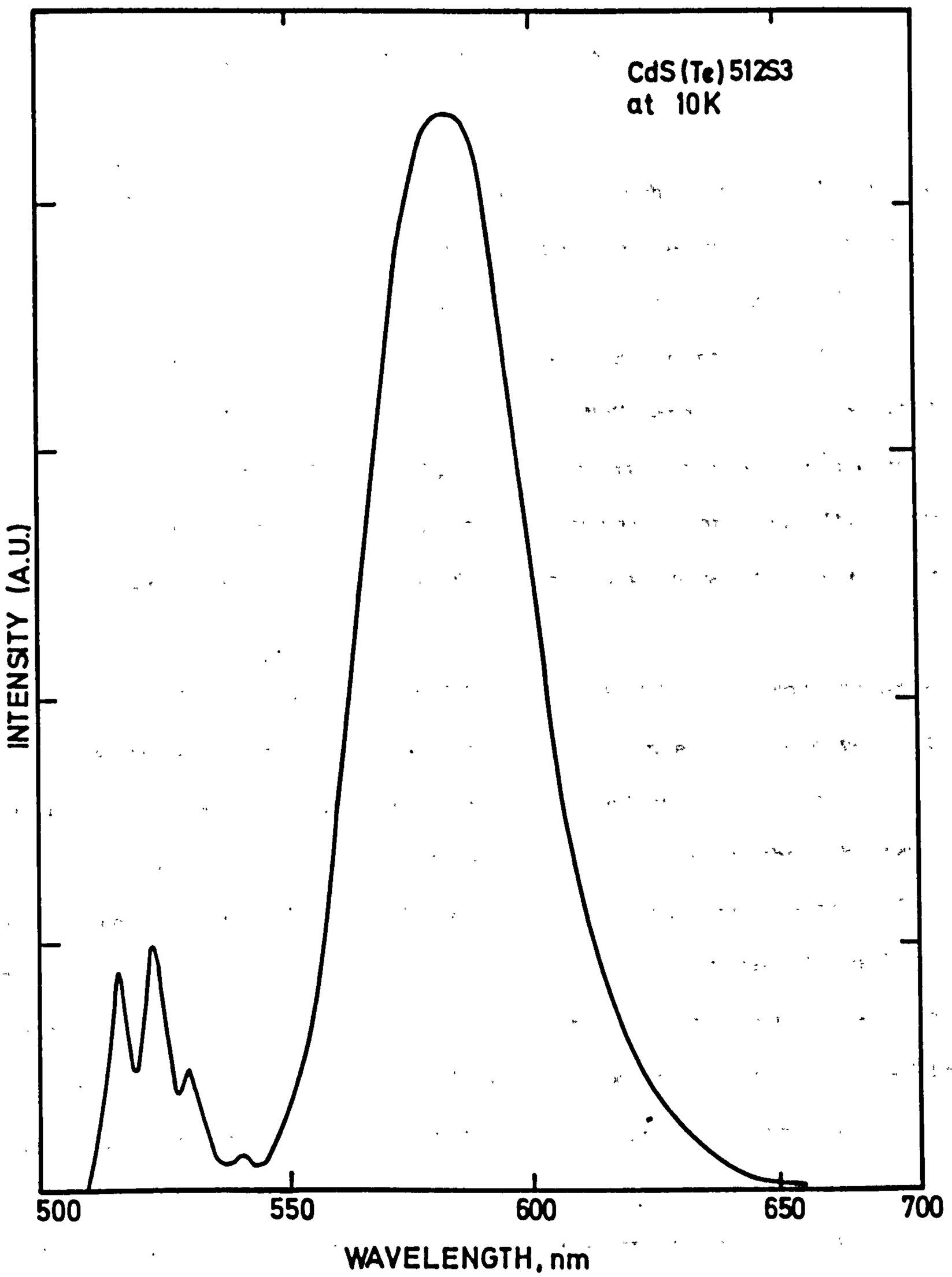

FIGURE 5.2 Luminescent emission spectrum of a CdS(Te) sample (boule) at 10K excited by 365nm UV radiation.

there was little useful information derivable from these measurements at very low temperatures.

5.3 Alpha-Induced Radioluminescent Properties

5.3.1 General

The decay profiles and the thermal quenching of the luminescent emission from various CdS(Te) samples were examined using the technique and arrangement described in Chapter 4. Highly ionizing 5.5 MeV α-particles from an ^{241}Am source were used for excitation. About 20 μm thickness of CdS(Te) is enough to stop 5.5 MeV α-particles as estimated from the data given by Birks (5), on the assumption that the range energy curve given for NaI is approximately valid for CdS. Thus, very thin samples were adequate to produce results with α-particle excitation.

The light pulses produced by the 60 keV X-rays from the same source were easily eliminated electronically since they were very low in amplitude compared with the pulses produced by the 5.5 MeV α-particles. The strength of the source used was such that the samples were irradiated with a flux of about 5000 particles per second. To minimize the dead-time error, the stop-to-start rate was always kept less than 1% so that there was no need for photon pile-up corrections. The time resolution of the decay system was kept as short as possible by maximizing the light collection from the samples on to the start-PMT and controlling the threshold of the pulse-height discriminator 1 (see Figure 4.1). In some cases, poor time-resolution became inevitable because of the severe decrease in the luminescence efficiency of the CdS(Te) sample at high temperatures. In addition to this poor time resolution, background counts superimposed on the signal (decay curve)

became significant. This constant background was subtracted from the observed decay curve before deriving any results. The background counts are particularly significant in the thermal quenching results and subtraction was therefore carried out carefully for every thermal quenching point.

The radioluminescent properties of most of the CdS(Te) crystals were examined at temperatures between 80 K and 300 K. Temperatures of 70 K were reached by pumping the liquid nitrogen inside the cryostat. In the following sections, the results obtained on various CdS(Te) samples by α-excitation are summerized.

5.3.2 The Decay Profiles

In general, rather interestingly, significantly shorter decay lifetimes were observed in the CdS(Te) samples when they were excited by α-particles. This contrasts with the results obtained by Cuthbert and Thomas (2).

The platelet 108S8, a small platelike CdS(Te) sample from the crystal growth run No.108 (1.43×10^{19} atoms/cc average tellurium concentration) was first studied to determine the decay of the light intensity with time. The curve illustrated in Figure 5.3 represents the decay profile obtained at temperatures of 80 K. The very fast rise time and the sensitivity of the systems over the two decades is clearly illustrated. The value of the half-width of the front edge (hwfe) at half-maximum of this decay is about 1.5 ns which shows the good time resolution of the system (see Figure 5.5 to understand this definition and other decay parameters). From this distribution measured at 80 K, the $t_{1/e}$ and t_{1/e^2} decay times (the times taken for the luminescent intensity to decay to 1/e and $1/e^2$ respectively of its peak value) were derived as 52 ns and 195 ns respectively. Clearly,

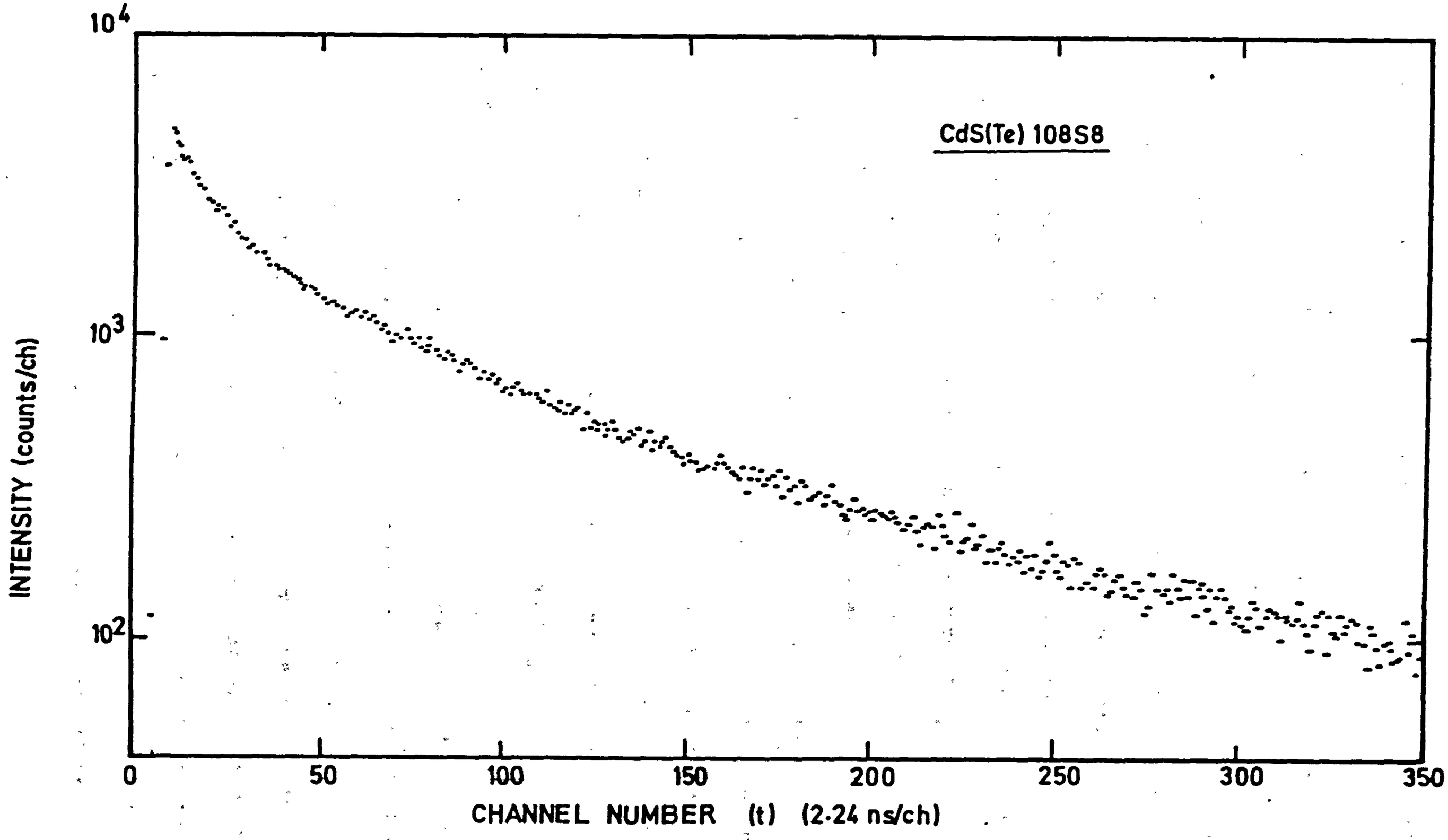

FIGURE 5.3 The decay profile of the luminescent emissions from platelet 108S8 at 80 K when excited by 5·5 MeV alpha-particles.

this is a very fast decay (the $t_{1/e}$ value that Cuthbert and Thomas (2) found for their similar platelets when excited by 400 keV electrons was more than 500 ns at this temperature). It was also non-exponential, the ratio of $t_{1/e}$ to t_{1/e^2} being 0.26.

Bateman and Jones (67) tried to estimate the error in the measured decay times of CdS(Te) due to finite time resolution of the system by relating the values of hwfe measured to the standard deviation σ of the Gaussian type resolution function. They showed that the actual decay times were longer than the measured ones. The error was negligibly low (1-2%) for t_{1/e^2} values; but, it was considerable for $t_{1/e}$ values depending upon the values of hwfe and $t_{1/e}$. In this way, it was discovered that the error in the measured $t_{1/e}$ values ranged from 20% (where the decay time under consideration is approximately equal to σ) to a negligible magnitude (where the decay time under consideration is larger, at least 30 times, than σ). Applying their method to the decay times measured herewith, the error was calculated for each $t_{1/e}$ value and this data was included in Table 5.1 and 5.2 where the radioluminescent parameters for various CdS(Te) crystals have been tabulated. In this way, an error of less than 1% was found for the 52 ns value of the platelet 108 at 80 K so that the actual $t_{1/e}$ value was only about 52.5 ns.

The statistical errors of the measured intensities in each channel of the decay curve are indicated by the scatter of the points about the smooth curve in Figure 5.3. In the measurement of these decays the runs were allowed to proceed for a period of from hours to days, depending upon the efficiency of the sample, in order to obtain good statistical accuracy. The statistical fluctuations are not shown point by point on the decay profiles represented in the rest of this work, instead a smooth curve averaging these small fluctuations is drawn.

TABLE 5.1

Summary of α-induced radioluminescent results on various CdS(Te) crystals

		Sample No.					
		108	512	513	518	534	535
Type		Platelet	S tail	Cd tail	Cd tail	Cd tail	S tail
Te , 10^{18}/cc		14.3	1.1	5.1	7.2	8.6	9.7
I	$t_{1/e}$, ns	52	145	78	64	56	78
	$t^*_{1/e}$, ns	52.5	147	79	65	56.6	79
	t_{1/e^2}, ns	195	390	300	210	190	228
	$t_{1/e}/t_{1/e^2}$	0.26	0.37	0.26	0.30	0.29	0.34
II	$t_{1/e}$, ns	15	20	15	14	20	24
	$t^*_{1/e}$, ns	15.2	20.3	15.3	14.3	20.3	24.4
	t_{1/e^2}, ns	61	62	56	56	68	84
U_1 , eV		0.14	0.17	0.24	0.14	0.14	0.24
U_2 , eV		0.037	0.027	0.041	0.037	0.043	0.019
$A_1 \times 10^4$		0.12	4.4	185	0.54	0.11	80
A_2		13	10.8	15.6	15.6	12	22
I(294)/I(0)		11	2.5	2	4	12%	2

I = Values at 90 K

II = Values at 294 K

$t^*_{1/e}$ = Corrected value of $t_{1/e}$ (67)

Increasing the temperature in steps up to room temperature the decay profiles of this platelet were examined in the same way. The decay times remained fairly constant in the temperature range from 80 K to 110 K, and began to decrease smoothly beyond 110 K. The variation of the decay times with reciprocal temperature is illustrated in Figure 5.4. As this figure shows, the decay times decreased monotonically from 80 K to 300 K; there was no maximum in the lifetime which again contrasts with the result of Cuthbert and Thomas. The decay profile from the same platelet at 294 K is shown in Figure 5.5. At this temperature, the decay times (i.e. $t_{1/e}$ and t_{1/e^2} times) were found to be 15 ns and 61 ns respectively (the value of $t_{1/e}$ found by Cuthbert and Thomas was about 400 ns). The time resolution of the system in this decay measurement was as good as the one found in the decay profile at 80 K so that the decay times derived from the observed curves was still very accurate (i.e. an error of less than 1%). The high performance of the system at this high temperature measured was achieved partly because of the efficient light collection from the transparent and thin platelet on to the start-PMT and partly because the luminescent emission from this sample did not quench appreciably at room temperature compared with the quenching in the boules of CdS(Te).

Further decay measurements were made on the boules. Boule 512 was grown in sulphur vapour and had an average tellurium concentration of 1.1×10^{18} atoms/cc. Its optical quality (transparency) was better than that of the other boules. The curve in Figure 5.6 illustrates the decay from this boule measured at 80 K, from which the decay times were found to be 145 ns and 390 ns respectively. These values are at least twice as great as the values found for the platelets 108 at the same temperature (see Table 5.1). The decays of both samples in this low temperature range were found to be non-exponential; the ratio of

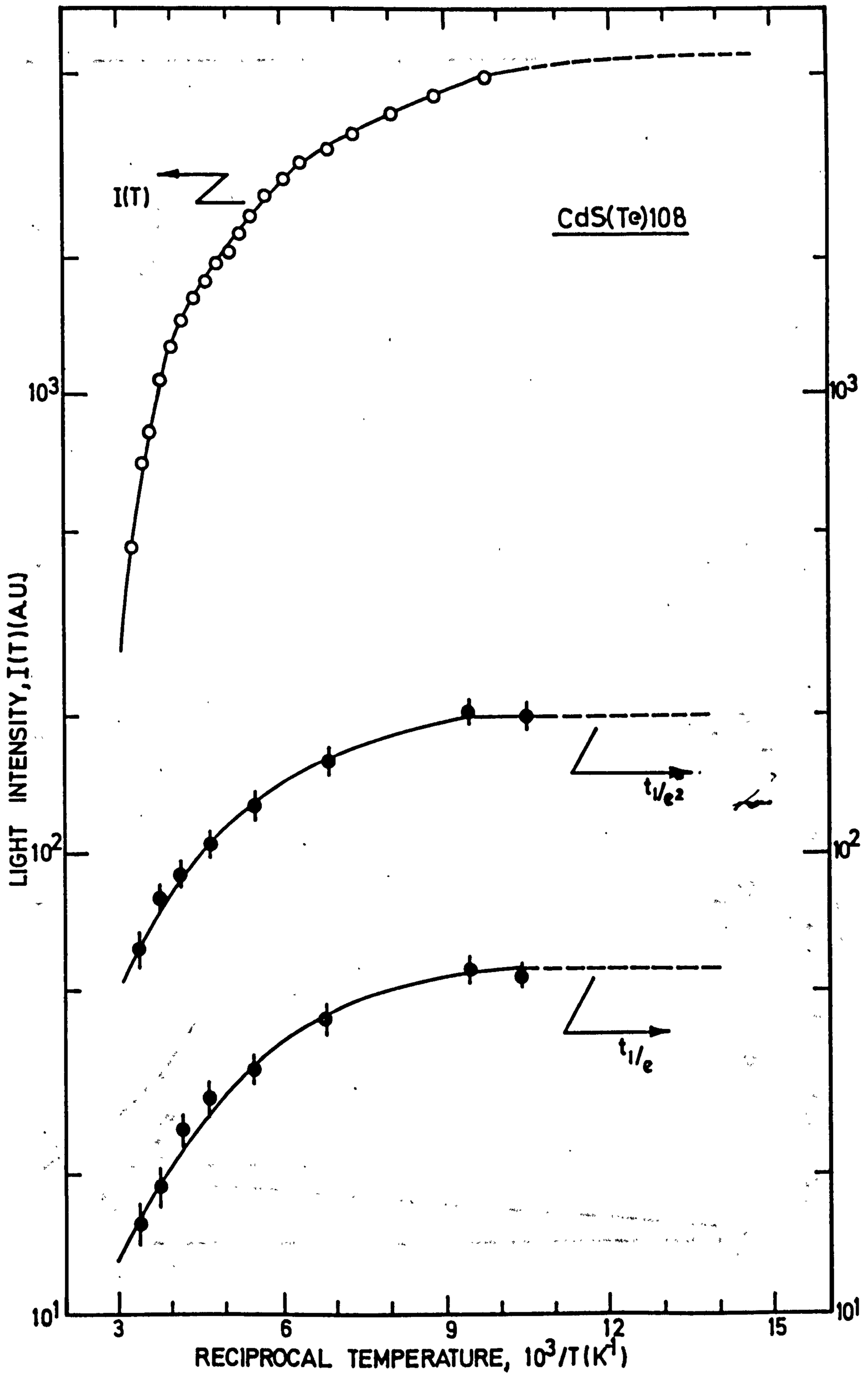

FIGURE 5.4 Variations of intensity and decay times of alpha-induced luminescence with temperature in CdS(Te) 108S8.

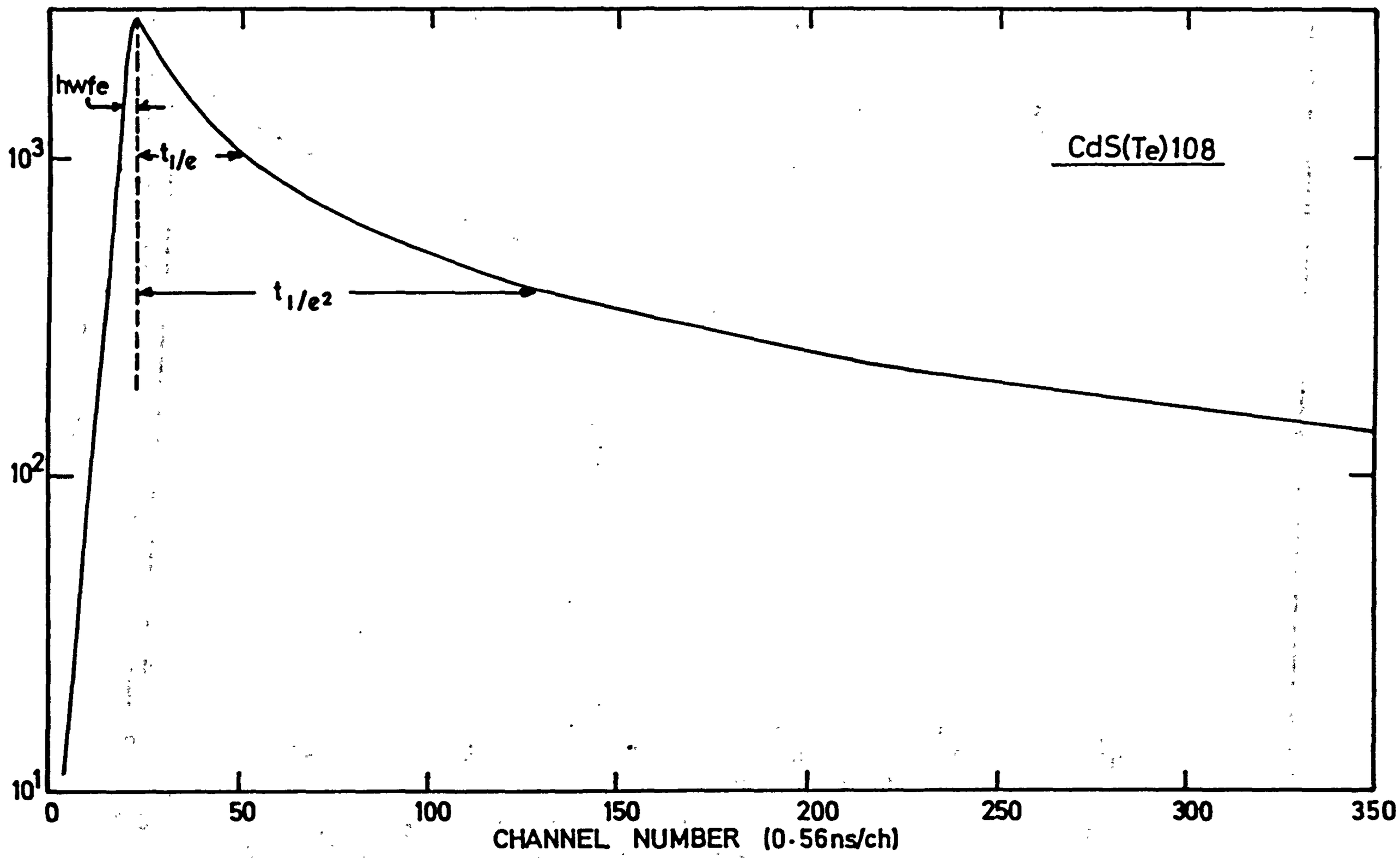

FIGURE 5·5 The decay profile of the luminescent emission from platelet 108S8 at 294K when excited by 5·5 MeV alpha-particles.

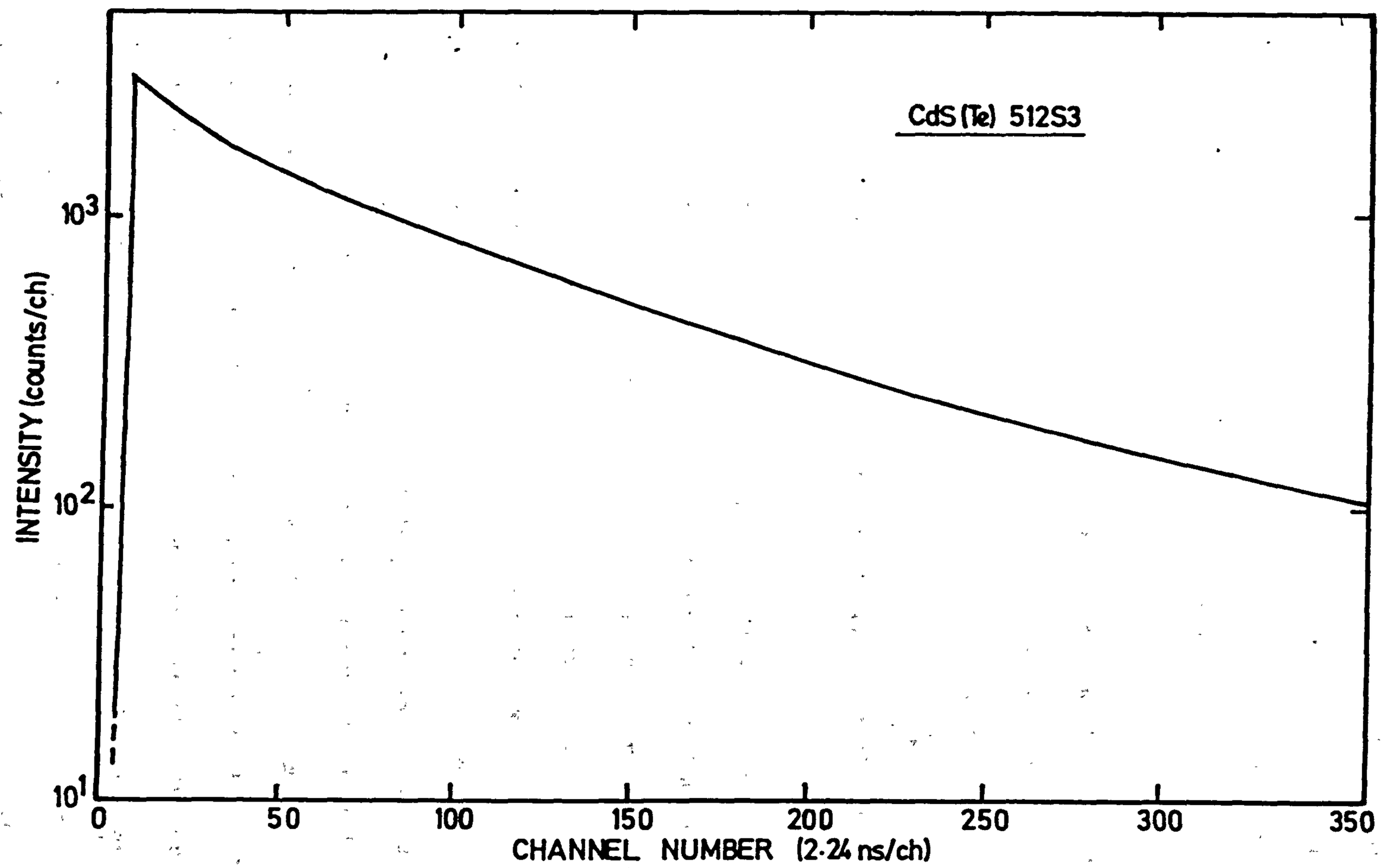

FIGURE 5·6 The decay profile of the luminesent emission from boule 512S3 at 80K when excited by 5·5 MeV alpha-particles.

$t_{1/e}$ to t_{1/e^2} for this boule was 0.37 (nearer to exponential than the platelet one). The variation of the decay times of this boule with temperature showed a similar pattern to that observed in the platelets. The decay remained constant in shape from 70 K to 170 K. Beyond this temperature the $t_{1/e}$ and t_{1/e^2} values started to decrease very rapidly as illustrated in Figure 5.7. At 294 K, they were 20 ns and 62 ns respectively.

Boule 518 was grown in cadmium vapour and had an average Te concentration of 7.2×10^{18} atoms/cc. It had rather poor optical quality. In general, the luminescent decays from this boule also were found to be fast and non-exponential. The decay times from this boule stayed unchanged up to 120 K, maintaining their values respectively at 64 ns and 210 ns. Beyond this temperature they started to decrease, reaching values of 14 ns and 56 ns respectively at 294 K as illustrated in Figure 5.8. In general, with this boule the values of the decay times and their variations with temperature were more similar than those of boule 512 to the values observed for the platelets 108.

The decay profiles of other boules examined were found to be similar, i.e. fast and non-exponential. They showed the same behaviour when the variation of decay time with temperature was investigated.

Boule 513 and 534 were grown in cadmium vapour and had an average tellurium concentration of 5.1×10^{18} and 8.6×10^{18} atoms/cc respectively. Their optical quality was not very good. At 98 K, the decay times were found to be 78 ns and 300 ns respectively for the former boule. At 294 K, they decreased to 15 ns and 56 ns respectively. As for the latter boule its decay times were found to be similar to the values observed in the platelets 108; namely, 56 ns and 190 ns respectively at 90 K, decreasing to 20 ns and 68 ns respectively at 294 K.

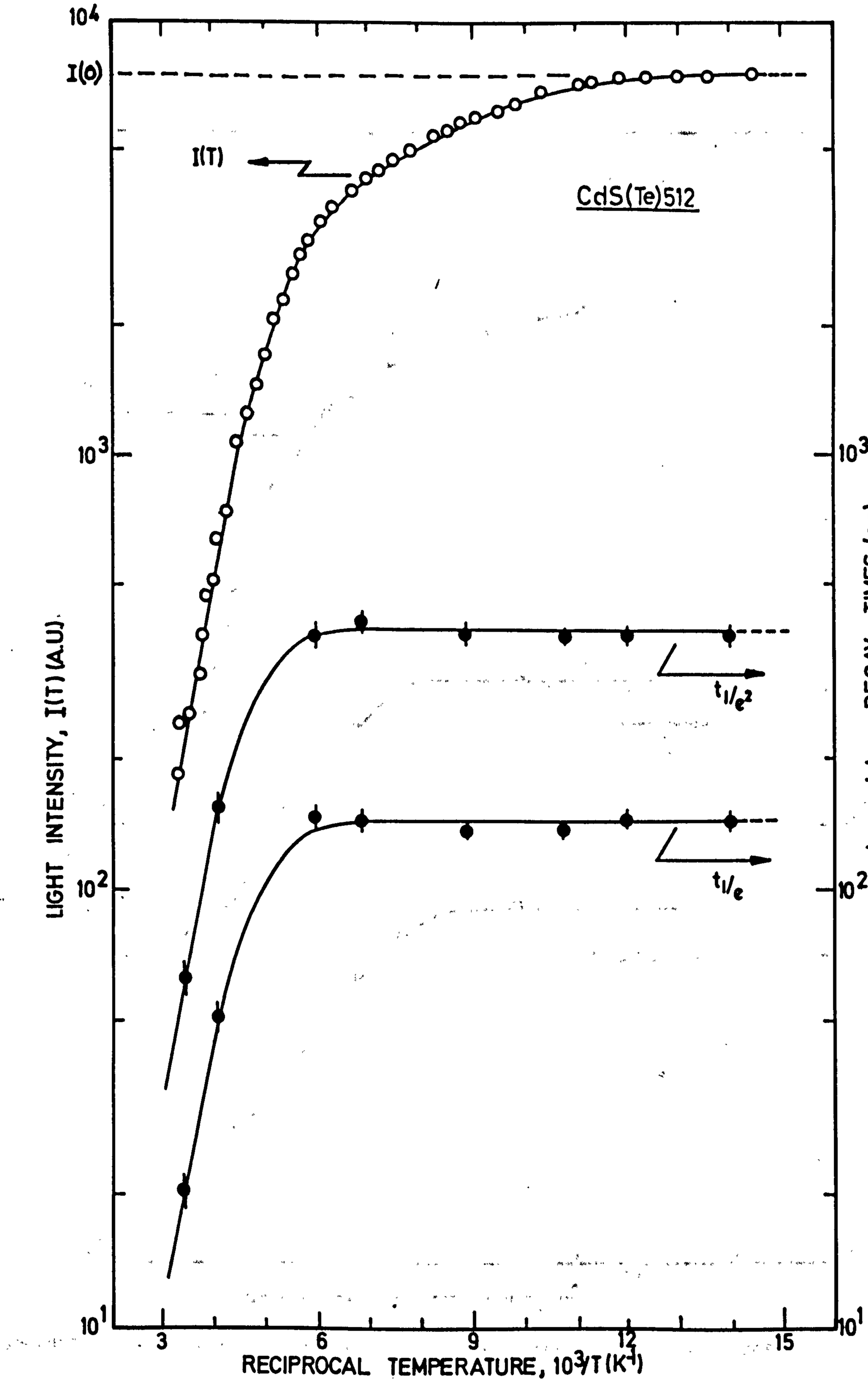

FIGURE 5.7 Variations of intensity and decay times of alpha-induced luminescence with temperature in CdS(Te) 512.

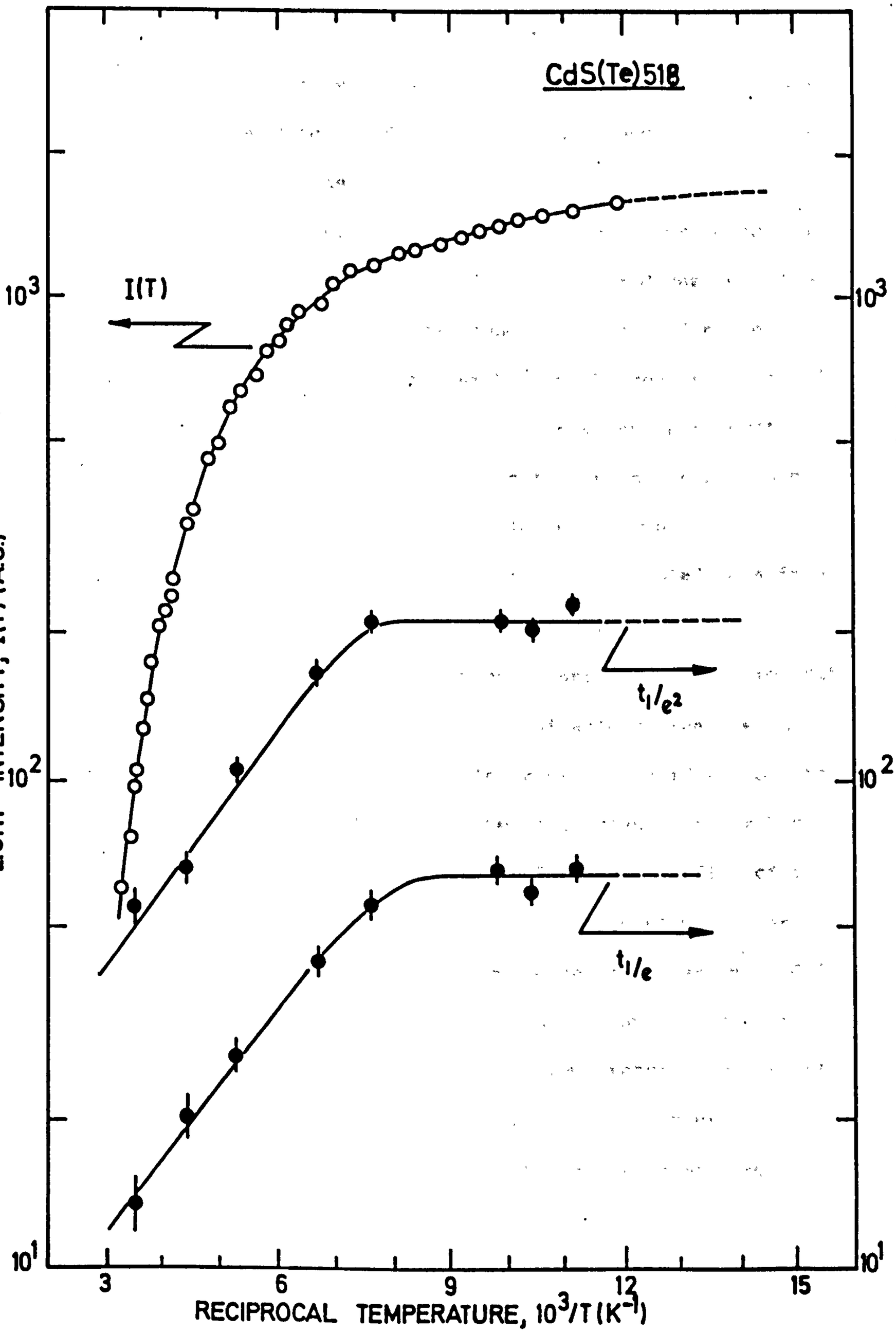

FIGURE 5.8 Variations of intensity and decay times of alpha-induced luminescence with temperature in CdS(Te) 518S1.

Boule 535 which was grown in sulphur vapour was the last one examined in detail. It had an average tellurium concentration of 9.7×10^{18} atoms/cc and was slightly darker than boule 512. The decay times at 95 K were found to be 78 ns and 228 ns respectively whereas at 294 K they decreased to 24 ns and 84 ns.

The heavily-doped boule 511 with an average tellurium concentration of 9.5×10^{19} atoms/cc exhibited a dark red colour and was very opaque. Since its luminescence efficiency was found to be low and since its emission spectrum was dominated considerably by the red band, we did not attempt a serious study of this sample. Only few decay profile measurements were made using α-particle excitation and decay times faster than those of the lightly-doped boules were found.

Lastly, it was decided to examine the pure CdS platelets from crystal growth run No.109 which had been grown under the same conditions of the CdS(Te) 108 platelets except there was no CdTe impurity added to the growth tube. It was thought desirable to measure the radioluminescence of pure CdS crystals in order to see if any of the radioluminescent properties of CdS(Te) are attributable to the host lattice and not to the tellurium impurity. The decay profile of a platelet 109 at 100 K was very fast (a few nanoseconds) which was consistent with the generally accepted luminescence mechanism in CdS (45,46). At room temperature, the signal was very small (and the existing signal was even faster than the low temperature one), so it was difficult to obtain a reliable decay profile. The thermal quenching of the luminescent emission was also found to be different from that of the CdS(Te) crystals, as shown below.

5.3.3 The Thermal Quenching Curves

The thermal quenching data for the α-induced luminescent emission from the CdS(Te) crystals was obtained by warming up the sample crystal

slowly from 70 K to 300 K and at the same time, counting the single-photons emitted (stop pulse rate). The background counts (obtained by closing the slit of the stop-PMT) were subtracted from the measured intensities. The stop-rate was again maintained at a low fraction of the known source intensity to avoid pile-up errors. In this way, the variation of the luminescent (light) intensity, I(T), with temperature was obtained for the various samples, and the results were plotted against the reciprocal temperature in order to perform graphical analysis. The thermal quenching curves were found to be smooth and almost identical in structure for all the samples examined, i.e. I(T) seemed asymptotic below 80 K but quenched rapidly at temperatures above 160 K. Since it was observed that the emission intensity from the CdS(Te) samples stayed nearly constant below 70 K down to 10 K (see Section 5.2.2), the asymptotic value of I(T) around 70 K was approximated to I(0), the luminescent intensity at 0 K. The accuracy of the analysis was slightly affected by the fact that the measurements stopped mostly before this asymptotic I(0) value was reached. Thus, the value of I(0) was varied (with strict limits) so as to optimize the fit in the quenching curves. The I(0) values derived in this way always allowed smooth extrapolation of the experimental data to lower temperatures.

In Figures 5.4 and 5.7 the thermal quenching curves for the platelet 108 and boule 512 are shown. All the curves observed generally showed the same basic trend, with the emission substantially quenched at room temperature.

It is usual to investigate the activation energies controlling the radiative recombination process graphically using a plot of $\log(I(0)/I(T)-1)$ vs $1/T$ as explained in Section 2.4.3. Such a plot is illustrated for the boule 512S1 in Figure 5.9. Rather striking and consistent results were obtained from this type of analysis. Below

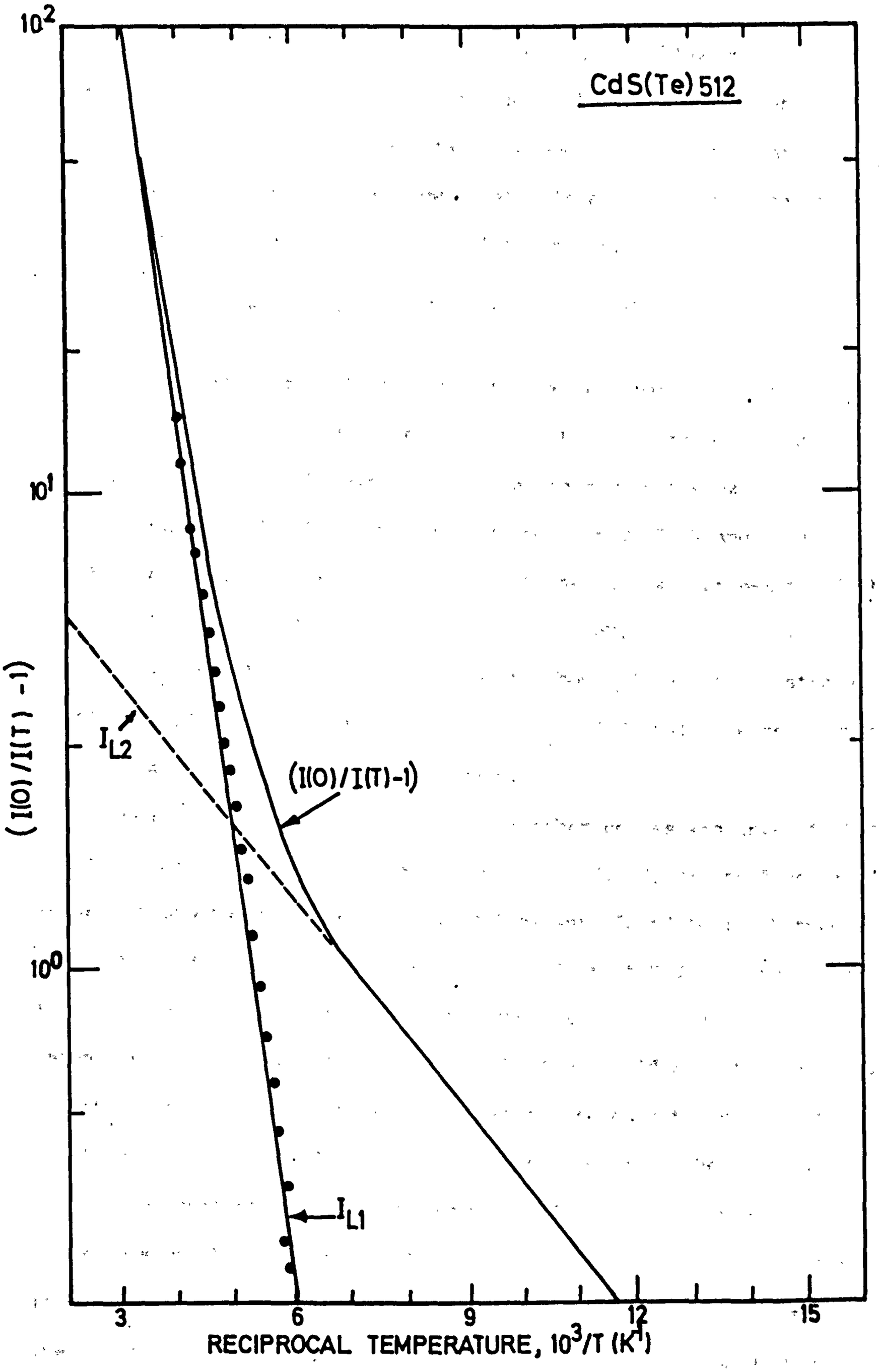

FIGURE 5.9 Graphical analysis of the thermal quenching curve I(T) of CdS(Te) 512S1 .

145 K, a very good fit to a straight line I_{L2} was obtained on a log-linear plot. Extrapolation of this line backwards and the subtraction of this contribution from the total gave another good straight line I_{L1} of much steeper slope. This shows that this analyzed function can be written as the sum of two exponential functions, i.e.

$$(I(0)/I(T)-1) = A_1 e^{-U_1/kT} + A_2 e^{-U_2/kT} \quad . \quad . \quad . \quad . \quad . \quad (5.1)$$

The slopes of the straight lines provide two activation energies, U_1 and U_2, which can readily be identified with the depth of the hole trap on the Te centre and the electron binding energy in the exciton (1,2). For the boule 512S1, the values were found U_1 = 0.17 eV and U_2 = 0.027 eV. In the same way, for the platelet 108S8 these values were estimated graphically to be U_1 = 0.14 eV and U_2 = 0.037 eV.

The thermal quenching curve for the boule 518S1 is illustrated in Figure 5.8 from the analysis of which U_1 and U_2 values were calculated to be 0.24 eV and 0.041 eV respectively.

When the thermal quenching of the other boules was investigated, similar pairs of activation energies were found. U_1 values fluctuated between 0.14 eV and 0.24 eV, and U_2 values were found to lie between 0.019 eV and 0.041 eV. These values for different CdS(Te) samples are tabulated in Table 5.1, together with the ratios of I(294), the luminescent intensity at 294 K, to I(0) which gives an idea of the degree of quenching at room temperature. This ratio was found to be a maximum (11%) in the platelet 108, but had decreased to 2% in the boules.

The constant multiplying terms A_1 and A_2 can be derived from the intercepts of the two straight lines I_{L1} and I_{L2} on the y-axis. The interpretation of these intercepts is heavily dependent on the exact quenching mechanism involved in each sample as shown by Klasens (68). It is interesting to note (Table 5.1) that A_1 (the hole intercept) varies over two orders of magnitude, A_2 (the electron intercept) remains

substantially constant at a value of 15. Clearly the magnitude of A_1 is sensitive to sample to sample variations but no meaningful correlations with any of the principal variables (Te concentration and stoichiometry) could be established.

A rather different structure was found in the thermal quenching curve of the platelet 109 (pure CdS). The α-induced radioluminescent intensity was constant up to 85 K. Then it began to decrease as the temperature was raised to 150 K. There was a plateau between 150 K and 195 K followed by another quenching drop, this time with a faster slope. Using the standard analysis, the following data were derived from these two slopes. Namely, $U_1 = 0.14$ eV, $A_1 = 3.7 \times 10^6$, $U_3 = 0.43$ eV and $A_3 = 7.4 \times 10^{10}$. The 0.030 eV electron activation energy was not apparent because the measurements were not extended to a sufficiently low temperature. A value of U_1 of 0.14 eV is characteristic of the hole traps in CdS. U_3 was not identified.

5.4 Beta-Induced Radioluminescent Properties

5.4.1 General

The same series of measurements, e.g. of decay profiles and thermal quenching were repeated at temperatures between 80 K and 300 K, using β-irradiation from a ^{90}Sr source. Since the ionization density with β-particles is lower than with the 5.5 MeV α-particles by a factor of ∿250 (5), one might expect significant differences in the behaviour of the luminescence. The β-induced luminescence is also interesting in that direct comparison can be made with the results of Cuthbert and Thomas (2) who used 400 keV pulsed electron-beam excitation in their work on CdS(Te) platelets.

The same cryostat and arrangements which had been used in the α-induced measurements were again employed. The β-source was located

inside the cryostat as near to the sample as possible. The light collection by the start-PMT was optimized and the usual precautions against pile-up were taken. Adequate time resolution for the purposes of the experiments was thus maintained. But, in general, the time resolution of the decay system was worse with these β-induced measurements. This was partly because the electrons coming from the β-source were of lower energy (∿1.0 MeV mean), and not monoenergetic, so that the light pulses produced by the particles were generally small and varied considerably in amplitude. Also, the larger volume of the samples used (since 2-3 mm thickness of CdS(Te) is required to stop the exciting β-particles) made the light collection from the samples difficult, and this was another source of spread in the time resolution. Fortunately, however, it was again possible to estimate the error in the measured values of $t_{1/e}$ (68) and therefore to calculate the actual decay time which was again found to be longer than the measured value.

5.4.2 The Decay Profiles

In general, the β-induced decays were found to be different, i.e. longer than α-induced ones. This difference was mainly apparent at the very start of the decay, i.e. in the fast component of the decay. This is clearly seen in the two β-induced decay profiles for platelet 108 shown in Figure 5.10, (a) at 150 K and (b) at 114 K. The decay times ($t_{1/e}$ and t_{1/e^2}) were calculated to be 205 ns and 507 ns respectively at 114 K using the curve in Figure 5.10(b). The hwfe of this curve was 3 ns so that the accuracy of the observed decay time was very high (an error of less than 1%). At 150 K the decay times were 220 ns and 715 ns respectively. As will be noticed from these two sets of values, the variation of the decay times when the temperature was increased from 80 K to 300 K showed an increase around 170 K. This

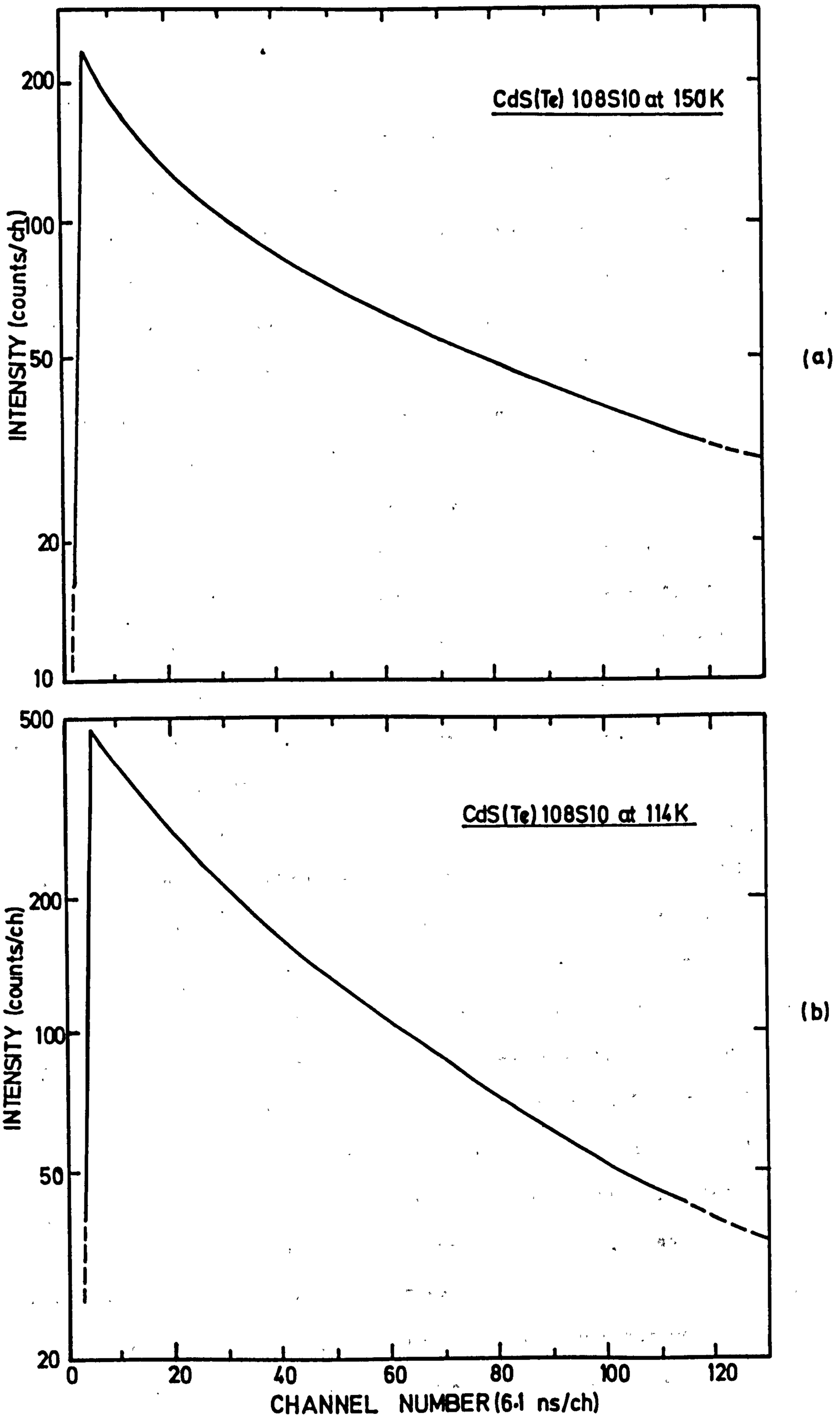

FIGURE 5.10 Decay profiles of beta-induced luminescent emission from platelet 108S10 at temperatures 150 and 114K.

was more apparent at long times, i.e. in the values of t_{1/e^2} as illustrated in Figure 5.11. Beyond this temperature, the decay times began to decrease reaching values of 12 ns and 43 ns respectively at 294 K. The hwfe of the decay at this temperature was about 10 ns; so this time, an error of about 11% was involved. Other useful information derived from the decay profile was the value of the ratio of $t_{1/e}$ to t_{1/e^2} at 90 K which was found to be 0.45 for this platelet. These ratios and the decay times (including the errors estimated (67) on them) for various samples are tabulated in Table 5.2.

The decay profiles from the boules were again found to be similar to those from the platelets. In Figure 5.12 the variation of the decay times with temperature observed with boule 512 is illustrated. At 90 K, the decay times were 255 ns and 640 ns respectively, the ratio of which is 0.40. Around 155 K, there was a larger increase in the decay times, after which they decreased rapidly becoming 18 ns and 56 ns respectively at 294 K.

Boule 518 responded in the same fashion to the β-particles and similar decay times were observed as shown in Figure 5.13. At 90 K, the values were 265 ns and 590 ns respectively (similar to the values found for the boule 512, see Table 5.2). Again, there was a maximum at about 180 K. The decrease of the decay times beyond this temperature was not as rapid as in the other samples. Consequently, the decay times were found to be much longer at 294 K; namely, 185 ns and 600 ns.

Values of 225 ns and 610 ns were found for the decay times of boule 534 at 90 K. Their variation with temperature showed a less pronounced maximum (see Figure 5.14). Beyond 155 K, $t_{1/e}$ and t_{1/e^2} decreased as expected to 28 ns and 65 ns at 294 K.

The last sample examined with the β-particle excitation was boule 535 which also responded in the same way as the platelet 108.

TABLE 5.2

The summary of β-induced radioluminescent results on various CdS(Te) crystals.

		Sample No.				
		108	512	518	534	535
Type		Platelet	S tail	Cd tail	Cd tail	S tail
I	$t_{1/e}$, ns	205	255	269	225	240
	$t^*_{1/e}$, ns	207	258	271	227	242
	t_{1/e^2}, ns	465	640	590	610	520
	$t_{1/e}/t_{1/e^2}$	0.45	0.40	0.45	0.37	0.46
II	$t_{1/e}$, ns	12	18	185	27	29
	$t^*_{1/e}$, ns	14	20	187	28	30
	t_{1/e^2}, ns	43	56	600	65	56
	U_1 , eV	0.18	0.20	0.19	0.22	-
	U_2 , eV	0.05	0.039	0.046	0.045	-
	I(294)/I(0)	1%	0.8%	2.3%	0.9%	-

I = Values at 90 K

II = Values at 294 K

$t^*_{1/e}$ = Corrected value of $t_{1/e}$ (67).

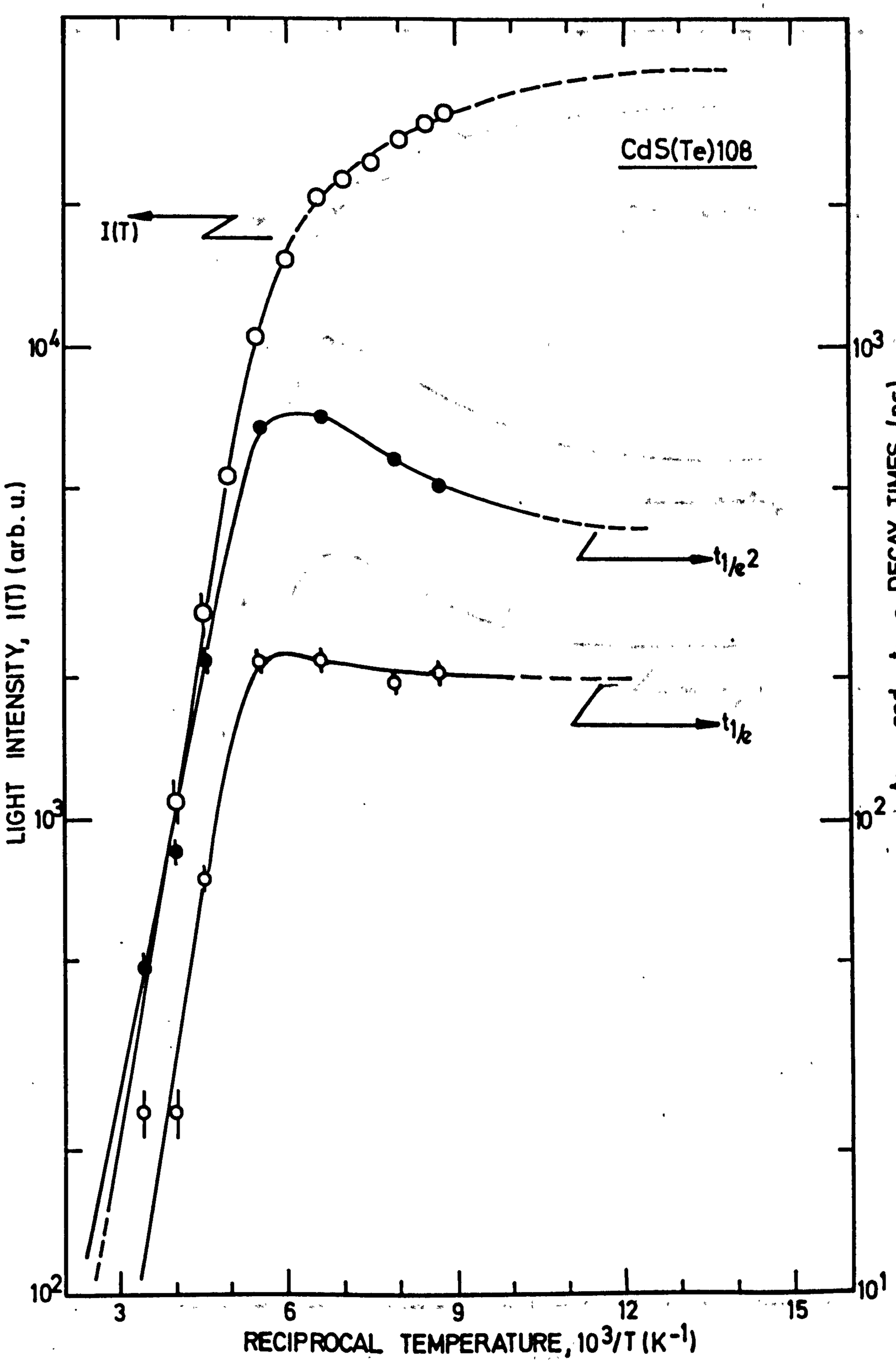

FIGURE 5.11 Variation of intensity and decay times of the beta-induced luminescence in CdS(Te)108S10.

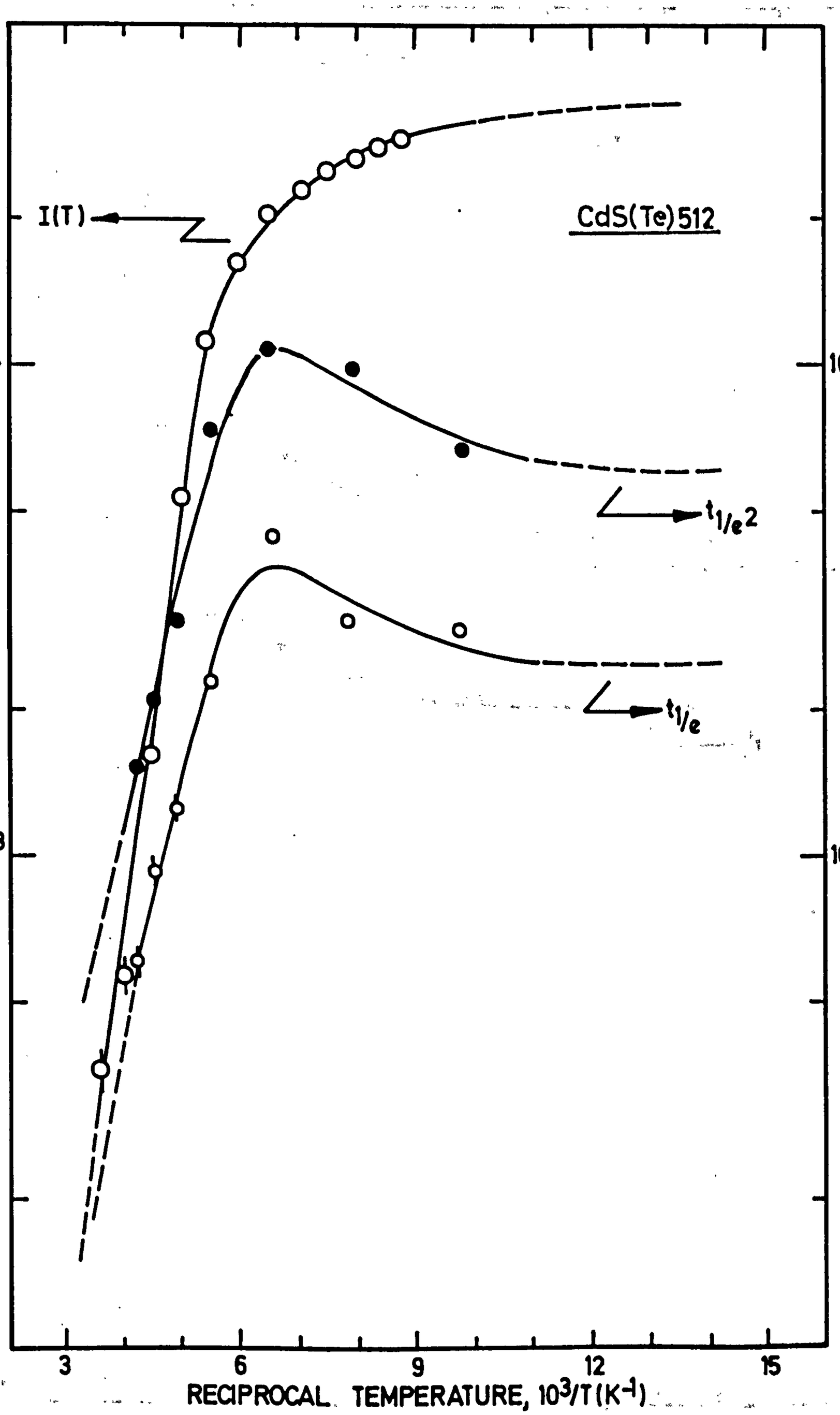

FIGURE 5J2 Variation of the intensity and decay times of the beta-induced luminescence with temperature in CdS (Te) 512S1.

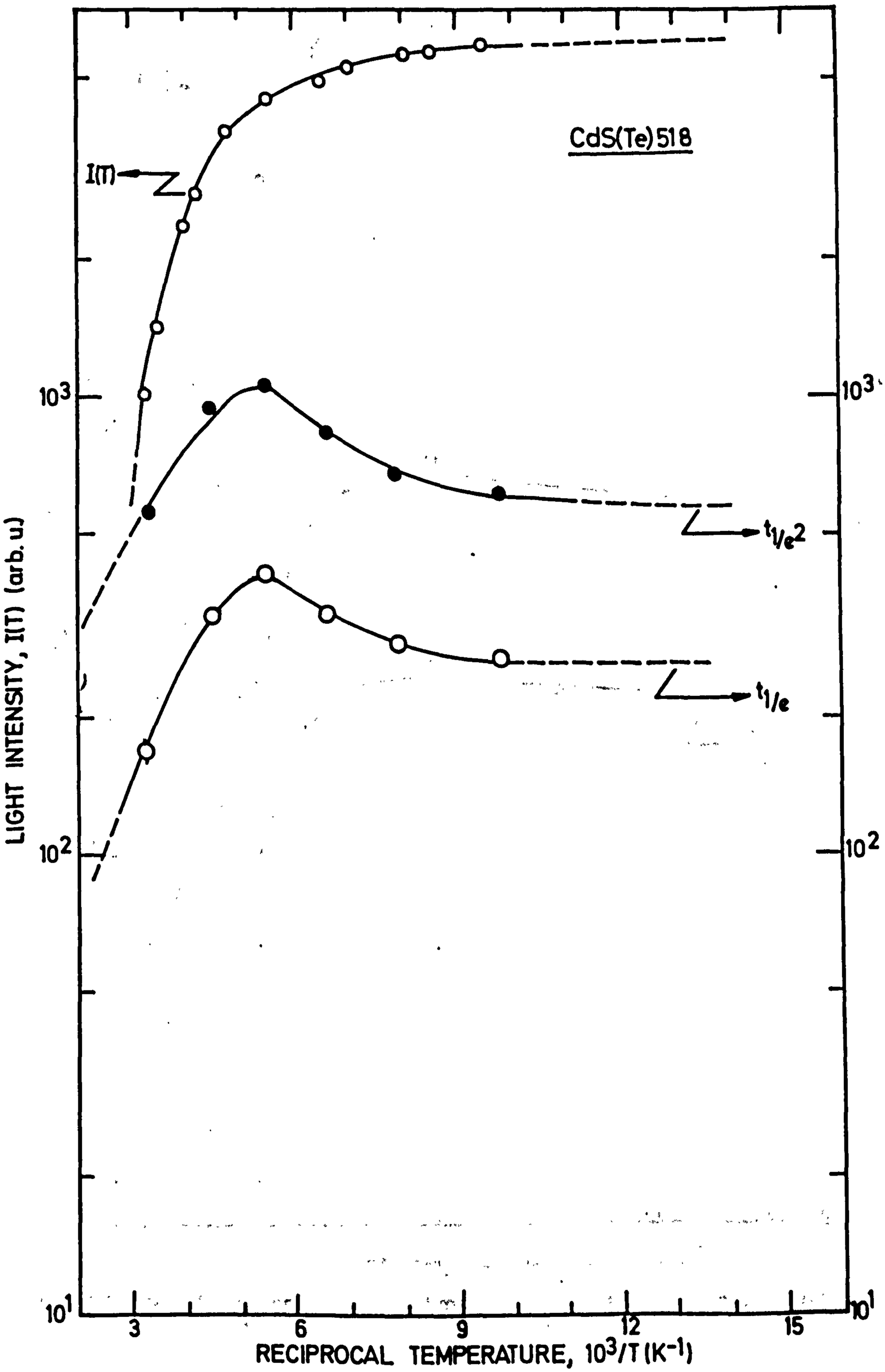

FIGURE 5.13 Variations of intensity and decay times of the beta-induced luminescence with temperature in CdS(Te) 518S1.

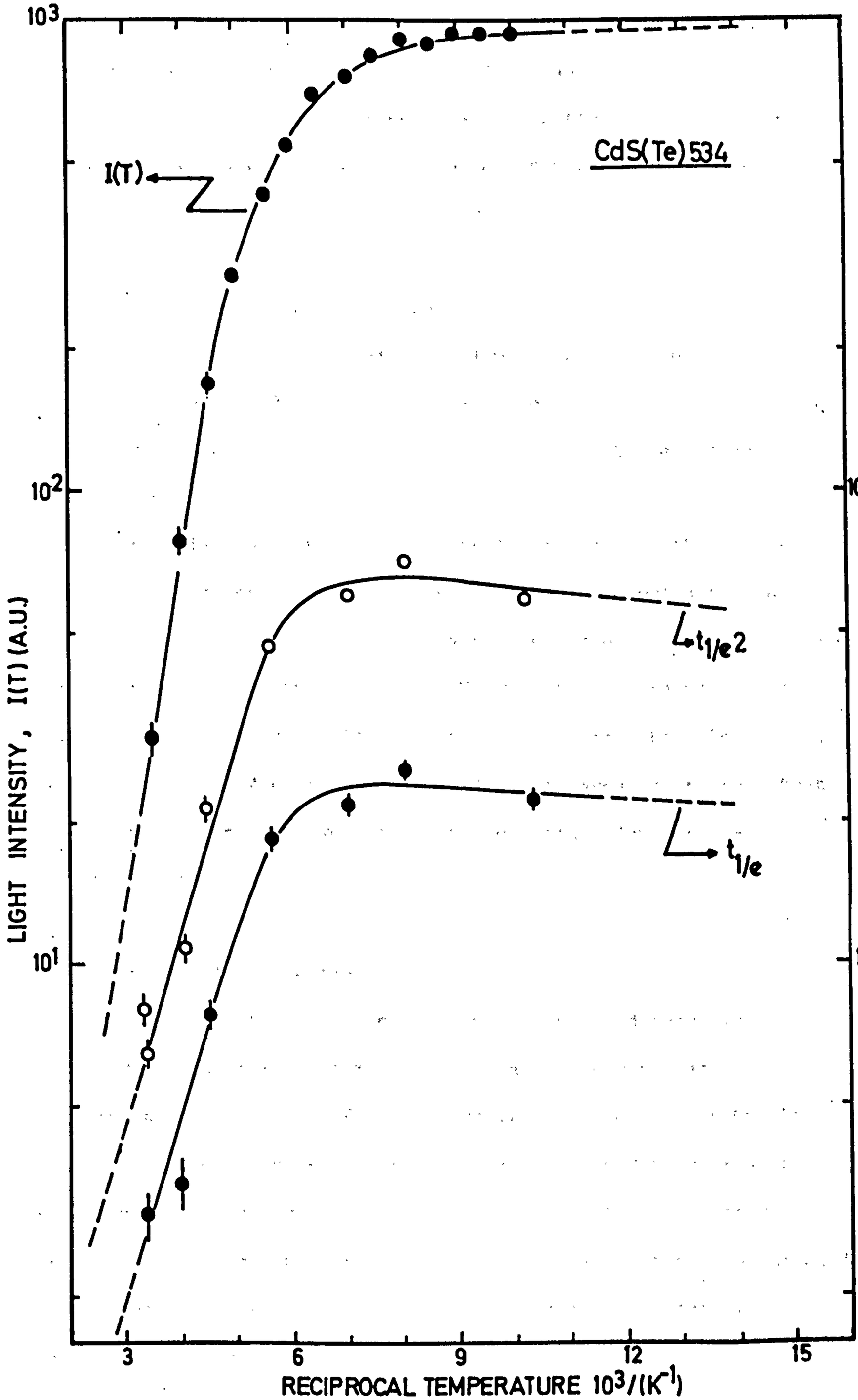

FIGURE 5.14 Variations of decay times and intensity of beta-induced luminescence with temperature in CdS(Te)534S1.

The two decay times were found to be 240 ns and 520 ns at 90 K. Their variation with temperature is shown in Figure 5.15. The values of decay times decreased rapidly beyond 155 K and became 29 ns and 56 ns respectively at 294.

5.4.3 The Thermal Quenching Curves

The variation of the β-induced luminescence intensity with temperature between 90 K and 300 K was also studied. In general, the thermal quenching curves were similar to those obtained using α-particles.

The variation of the luminescent intensity with the reciprocal temperature has been plotted on the same diagram showing the variation of decay times with 1/T. The activation energies derived from these curves are tabulated in Table 5.2. U_1 was found to range between 0.18 eV and 0.22 eV for different samples, whereas the values of U_2 varied between 0.04 eV and 0.05 eV. It is interesting to note that the activation energies were found to be similar for both α- and β-induced luminescence.

5.5 Time Resolved Spectra

Time-resolved spectroscopy is one method of determining the mechanism of radiative recombination in a luminescent material. Cuthbert and Thomas (2) made time-resolved measurements on CdS(Te) samples because the non-exponential decay, together with broad band emission from this material, suggest donor-acceptor pair recombination as the origin of the 600 nm emission band. However their measurements showed that this was not the case since no change was observed in the emission spectrum during the decay.

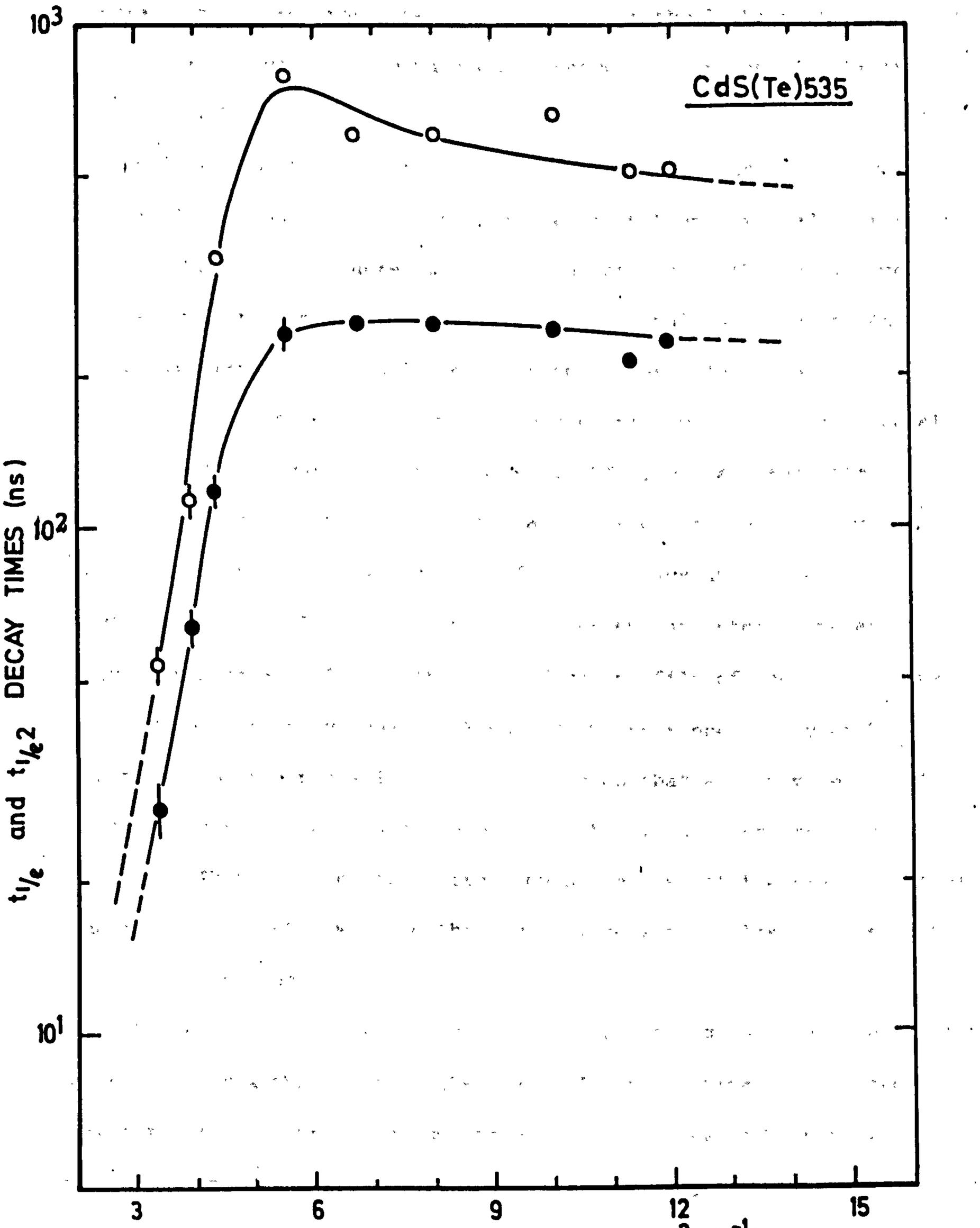

FIGURE 5.15 Variations of decay times of the beta-induced luminescence with temperature in CdS(Te)535S5.

Similar measurements on our samples were carried out. The adjustable monochromator (MS-1) was located in the light path to the stop-PMT and by varying the wavelength between 530 nm and 670 nm the decay time of the decay at different wavelengths was examined (i.e. the complement of the time-resolved spectroscopy). For this purpose, the platelet 108 was held at a temperature of 90 K and excited by the 5.5 MeV α-particles. There was slight variations in the decay times observed with this method. The $t_{1/e}$ and t_{1/e^2} values showed a decrease in the same manner towards longer wavelengths as illustrated in Figure 5.16. In order to minimize the possibility of any instrumental error, the decay system parameters (e.g. EHT's, pulse rates, time resolution) were maintained constant at their optimum values throughout the measurements. The hwfe values of these decays at various wavelengths were about 1.2 ns. Keeping all system parameters constant and removing the optical filter (MS-1), a decay profile of the platelet was obtained, with decay values of 52 ns and 195 ns respectively at 90 K. Examination of the plots in Figure 5.16 shows that at a wavelength of about 590 nm the decay times are equal to the values measured without a filter. This is a sensible situation since most of the single photons reaching the stop-PMT will be those with wavelengths close to the peak of the emission band.

While the magnitude of the effect shown in Figure 5.16 is not large (∿15% maximum) it is quite real. The statistical errors are less than 3% as shown by the smooth behaviour of the data points. Systematic errors have been eliminated by retaining all the system parameters constant, the filter position only being changed. These results illustrate the sensitivity of the present technique and provide clear evidence that when α-particles are used, the radioluminescent spectrum from CdS(Te) crystals is not time invariant as Cuthbert and Thomas found it to be with electron excitation.

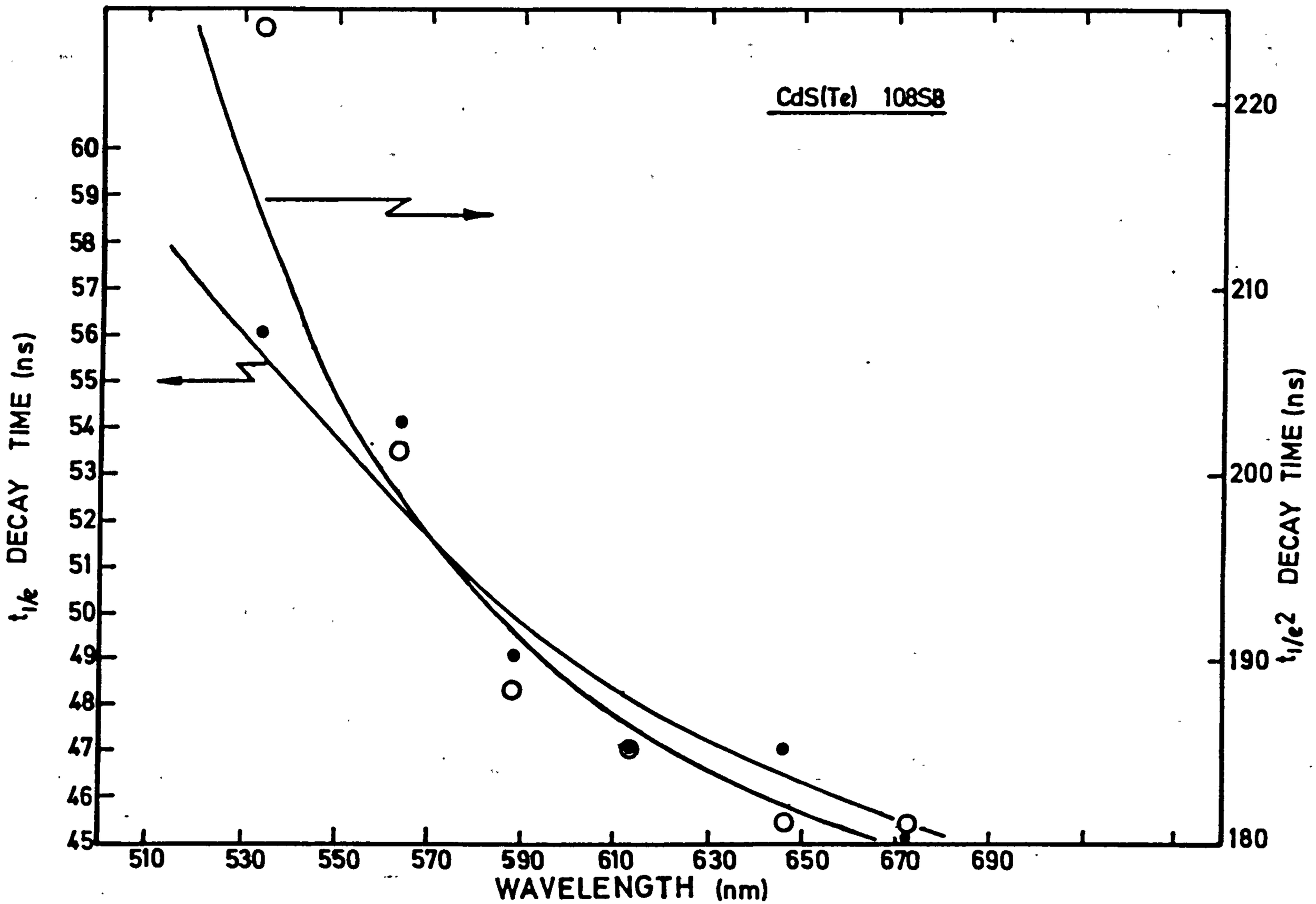

FIGURE 5.16 Variations of the decay times of platelet 108S8 with the wavelength of the luminescent emission at 90K, when excited by 5.5 MeV α-particles.

5.6 The Scintillation Efficiency of the Boules

The results outlined in the previous sections have shown the similarities between the radioluminescent properties of the platelets and boules of CdS(Te). Both types of crystal had the same radioluminescent emission band centred around 600 nm and the decay times of light from both crystals have been found to be similar with, however, the alpha decay times significantly shorter than the beta ones (by a factor of four in most cases). The last important parameter to be checked with the boules, before their usefulness as scintillators could be verified, is whether these large CdS(Te) crystals have as high a luminescence (scintillation) efficiency as that of the platelet crystals.

In order to estimate the luminescent efficiency, the boule examined was coupled optically to K-22 silicon photodiode and was irradiated with γ-rays of known energy (see Chapter 3). W_{eff}, the observed effective γ-energy required per ion pair, was calculated from the pulse-height spectrum obtained in each case. These results obtained with different γ-rays and the experimental arrangements etc. will be described in the next chapter where the response of the proposed γ-ray detector will be discussed in detail.

Among the various boules grown No.512 provided the best results because of its better optical quality, i.e. transparency to its own light. With this boule of about 0.5 cc volume values of W_{eff} were measured and found to be ranging from 22 eV/ip to 32 eV/ip, depending on the γ-energy used, the geometry of the detector and the light collection. (This compares with 24 eV/ip measured in a thin platelet crystal). These values indicate the existence of a high luminescence (scintillation) efficiency in this boule. This large crystal was about 5 mm thick and some correction for self absorption of the luminescence would be necessary to calculate the true quantum

efficiency. Clearly, if Equation 3.2 is used the scintillation efficiency of this boule is found to be comparable with that of the platelets (i.e. the quantum efficiency of the luminescent recombination is ∿70%).

5.7 Conclusion

Radioluminescent measurements have been carried out on CdS(Te) crystals, both platelets and boules and, as the result, new features have been observed. The lightly-doped (10^{18} - 10^{19} atoms/cc) crystals produced almost the same emission spectrum and the same thermal quenching parameters found by the others, but some discrepancies were observed in their decay profiles and the time-resolved spectra.

When different excitations (UV and α-particle) were used, the emission spectra at low temperatures remained almost the same, that is, a broad featureless band varying around 590-600 nm was observed. Some small deviations in the peak position of this orange band were thought to be caused by the use of different spectrometers. The runs at very low temperatures (10 K) did not provide any extra information except to confirm that the efficiency of the orange emission is almost constant between 10 K and 70 K.

The first striking results were observed when the decay profiles induced by α- and β-particles were investigated at temperatures between 70 K and 300 K. Cuthbert and Thomas (2) established that the decay for excitation by electrons is exponential and at the same time $t_{1/e}$ increased in value above 20 K reaching a maximum of 4 μs at ∿200 K. Above this temperature the decay time showed a sudden decrease following the quenching of the luminescence and decreased to a value of about 300 ns at room temperature (see Figure 2.6). The decay times found in our samples were always faster than reported by Cuthbert and Thomas. Though there were slight variations in our samples, the decay times

were of the order of 250 ns when excited by β-particles and became very fast, i.e.~100 ns or less, when excited by α-particles. When the temperature was increased the decay times did not change very much, staying almost constant up to ~150 K with α-excitation. In some of the β-induced decays, there was a small increase around ~170 K, especially at long times so that $t_{1/e}$ did not change very much; the effect was small but quite consistent as observed in several samples, particularly with the t_{1/e^2} values. With increasing temperature, the decays started to decrease to a value $\lesssim$ 20 ns. There was an exceptional case where the decay did not quench appreciably. This was observed with the β-excitation of boule 518 which was grown in excess Cd. The intensity of luminescence from this boule did not quench very much either, in comparison with the other samples. This is thought to be due to the excess S vacancies in this crystal which introduce donor states. Roessler (3) showed that the addition of donors to CdS(Te) leads to an increase in the efficiency of the luminescence at room temperature.

The implications of the above results on the proposed models of the luminescence mechanism in CdS(Te) will be discussed in detail in Chapter 7. However, it is interesting to note that at the lowest temperatures reached in our samples the value of $t_{1/e}$ for β-excitation was already ~200-250 ns (i.e. lower than the proposed fundamental Te^* exciton lifetime of 300 ns proposed by Cuthbert and Thomas for the isoelectronic Te trap). This tends rather to cast doubt on the validity of their model as will be shown in Chapter 7.

The observed decay lifetimes and quenching characteristics are quite attractive from the point of view of applications to scintillation detection. The lifetimes are acceptably short (~250 ns at 100 K) and intensity can be traded off for a shorter response time at higher

temperature. It is clear, however, that cryogenic (i.e. ∿100 K) operation is necessary for good luminescent efficiency. Obviously the possibility of particle discrimination exists because of the very different decay times under α- and β-excitations.

CHAPTER 6

CRYOGENIC CdS(Te)-Si(Li) GAMMA DETECTOR

6.1 Introduction

The high luminescence efficiency, the high atomic number and the fast luminescent decay in CdS(Te) makes this material an attractive scintillator in radiation detection as already discussed in Chapter 1. Up until now it had only been possible to grow small platelets of this material with the desired properties. Attempts by Madden et al (7) and others to grow boules of CdS(Te) which are necessary for detecting the penetrating γ-rays were unsuccessful in that the large crystals grown by them showed very poor luminescent and optical properties compared with those of the small platelets of the same material. Even Mikulyak (56) recently grew some large CdS(Te) crystals, he did not report much about their suitability in gamma-work.

On the other hand, both the platelet and the boule type crystals of CdS(Te) grown by us exhibited similar radioluminescent properties (see Chapter 5). There would appear, therefore, to be no obstacle to the use of a boule of CdS(Te) as a scintillator in conjunction with a cryogenic Si(Li) photodiode to make a composite nuclear particle detector.

We tested the performance of such a composite detector using first 5.5 MeV α-particles and then various γ-rays, the energies of which ranged from 60 keV up to 1 MeV. At the same time as generating pulse-height spectra from the nuclear radiations these measurements permitted an estimation of the luminescence efficiency of the crystal to be made. During this work, we examined the light collection from these scintillators since it plays an important role

in the final response obtainable from any scintillation detector. In this chapter, we give the results of these investigations made on the application of CdS(Te) crystals to nuclear particle detection.

6.2 The Cryogenic Photodiode, the Cryostat and the Electronic Arrangement

The comparison of lithium-drifted silicon diodes with photomultipliers as scintillation light sensors has already been made in Section 1.5 of Chapter 1. There it was pointed out that at the wavelength concerned (600 nm) a Si diode is superior to a photomultiplier because it has a higher quantum efficiency. But, we have also pointed out that the high noise from Si at room temperature reduces this advantage. On the other hand, if one uses a cryogenic Si(Li) photodiode as indicated by Bateman and Özsan (32) the noise performance improved considerably.

Two stringent conditions are therefore imposed on the cryogenic Si(Li) diode by the proposed application, namely

(1) Very low noise.

(2) A capacity to be coupled directly to the scintillator.

The 2π K-line detectors manufactured by Simtec Industries Ltd. meet both these criteria. The detector noise contribution is reckoned at less than 0.5 keV fwhm at 77 K by the manufacturers and the devices feature a deep diffused junction with a silicon window of 0.2 μm thick. An additional advantage is that storage of the device at 77 K is not essential. The model K-22 diode which was used successfully in our previous work (32) was found suitable for this work as well. Having 20 mm diameter and 2 mm active depth, it provides a suitable diameter for coupling to a cm diameter scintillator and adequate depth for light absorption. It also has a low capacity (25 pf).

Since the window of K-22 could be coupled to the scintillator directly, the light collection was improved considerably, and with it the energy resolution as explained in Section 1.3.3 of Chapter 1. This direct coupling facility of the scintillator to the photodiode at low temperature was also desirable since the luminescence efficiency of the CdS(Te) was a maximum at these temperatures.

A cryostat for our composite detector was developed and a sectional diagram is shown in Figure 6.1. The K-22 diode was mounted vertically on the top of a cold finger cooled through a liquid nitrogen reservoir made from stainless steel. The CdS(Te) scintillator was directly coupled to the photodiode by a silicone compound. Signal leads to the charge-sensitive and preamplifier and the thermocouple wires (copper-constantan) to the thermocouple amplifier passed out through the vacuum sealthrough terminals on the side windows as shown in Figure 6.1.

The noise of the cryogenic Si(Li) diode is lower than the noise of the best room temperature charge-sensitive amplifier. Selection of the preamplifier therefore determines the system performance. The Ortec model 130-3F was found to give the best results - namely, a noise fwhm of 1.9 keV(Si). In order to avoid any pick-up due to long connecting leads, the 130-3F preamplifier was located immediately beside the cryostat.

A block diagram of the electronic arrangement used for our composite radiation detector is shown in Figure 6.2. The pulses from the 130-3F preamplifier were shaped in a University Series amplifier, model 250 (4 μs time constant) and passed to a 512 channel pulse-height analyzer (NS-605). A HT unit supplied the bias up to 200 V for the diode and a mercury relay pulser provided calibration for

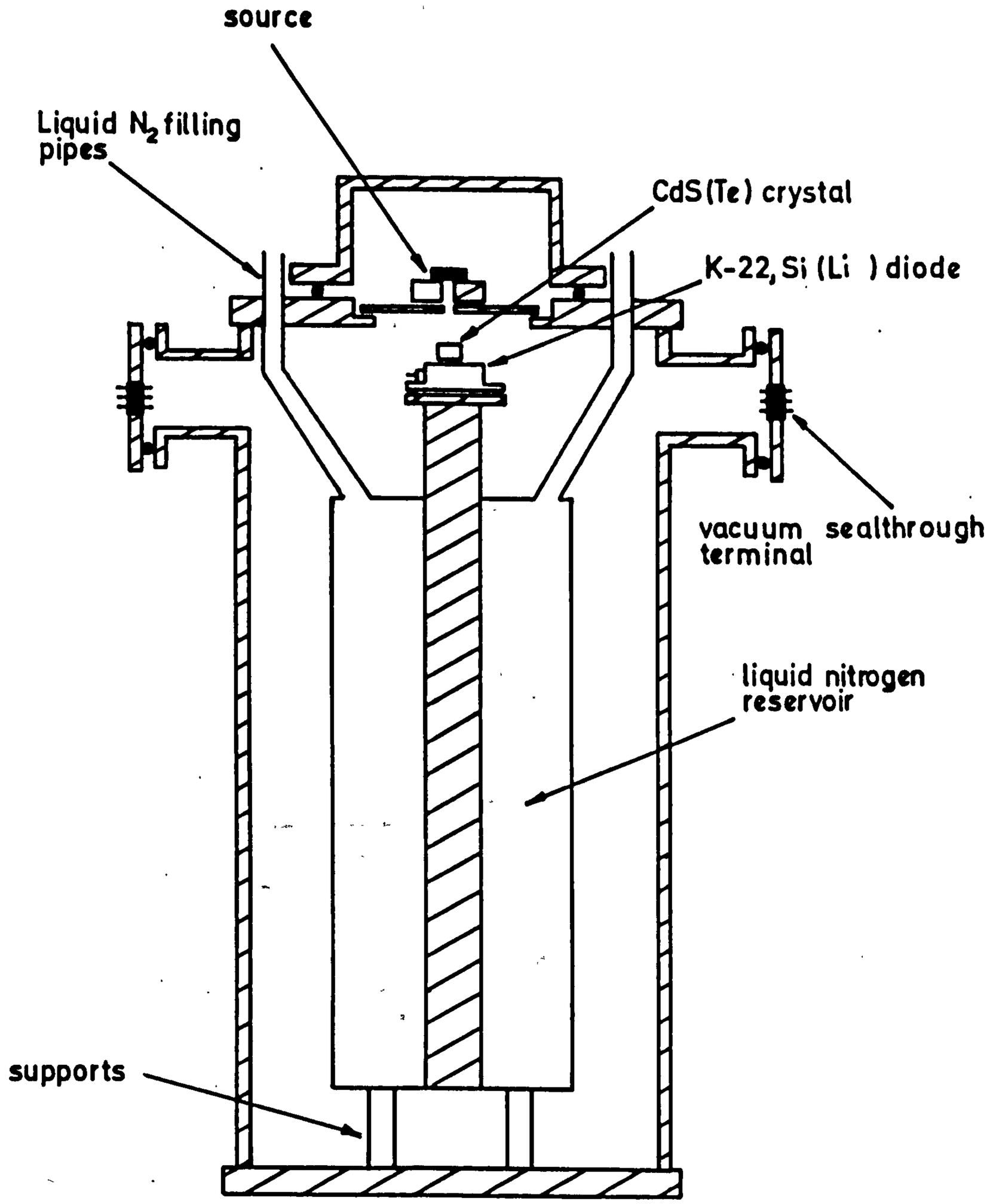

FIGURE 6.1 A sectional diagram of the photodiode cryostat

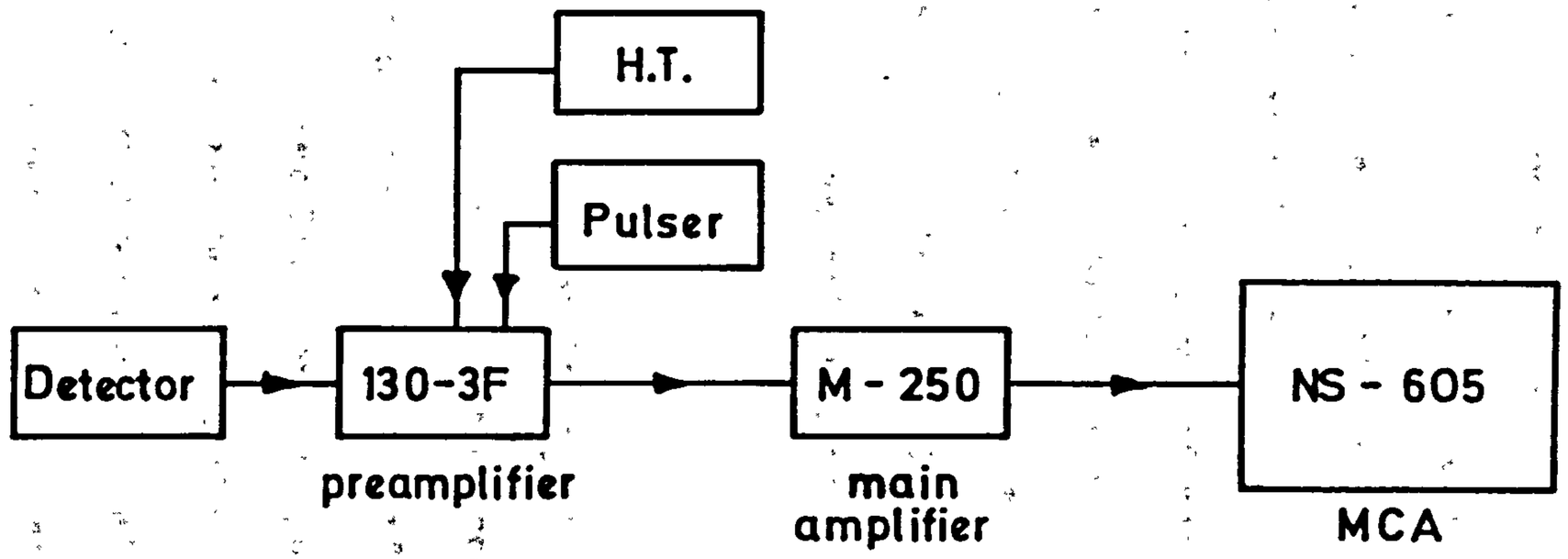

Figure 6.2 Block diagram of the electronic set-up used for CdS(Te)-Si(Li) detector

the system as will be shown in the next paragraph. This calibration permitted the charge deposited in the photodiode by the light from the CdS(Te) scintillator to be measured in terms of the energy which would be required to be deposited directly in the silicon to produce the same number of ion pairs. This quantity was referred to as keV(Si) to distinguish it from the energy of the particle incident on the scintillator. The number of ion pairs in any given signal may be found by dividing this quantity by 3.6 eV, the mean energy required to produce one ion pair in silicon (34).

The mercury pulser supplied pulses precise in amplitude to the test capacitor at the input of the 130-3F preamplifier for the calibration of the electronic chain. The dial of the mercury pulser itself was calibrated in terms of keV(Si) with the help of pulses produced in the Si(Li) diode by 59 keV γ-rays from an ^{241}Am source so that the output from this pulser in divisions was proportional to energy in keV(Si).

6.3 Results Using α-Particles and Platelets

The estimates of the luminescence efficiency of the first CdS(Te) crystals grown by us were performed using the cryogenic Si(Li) detector (see Chapter 3). For this purpose a small platelet from the crystal growth run No.108 was coupled to the K-22 silicon photodiode at 90 K and then irradiated by 5.5 MeV α-particles. The pulse-height distribution corresponding to this detection arrangement has already been given in Figure 3.3. In this section, we discuss some further detail of this α-particle detection system.

When we irradiated a small platelet, 108S1, with 5.5 MeV α-particles, most of the scintillation induced emerged from the thin edges and the sharp corners of the sample. This is due to high

refractive index of the material ($\sim$2.5). To overcome this difficulty, a thin aluminium reflecting foil was placed around the sample. This improved the light collection considerably. In this way, the pulse-height distribution shown in Figure 3.3 was obtained. The main α-peak in this distribution corresponds to a signal of 2.2×10^5 ion pairs in the silicon photodiode from which an overall scintillation efficiency figure, W_{eff} of 24 eV/ip for 5.5 MeV α-particles was deduced. Assuming a 50% light transfer efficiency from the scintillator to the photodiode, we derived a quantum efficiency of luminescence of 60-70% (see Chapter 3). In the pulse-height spectrum, in addition to the low energy tail due to straggling a small, high-energy peak was observed close to the main α-peak. This is due to irregularities and the crystalline boundaries in the platelets which lead to different light collection paths from different parts of the scintillator to the photodiode.

The energy resolution of this main α-peak is found to be 6.6% fwhm. This is a reasonable resolution figure, but much poorer than one would expect from the ion pair statistics, viz. $\frac{2.36}{\sqrt{2.2 \times 10^5}} = 0.5\%$. It seems reasonable to assume that poor light collection due to the high refractive index and bad sample geometry is responsible for the discrepancy.

6.4 Light Collection from CdS(Te) Boules

Increasing the volume of a scintillator for better detection efficiency we sacrifice the light collection efficiency. At the same time, the extra variance arising from the differential light collection from the large volume of the scintillator introduces broadening to the pulse-height spectrum. Therefore, the final shape of the pulse-height

spectrum recorded depends considerably on the optical properties of the scintillator (e.g. its transparency and refractive index), its geometry and the perfection of the optical coupling between the scintillator and the photon detector.

Some preliminary experiments on the various large CdS(Te) boules were carried out with a view to increasing the light transfer efficiency to the K-22 diode. At the same time, by comparing the results obtained, the best boule for gamma-detection was selected. Some measurements were carried out using the cryogenic photodiode system and some at room temperature with a photomultiplier. Polished, roughened and white painted (TiO_2) finishes were tried and the last named adopted by far the best.

In general, the boules were less transparent than the platelets. Among the various boules, the ones grown under excess S vapour pressure and containing a smaller Te concentration had a better optical quality. Boule 512 was one of them. An attempt was made to find out the transparency of this boule to its own radiation by measuring its absorption length at 600 nm. For this purpose, the "Optica Spectrometer (CF 4N1)" in the Applied Physics and Electronics Department of this University was used. From the absorption spectrum of the sample at room temperature, an absorption length of 3.5 mm at 600 nm was calculated assuming the refractive index of the material as 2.5. This is rather a short absorption length for a scintillator, a value greater than one centimetre is required. On the other hand, the transparency of the CdS(Te) boules improved considerably at low temperatures as observed visually. (Unfortunately no absorption measurements could be made at low temperatures to verify this).

As for the measurements made to compare the amplitudes of the light pulses from various boules, sample 518S1 was used initially. This was a conically shaped sample cut from boule 518 grown under excess Cd. It had a height of 1 cm, large diameter of 1 cm and small diameter of about 2.5 mm. 5.5 MeV α-particles from an ^{241}Am source were used to induce the scintillations and the variations in the light pulses were studied with respect to conditions of the surfaces of the sample, i.e. by roughening or polishing them. We found that bigger pulses were obtained if both ends of the crystal were polished. The polishing was done on a lapping wheel with a diamond paste down to a grit size of 1 μm to ensure a good optical finish.

We carried out similar measurements on another boule and found similar results. Sample 513S2 cut from boule 513, grown under excess Cd, was a disc of 2 mm thick and 10 mm in diameter. When one side of it was roughened, the light collection efficiency became poorer, whereas larger pulse-heights were again observed when both surfaces were polished. At this stage an attempt was made to find a reflective coating for the scintillator in order to maximize the light collection on the photodiode. A reflective aluminium foil was not a good solution. What is needed is a diffuse type coating with around 100% reflectivity at 600 nm wavelength so that most of the light will come out from the polished and uncoated surface looking towards the photodiode. A diffuse white paint, TiO_2, was found to be ideal for this purpose. We observed pulses which were about 25% larger when 513S2 was coated with this paint.

Both boules 518 and 513 were opaque and so their optical quality was not very good. Thus, most of the light produced by efficient radiative recombination in these crystals was absorbed in the volume before it could reach the photodiode. Having a low Te concentration, boule 512 (grown under S excess) had a better optical quality. Since

this was the most transparent boule, we selected this crystal for our gamma work. From this boule with its original cylindrical shape we tried to cut a uniform piece with no cracks in it. We ended with sample 512S1 which had a volume of about 0.5 cc but an undesirable geometry. It took the form of a non-uniform semidisc 5.7 mm thick and 10 mm in diameter. This shape was unavoidable because we did not wish to sacrifice any of the bulk volume (more important for gamma detection) in shaping the sample to a regular geometry.

After polishing all the surfaces, the light collection from various alternative surfaces of the sample 512S1 was examined. There was maximum light coming from one surface when the sample was irradiated by penetrating gamma-rays. This surface therefore was coupled to the photodiode using a very thin layer of a silicon fluid (MS200/60.000 CS from Hopkin and William Ltd.). This optical coupling material improved the light transfer efficiency from the scintillator to the photodiode and, at the same time provided good mechanical stability and thermal contact. In this way, a composite detector, i.e. the CdS(Te) scintillator — K-22 silicon photodiode was prepared for the γ-ray studies. The light transfer efficiency was again increased using the diffused reflective coating (TiO_2) on all the surfaces of the sample except that looking into the photodiode.

6.5 Gamma-ray Spectra

6.5.1 Introduction

With the cryogenic detector described above, various γ-rays of different energies were used and the resultant pulse-height spectra studied. The low temperature (about 110 K) for the operation of the detector was maintained in the cryostat, in which the source was located as well.

6.5.2 Response to 59 keV Gamma-Rays

First the detector was irradiated with 59 keV γ-rays from an ^{241}Am source. The source was located about 2" above the detector and a glass absorber of 1/8" thickness was used to stop α-particles from the same source reaching the detector.

The distribution in Figure 6.3 containing three separate peaks was obtained with the unpainted scintillator. The 8.5 keV(Si) peak corresponds to the detection via the CdS(Te) scintillator, i.e. the production of scintillations by γ-rays in 512S1 and the detection of these visible photons by the silicon diode. Not all of the γ-rays were detected in the scintillator. Some of them penetrated directly to the diode and were detected there. The 59 keV(Si) peak is produced in this way. The third peak is the pulser test signal which gives the expected 2 keV(Si) fwhm. From the genuine 8.5 keV(Si) photopeak, the value of W_{eff} was calculated in the following way:

$$\text{Number of i.p's produced in the Si diode} = (8.5\times10^3)/3.6$$
$$= 2360$$

$$W_{eff} = (\text{input } \gamma\text{-ray energy})/(\text{i.p's produced})$$
$$= (59\times10^3)/2360$$
$$= 25 \text{ eV/ip}$$

The resolution of this photopeak was found to be about 36%.

The scintillator was painted with TiO_2 and then re-irradiated with the same source. This time, the effect of the collimation of γ-rays was examined as well. The results are given in Figures 6.4 and 6.5. There are X-rays coming from the source ranging in energy from 16 keV to 48 keV and detected directly in the Si(Li) diode in the same way as the 59 keV ones. The spectrum in Figure 6.4 was obtained when the source was not well-collimated. Because of the action of the

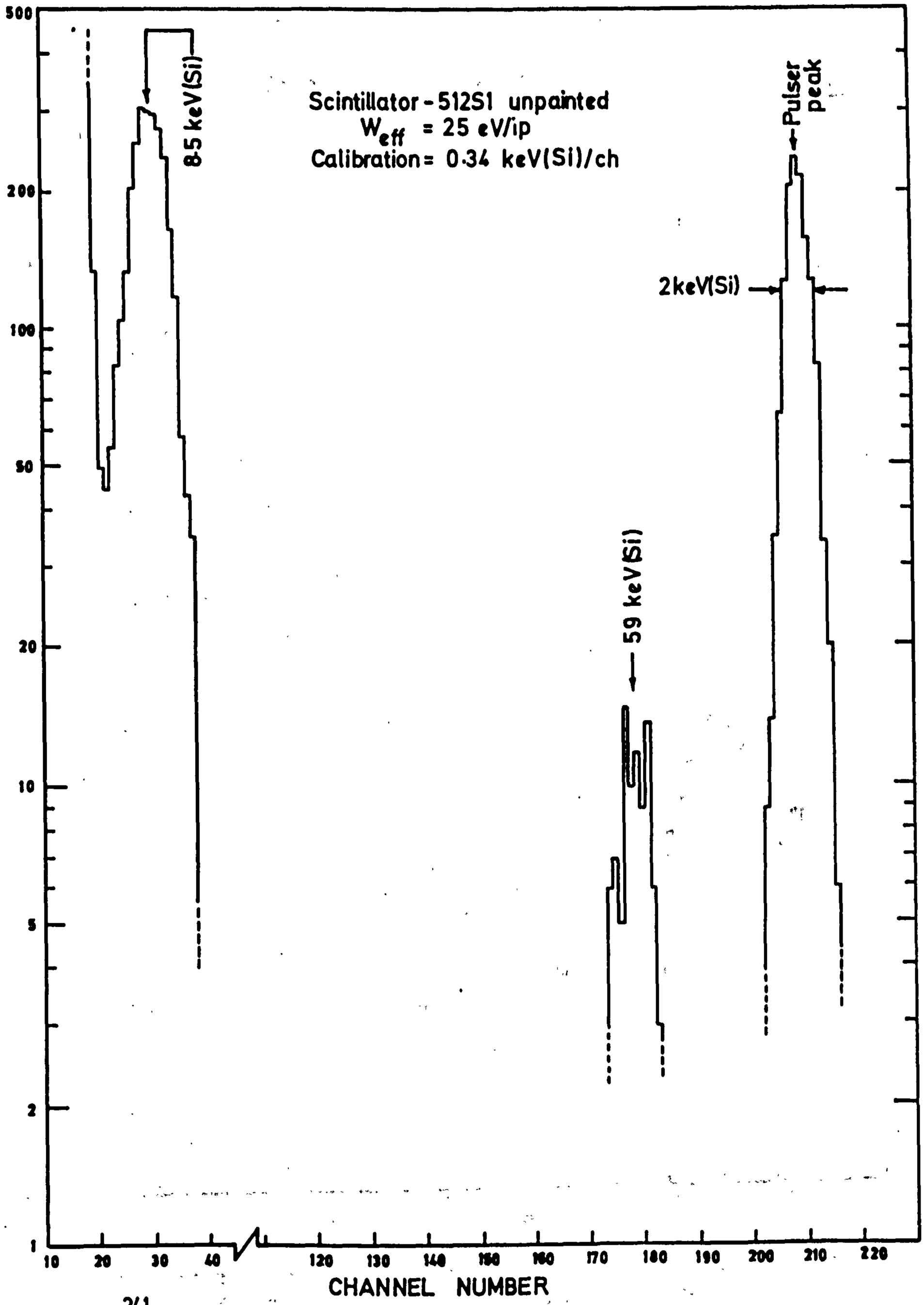

Figure 6.3 ^{241}Am gamma-ray spectrum taken with the CdS(Te)-photodiode detector cooled at 110K

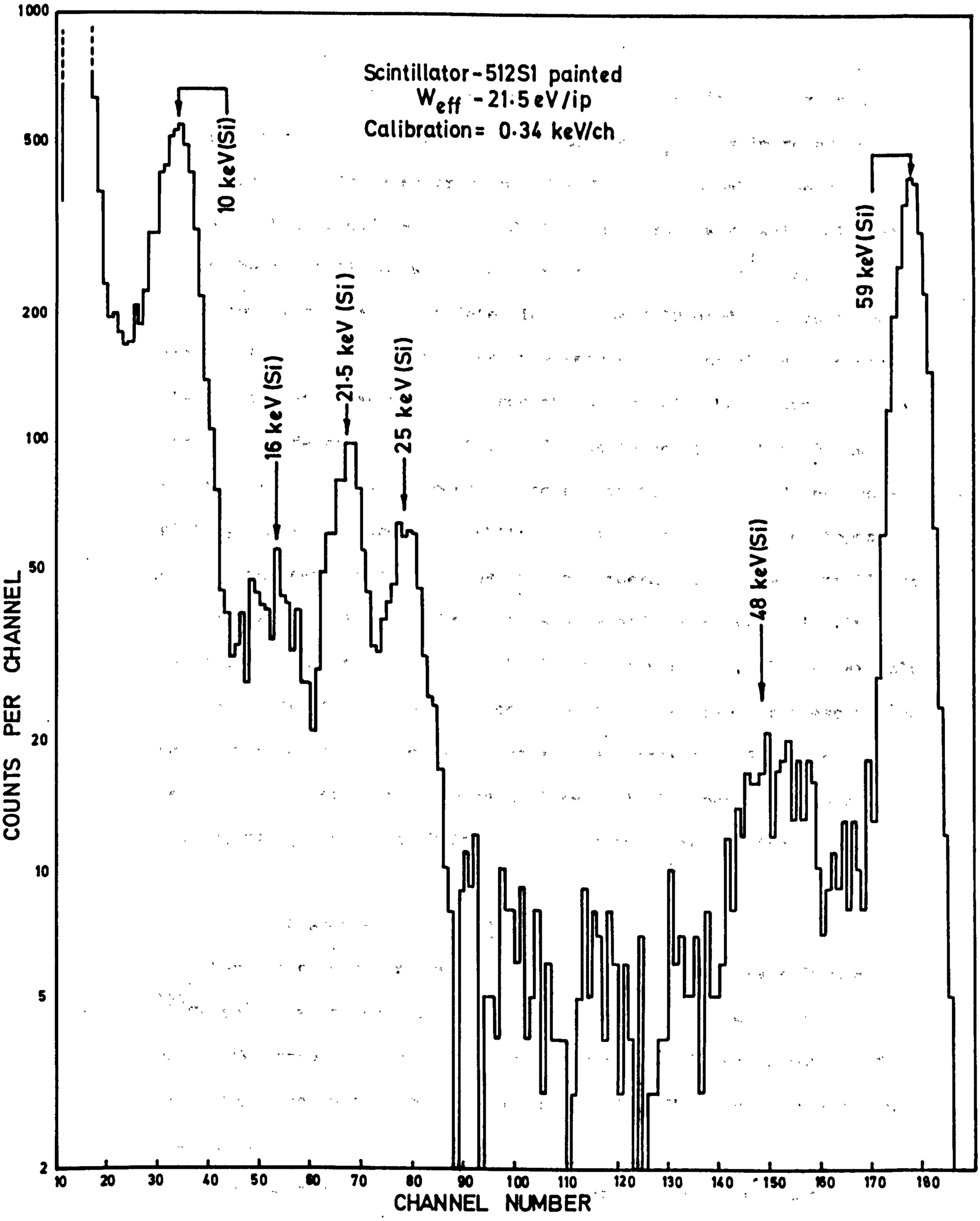

Figure 6.4 ^{241}Am gamma-ray spectrum taken with the CdS(Te)-photodiode detector cooled at 110K (source is not well collimated on the crystal)

TiO_2 reflective coating, more light was collected from the scintillator by the diode. Therefore, the value of W_{eff} was improved to 21.5 eV/ip as calculated from the 10 keV(Si) photopeak. The distribution in Figure 6.5 was obtained when the γ-rays were well-collimated on to the scintillator with the help of a copper collimator. This time there was less direct detection by the K-22 diode, so that the intensity of the 59 keV(Si) peak was reduced. Since the volume of the scintillator was not large enough to stop all the γ-rays, and since the effective area of the diode was larger than that of the scintillator, it was not possible to eliminate this 59 keV peak completely. A slight oberseved shift in the position of the photopeak could have been due to a change in the temperature of the scintillator to a lower value so that the luminescence efficiency was slightly increased. On the other hand, the low amplitude of the 59 keV signals in the CdS(Te)-Si(Li) detector could make the accuracy of these values poor. Consequently a pulse-height analyser offset of 2 channels would lead to 20% error. From the main 11 keV(Si) photopeak in Figure 6.5, a value of W_{eff} of 19.5 eV/ip was calculated at resolution of 21.5%.

6.5.3 Response to 662 keV γ-Rays

Next, the detector was irradiated with 662 keV γ-rays from a ^{137}Cs source which was located about 2" above the detector and collimated through a hole in a copper cylinder. A lead absorber of 1/32" thickness was introduced to prevent 30 keV X-rays from reaching the source.

The spectrum in Figure 6.6 was obtained with the unpainted CdS(Te) 512S1 scintillator. The 75 keV and 84 keV peaks were due to the direct detection of fluorescent X-rays from lead by the diode.

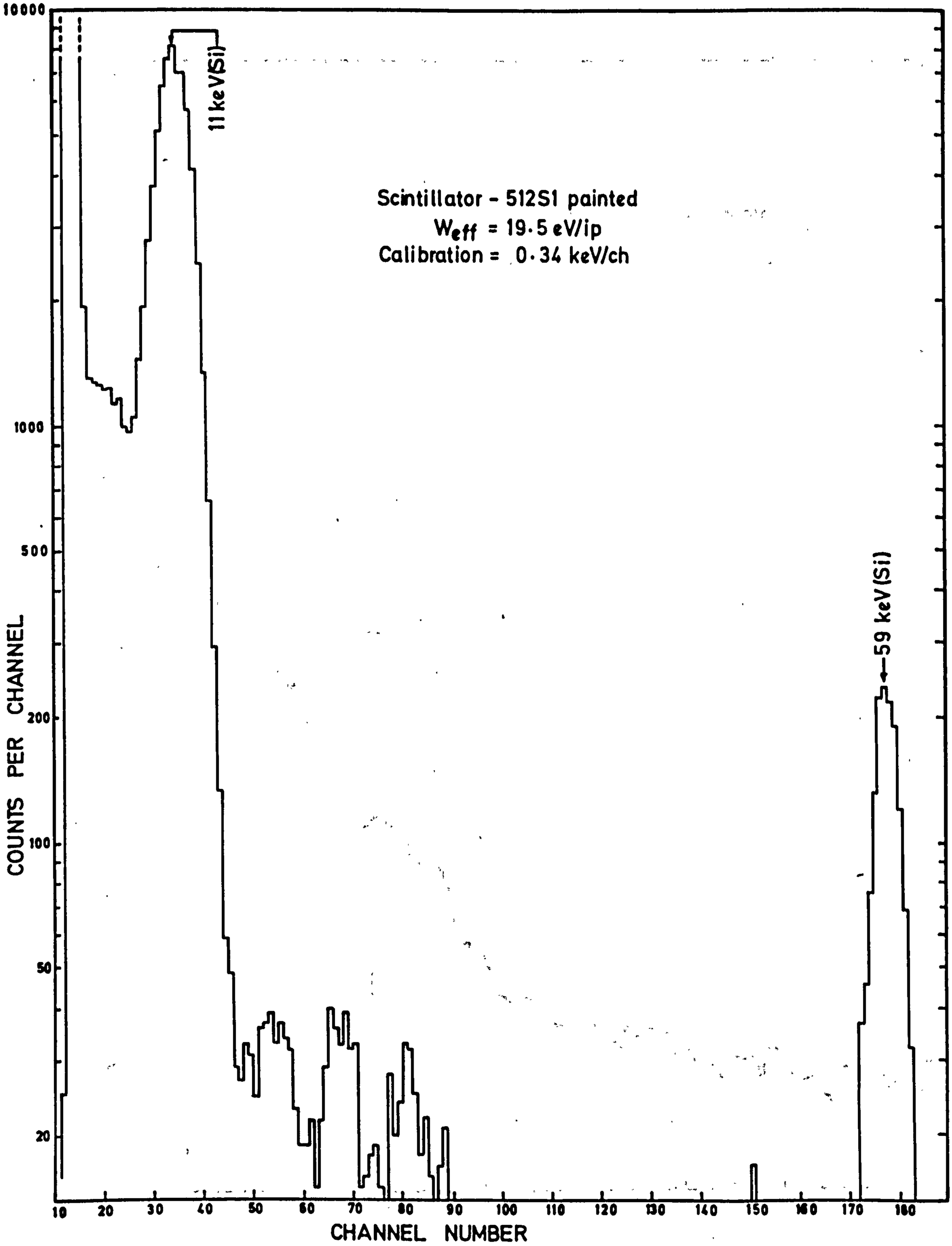

Figure 6.5 ^{241}Am gamma-ray spectrum taken with the CdS(Te)-photodiode detector cooled at 110 K (source is well collimated on the crystal)

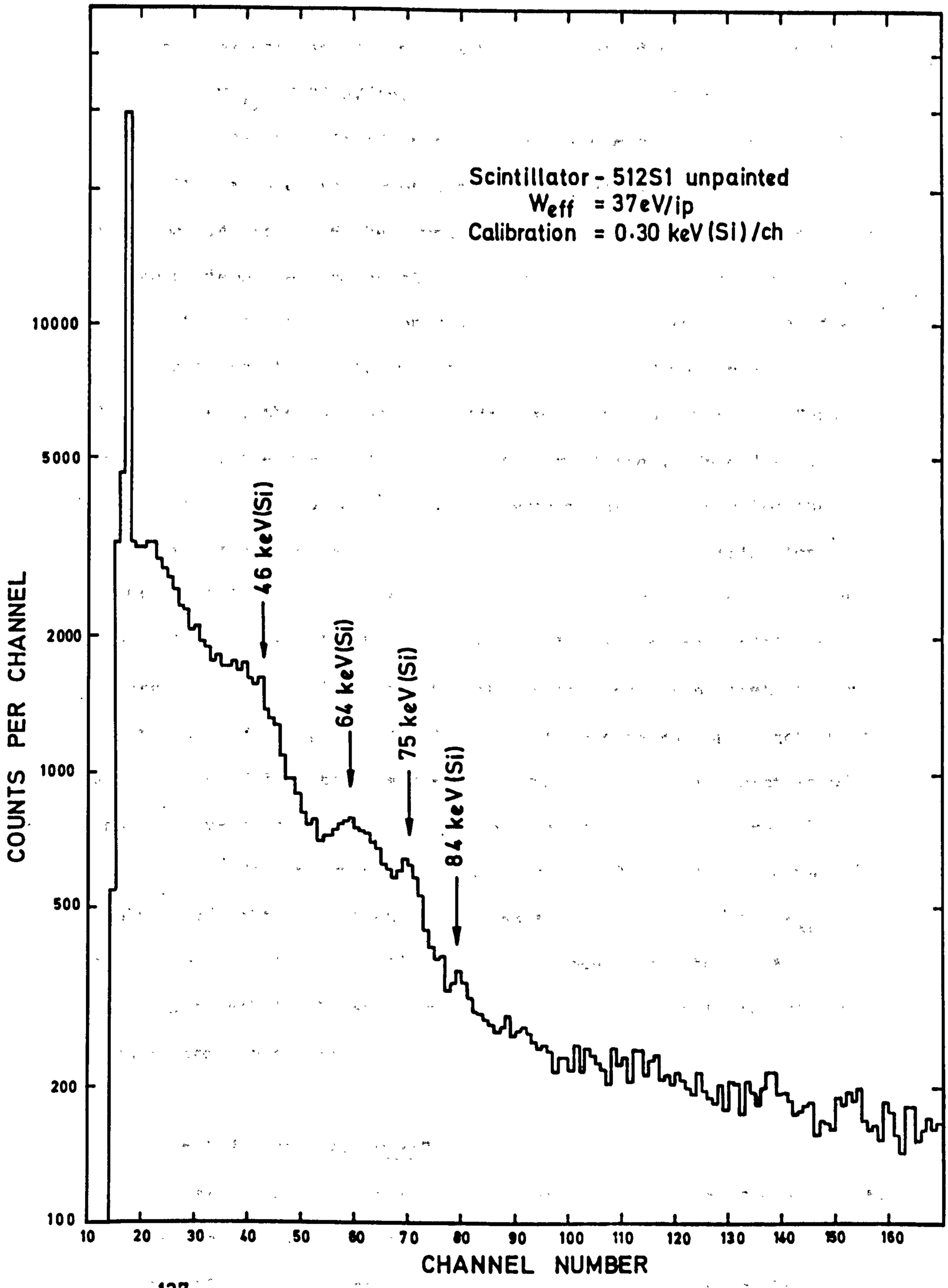

Figure 6.6 ^{137}Cs gamma-ray spectrum taken with the CdS(Te)-photodiode detector cooled at 110 K

The photopeak corresponds to 64 keV(Si) in this distribution, with a value of W_{eff} of 37 eV/ip. But, the resolution of this peak was very poor. On the left of this photopeak a Compton continuum can be seen. The value of the Compton edge energy E', was found using Equation 1.4, to be 480 keV, which corresponds to 46 keV(Si) in terms of energy deposited in the silicon diode, as shown in the spectrum.

When the scintillator was coated with TiO_2 and irradiated with the same source the distribution (a) of Figure 6.7 was obtained. Unfortunately, the photopeak coincided with the 75 keV(Si) Pb X-ray peak so that the spectrum looks rather complicated. In order to clarify the situation a background spectrum was recorded using the same arrangement but without the scintillator. The distribution (b) of Figure 6.7 was then obtained; i.e. ^{137}Cs spectrum as detected by the silicon diode. In this picture, the Pb X-rays can readily be observed superimposed on the uniform Compton scattering distribution of the 662 keV γ-rays in the diode. When this background spectrum (b) was subtracted from the observed spectrum (a), a clearer picture of the ^{137}Cs γ-ray spectrum was revealed, see curve (c), Figure 6.7. The Compton edge energy was calculated to be 52 keV(Si). Because of the better light collection, there was an improvement in the W_{eff} value, to 31.3 eV/ip. The resolution of the photopeak was about 13%. The very first peak in the spectrum is due to the backscattering of the γ-rays from the cryostat lid.

6.5.4 Response to γ-Rays from ^{207}Bi Source

Next, the ^{137}Cs source was replaced with a ^{207}Bi one which has two distinct γ-ray components at 0.570 MeV and 1 MeV. The lead absorber of 1/32" thickness was still in operation to stop the low energy X-rays reaching the detector.

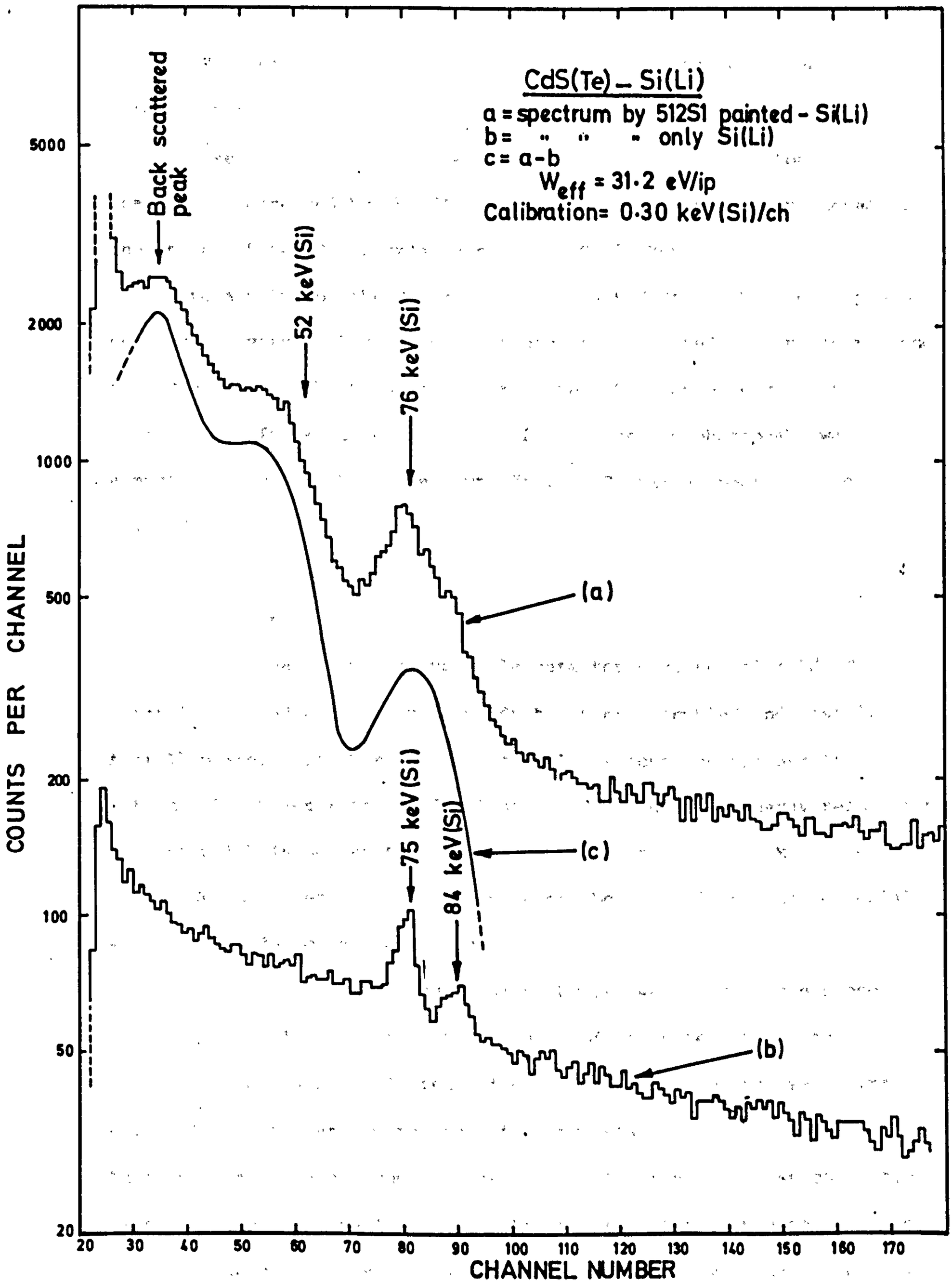

Figure 6.7 ^{137}Cs gamma-ray spectra taken at various conditions (intensity scale is arbitrary for each spectrum)

The spectrum shown in Figure 6.8 was obtained with the painted (TiO_2 coated) scintillator. Once again two Pb X-ray peaks appeared (i.e. those at 75 keV and 84 keV) superimposed on the Compton scatterings detected by the diode. However, there are two photopeaks, the one at 65 keV(Si) corresponds to the 0.570 MeV γ-rays, which in turn give a value of the Compton edge of 44 keV(Si). The second photo-peak is not very well resolved. It occurs at 116 keV(Si) and corresponds to 1 MeV γ-rays, which in their turn give a Compton edge value of 93 keV(Si). The W_{eff} value derived from these two photopeaks was almost the same as the value found from ^{137}Cs gamma spectrum, i.e. 31.2 eV/ip.

6.6 Discussion

A cryogenic nuclear particle detector composed of a CdS(Te) scintillator and a Si(Li) photodiode has been assembled and tested. A small platelet of this high-Z material was found sufficient to detect 5.5 MeV α-particles efficiently and produced an energy resolution of 6.6% which is better than the value of 15% reported by Madden et al (7). On the other hand, larger volumes (boules) of the same material were used to detect various γ-rays.

Among the various boules grown by us, we selected the piece 512S1 as a sample γ-scintillator because of its superior optical quality. The overall efficiency figures obtained from the γ-spectra with this scintillator were found to vary between 20 and 32 eV/ip. These variations are thought to be due to differential light collection caused by the large variations in the shapes of the sample scintillators. However, the most important feature is that these low values of eV/ip, which are similar to those observed in the platelets, indicate the

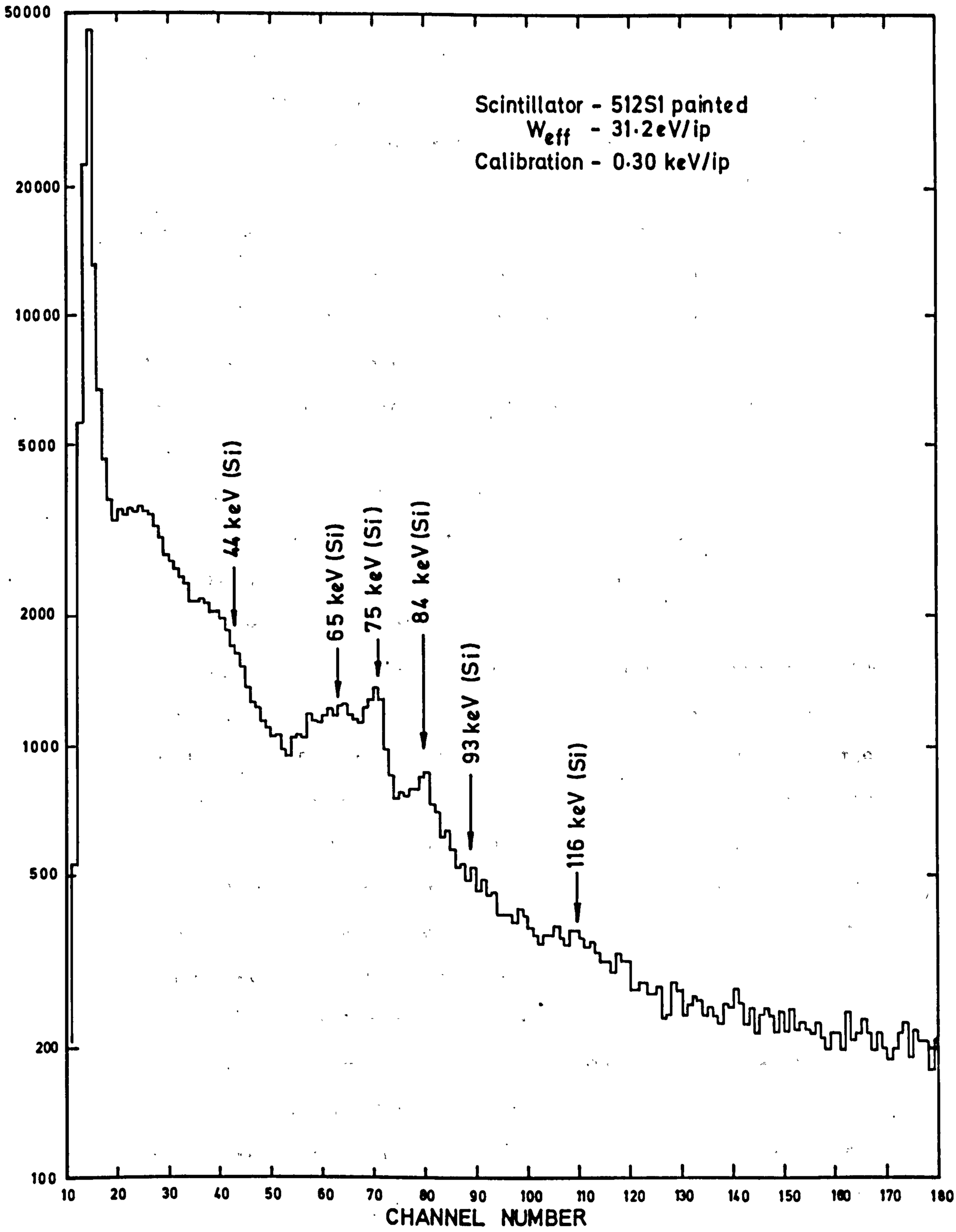

Figure 6.8 ^{207}Bi gamma-ray spectrum taken with the CdS(Te)-photodiode detector cooled at 110K.

existence of high luminescence efficiency in the boules.

In contrast with the low measured values of the eV/ip the resolution of the photopeaks in the γ-spectra was poor. If we insert the value of 31 eV/ip found from the detection of 662 keV γ-rays with our detector into Equation 1.5, a resolution (ΔE/E) value of 1.6% is suggested which is much less than that value of 25% found experimentally. The values obtained with Ge(Li) and NaI(Tl)-PMT detectors for the same γ-rays are 0.3% and 8% respectively (see Chapter 1). The main reasons postulated for this poor energy resolution are:

(1) the high refractive index of this material,

(2) the unusual shape of the sample scintillator,

(3) the self-absorption of CdS(Te) to its own light.

Because of the high refractive index of CdS(Te) and the associated total internal reflection, it is rather difficult for the light to escape from the crystal. Trapping of light is a function of the point of origin of the scintillation and so leads to a large variance which ruins the energy resolution. Considerable improvement was made if all the surfaces of the CdS(Te) scintillators were polished to a fine grade and coated with a diffuse reflector. The coupling material also played an important role in increasing the light transfer efficiency from the scintillation on to the photodiode.

The unusual shape of the sample scintillator introduced extra broadening in the photopeaks observed. The growth of new CdS(Te) boules with proper cylindrical geometry and a minimum number of edges should reduce trapping and improve the resolution. In fact, the volume of the sample scintillator 512S1 was insufficient to resolve 1 MeV γ-rays of 207Bi, i.e. the detection efficiency f was low. We

need a volume of at least 6 cc to achieve a useful photopeak detection efficiency at high energies (see Table 1.1). The high background of Compton events in the Si(Li) photodiode was aggravated by the small volume of the scintillator which was not large enough to stop all the γ-rays reaching the Si(Li) photodiode.

The last, but the most important factor affecting the energy resolution of the boules is their poor transparency. Measurements at room temperature showed that the absorption length in these crystals did not exceed 3.5 mm. Given a recently observed improvement of the transparency at low temperatures, the question still remains whether the boules we have grown are good enough in respect of their self-absorption.

The present work has taken us a considerable part of the way to the realisation of a successful scintillation counter based on the use of CdS(Te). Large boules of centimetric dimensions have been grown with radioluminescence efficiencies comparable to those of the best platelets. The boules have been matched to an Si(Li) diode to yield an overall energy per ion pair (∿25 eV) which is unmatched by any other type of scintillation detector (NaI(Tl) and a good PMT yield at best ∿300 eV/ip). Unfortunately, the pulse-height resolution was very poor compared with what might be anticipated from the high radioluminescence efficiency. This has been attributed to the combination of bad sample geometry with the very high refractive index of the material leading to a bad transfer variance caused by light trapping and made worse by the poor transparency of the material to its own radiation. We believe that further improvements will result if more transparent boules are grown. The growth of such large crystals is a matter of experience and patenience, and the attainment

of the necessary absorption coefficient ($\sim$0.1 cm^{-1}) seems quite feasible. It looks probable that if a scintillator of good geometry is prepared from a crystal of better transparency one migh obtain a 2% energy resolution for 662 keV γ-rays using the cryogenic detector described here.

CHAPTER 7

CONCLUSIONS

7.1 Some Insights into the Luminescent Mechanisms in CdS(Te)

7.1.1 Introduction

The present work has extended the data on radioluminescence (RL) in CdS(Te) in three directions:

(1) Decay and quenching data were taken with both α- and β-particles whereas the previous workers used only β-particles. This has introduced a new parameter; namely, ionization density. The mean ionisation density created by a 5.5 MeV α-particle in CdS is ~250 times that of a 1 MeV β-particle (the energy loss data given in Birks (5) for NaI was used to derive this relation). This very large factor introduces very different initial conditions in the decay kinetics. The differences in decay waveform already noted in Chapter 5 are discussed in more detail later in this section.

(2) In the boule crystals we have control of the stoichiometry and crystals with excess of either sulphur or cadmium (previous results reported describe only platelet crystals of which the stoichiometry can only be guessed and certainly not controlled). The stoichiometry would in general be expected to control the luminescent properties of the crystals and as shown later, this is indeed the case.

(3) A sufficient number (six) of different crystals with a good spread of tellurium concentration ($1x10^{18}$-$1.5x10^{19}$/cc) have been grown and measured so that some attempt at correlating the RL properties with [Te] (tellurium concentrations) became possible.

Only in one important respect is the present work deficient from the point of view of studying the RL process and that is the lack of data below 80 K. For scintillation counter applications there is no

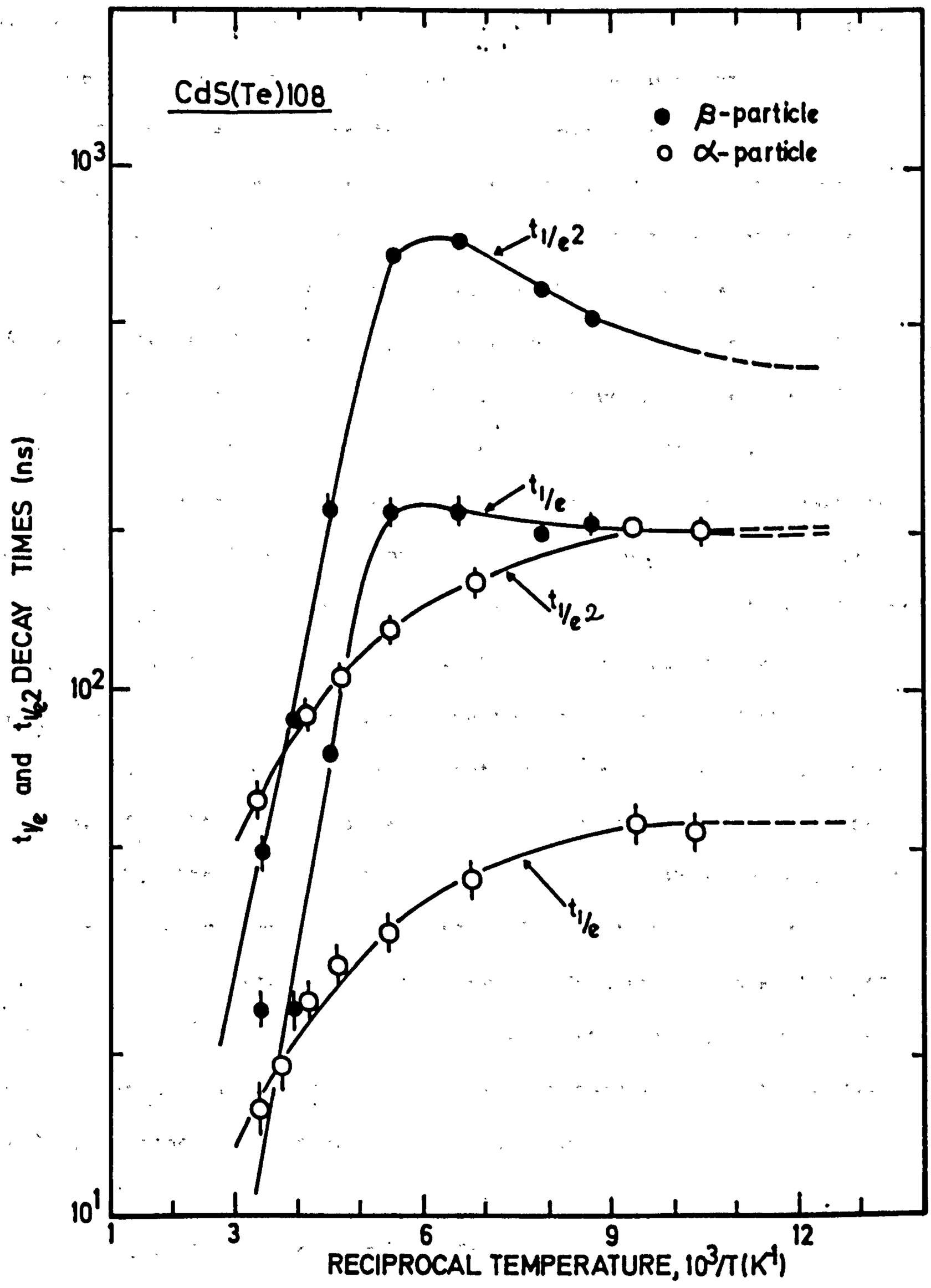

FIGURE 7.1 Variations of decay times of alpha and beta induced luminescence with temperature in CdS(Te)108.

need to go to lower temperatures but clearly for future study of the material a helium cryostat would be essential to complete the picture outlined in this section and solve the remaining problems.

Before discussing in detail the respects in which our data differs from the results of previous workers, it is well to recall (see Chapters 3 and 5) the constant features of the RL output from CdS(Te). Similar to the samples examined by Cuthbert and Thomas (2), our crystals at low temperatures showed a broad emission band of ∿50 nm fwhm centred between 580 and 600 nm. No structure is evident in the band even at 4.7 K. (This was checked down to ∿10 K (Figure 5.2) where there was no sign of zero-phonon lines). Activation energies of ∿ 0.2 eV and ∿ 0.03 eV were found to control the quenching of the luminescence. A high luminescent efficiency was observed in all samples and, in those that were measured with the photodiode the radiative recombination fraction (i.e. the quantum efficiency of Cuthbert and Thomas) was of the same order as that previously observed, i.e. 60-70%. Because of light collection problems, an accurate estimate was not possible but the figure quoted is a lower limit. When, however, our lifetime data is compared with that of Cuthbert and Thomas a very different picture emerges as explained in Chapter 5. This RL lifetime (decay time) data is examined here in context of the parameters which we have under our control, viz. ionisation density, stoichiometry, tellurium concentration and output wavelength.

7.1.2 Ionisation Density Effects on the RL Lifetime

In Figure 7.1, the decay times $t_{1/e}$ and t_{1/e^2} plotted against 1/T are seen for the stimulation of a platelet crystal (108) with α- and β-particles. At ∿100 K, the α-induced $t_{1/e}$ value is four times shorter than the β-induced one. The beta $t_{1/e}$ value is ∿220 ns,

already much shorter than the 300 ns value observed by Cuthbert and Thomas at helium temperatures. They interpreted the exponential decay of 300 ns observed below 20 K as the intrinsic lifetime of the Te* exciton and this idea seems to be in accord with the results of Cuthbert (1) who showed that the free carrier density drops rapidly below 20 K and all carrier movement stops in nanoseconds. However, when Henry and Nassau (45) applied the model which had been extremely successful in predicting the oscillator strength (and thus the decay lifetimes) of the excitons bound to donors and acceptors in pure CdS (the I_1 and I_2 lines in the spectrum) to excitons bound to Te in CdS, they predicted a lifetime of 27 ns, i.e. an order of magnitude shorter than the lifetime measured by Cuthbert and Thomas.

Now, according to the model proposed by Cuthbert (1), the lengthening of the luminescent lifetime above 20 K is due to thermalisation of the weakly bound excitonic electron (0.03 eV activation energy) and the final collapse of the decay time (and the RL efficiency) above $\sim$200 K is due to the ionisation of the hole (with 0.20 eV activation energy). This accounts for the sharp peak on the RL decay time observed in Figure 2.6. Our samples (Figure 7.1 is typical) show no such dramatic peak in $t_{1/e}$. Something of a peak is seen in t_{1/e^2} decay times at $\sim$180 K which tends to confirm the basic idea at least in the case of β-excitation. No peak of any sort is observed with α-excitation. If our observed decay times (with betas) were to be shorter than the fundamental excitonic decay at $\sim$100 K then some non-radiative quenching process would have to be involved. However, the high luminescent efficiency observed in all our samples at $\sim$100 K makes this extremely improbable and our short decay values of $\sim$220 ns, which (according to the model proposed) should decrease even further as T is reduced, throw serious doubt on the idea that the fundamental excitonic lifetime can be as long as 300 ns.

Considering the α-induced RL lifetime as a function of temperature (e.g. Figure 7.1), we again find evidence which seems to contradict the model proposed by Cuthbert (1). At 100 K when the luminescent efficiency is very high the α-particles reveal a lifetime of 55 ns which is clearly incompatible with a 300 ns intrinsic lifetime but still compatible with a 27 ns one.

The activation energies observed in the quenching curve (taken with the data of Cuthbert and Thomas (2)) indicate that, above 20 K the electrons produced by the ionising event are mobile, i.e. subject to continual trapping and detrapping and, above ∿150 K the holes are similarly affected. It is not an unreasonable hypothesis, therefore, that the decay kinetics might become dominated by a diffusion type form in the region of ∿100 K. This would be particularly understandable in the case of α-excitation when the initial carrier density is very high. The success of this idea is shown in Figure 7.2 where $(I(o)/I(t))^{\frac{1}{2}}$ is plotted against t for the decay of several samples when excited by α-particles at ∿95 K. Here, I(o) and I(t) are the luminescent intensities derived from the decay profile under consideration at times o and t respectively. Very good straight lines result with deviations near t = o which indicate a much faster contribution to the signal. The straight lines in Figure 7.2 represent fits to a bimolecular decay curve of the form $I(t) = \frac{a}{(b+t)^2}$, where a and b are constants. However, the bimolecular form need not be interpreted literally since a wide range of diffusion type processes involving two carrier recombination (with at least one very mobile) can result in similar forms of decay.

As Figure 7.3 shows, the behaviour of the decay curves of a single sample (108) for α-excitation as the temperature is varied

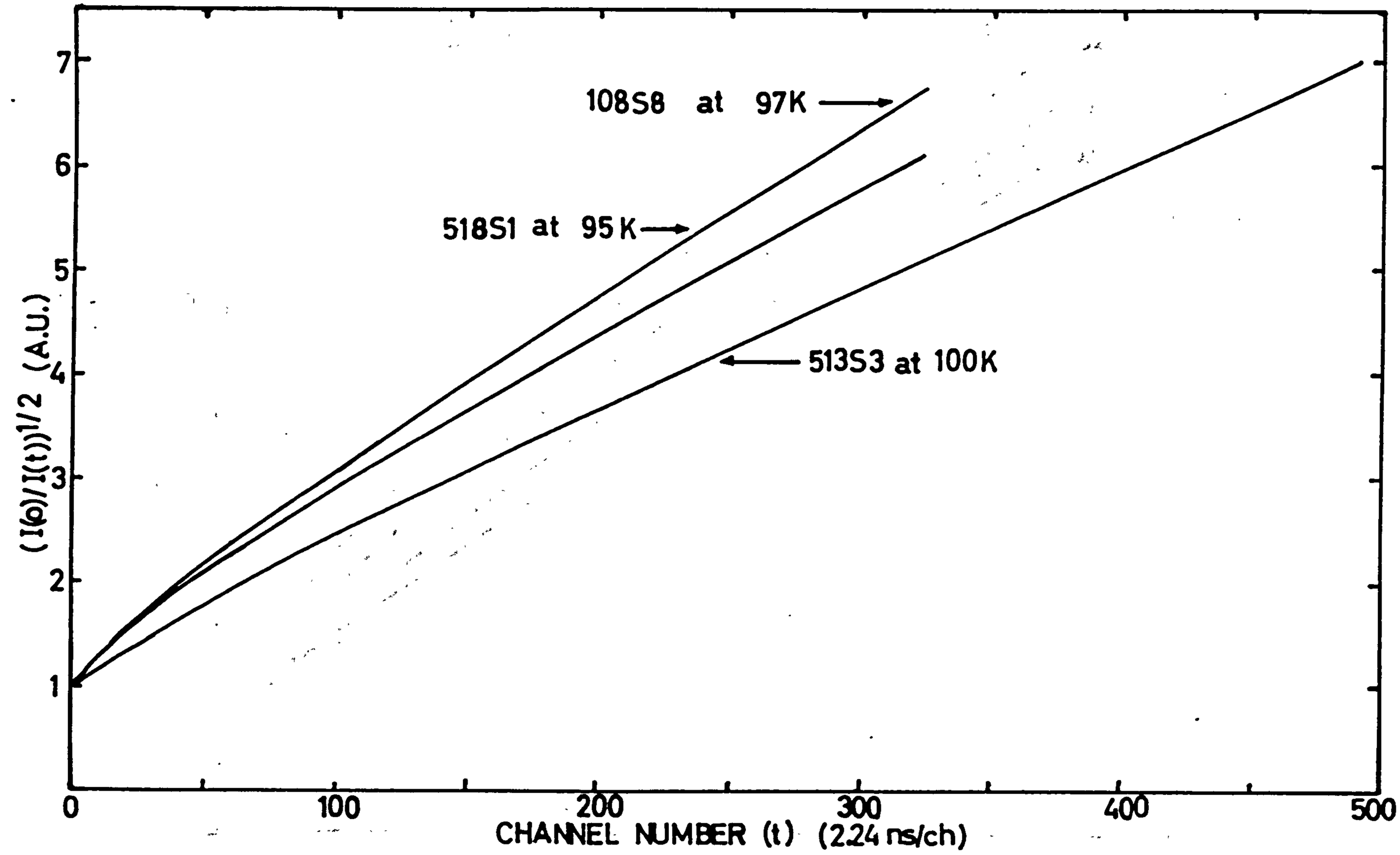

FIGURE 7.2 Analysis of α-induced decay profiles of various CdS(Te) crystals for bimolecular decay mechanism.

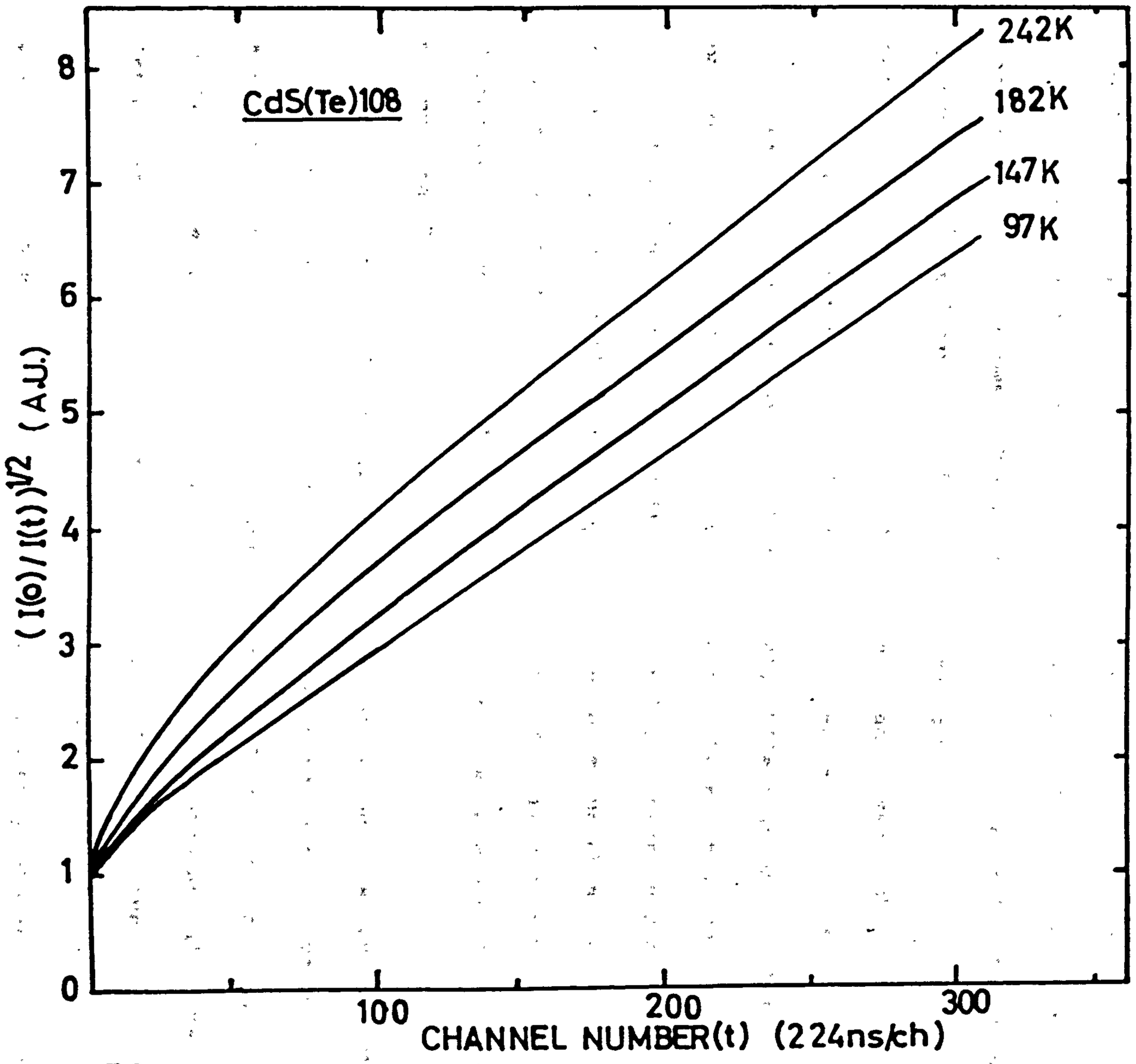

FIGURE 7.3 Analysis of α-induced decay profiles of platelet 108 at various temperatures for bimolecular decay mechanism.

presents a striking simple picture. At long times the decay fits a straight line on the plot at all temperatures and the slope of the line (k) is constant. However, the relative fraction of the fast part of the decay increases considerably with increasing temperature. Thus, the picture emerges of a decay composed of two independent contributions, i.e. a bimolecular part and a fast part which, when the bimolecular contribution is subtracted off, yields a reasonable fit to an exponential form as Figure 7.4 shows. The slope of the main part of this fast decay component gives a decay time of $\sim$30 ns which is very suggestive of the intrinsic exciton lifetime calculated by Henry and Nassau (45). As the temperature is increased to 242 K the slope of the main part of the fast component remains constant (Figure 7.4), while a second shorter part of lifetime $\sim$9 ns becomes more prominent. The relative constancy of the shape and magnitude of this fast (30 ns) component over a temperature range in which the main luminescence is quenching very rapidly tends to suggest the view that it may indeed result from some direct excitation of the tellurium ion by the high electric field of the moving α-particle.

In sample 108 the tellurium concentration is such that every tenth sulphur atom along a line is replaced by a tellurium atom on average. A reasonable degree of direct excitation is therefore possible (i.e. $\sim$10%). Since both parts of the decay fit analytic mathematical forms, integration is straight forward and evaluation of the relative signal content (number of photons) in the two parts yields the following results: At 97 K, the fast component represents 8.8% of the total light and, at 242 K, this ratio becomes 20.7%. The fast component quenches by a factor of 1.67 in this temperature interval and the total signal quenches by a factor of 3.92. The reduced quenching also suggests that carrier movement is not heavily involved in the fast decay.

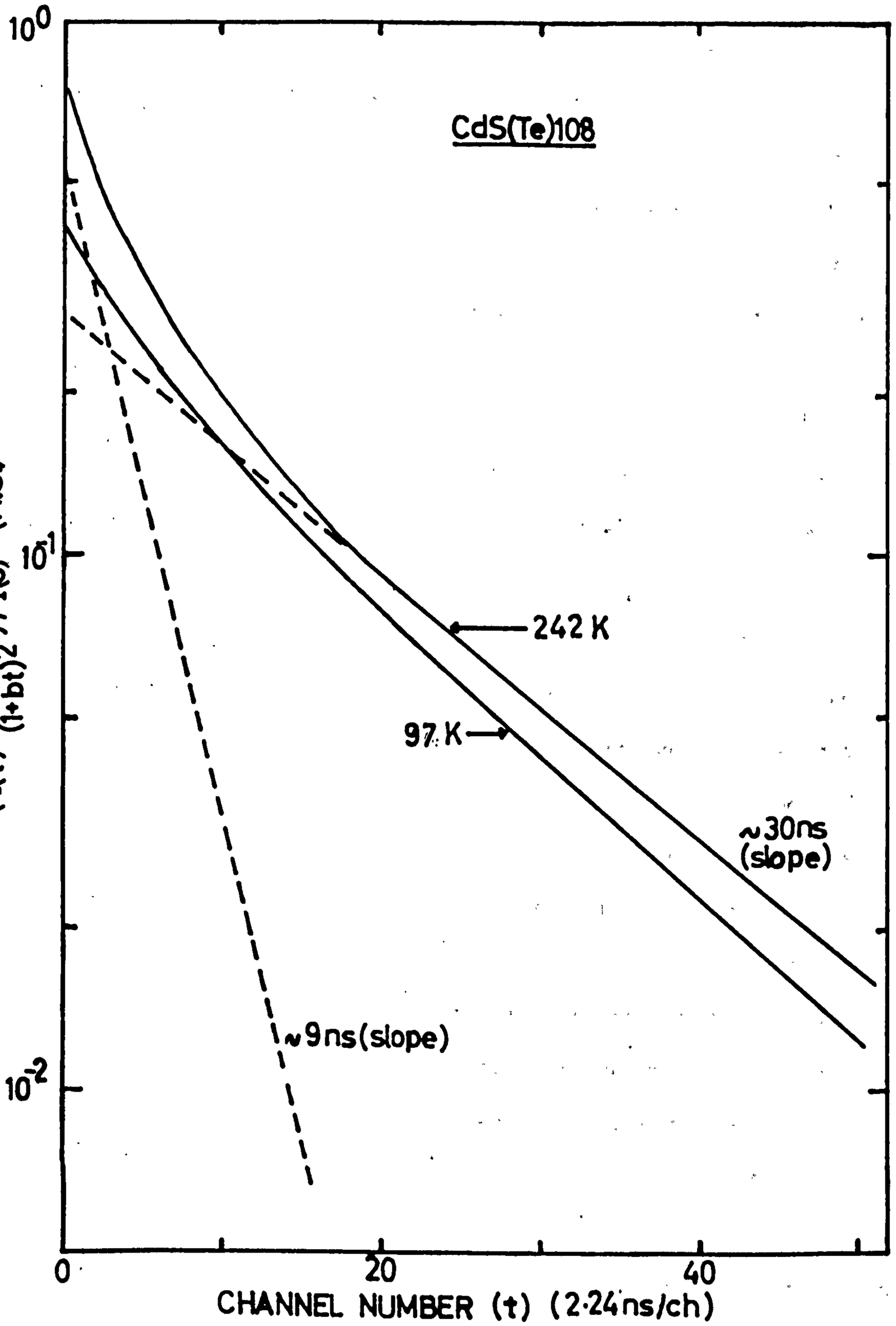

FIGURE 7·4 Fast part of decay components of platelet 108 at two different temperatures after bimolecular parts are subtracted from the α-induced decay profile.

The behaviour described above is common to all crystals grown with a reasonably high tellurium concentration and a cadmium excess as Figure 7.5 shows. The decay lifetime found for the fast decays in all these samples range between 17 and 30 ns. Fits to an exponential form are good in all cases with a faster component sometimes visible. The concept of this as a direct interaction phenomenon is further reinforced by the behaviour of samples 512 and 535 which have grown with a sulphur excess. The former shows no sign of a fast component but the latter clearly has a fast decay component of $\sim$22 ns (Figure 7.6). The difference between the two is simply that 512 has [Te] of 1.1×10^{18}/cc and 535 has [Te] of 9.7×10^{18}/cc. The amount of direct interaction between the alpha and the tellurium ion would be expected to depend on the density of tellurium ion.

The behaviour of the β-induced decay curves, on the other hand, is much more complex than that of the α-ones. First, there is no very fast component at all (presumably due to the very weak ionising field of the β-particle). Second, while in certain regions, around 120 K bimolecular fits are obtained, the decay shape is very unstable as the temperature varies with rapid shortening setting in at $\sim$200 K as the holes become ionised (Figure 7.7). It is clear that in the case of the β-excitation, no simplifying condition is imposed by the high ionisation densities and, the interaction of the various ionisation and trapping processes produces complex variations of the decay waveform. However, it is interesting to note that near 120 K a good straight line fit is obtained in all cases.

If the bimolecular model is meaningful in the temperature range around 100 K where the holes are still fairly well trapped on the tellurium ions then the slope k of the bimolecular decay fits should correlate with the tellurium density. In Figure 7.8, k is plotted

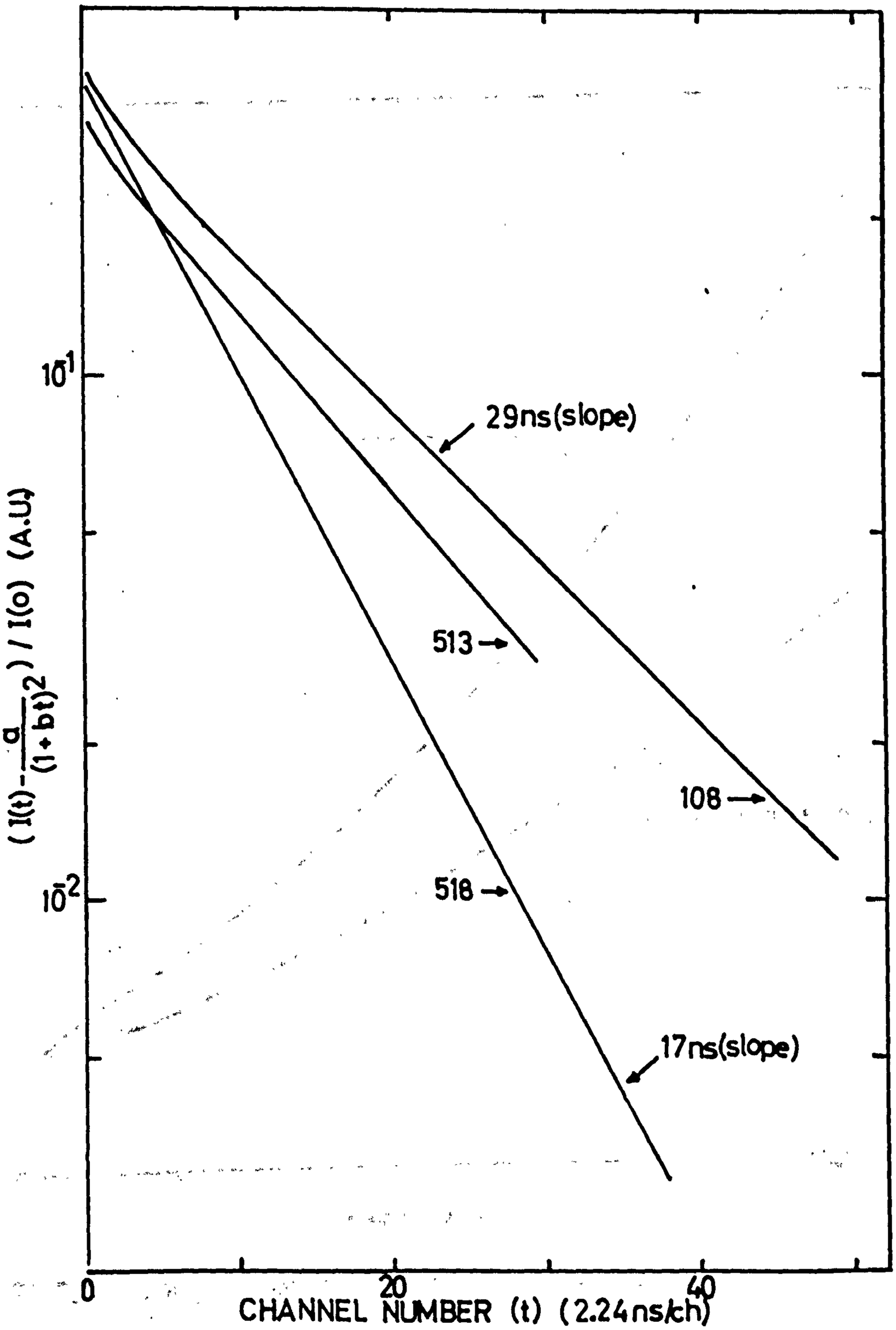

FIGURE 7.5 Fast part of decay components of various CdS(Te) samples after bimolecular contribution is subtracted from the α-induced decay profile.

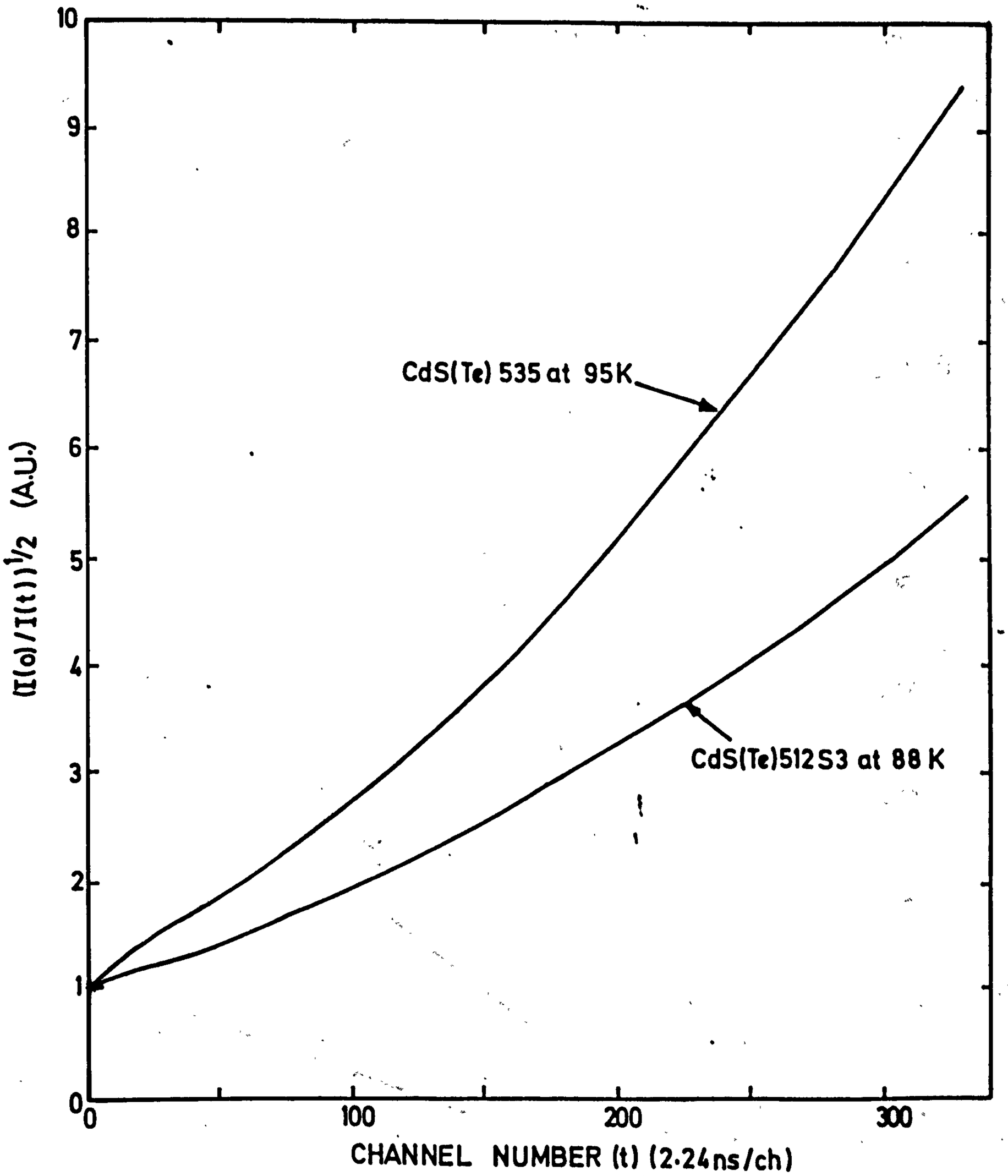

FIGURE 7.6 Analysis of α-induced decay profiles of two different CdS(Te) crystals for bimolecular decay mechanism.

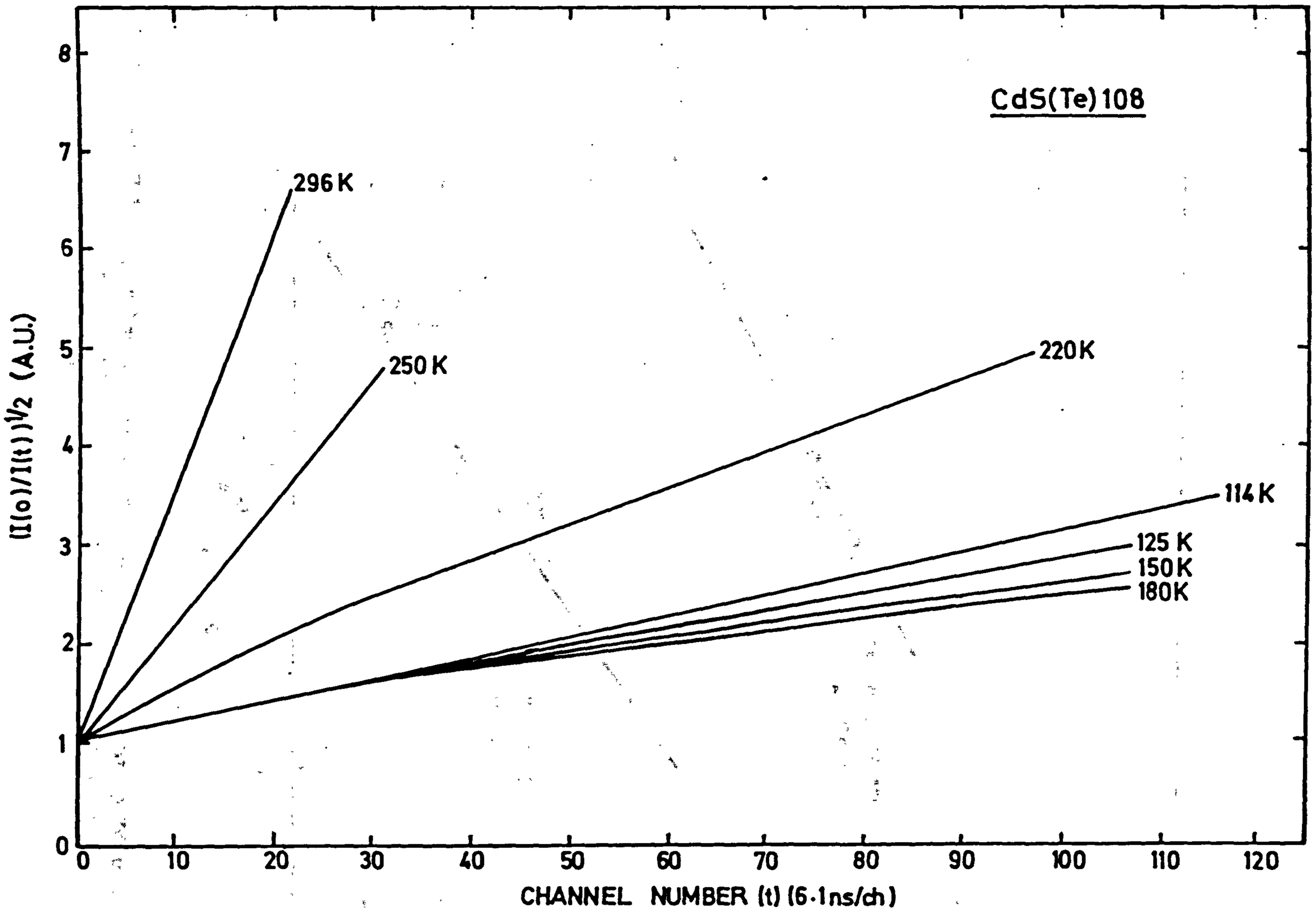

FIGURE 7.7 Analysis of β-induced decay profiles of platelet 108 at various temperatures for bimolecular recombination mechanism.

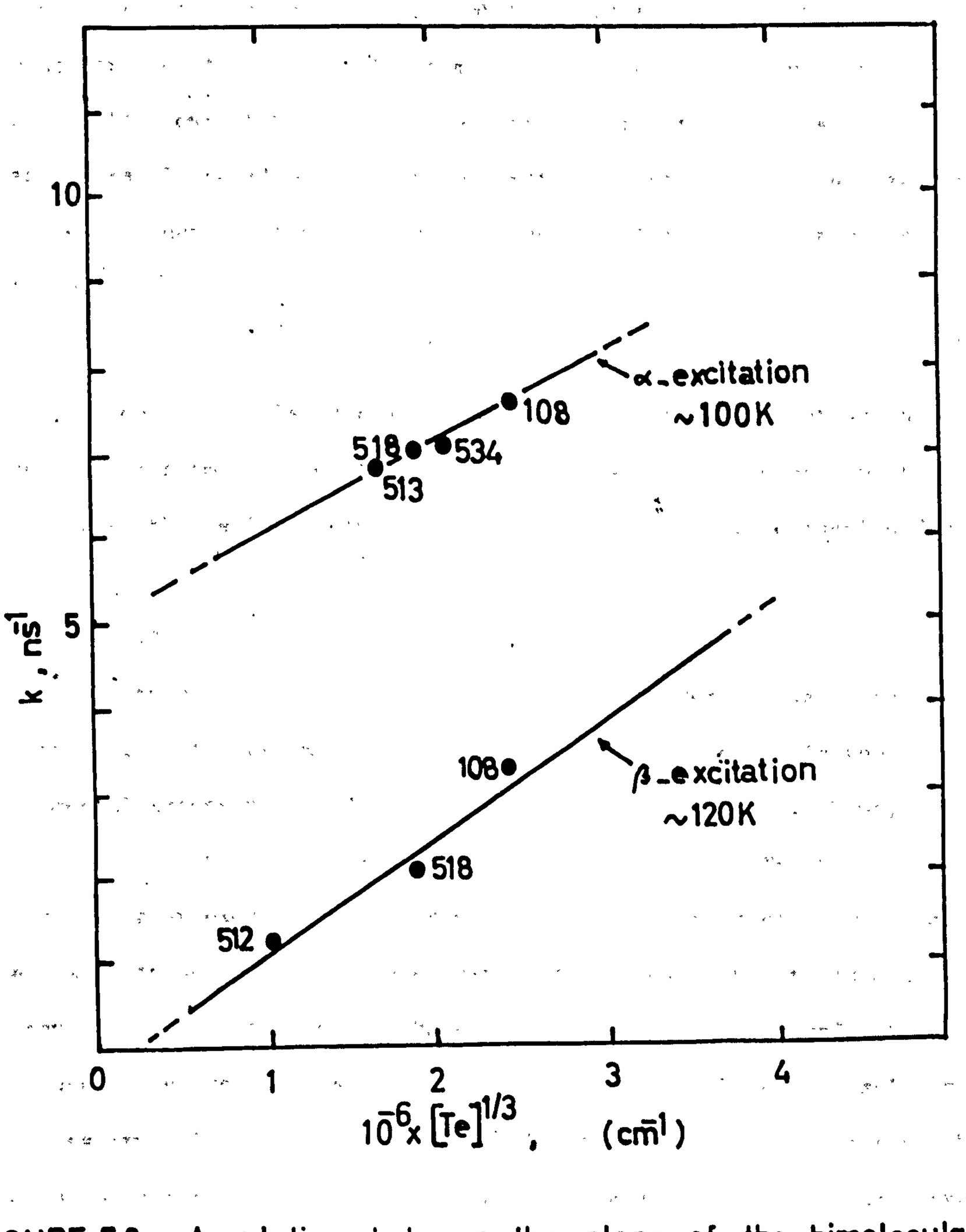

FIGURE 7.8 A relation between the slope of the bimolecular decay component and the tellurium concentration among various CdS(Te) crystals.

against $[Te]^{1/3}$, i.e. the number of tellurium ions per unit length along a line in the lattice. As expected, an orderly (approximately linear) relation exists with a high k correlating with a high tellurium concentration for α-particle stimulation. β-excitation yields substantially lower k values but the correlation with $[Te]^{1/3}$ is a line approximately parallel to that for α-stimulation. This is as expected since k appears in the differential equation for recombination as follows,

$$\frac{dn}{dt} = -kn^2 \qquad \ldots\ldots\ldots (7.1)$$

and, in our case, also contains the initial carrier concentration N_o due to our normalisation to I(o). Hence k should correlate positively with both the tellurium concentration and the initial ionisation density.

7.1.3 Stoichiometric Effects

Fortunately, two boules have been grown under similar conditions with similar tellurium concentrations and only differing in the elemental excess provided by the tail of the growth tube. Thus, 534([Te] = 8.6×10^{18}/cc) had a cadmium excess and 535([Te] = 9.7×10^{18}/cc) had a sulphur excess. Apart from the tendency for crystals with cadmium excesses to suffer less severe quenching at room temperatures quite dramatic differences in the shape of the RL decay were noted. As Figure 7.9 shows, over most of the range of temperatures the sulphur excess crystal exhibits longer decay times under β-excitation than the cadmium excess sample. Also the decay shape at ∿100 K is nearer exponential in the case of the sulphur excess ($t_{1/e}$ / t_{1/e^2} = 0.45 for 535 as compared with 0.35 for 534). However, the really striking difference between samples 534 and 535 shows up when the α-particle induced RL decay at ∿90 K is examined in the two crystals. Figure 7.10 shows a

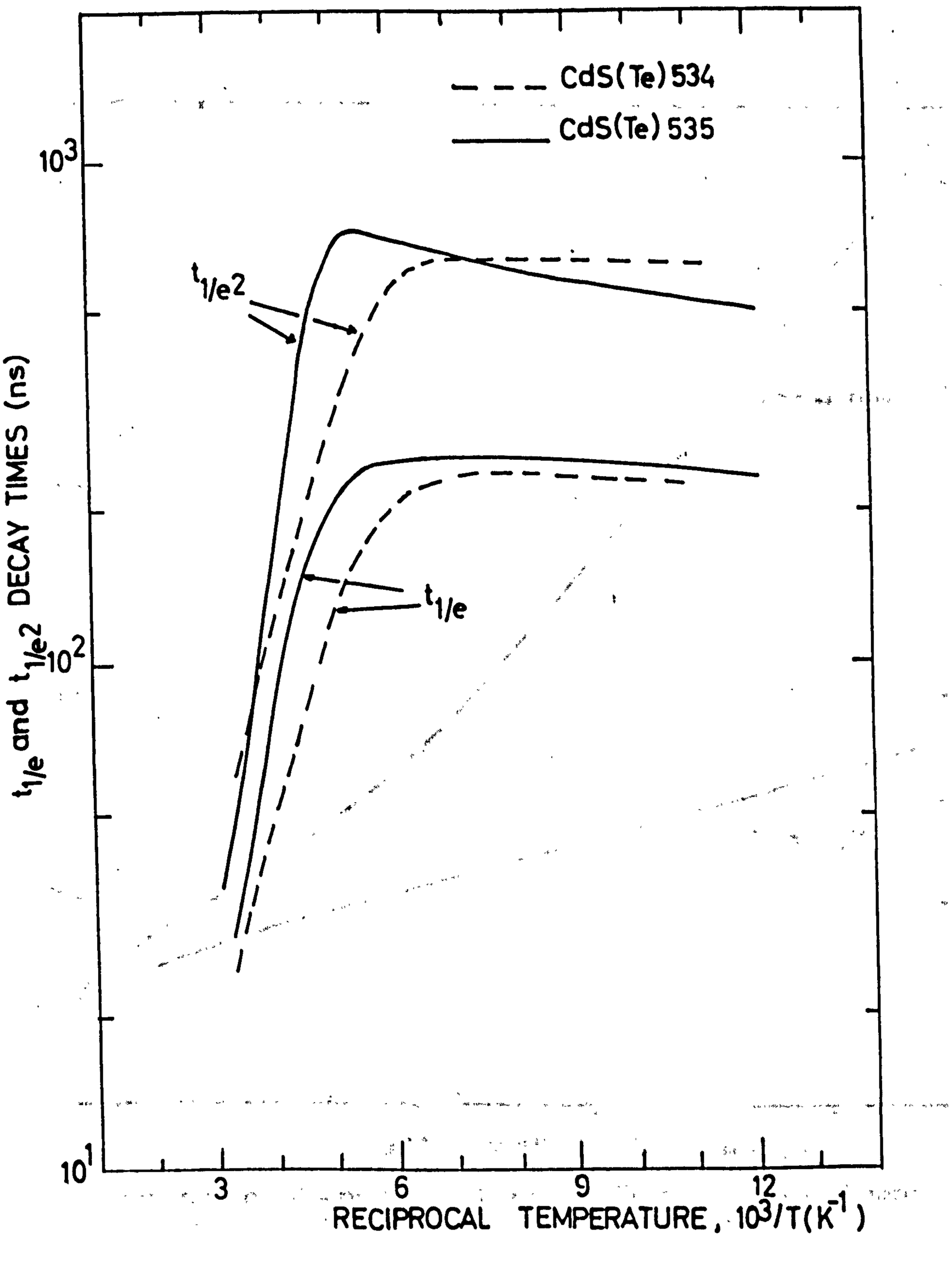

FIGURE 7.9 Variations of β-induced decay times with temperature in two different CdS(Te) crystals.

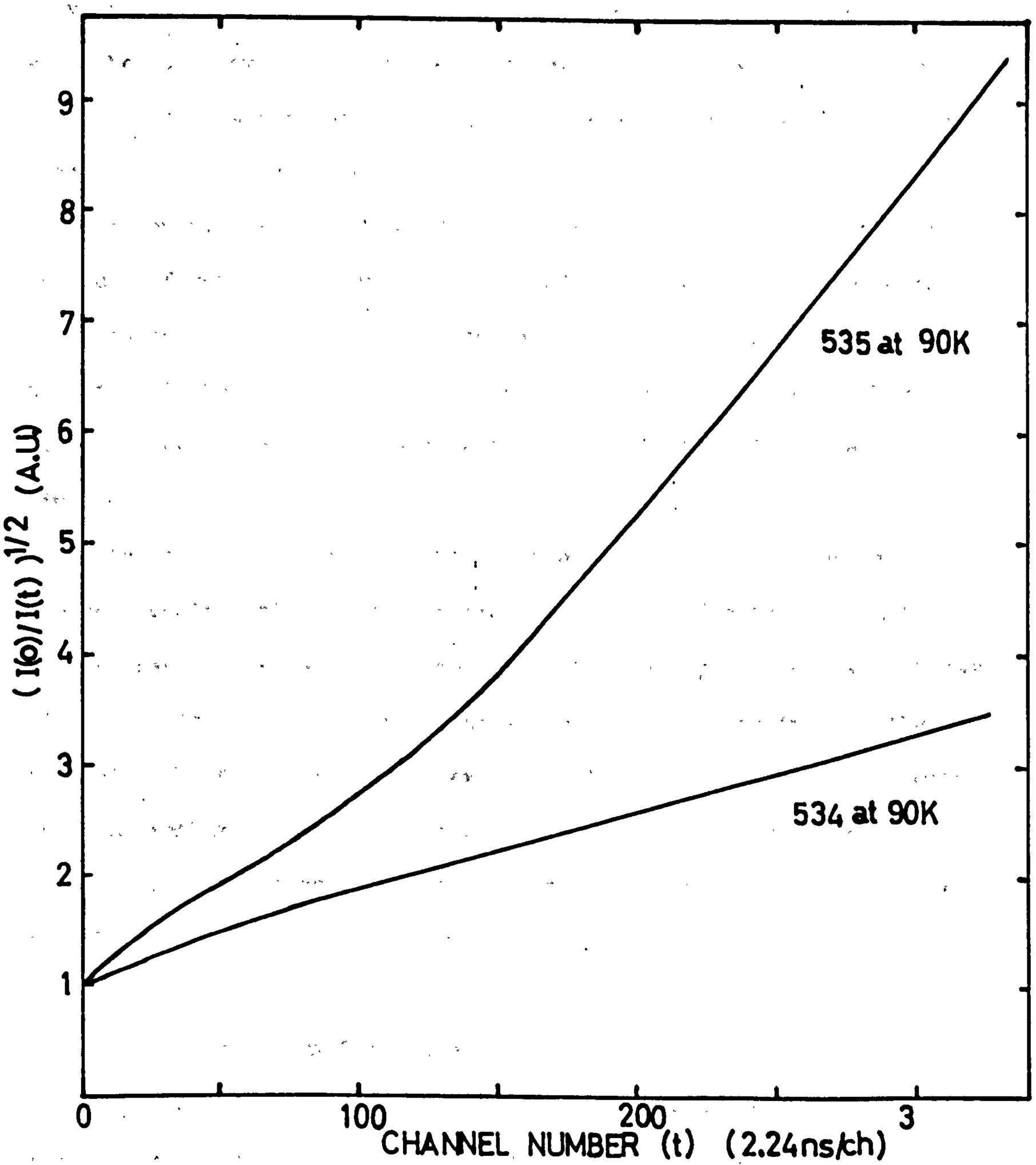

FIGURE 7.10 Analysis of α-induced decay profiles of two different CdS(Te) crystals for bimolecular decay mechanism.

$\left(I(o)/I(t)\right)^{\frac{1}{2}}$ vs t plot of these decays. 534 shows a good straight line fit at longer times with the usual fast component producing a curve near t = o. 535, on the other hand, shows a concave up curve with the fast component again evident within the first 30 ns. When the 535 decay is plotted on a log plot a reasonably straight line is obtained with a time constant of $\sim$150 ns after the 22ns component has died away. Here, the two distinct trends induced by the stoichiometric difference are seen as, (i) a cadmium excess favours bimolecular kinetics and (ii) a sulphur excess favours a quasi exponential form. A review of the results on all the samples available confirm this, i.e. 512 and 535 are quasi exponential and 513, 518, 534 give bimolecular fits.

The above results show that crystals with a sulphur excess produce results which tend to reproduce similar effects (though far from comparable in magnitude) to those observed by Cuthbert and Thomas (2), i.e. slower and more exponential decays with a maximum in the decay time at $\sim$170 K (in β-particle excitation). This prompts the hypothesis that the rather unusual behaviour they observe may result from extreme stoichiometric unbalance towards a sulphur excess resulting from their growth conditions.

7.1.4 Tellurium Concentration Effects

The correlation with the k values of the bimolecular fits with the tellurium concentration in the case of α- and β-excitation has already been noted (Figure 7.8). In the case of β-excitation, however, at temperatures of $\sim$90 K we clearly have different carrier kinetics with the decay form approaching exponential. At this temperature, it seems reasonable to visualise the holes firmly bound on the tellurium ions and the electrons trapping and detrapping very rapidly until

overtaken by recombination while in the trapped state. In this situation one would expect an inverse correlation between the decay lifetime observed and the tellurium concentration. In fact, as it is seen from Figure 7.11, $t_{1/e}$ correlates very well with $[Te]^{-1/3}$ (i.e. the mean distance between tellurium ions).

The first point to be made is that Figure 7.11 makes it seem very unlikely that the Te* excitonic lifetime is 300 ns as conjectured by Cuthbert and Thomas (2) since, as pointed out previously, the quantum efficiency in samples 108, 534, 545, 518 is uniformly very high (60-70%). Secondly, we have the problem of the approximately linear dependence of $t_{1/e}$ on the tellurium ion separation. While admitting that for a firm hypothesis to be made, the measurements should be made at 4.2 K, the following ideas can be put forward.

A possible mechanism for a lifetime dependence on $[Te]^{-1/3}$ such as is shown by Figure 7.11 is that the retrapping of an electron on a tellurium ion with a hole should take place via some tunnelling mechanism. This is perhaps not unreasonable in view of the following considerations: (i) the lifetime of a free electron in the conduction band is very short in CdS, i.e. 10^{-10} seconds, and therefore the electrons produced by the ionising event spend most of their time during the decay either in a tellurium exciton form or in some other trap, almost certainly a sulphur vacancy. (ii) In pure CdS, activation energies of 0.03 eV and 0.16 eV, are routinely found corresponding to the usual donor and acceptor centres. It is not therefore impossible to think of a situation in which the RL emission at low temperatures is a form of pair recombination between, say, a tellurium ion with a trapped hole and a nearby sulphur vacancy with an electron. Since the available energy is stored on the tellurium ion one could expect a luminescent spectrum determined largely by it but with the tunnelling between the two partners washing out any

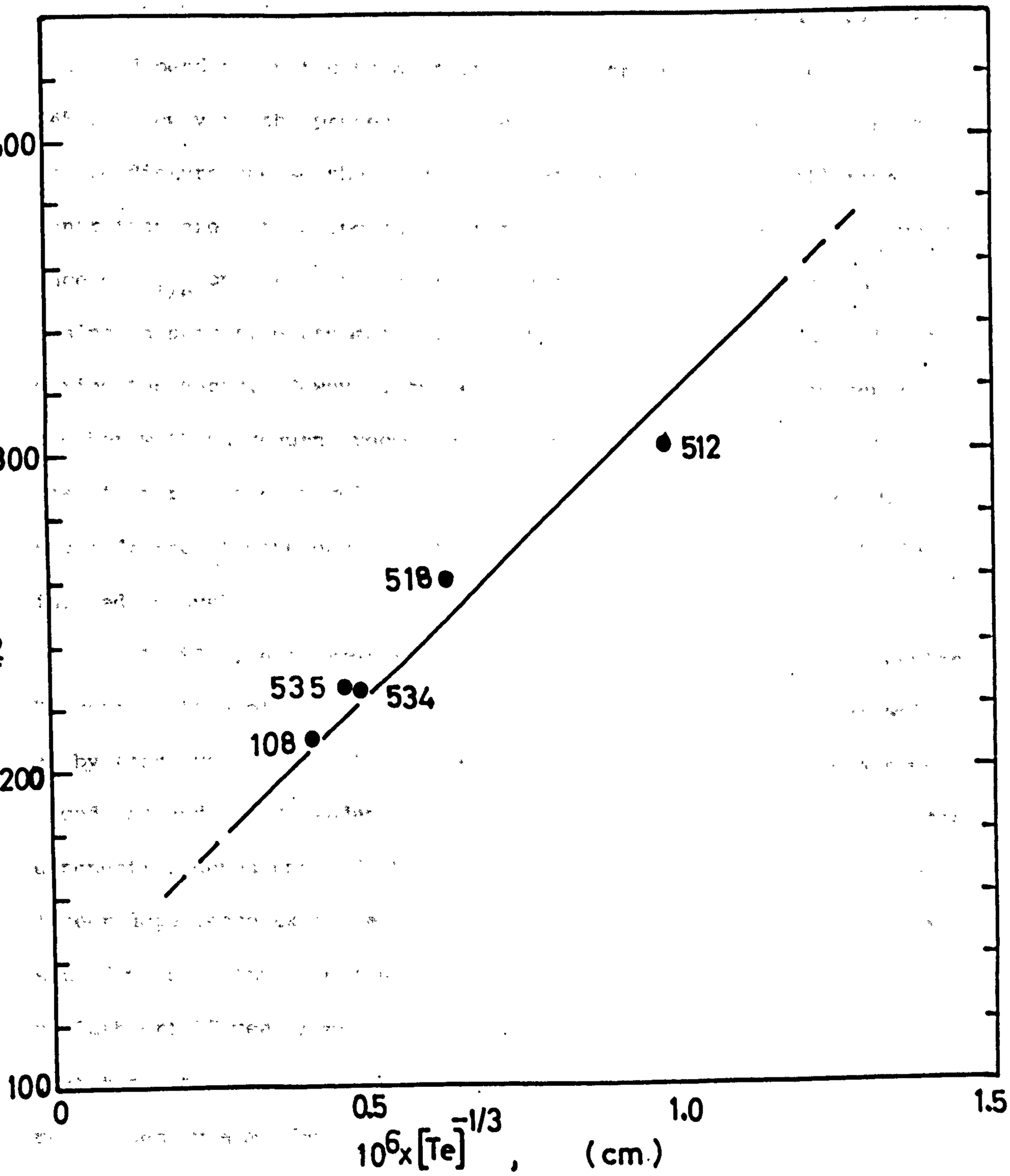

FIGURE 7.11 A relation between β-induced $t_{1/e}$ decay times and tellurium concentration among various CdS(Te) crystals at 90K.

phonon structure and producing a broad band. (As noted previously in Chapter 2, the band structure remains very broad and no zero-phonon lines are visible even at 4.2 K).

Such a pair recombination would show a time constant exponentially dependent on the separation of the partners (see Henry and Nassau (45)). However, the presence of the Te atom in the lattice does itself create disturbance so the vacancy concentration and the tellurium concentration are not independent variables. The nature of exact dependence of $t_{1/e}$ on $[Te]^{-1/3}$ is therefore rather obscure. An argument against a pair type recombination is the lack of wavelength shifting during the decay. However, tunnelling of a carrier from one centre to another with subsequent recombination on the Te ion would not in fact lead to first order wavelength shifting (as will be shown below, a small degree of wavelength shifting has been observed in α-particle induced decays).

At 90 K, electrons will in general reach the charged Te centre by reionisation of the carriers trapped on sulphur vacancies as well as by this hypothetical tunnelling. The process is therefore a compound one and the dependence of $t_{1/e}$ on $[Te]^{-1/3}$ would be weaker than the exponential dependence of the simple model. This could explain the linear dependence exhibited in Figure 7.11. Clearly, this particular set of measurements requires to be repeated at $\lesssim$ 20 K when (according to Cuthbert RF measurements (1)) the free carrier signal vanishes. At that temperature, electrons trapped elsewhere than on Te ions must reach them by some form of tunnelling.

7.1.5 Radioluminescent Output Spectrum

If, as hypothesised by Cuthbert and Thomas, the RL output results directly from the de-excitation of an exciton on a Te ion,

then even at $\sim$100 K one would not expect to see ionisation density effects in the output spectrum. However, as Figure 7.12 shows, α- and β-particles, and UV light all produce significantly different results (69). Unfortunately, the system wavelength resolution available was poor but extremely good statistics (2.5×10^4 counts in the peak point) were used and the smooth behaviour of the curves indicates that the effect is genuine. (Clearly, a much better demonstration could be made with better equipment). An interesting feature of Figure 7.12 is the way in which the alpha RL output spectrum is seen to be in some sense intermediate between the UV and the β-induced curves. This can be understood in terms of the initial separation of the electron and hole produced by the ionising event (i.e. the initial ionisation density).

In the UV case, the ejected electron and hole have only $\sim$1 eV of kinetic energy to share and, therefore, thermalise and trap very rapidly, i.e. in 10^{-10} secs. They are thus separated by only a very short distance and are candidates for the tunnelling process postulated above. Similarly, the α-particle produces very dense ionisation and many carrier pairs are trapped in close proximity. However, α-particles generate a small number of energetic δ-rays ($\geq$ 100 eV) which dissipate their energy in the low density ionisation, typical of β-particles (hence the intermediate position of the α-curve). Clearly the β-curve represents initial conditions in which the carrier pairs are well separated.

The movement of the UV and α-induced spectra towards the red relative to the β-curve can again be plausibly interpreted as due to the fact that in the former cases electron capture by a hole carrying tellurium ion is predominantly via tunnelling from an adjacent electron

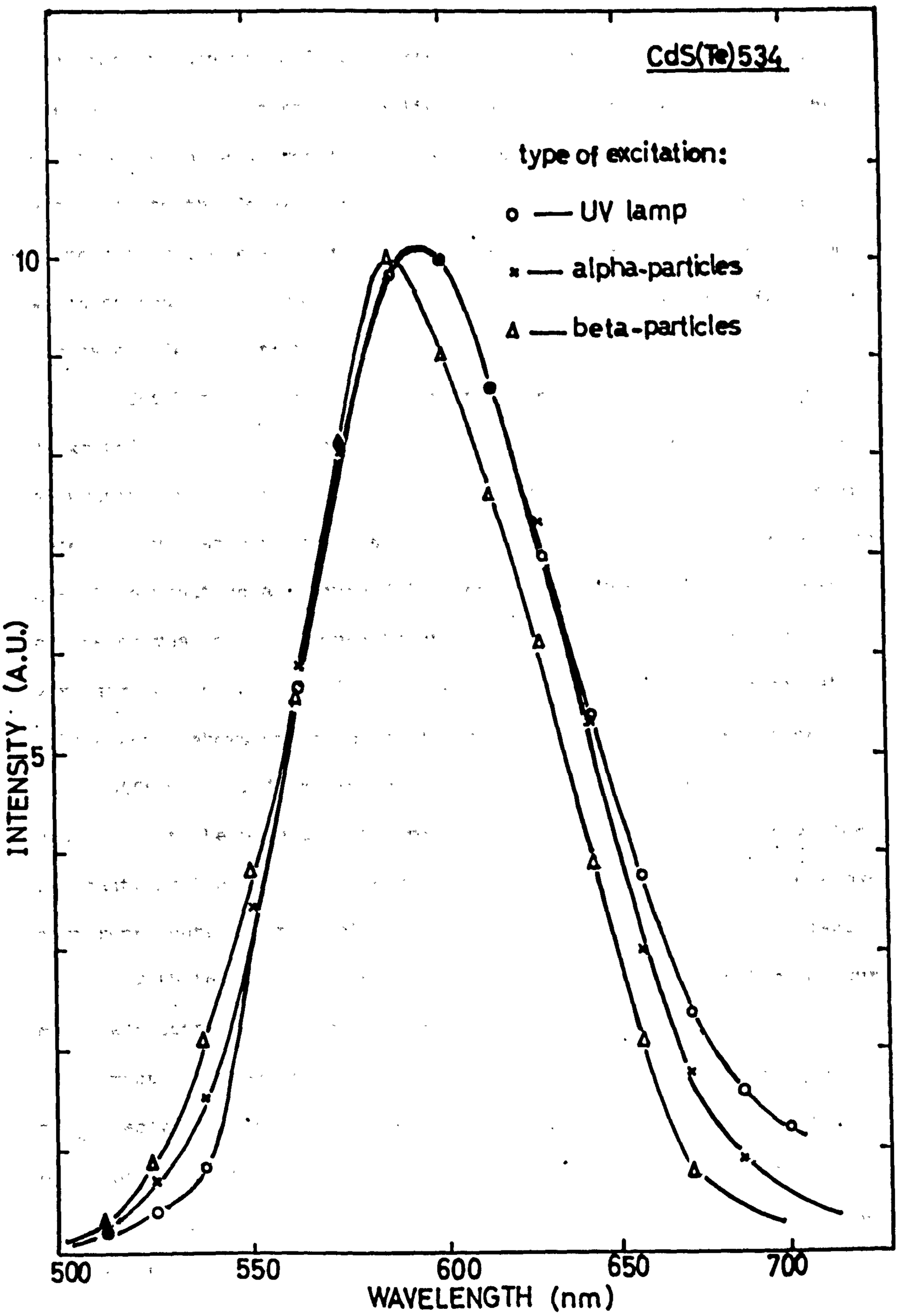

FIGURE 7.12 Luminescent emission spectra from boule 534 when excited by different sources (69).

trap rather than via a free carrier from the conduction band as in the latter case. In the tunnelling case, the binding energy of the electron in the electron trap is not available and the energy available to the Te exciton is less by this amount. It is interesting to note that the wavelength shift observed in Figure 7.12 is 12.5 nm which corresponds to an energy of 0.045 eV, the characteristic binding energy of electron traps in CdS.

Cuthbert and Thomas applied time-resolved spectroscopy to β-excited RL in CdS(Te) and found no observable effect. This is not surprising in the light of the ideas under discussion. However, when time-resolved spectroscopy is applied in the case of α-excitation, the result is positive as Figure 7.13 shows (69). The outstanding feature of the curves in this figure is that the prompt signal (0-60 ns) is very similar in distribution to the beta-curve and, the characteristic 'alpha-ness' shows up at longer times (454 - 738 ns). Again there is a shift of $\sim$ 0.045 eV in the peaks. The interpretation in this case is that the prompt part (corresponding to the $\sim$ 30 ns decay time constant) is the intrinsic Te excitonic decay spectrum while the slower part represents the recombination held up by the tunnelling process.

With the present apparatus the resolution in decay time measurements was considerably better than in wavelength and, therefore, the complement of time-resolved spectroscopy was used, i.e. the $t_{1/e}$ and t_{1/e^2} decay times were measured at different wavelengths across the emission spectrum (see Chapter 5). As Figure 5.16 shows for sample 108 the results are positive and quite striking. Both time constants decrease by 20% from 530 nm to 670 nm, Figure 7.14 shows similar results for 534 (to compare with Figure 7.13) with an even greater effect, but poorer statistics in the decay curves from which the time constants are derived. The interpretation of Figures 5.16 and 7.14 is

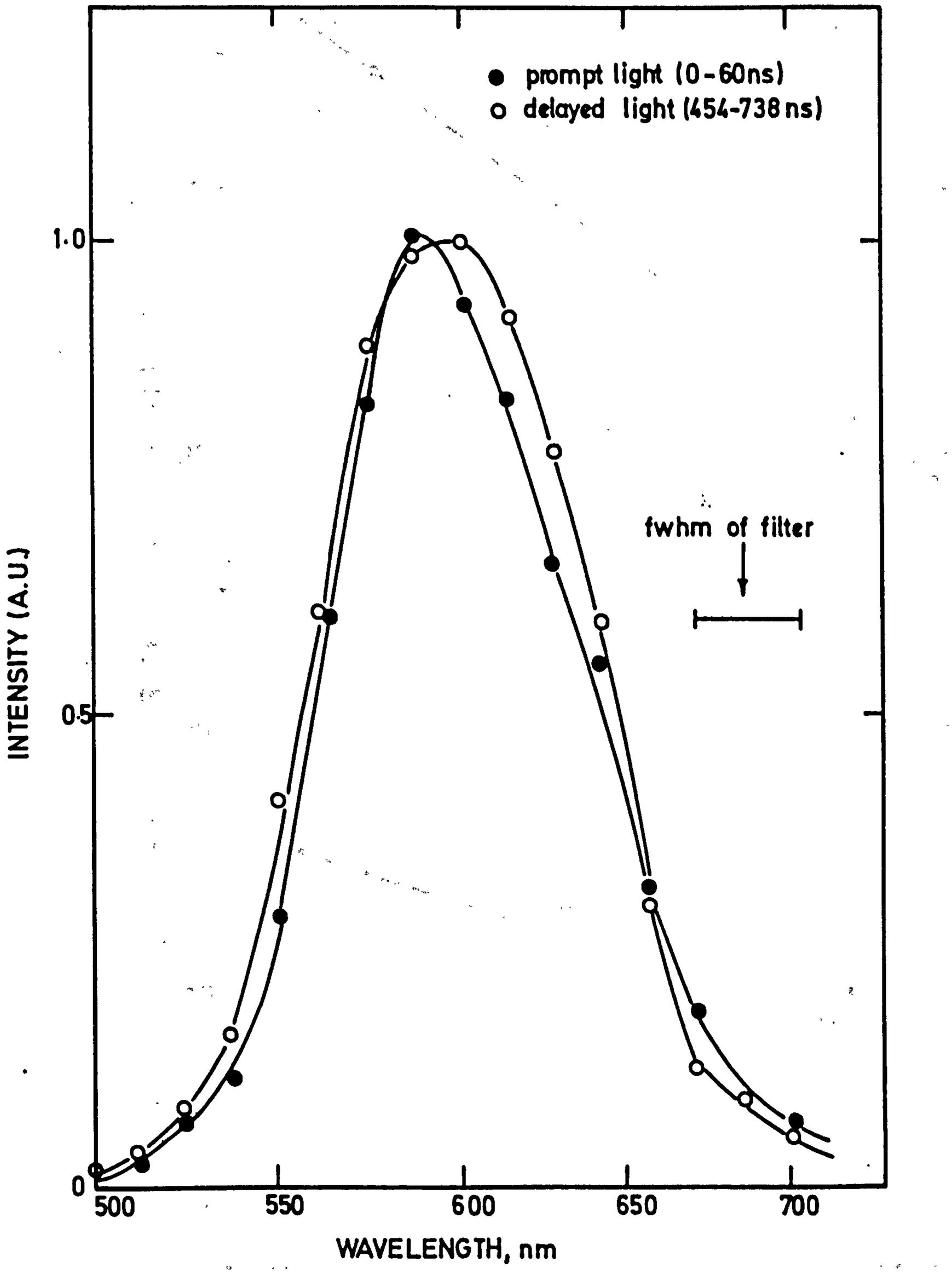

FIGURE 7.13 Time-resolved spectra for CdS(Te)534 crystal excited by 5.5 MeV α-particles at 100K(69).

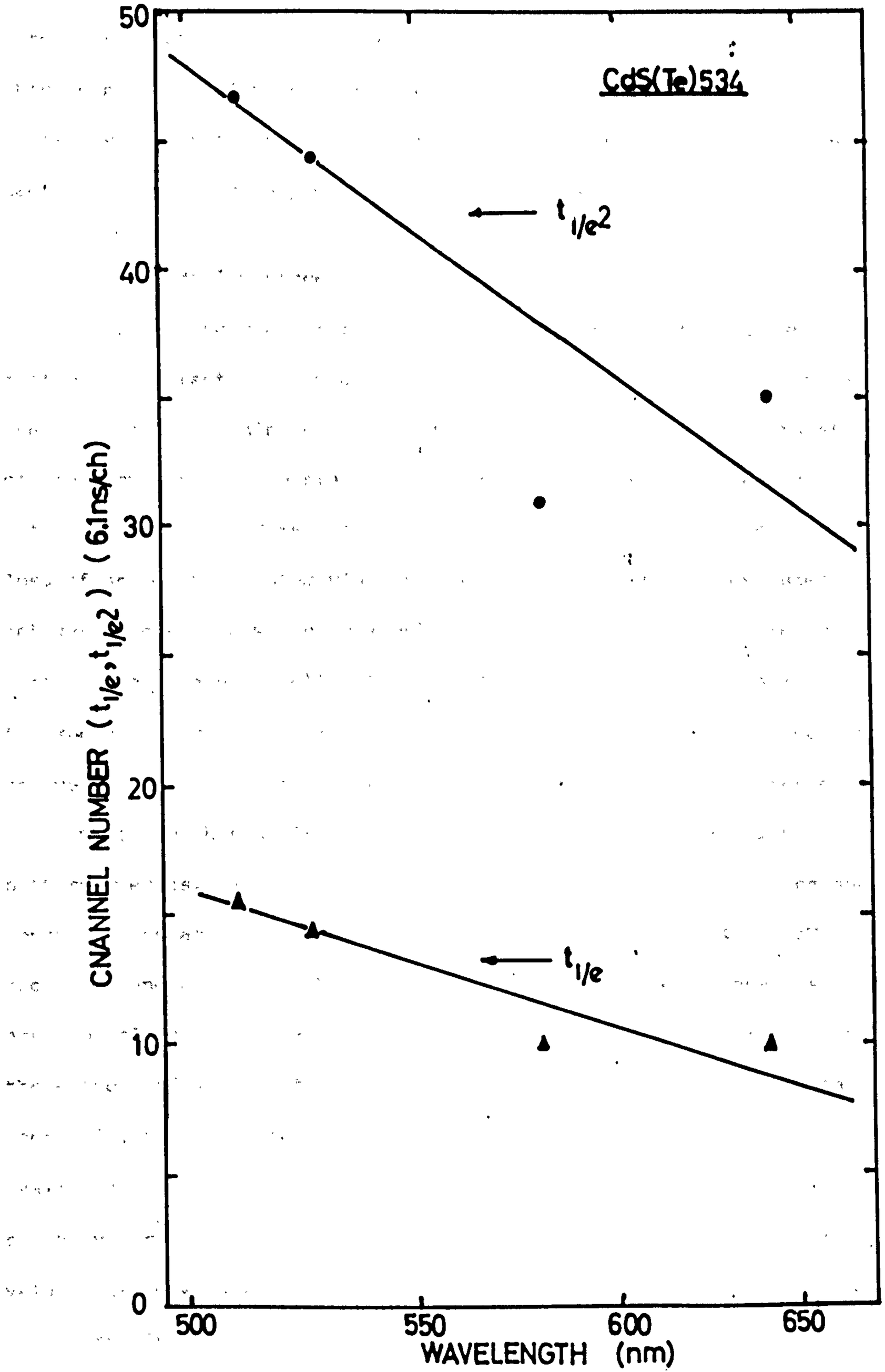

FIGURE 7.14 Decay time variations with the wavelength of emission when boule 534 is stimulated by α-particles at 95K (69).

rather obscure since they show the change in distribution of signal between the two parts of the decay kinetics as the wavelength changes. This is not a readily determined quantity and the main purpose of these results is to show clearly that time-wavelength effects do in fact exist as indicated by the time-resolved spectroscopy results.

7.1.6 Radioluminescent Quenching Effects

The quenching characteristics of the CdS(Te) crystals grown, show most of the effects that might be expected. Thus, Figure 7.15 shows the different quenching curves obtained with α-, β- and UV stimulation of the sample 534. The standard analysis of quenching curves in materials such as CdS relies on the simple concept of non-radiative loss of an excited system via a pathway accessible only above some activation energy U which is supplied by thermal excitation from the lattice (see Klasens (68)). A log plot of $(I(o)-I(T))/I(T)$ against $1/T$ is expected to yield a straight line from the slope of which U can be derived as described in Chapter 5. Subjecting the quenching curves of all samples to this analysis (see Chapter 5), a very consistent pattern emerges. α- and β-particles and UV all stimulate luminescence controlled by activation energies lying in the ranges 0.14-0.2 eV for the holes and 0.03-0.05 eV for the electrons. The variations observed are probably not physically significant because, (i) no correction for the effects of wavelength shifts on the steep PMT characreristic have been made, and (ii) because of the lower limit of temperature (80-90 K) available in the cryostat I(0) has to be estimated and the fitting is not very accurate. As summarised in Tables 5.1 and 5.2, the observed values agreed well with typical electron and hole trap depths in CdS.

Referring back to Table 5.1, it is observed that some trends are visible in the intercepts of the fits to the two parts of the

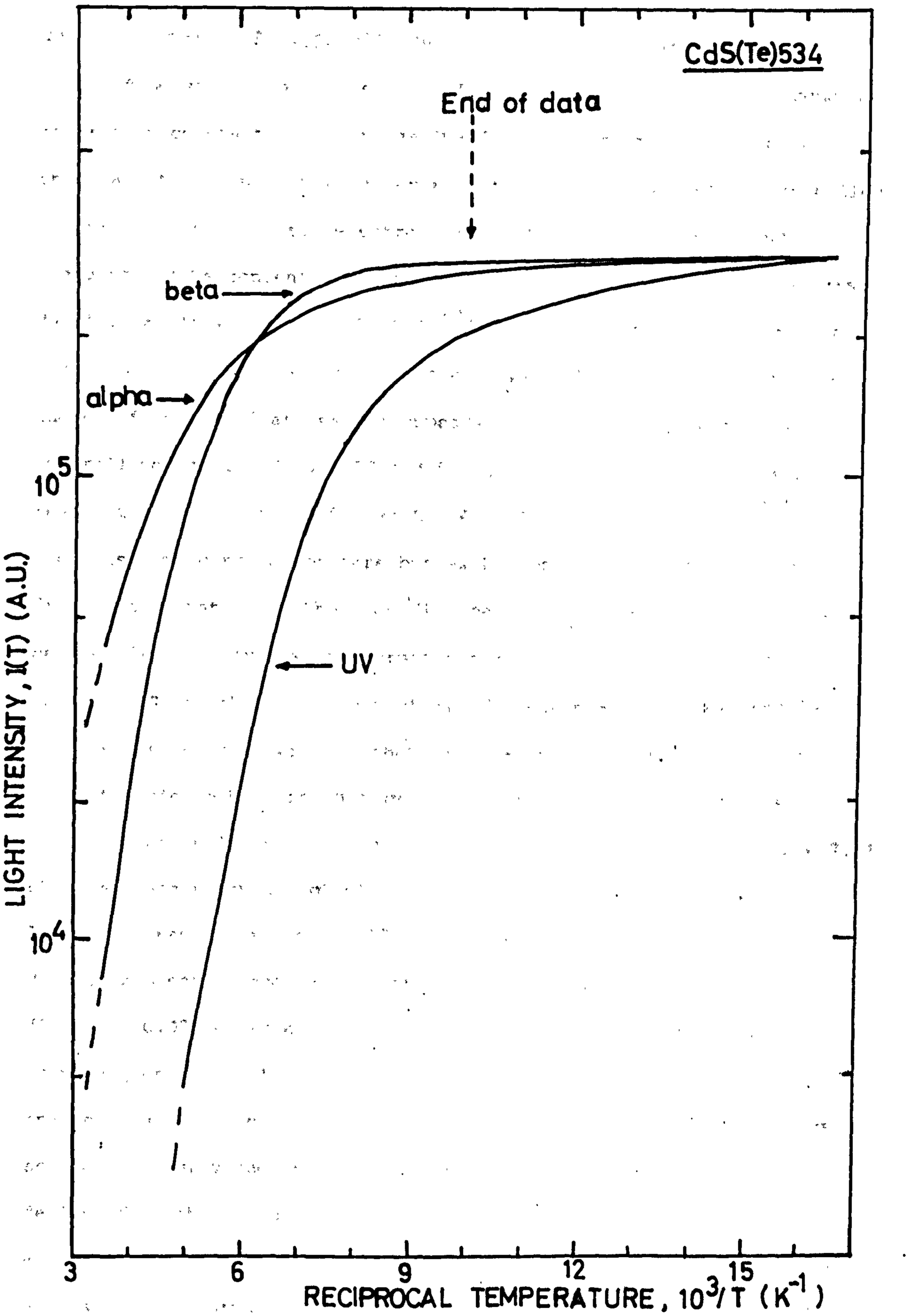

FIGURE 7.15 Thermal quenching of luminescence in boule 534 when stimulated by different sources(69).

quenching curve. A_1 typically runs from 10^3 - 10^5 and fluctuates wildly from sample to sample while A_2 (the electron intercept) remains remarkably constant in the range 10-20. The latter fact tends to encourage the view expressed above that electron trapping is controlled largely by the "natural" electron traps of the host lattice and changing the Te concentration makes little difference to the mean trap density (at least up to $[Te] \sim 2 \times 10^{19}$/cc). The intercept of the hole line does vary from sample to sample. Apart from 513 (which shows a number of curious features) it appears that the stoichiometry is the controlling factor. Thus 518 and 534 give $A_1 \sim 5 \times 10^3$ and $\sim 1 \times 10^2$ respectively. 512 and 535 give $A_1 \sim 4.4 \times 10^4$ and 80×10^4. Clearly, there is some correlation here but as Klasens (68) points out, it is difficult to interpret the significance of quenching data when killer centres (i.e. centres which permit non-radiative recombination) are present. Given that some sort of killer centre must be responsible for the loss of carriers and that calculations of Klasens show that the activation energy found from plots such as Figure 5.9 may be spurious, an analysis based on his formula was carried out. Figure 7.16 shows a Klasens' type plot of $(I(0)/I(T))^{\frac{1}{2}} - (I(T)/I(0))^{\frac{1}{2}}$ against 1/T on log paper for sample 512. The result is again a good fit to a double exponential and the activation energies are little changed (0.14 and 0.023 eV as against 0.17 and 0.027 eV). A summary of α-induced quenching data obtained on various CdS(Te) samples with Klasens' analysis is given in Table 7.1. (In this table, E and D represent an activation energy and an intercept of straight line respectively, derived from the graphical analysis). The fact that the hole activation energies change more than the electron ones when the Klasens analysis is performed is perhaps not surprising in that hole trapping on non-radiative centres would be expected to be more severe than in

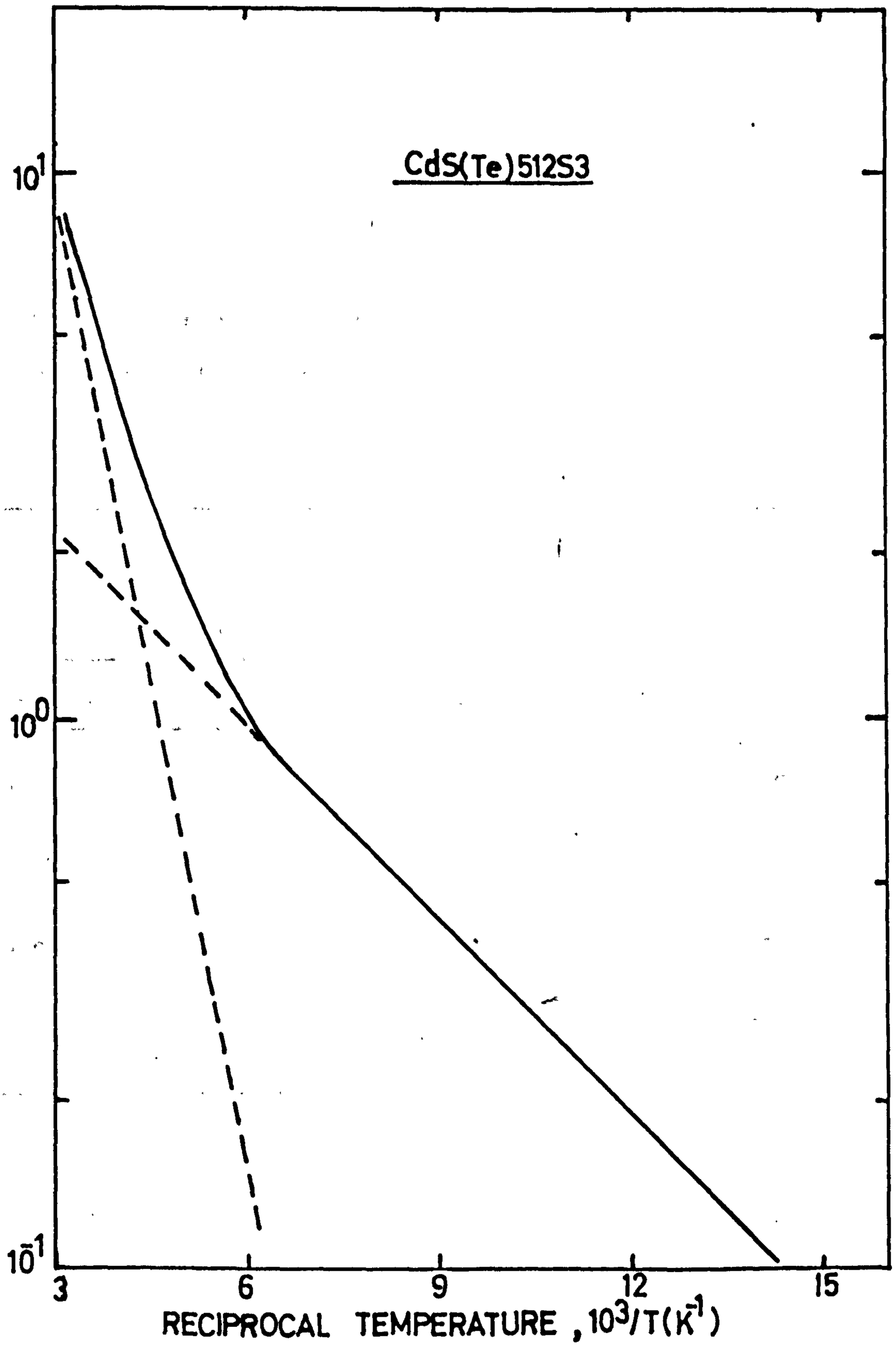

FIGURE 7.16 Klasens type analysis of the thermal quenching data given in Figure 5.7 for CdS(Te)512.

TABLE 7.1

Summary of α-induced thermal quenching data obtained on various CdS(Te) crystals using Klasens (68) analysis.

	Sample No.				
	108	512	513	518	535
Type	Platelet	S tail	Cd tail	Cd tail	S tail
E_1 , eV	0.17	0.14	0.17	0.11	0.19
$D_1 \times 10^4$	1.16	1.41	8.22	0.22	23
E_2 , eV	0.030	0.023	0.033	0.030	0.024
D_2	81	141	211	81	182

the electron case and Klasens predicts that the activation energy observed in such a case is some function of both the activation energy of the hole on the luminescent centre and the height of the trapping level above the valence band. The fact that the shifts are not dramatic probably reflects the well known fact that most hole traps in CdS generally lie $\sim$0.16 eV above the valence band.

Thus, while the quenching data confirms some broad features of the situation in the radioluminescence of CdS(Te), it can offer very little in the way of detailed tests of any model.

7.1.7 Models

The idea that, while all recombination takes place as excitons on a Te ion, some of the recombining electrons are collected by a tunnelling process from a neighbouring lattice electron trap seems to accommodate the new data presented in this work. This idea can explain the $\sim$0.045 eV red shift of the alpha and UV output spectrum relative to the beta one in terms of the degree of proximity of the initial carriers. Those generated at high density (e.g. the ones produced by alphas) tunnel rather than hop around from trap to trap so giving shorter decays with less energetic photons. Furthermore, in the case of alphas, two recombining species can be defined, viz. hole bearing Te ions and electron bearing lattice traps. The appearance of bimolecular kinetics is not therefore a surprise nor is the fact that the slope of the bimolecular plot is independent of temperature.

The fast part of the alpha decay curves shows a rather constant decay time of $\sim$20 - 30 ns, invariant with temperature and reasonably constant over a wide range of crystals, independent of stoichiometry and requiring only a [Te] $\geq 5\times10^{18}$/cc. It tends to

strike one as direct excitation of the Te ion to its excitonic state. The lifetime value of ∿25 ns agrees with the calculations of Henry and Nassau (45) for this system but disagrees with the 300 ns value which Cuthbert and Thomas (2) observed as the decay constant at 4.2 K and interpreted as the exciton lifetime. Cuthbert (1) showed that the free electron lifetime drops very rapidly towards 20 K and we must presume that it falls to ∿1 ns at 4.2 K. If we are to accept that the 300 ns exponential decay observed by Cuthbert and Thomas is the intrinsic excitonic lifetime we must require sequential trapping of 84% of holes on tellurium ion$and 84% of electrons on the Te^+ ions so created. Assuming that the competing lattice electron trap density was ∿16% of the local Te^+ concentration (an extremely unlikely assumption in the case of a very weakly ionising β-particle track), the quantum efficiency of any given sample should vary substantially with [Te] and the stoichiometry. This was not observed either by Cuthbert and Thomas or by ourselves. In fact, the uniform high efficiency of all samples at low temperatures is one of the striking features of CdS(Te). It thus seems that transport of electrons from lattice traps to Te^+ centres must occur. Since ionisation to the conduction band is not energetically possible, only tunnelling is available. How such a situation could result in the exponential decay over a factor of twenty in intensity observed by Cuthbert and Thomas is not clear; but, it is already evident that most of our samples will have decay times substantially less than 300 ns at 4.2 K. It may be therefore that this observed property of their crystals will be as different in our case as the decay lifetime behaviour with temperature which bears no relation to our results by an order of magnitude. Measurements of the decay profiles of our samples at $\lesssim$ 10 K is clearly important and if the above hypothesis is correct we could certainly expect to see

time-resolved effects.

In the absence of results at $\lesssim 10$ K it is difficult to be categorical about the ideas expressed above. However, it is clear that the present work has yielded considerable new insights into the RL mechanism in CdS(Te) and possibly paved the way to a definite model by

(a) successfully producing a series of good crystals of known [Te] and stoichiometry,

(b) providing new diagnostic situations through the use of α- and β-particles and time-resolved spectroscopy.

7.2 CdS(Te) as a Practical Scintillation Detector

At the start of this work the outstanding problems in the application of CdS(Te) as a scintillator were those of successfully producing large volume crystals of good optical quality and high luminescent efficiency, and finding a suitable photon detector at the wavelength of luminescent emission concerned. The results of Chapter 6 show how far these problems have been solved. It is clear that the boules produced (512 for example) have dimensions of order 1 cc, no grain boundaries or internal cracks, and a luminescent efficiency essentially the same as that observed in the platelets. The only outstanding problem is now the optical absorption of the crystals to their own emission. From the samples grown it is clear that the attenuation coefficient is very much determined by the stoichiometry since considerable variation is seen from sample to sample at constant tellurium concentration. In general, the sulphur excess crystals are clearer. Tellurium concentration does not seem to be critical at least up to [Te] values of $\sim 2\times10^{19}$/cc since the platelets (108) show lower attenuation than the boule with lowest [Te] (i.e. boule 512).

The measured room temperature attenuation coefficient of 512 was ~ 3 cm^{-1} at 600 nm. Work in pure CdS has indicated that the attenuation coefficient in the wavelength region above the band edge is limited to ~ 1 cm^{-1} by impurities and the attainment of the lower values ($\lesssim 0.1$ cm^{-1}) necessary for large scintillation counter depends very much on the growth technique. This, then, is an area in which further work would be necessary before adequate performance could be guaranteed for the large volume (i.e. ~ 100 cc) scintillators desirable for γ-ray detection. One effect has been noted, however, which promises lower effective attenuation than that measured in the test at room temperature. In the course of decay measurements at ~ 100 K on samples with cadmium excess (e.g. 534) a dramatic change in body colour to pale green and an obvious increase in transparency was noted. No quantitative measurements of this effect have so far been possible, but it is clear that at ~ 100 K (which is a very suitable operating temperature for CdS(Te)), the attenuation coefficient may well be less than 1 cm^{-1}. The effect is probably explicable in the terms of the shift of the band edge with temperature and the reduction of the free carrier density induced by the ionisation of donor states produced by the cadmium excess. Quantitative measurements of this effect is a high priority for future work on CdS(Te).

The problem of finding a suitable light detector to match the CdS(Te) emission at 600 nm was neatly solved by using the cryogenic Si(Li) diode described in Chapter 6. The high quantum efficiency of the silicon diode at 600 nm ($\sim 70\%$ for light incident from vacuum) shows up in the incredibly low energy per ion pair observed with CdS(Te), i.e. 24 eV. Optical coupling between the CdS(Te) crystal with refractive index of ~ 2.5 and a silicon surface of refractive

index ∿4 is obviously a problem. Curiously enough, this did not reflect in the total transmission but some of the degradation of the pulse-height resolution is attributed to this effect. Silicone oil with a refractive index of ∿1.5 is clearly not ideal, but no alternative was found. Theoretically, a coupling medium of refractive index ∿2.5 or greater should be ideal in that total internal reflection would be prevented.

One drawback of the Si(Li) diode is the slow time response of the system. Electronic time constants of 2-5 μs were routinely used. While the timing information from the fast front edge of the CdS(Te) luminescent pulse is inherent in the electronic output and can be recovered by a zero-crossing or constant fraction discriminator, for some applications it is important to have a short response time to combat pile-up. In this case, a PMT is the better light detector and, provided the temperature differential between crystal and PMT can be dropped across a suitable light pipe, the new photocathodes developed for laser work will permit an overall energy per photoelectron of 100-150 eV. This is better than can be achieved with NaI(Tl) and, a further advantage is that a crystal grown under cadmium excess will yield a decay time of ∿200 ns for γ-rays and ∿50 ns for α-particles. Thus, time constants are shorter than those of NaI(Tl) with a high degree of particle discrimination available. Very much faster response times are available if the temperature of the crystal is raised from 100 K to 300 K. The luminescent efficiency drops by a factor of 10 giving ∿1 keV per photoelectron in a PMT (comparable to, say, NE 102 plactic scintillator) with decay times of ∿50 ns for γ-rays and ∿15 ns for α-particles. In this case we could have a γ-ray detector with the detection efficiency of NaI(Tl) and a speed of response approaching that of plastic scintillator.

The serious problem remaining in the present work is that of determining the reason for the extremely poor pulse-height resolution observed with ^{137}Cs γ-rays in the cryogenic CdS(Te) 512 - Si(Li) detector. We have to compare the photopeak resolution in Figure 6.7c with the anticipated spectrum of Figure 1.7. Extensive work on NaI(Tl) (5,11,12) has shown that the transfer variance induced by differential light collection from the various regions of the scintillator responsible for the fact that the resolution of the ^{137}Cs γ-ray photopeak is a factor of two greater than the Poisson statistics predict (see Chapter 1). The factors which aggravate the transfer variance problem are as follows:

(i) crystal refractive index,

(ii) crystal absorption of the signal

(iii) crystal geometry.

Clearly all three factors apply in the case of our CdS(Te) crystals.

Factor (i) is inescapably present in CdS(Te) since, as already noted, the refractive index is 2.4. This simply serves to aggravate problems (ii) and (iii) by increasing the total internal reflection at the output face of the crystal. Factor (ii) leads to absorption of light rays trapped in the crystal by unfavourable features of crystal geometry (factor iii) such as corners and angles. The fact that the observed energy per ion pair is very nearly the same in the thick crystal (e.g. 512) as in the thin platelets shows that absorption is not very severe and the main source of the transfer variance is thought to lie in bad geometry. In order to get the maximum volume out of an irregularly shaped boule, sample 512 was cut with several flats, each bounded by an angle approximating 90^{o}. The resulting light trapping is believed to be the main cause of the poor resolution observed with

the ^{137}Cs source. For future work, crystals of more orthodox shape are required, i.e. right cylinder, possibly with spherical ends away from the output face.

Other factors which can affect the pulse-height resolution are temperature variation throughout the crystal and the slight degree of birefringence of CdS. Neither of these two effects are thought capable of producing the level of dispersion observed.

The state of development of CdS(Te) as a useful scintillator may now be summarised as follows:

(a) Cubic centimetre volume boules have been produced and shown to possess essentially the same characteristics as the original platelet crystals. The only difference is that considerable control of the properties of the crystals is available through manipulation of the stoichiometry during the growth.

(b) The crystal can be used at $\sim$100 K with a Si(Li) photodiode to give an extremely low energy per ion pair and the potential of very good pulse-height resolution if the problems of light collection can be solved. Alternatively, a PMT can be used with reduced statistics available but greater speed or response.

(c) Control of the scintillator temperature enables one to sacrifice signal for response time and so get a γ-ray detector with the detection efficiency of NaI(Tl) but a response time comparable with organic scintillators.

(d) The material shows ideal properties for pulse shape discrimination. The decay time is sensitive to ionisation density without showing the change of luminescent efficiency which accompanies this effect in most other scintillators. Typically, the decay time of the α-particle is four times shorter than that of the β-particle at 100 K.

Clearly, future work on this material should concentrate on two main problems, i.e. the study and growth of crystals with very low optical absorption in the region of the emission band, and the study of the longstanding problem of extracting light from a material of high refractive index without introducing severe pulse-height dispersion. Progress in these two matters would make CdS(Te) a useful addition to the available nuclear radiation detecting materials.

Publications

1. "A Cryogenic Scintillator-Photodiode Detector for Penetrating Charged Particles", J.E. Bateman and F.E. Özsan, Nucl. Instr. and Meth. 108 (1973) 403.

2. "Radioluminescence in Large Single Crystals of Cadmium Sulphide Doped with Tellurium", J.E. Bateman, F.E. Özsan, J. Woods and J.R. Cutter, J. Phys. D: 7 (1974) 1316.

REFERENCES

1. J.D. Cuthbert, J. Appl. Phys. 42 (1971) 739

2. J.D. Cuthbert and D.G. Thomas, J. Appl. Phys. 39 (1968) 1573

3. D.M. Roessler, J. Appl. Phys. 41 (1970) 4589

4. J. Sharpe, "Nuclear Radiation Detectors", Methuen, London, 1964

5. J.B. Birks, "The Theory and Practice of Scintillation Counting", Pergamon, Oxford, 1964

6. S.C. Curran, "Luminescence and Scintillation Counters", Butterworths, London, 1953

7. T.C. Madden, J.L. Merz, G.L. Miller and D.G. Thomas, IEEE Trans. on Nucl. Sci. NS-15 / No.6 (1968) 47

8. I. Kaplan, "Nuclear Physics", Addison-Wesley, London, 1964

9. G. Bertolini and A. Coche, "Semiconductor Detectors", North-Holland, 1968

10. K. Siegbahn, "Alpha-, Beta- and Gamma-ray Spectroscopy, Vol. 1", North-Holland, 1965

11. J.R. Prescott and P.S. Takhar, IRE Trans. on Nucl. Sci. NS-9 (1962) 36

12. I.R. Gulakow, A.D. Levkovich, A.N. Perstev, and P.N. Tolkach, Instr. and Exp. Tech. 2 (1970) 404

13. P. Kisijper, C.J. Tiesinga and C.C. Jonker, Nucl. Instr. and Meth. 42 (1966) 56

14. A.I. Kilvington, C.A. Baker and P. Illiness, Nucl. Instr. and Meth. 80 (1970) 177

15. G.A. Morton, H.M. Smith, H.R. Krall, IEEE Trans. on Nucl. Sci. NS-16 (1966) 92

16. A.H.F. Muggleton, Journ. Phy. E: Scientific Instr. 5 (1972) 390

17. Proc. of the Total Absorption Gamma-ray Spectrometry Symp., Gattinburg, Tennessee, May 1960, U.S. Atomic Energy Commission Office, Report TID-7594

18. U.C. Mishra and Sadasivan, Nucl. Instr. and Meth. 69 (1969) 330

19. J.M. Hollander, Nucl. Instr. and Meth. 43 (1966) 65

20. Ortec, Application report on germanium detector systems

21. G.L. Miller, IEEE Trans. on Nucl. Sci. NS-19 (1972) 252

22. "An introduction to the operation and applications of semiconductor detectors", Nuclear Enterprises (1972)

23. R.Y. Deshpande, Nucl. Instr. and Meth. 57 (1967) 125

24. L. Malm, T.W. Raisdorf, M. Martini and K.R. Zanio, IEEE Trans. on Nucl. Sci. NS-20 (1973) 500

25. E.M. Gunnersen, Rep. Prog. Phys. 30 (1967) 27

26. K. Zanio, W. Akutagawa and H. Montana, IEEE Trans. on Nucl Sci. NS-19 (1972) 257

27. W. Akutagawa, K. Zanio, and J.W. Mayer, Nucl. Instr. and Meth. 55 (1967) 383

28. W. Akutagawa and K. Zanio, IEEE Trans. on Nucl. Sci. NS-15 (1968) 266

29. K. Zanio, J. Neeland and H. Montano, IEEE Trans. on Nucl. Sci. NS-17 (1970) 287

30. P. Siffert and A. Cornet (Ed.), Proc. of Int. Symp. on CdTe, June 1971, Strasbourg

31. J.E. Eberhardt, R.D. Ryan and A.J. Tavendale, Nucl. Instr. and Meth. 94 (1971) 463

32. J.E. Bateman and F.E. Özsan, Nucl. Instr. and Meth. 108 (1973) 403.

33. J.E. Bateman, Nucl. Instr. and Meth. 67 (1969) 93

34. J.E. Bateman, Nucl. Instr. and Meth. 71 (1969) 261

35. J.E. Bateman, Nucl. Instr. and Meth. 71 (1969) 269

36. EG & G Inc., Photodiode Application Notes for SGD-100 and SGD-444

37. L. Clark and J. Woods, J. Cry. Growth 3 (1968) 126

38. M. Aven and J.S. Prener, "Physics and Chemistry of II-VI Compounds", North Holland, 1967

39. D.G. Thomas and J.J. Hopfield, Phys. Rev. 116 (1959) 573

40. J.O. Dimmock, Int. Conf. on II-VI Semiconductor Compounds", Ed. by D.G. Thomas, Benjamin 1963

41. T.S. Moss, "Optical Properties of Semiconductors", London, Butterworths, 1959 p.215

42. H. Gobrecth and A. Bartshat, Z. Physik 156 (159) 131

43. J.J. Hopfield and D.G. Thomas, Phys. Rev. 122 (1961) 35

44. D.G. Thomas and J.J. Hopfield, J. Appl. Phys. 33 (1962) 3243

45. C.H. Henry and K. Nassau, Phys. Rev. B1 (1970) 1628

46. K. Colbow, Phys. Rev. 141 (1966) 742

47. K. Colbow and K. Yuen, Can. J. Phys. 50 (1972) 1518

48. J.L. Merz and R.J. Lynch, in reference 40.

49. J.J. Hopfield, D.G. Thomas and R.T. Lynch, Phys. Rev. Let. 17 (1966) 312

50. D.G. Thomas and J.J. Hopfield, Phys. Rev. 150 (1966) 680

51. F.A. Trumbore, M. Gershenzon and D.G. Thomas, Appl. Phys. Let. 17 (1966) 4

52. J.D. Cuthbert and D.G. Thomas, Phys. Rev. 154 (1967) 763

53. A.C. Aten, J.H. Haanstra and H. de Vries, Phillips Research Reports 20 (1965) 395

54. R. Dingle, Phys. Rev. 184 (1969) 788

55. O. Goede and E. Nebauer, Phys. Stat. Sol. (a) 7 (1971) K85

56. R.M. Mikulyak, J. Cry. Growth 8 (1971) 149

57. L.M. Bollinger and G.E. Thomas, Rev. Sci. Instr. 32 (1961) 1044

58. J.A. Miehe, G. Ambard, Z. Zampach and A. Coche, IEEE Trans. on Nucl. Sci. NS. 17 (1970) 115

59. T.H. Binkkert, H.P. Tschanz and P.E. Zinsli, J. Lum. 5 (1972) 187

60. H.R. Stacklman, J. Lum. 3 (1970) 143

61. P.G. Sjolin, Nucl. Instr. Meth. 37 (1965) 45

62. P.B. Coates, J. Phys. E (Sci. Instr.) 2 (1968) 878

63. C.C. Davis and T.A. King, Rev. Sci. Instr. 41 (1970) 407

64. C.C. Davis and T.A. King, J. Phys. A (Gen. Phys.) 3 (1970) 101

65. P.B. Coates, J. Phys. E (Sci. Instr.) 5 (1972) 148

66. I.M. Blair, D. Pooley and D.S. Smith, J. Phys. C (Sol. St. Phys.) 5 (1972) 1537

67. D.E. Bateman and R.E. Jones (at Rutherford High Energy Laboratories), private communication

68. H.A. Klasens, J. Phys. Chem. Sol. 9 (1959) 185

69. J.E. Bateman (at Rutherford High Energy Laboratories), private communication